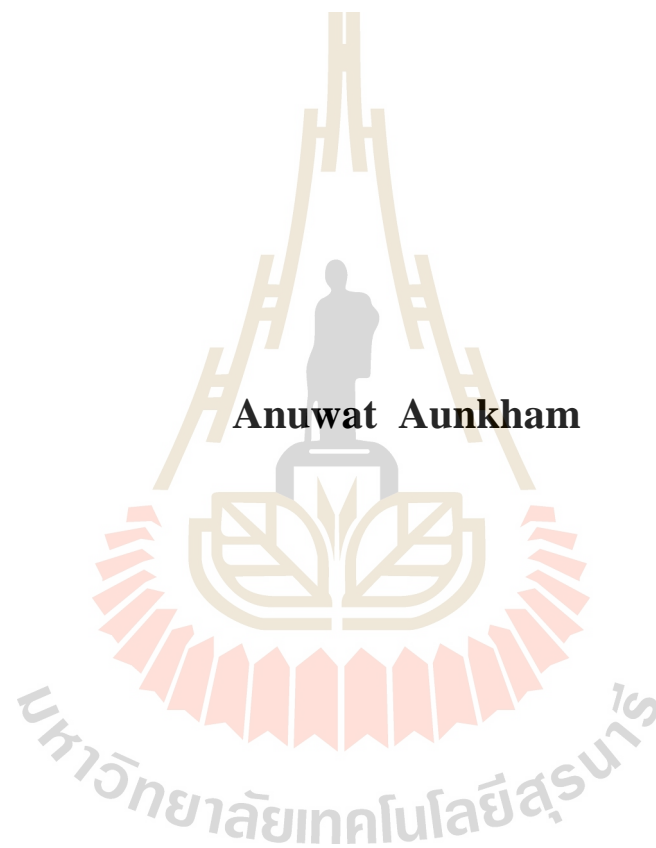


**STRUCTURE AND FUNCTION OF OUTER MEMBRANE  
PROTEINS FROM PATHOGENIC BACTERIA**



**A Thesis Submitted in Partial Fulfillment of the Requirements for the  
Degree of Doctor of Philosophy in Biochemistry  
Suranaree University of Technology  
Academic Year 2016**

การศึกษาโครงสร้างและหน้าที่ของโปรตีนที่เยื่อเซลล์ชั้นนอก  
ของแบคทีเรียก่อโรค



วิทยานิพนธ์นี้เป็นส่วนหนึ่งของการศึกษาตามหลักสูตรปริญญาวิทยาศาสตรดุษฎีบัณฑิต  
สาขาวิชาชีวเคมี  
มหาวิทยาลัยเทคโนโลยีสุรนารี  
ปีการศึกษา 2559

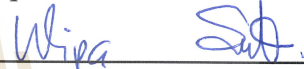
**STRUCTURE AND FUNCTION OF OUTER MEMBRANE  
PROTEINS FROM PATHOGENIC BACTERIA**

Suranaree University of Technology has approved this thesis submitted in partial fulfillment of the requirements for the Degree of Doctor of Philosophy.

Thesis Examining Committee

  
\_\_\_\_\_  
(Prof. Dr. Jatuporn Wittayakun)

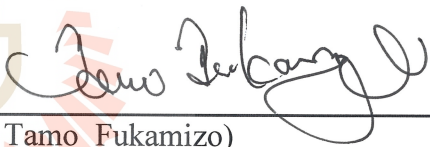
Chairperson

  
\_\_\_\_\_  
(Assoc. Prof. Dr. Wipa Suginta)


Member (Thesis Advisor)

  
\_\_\_\_\_  
(Prof. Dr. Bert van den Berg)

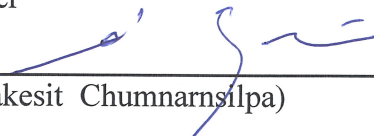
Member

  
\_\_\_\_\_  
(Prof. Dr. Tamo Fukamizo)

Member

  
\_\_\_\_\_  
(Dr. David Apps)


Member

  
\_\_\_\_\_  
(Dr. Sakesit Chumnarnsilpa)

Member

  
\_\_\_\_\_  
(Prof. Dr. Santi Maensiri)

Acting Vice Rector for Academic  
Affairs and Internationalisation

  
\_\_\_\_\_  
(Prof. Dr. Santi Maensiri)

Dean of Institute of Science

อนุวัต อนุคำ : การศึกษาโครงสร้างและหน้าที่ของโปรตีนที่เชื่อมเซลล์ชั้นนอก  
ของแบคทีเรียก่อโรค (STRUCTURE AND FUNCTION OF OUTER MEMBRANE  
PROTEINS FROM PATHOGENIC BACTERIA). อาจารย์ที่ปรึกษา :  
รองศาสตราจารย์ ดร.วิภา สุจินต์, 193 หน้า.

งานวิจัยนี้เป็นการศึกษาโครงสร้าง และหน้าที่ของช่อง โปรตีนที่เชื่อมหุ้มเซลล์ชั้นนอกของ  
แบคทีเรียแกรมลบที่ก่อโรคสองสายพันธุ์ที่มีชื่อว่า *BpsOmp38* จากเชื้อ *Burkholderia pseudomallei* และ  
*VhChiP* จากเชื้อ *Vibrio harveyi*

*BpsOmp38* มีคุณสมบัติเป็นช่องแพร่ผ่านสารที่ไม่จำเพาะ ซึ่งประกอบด้วยหน่วยย่อย ที่  
เหมือนกัน 3 หน่วย จากการศึกษาโครงสร้างสามมิติของผลึกโปรตีน ซึ่งสามารถหักเหรังสีเอกซ์ได้ความ  
ละเอียด 2.8 อังสตรอม พบว่าแต่ละหน่วยย่อยมีโครงสร้างโดยรวมประกอบด้วย 16 anti  $\beta$ -strands ต่อด้วย  
8 loop ขนาดยาวที่ยื่นออกไปด้านนอกเซลล์ และ 7 loop ขนาดสั้นที่ยื่นเข้าไปใน periplasmic ลักษณะ  
ภายในช่องโปรตีนมีคุณสมบัติเป็นไฮโดรฟิลิกสูง ซึ่งจากโครงสร้างพบว่า กรดอะมิโน Tyr119 ยื่นเข้าไป  
ตรงกลางของช่องโปรตีน และจากการศึกษาผลของยาต่อเชื้อ *B. pseudomallei* ด้วยวิธี Minimum inhibitory  
concentration (MIC) พบว่า เชื้อมีการต้านทานต่อยาเกือบทุกชนิดยกเว้นยา 2 ชนิด คือ ceftazidime และ  
meropenem ผลการทดลองสอดคล้องเป็นอย่างดีกับการศึกษาการแพร่ผ่านของยา ด้วยเทคนิค liposome  
swelling และ เทคนิค planar lipid membrane (BLM) ยาสองชนิดนี้แพร่ผ่านช่องโปรตีนได้ดีกว่ายาชนิด  
อื่นๆ และจากการศึกษาผลการกลายพันธุ์ของกรดอะมิโน Tyr119 มีหน้าที่สำคัญต่อการควบคุมการแพร่  
ผ่านของยา และน้ำตาลผ่านช่อง *BpsOmp38* ซึ่งการดัดแปลงกรดอะมิโน Tyr119 ให้เป็น Ala ส่งผลให้มีการ  
การแพร่ผ่านของยาและน้ำตาลเพิ่มขึ้น เนื่องจากกรดอะมิโน Ala มีขนาดเล็กกว่า Tyr จึงทำให้ช่องของ  
โปรตีนมีขนาดกว้างขึ้น การแพร่ผ่านของสารจึงแพร่ผ่านได้ดีขึ้น

*VhChiP* มีคุณสมบัติ เป็นช่องแพร่ผ่านสารที่จำเพาะสูงต่อน้ำตาล ไคโตแซกซะ โอส จากการศึกษา  
ผลการกลายพันธุ์ของกรดอะมิโน Tyr136 ด้วยวิธีการทำให้โปรตีนเสียสภาพด้วยการเพิ่มอุณหภูมิ พบว่า  
น้ำตาล ไคโตโอลิโกแซคคาไรด์ช่วยป้องกันการเสียสภาพ ในระดับโครงสร้างทุติยภูมิ และตติยภูมิของ  
ช่องโปรตีน นอกจากนี้ยังมีการศึกษาอัตราการจับของน้ำตาล กับช่องโปรตีนด้วยวิธีอุณหพลศาสตร์ และ  
เทคนิค fluorescence spectroscopy ผลการศึกษาช่วยยืนยันว่า Tyr136 มีบทบาทสำคัญต่อการแพร่ผ่านของ  
น้ำตาลผ่านช่องพอรินชนิด *VhChiP* จากการศึกษาโครงสร้างสามมิติของผลึกโปรตีน *VhChiP* refolded  
และ *VhChiP* native ที่ถูกหักเหด้วยรังสีเอกซ์ ด้วยความละเอียดสูงถึง 1.9 อังสตรอม ซึ่งโครงสร้าง  
โดยทั่วไปของ *VhChiP* พอริน ประกอบด้วยหน่วยย่อยที่เหมือนกันสามหน่วย แต่ละหน่วยย่อย  
ประกอบด้วย 16 strand ที่ถูกเชื่อมต่อกันด้วย 8 loop ขนาดยาวที่อยู่ด้านนอกผนังเซลล์ และ 7 loop ขนาดสั้นที่

ยื่นเข้าไปใน periplasmic อย่างไรก็ตาม โครงสร้างของโปรตีนทั้งสองมีความแตกต่างกัน โดยโครงสร้างของ *VhChiP* refolded ในส่วนของ *N-terminus* จะยื่นออกไปด้านนอกของช่องโปรตีน แต่โครงสร้างของ *VhChiP* native จะยื่นเข้าไปอุดอยู่ในช่องโปรตีนที่อยู่ติดกัน ส่วนของ *N-terminus* นี้ อาจมีผลช่วยต่อการนำเข้าน้ำตาล ผ่านช่อง *VhChiP* พอริน โครงสร้างของโปรตีน *VhChiP* refolded ที่จับกับไคโตเฮกซะไอส พิสูจน์ให้เห็นว่า กระจอะมิโนที่เป็นวงแหวน จะจับกับวงแหวนของน้ำตาลด้วยแรงไฮโดรโฟบิก และ กระจอะมิโนที่มีประจุ หรือมีขั้ว จะจับกับ หมู่  $C_2$ -อะซีตามิโด และ ไฮดรอกซิล ของน้ำตาล ด้วยเครือข่ายพันธะไฮโดรเจน นอกจากนี้ก็พบว่าน้ำตาลไคโตเตตระไอส สามารถจับกับโครงสร้างของโปรตีน *VhChiP* native และมีผลทำให้ *N-terminus* หลุด และยื่นออกมาจากภายนอกช่องโปรตีน



สาขาวิชาเคมี  
ปีการศึกษา 2559

ลายมือชื่อนักศึกษา อนุต คุ้มคำ  
ลายมือชื่ออาจารย์ที่ปรึกษา [Signature]

ANUWAT AUNKHAM : STRUCTURE AND FUNCTION OF OUTER  
MEMBRANE PROTEINS FROM PATHOGENIC BACTERIA.

THESIS ADVISOR : ASSOC. PROF. WIPA SUGINTA, Ph.D. 193 PP.

STRUCTURE AND FUNCTION OF OUTER MEMBRANE PROTEINS FROM  
PATHOGENIC BACTERIA

Two outer membrane channels from two Gram-negative pathogenic bacteria, namely *BpsOmp38* from *Burkholderia pseudomallei* and *VhChiP* from *Vibrio harveyi*, together with their mutants were expressed and characterised.

*BpsOmp38* was shown to act as a general diffusion channel, consisting of three identical subunits. The crystal structure revealed that *BpsOmp38* was solved to highest resolution of 2.8 Å. The final model of *BpsOmp38* showed that each *Bps* barrel consists of 16 anti  $\beta$ -strands with eight extracellular long loops and seven periplasmic turns. The channel interior is highly hydrophilic with Tyr119 amino acid protruding in the centre of the pore. Minimum inhibitory concentration (MIC) and liposome swelling assays showed that clinical *B. pseudomallei* strain was resistant to most antimicrobial agents. However, high sensitivity was observed for ceftazidime and meropenem. This observation was in good agreement with the BLM experiments of *BpsOmp38* where translocation was observed for two sensitive drugs; ceftazidime and meropenem. In contrast, no channel blockage was seen for the drugs to which the *Bps* was resistant to even at high concentration. Meanwhile, mutation of the residue Tyr119 greatly affected the permeability of antimicrobial agents and neutral sugars. The results indicated the important role of Tyr119 in regulating the passage of these molecules through

*BpsOmp38* channel. The higher permeability of *BpsOmp38Y119A* was ascribed to the widening of the pore interior as a result of the substitution of the bulky Tyr with the smaller Ala residue.

*VhChiP* was identified to be highly selective for chitohexaose uptake. The essential role of Tyr136 in kinetic binding affinity was proven by the observation of increased midpoint temperature ( $T_m$ ) of secondary and tertiary structural thermal unfolding for protein-chitooligosaccharide complex. Thermodynamic parameters of protein-chitooligosaccharide interactions obtained from fluorescent quenching technique also supported this phenomenon. In the later part of this study, the 3D structures of trimeric *VhChiP* both in refolded and native forms were solved to highest resolution of 1.9 Å. The overall structures of the native and refolded channels were essentially identical, to which each of the trimeric barrels comprised 16 strands, connected by 8 extracellular loops, and 7 periplasmic turns. However, the *N*-terminus in the refolded channel swings outside the  $\beta$ -barrel, making the channel interior more accessible to the sugar substrate. This *N*-terminal segment that protrudes towards the protein lumen in the native channel was presumed to help in regulating sugar translocation and stabilising the structure of *VhChiP*. The crystal structure of the refolded *VhChiP* in the presence of chitohexaose revealed that the four GlcNAc rings were in stacking position with the regional amino acid residues. Besides, the C<sub>2</sub>-acetamido and OH groups of the GlcNAc units also interact with several charge or polar residues. The *N*-terminus of the native protein was displaced by chitohexaose.

School of Chemistry

Academic Year 2016

Student's signature Anuwat Aunkham

Advisor's signature Wipa Suda

## ACKNOWLEDGEMENTS

I would like to express my deepest appreciation to my thesis advisor Assoc. Prof. Dr. Wipa Suginta for providing me a great opportunity to work on this project and pursue my Ph.D. degree in Biochemistry. Her valuable time for guiding, as well as her unconditional support, inspiration and encouragement are very much appreciated.

I am also deeply grateful to my co-advisors, Prof. Dr. Bert van den Berg at Newcastle University, England for giving me a chance to work on membrane protein crystallisation, and Prof. Dr. Mathias Winterhalter at Jacobs University Bremen, Germany for his guidance on electrophysiology in their laboratories. They have provided me with valuable technical skills, precious advice and also kind support throughout my stay in foreign countries, which was an unforgettable experience.

My special thank goes to the Royal Golden Jubilee Ph.D. Program for the financial support, and the Biochemistry-Electrochemistry Research Unit, Suranaree University of Technology for providing research facilities. This research would not have been possible without their support.

I would like to acknowledge all the lecturers of the Department of Biochemistry at Suranaree University of Technology for passing on to me their knowledge and lab techniques in biochemistry, which were later found to be useful for my research project development.

I wish to thank all my friends in the Biochemistry-Electrochemistry Research Unit, Suranaree University of Technology for giving me all the emotional support needed to get through all the difficult times in this Ph.D. journey.

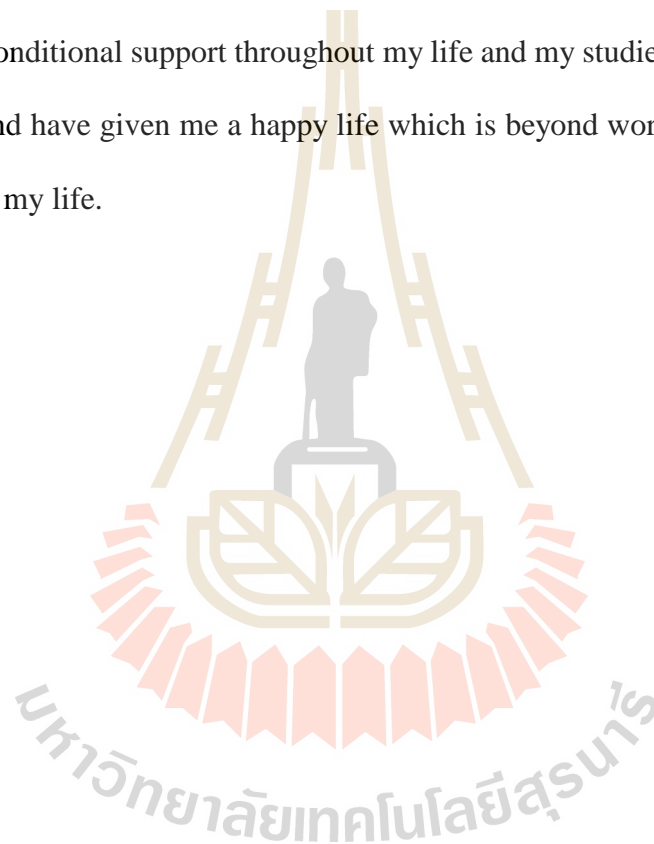


Thanks are also due to Mr. Wei Chung Sim for his precious critics and proofreading, which has profoundly improved the language and composition of this thesis.

Besides, I would like to thank those whose names are not mentioned here but have greatly inspired and encouraged me until this thesis comes to a perfect end.

Last but not least, my deepest gratitude goes to my family for their unflinching love and unconditional support throughout my life and my studies. They made me who I am today and have given me a happy life which is beyond words. I am very lucky to have them in my life.

Anuwat Aunkham



# CONTENTS

	<b>Page</b>
ABSTRACT IN THAI.....	I
ABSTRACT IN ENGLISH .....	III
ACKNOWLEDGEMENTS.....	V
CONTENTS.....	VII
LIST OF TABLES .....	XVI
LIST OF FIGURES .....	XVII
LIST OF ABBREVIATIONS.....	XXII
<b>CHAPTER</b>	
<b>I INTRODUCTION .....</b>	<b>1</b>
1.1 Gram-negative bacteria and their outer membrane proteins .....	1
1.1.1 Gram-negative bacteria.....	1
1.1.2 Classification of outer membrane proteins .....	3
1.1.3 Classification of integral or transmembrane proteins (porins) .....	4
1.1.3.1 General diffusion porins .....	4
1.1.3.2 Substrate-specific porins.....	6
1.2 <i>Vibrio harveyi</i> and <i>Burkholderia pseudomallei</i> .....	9

## CONTENTS (Continued)

	<b>Page</b>
1.2.1 <i>Vibrio harveyi</i> .....	9
1.2.2 <i>Burkholderia pseudomallei</i> .....	12
1.3 Porins involved in antibiotic resistance of pathogenic bacteria .....	14
1.3.1 Porins involved in membrane susceptibility .....	16
1.3.2 Antibiotic resistance of <i>B. pseudomallei</i> .....	17
1.4 Previous studies on porins from <i>B. pseudomallei</i> and <i>V. harveyi</i> .....	18
1.4.1 Liposome-swelling assays of outer membrane proteins from <i>B. pseudomallei</i> .....	18
1.4.2 Pore-forming properties and translocation of antibiotics through single channel of <i>BpsOmp38</i> by black lipid membrane (BLM) technique .....	20
1.4.3 Characterisation of chitooligosaccharide-specific porins from <i>V. harveyi</i> .....	21
1.4.4 Mutational effects on chitooligosaccharide permeability through <i>VhChiP</i> from <i>V. harveyi</i> .....	24
1.5 Research objectives .....	25
<b>II MATERIALS AND METHODS .....</b>	<b>28</b>
2.1 Design of oligonucleotide primers .....	28

## CONTENTS (Continued)

	<b>Page</b>
2.1.1 <i>BpsOmp38</i> from <i>Burkholderia pseudomallei</i> .....	28
2.1.2 <i>VhChiP</i> from <i>Vibrio harveyi</i> .....	29
2.2 Expression vectors and bacterial host cells .....	29
2.3 Chemicals and reagents .....	30
2.4 Instrumentation .....	31
2.5 Methodology .....	32
2.5.1 Structural and functional characterisation of <i>BpsOmp38</i> from <i>B. pseudomallei</i> .....	32
2.5.1.1 Antimicrobial susceptibility assay .....	32
2.5.1.2 Topology structure prediction .....	33
2.5.1.3 PCR amplification of the cDNA encoding <i>BpsOmp38</i> .....	34
2.5.1.4 Cloning of DNA encoding <i>BpsOmp38</i> into pET23d(+) and confirmation of DNA insert .....	35
2.5.1.5 Mutation design and site-directed mutagenesis of pET23d(+)/ <i>BpsOmp38</i> .....	36
2.5.1.6 Native protein expression and purification of <i>BpsOmp38</i> .....	37

## CONTENTS (Continued)

	<b>Page</b>
2.5.1.7 Immunological analysis .....	39
2.5.1.8 Pore conductance analysis .....	39
2.5.1.9 Liposome Swelling Assays.....	40
2.5.1.10 Statistical analysis.....	42
2.5.1.11 Binding studies using BLM technique .....	42
2.5.1.12 Thermal unfolding using circular dichroism (CD) spectroscopy .....	43
2.5.1.13 Thermal unfolding using fluorescence spectroscopy ...	44
2.5.1.14 Binding studies using fluorescence quenching.....	45
2.5.1.15 Thermodynamic parameters and the binding using fluorescence quenching .....	46
2.5.1.16 Crystallisation and structure solution of <i>BpsOmp38</i> ....	47
2.5.2 Structure and functional properties of outer membrane protein ( <i>VhChiP</i> ) from <i>Vibrio harveyi</i> .....	48
2.5.2.1 Structure Prediction of <i>VhChiP</i> .....	48
2.5.2.2 Expression and purification of <i>VhChiP</i> variants.....	48
2.5.2.3 Confirmation of <i>VhChiP</i> expression by immunoblotting .....	50

## CONTENTS (Continued)

	<b>Page</b>
2.5.2.4 Thermal unfolding assay using circular dichroism (CD) .....	50
2.5.2.5 Thermal unfolding assay using fluorescence spectroscopy .....	51
2.5.2.6 Binding studies using fluorescence quenching.....	51
2.5.2.7 Thermodynamic parameters and binding assay using fluorescence quenching .....	52
2.5.2.8 Cloning and expression of OM-expressed <i>VhChiP</i> .....	52
2.5.2.9 Inclusion body expression of SeMet-labelled <i>VhChiP</i> and <i>in vitro</i> folding.....	53
2.5.2.10 Crystallisation and structure solution of <i>VhChiP</i> .....	54
2.5.2.11 Single channel electrophysiology of <i>VhChiP</i> .....	55
2.5.2.12 Liposome swelling experiments .....	56
<b>III RESULTS.....</b>	<b>58</b>
Part I: Outer membrane protein ( <i>BpsOmp38</i> ) from <i>Burkholderia pseudomallei</i> .....	58
3.1 Functional and mutational effects of Tyr119 <i>BpsOmp38</i> .....	58
3.1.1 Antimicrobial susceptibility of <i>Burkholderia pseudomallei</i> .....	58

## CONTENTS (Continued)

	<b>Page</b>
3.1.2 Recombinant expression, purification and protein identification of <i>BpsOmp38</i> .....	62
3.1.3 Effects of Tyr119 mutations on antimicrobial properties .....	69
3.1.4 Effects of Tyr119 mutations on the pore conductance of the <i>BpsOmp38</i> channel .....	71
3.1.5 Effects of Tyr119 mutation of sugar and antibiotic permeability of <i>BpsOmp38</i> .....	75
3.2 Structure, thermal stability and thermodynamic parameters of outer membrane protein ( <i>BpsOmp38</i> ) from <i>Burkholderia pseudomallei</i> .....	78
3.2.1 X-ray crystal structure of <i>BpsOmp38</i> .....	78
3.2.2 Thermal unfolding using circular dichroism (CD) .....	82
3.2.3 Thermal unfolding using fluorescence .....	84
3.2.4 Binding studies using fluorescence quenching .....	86
3.2.5 Thermodynamic parameters and the binding energy determined by fluorescence spectroscopy .....	89
3.2.6 Permeation of antibiotics through <i>BpsOmp38</i> studied by black lipid membrane (BLM) technique.....	96

## CONTENTS (Continued)

	<b>Page</b>
Part II: Chitoporin ( <i>VhChiP</i> ) from <i>Vibrio harveyi</i> .....	100
3.3 Thermal stability and thermodynamic parameters of mutation effects of Trp136 of outer membrane protein ( <i>VhChiP</i> ) from <i>Vibrio harveyi</i> .....	100
3.3.1 Model of <i>VhChiP</i> .....	100
3.3.2 Recombinant expression and purification of <i>VhChiP</i> variants .....	101
3.3.3 Thermal unfolding study using circular dichroism (CD).....	104
3.3.4 Thermal unfolding studies using fluorescence .....	106
3.3.5 Estimation of binding energies using fluorescence quenching.....	110
3.4 Structure and functional properties of chitoporin ( <i>VhChiP</i> ) from <i>Vibrio harveyi</i> .....	123
3.4.1 Expression, purification and crystallisation of <i>VhChiP</i> .....	123
3.4.2 <i>VhChiP</i> forms trimers with <i>N</i> -terminally plugged pores .....	126
3.4.3 Roles of the <i>N</i> -terminal plugs in ion and sugar transport through <i>VhChiP</i> .....	129

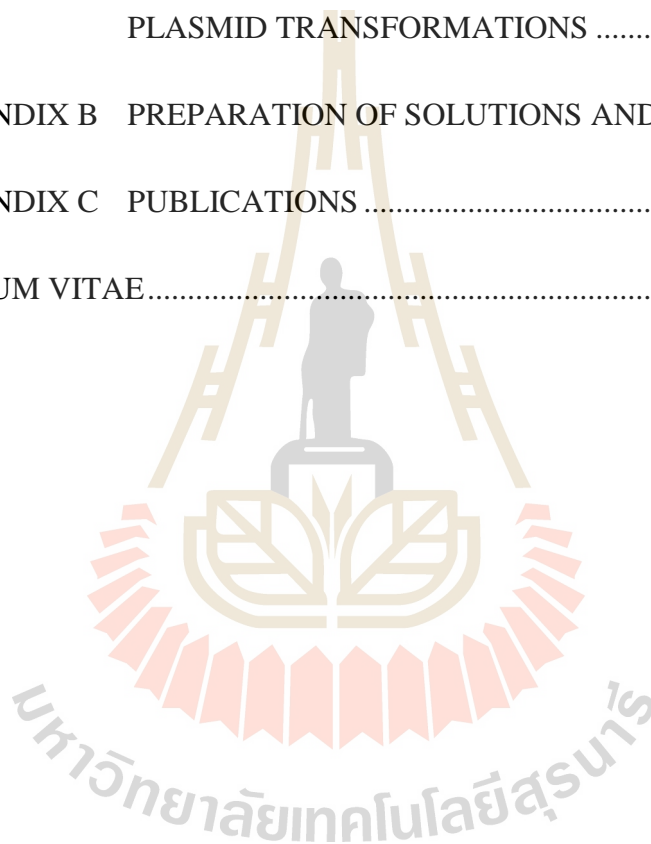


## CONTENTS (Continued)

	<b>Page</b>
3.4.4 Chitohexaose binding to <i>in vitro</i> folded <i>VhChiP</i> .....	131
3.4.5 Chitotetraose binding to natively-expressed <i>VhChiP</i> .....	134
3.4.6 Effect of the <i>N</i> -terminus on substrate binding and transport ....	135
<b>IV DISCUSSION.....</b>	<b>140</b>
Part I: Outer membrane protein ( <i>BpsOmp38</i> ) from <i>Burkholderia</i>	
<i>pseudomallei</i> .....	140
4.1 Functional properties and mutation effects of Tyr119 of <i>BpsOmp38</i> ..	140
4.2 Structure, thermal stability and thermodynamic parameters of outer	
membrane protein ( <i>BpsOmp38</i> ) from <i>Burkholderia pseudomallei</i> .....	145
Part II: Chitoporin ( <i>VhChiP</i> ) from <i>Vibrio harveyi</i> .....	152
4.3 Mutation effects of Trp136 on binding affinity and thermostability of	
<i>VhChiP</i> .....	152
4.4 Structure and functional properties of outer membrane protein ( <i>VhChiP</i> )	
from <i>Vibrio harveyi</i> .....	155
<b>V CONCLUSION .....</b>	<b>159</b>
<b>REFERENCES .....</b>	<b>161</b>

**CONTENTS (Continued)**

	<b>Page</b>
APPENDICES	
APPENDIX A COMPETENT CELL PREPARATIONS AND PLASMID TRANSFORMATIONS .....	183
APPENDIX B PREPARATION OF SOLUTIONS AND REAGENTS.....	185
APPENDIX C PUBLICATIONS .....	192
CURRICULUM VITAE.....	193



## LIST OF TABLES

Table		Page
2.1	Bacterium strain, the plasmids and the recombinant plasmids. ....	30
3.1	Antibiotic susceptibility of a clinically derived strain of <i>Burkholderia pseudomallei</i> . ....	59
3.2	Statistical analysis of MIC values of <i>Burkholderia pseudomallei</i> by one-way ANOVA and log <sub>2</sub> dilution methods. ....	61
3.3	Identification of tryptic peptides by nano LC/ESIMS. ....	68
3.4	Antimicrobial susceptibility of Omp-deficient <i>E. coli</i> expressing <i>BpsOmp38</i> variants. ....	70
3.5	Structural data and refinement statistics. ....	79
3.6	Thermal unfolding of <i>BpsOmp38</i> with the antibiotics. ....	86
3.7	The stability constants of binding determined by fluorescence spectroscopy. ....	89
3.8	Thermal unfolding of <i>VhChiP</i> with the substrate. ....	110
3.9	The binding constants estimated from fluorescence spectroscopy. ....	116
3.10	Structural data and refinement statistics. ....	125
3.11	The equilibrium binding constants <i>K</i> obtained by titrating 0 – 5 μM of chitohexaose on single channel of the three <i>VhChiP</i> variants. ....	138

## LIST OF FIGURES

Figure		Page
1.1	A segment of cell envelope of Gram-negative bacteria.....	2
1.2	Classes of membrane proteins.....	3
1.3	The 3D structure of general diffusion porin.....	6
1.4	The 3D structure of substrate-specific porins .....	7
1.5	Cross-section of maltoporin monomer.....	8
1.6	A) Milky seas, or mareel, is a condition on the ocean. B) <i>Vibriosis</i> due to shrimp swimming at the surface of the pond. ....	10
1.7	Model of the chitin degradation cascade of the marine bacterium <i>Vibrio harveyi</i> .....	11
1.8	Gram-stain of <i>B. pseudomallei</i> isolate VB976100.....	12
1.9	The symptoms of melioidosis .....	13
1.10	Mechanisms of antibiotic resistance .....	15
1.11	Multidrug resistance mechanisms associated with porin modification ....	16
1.12	Liposome-swelling assays of refolded Omp38.....	19
1.13	Kinetic analysis of antimicrobial agent translocation through <i>BpsOmp38</i> .....	21
1.14	Effect of chitooligosaccharides on chitoporin ion currents .....	22
1.15	Liposome swelling assays .....	23

## LIST OF FIGURES (Continued)

Figure		Page
1.16	The effect of transmembrane potentials at various concentrations of chitohexaose on the single channel conductance of trimeric <i>VhChiP</i> (WT) and its mutants .....	25
3.1	Agarose gel electrophoresis of recombinant DNA and SDS-PAGE of <i>BpsOmp38</i> protein .....	63
3.2	SDS-PAGE of cell non-induction and cell induction by 0.5% IPTG .....	64
3.3	A ribbon representation of the homology model of <i>BpsOmp38</i> .....	65
3.4	Purification, immunodetection, and mass analysis of the <i>BpsOmp38</i> variants, expressed in <i>E. coli</i> . (A) .....	67
3.5	Ion current recordings obtained by the black lipid membrane (BLM) reconstitution technique .....	73
3.6	Single channel recordings of <i>BpsOmp38</i> porin in artificial lipid membrane.....	74
3.7	Swelling of <i>BpsOmp38</i> -containing proteoliposomes, induced by neutral sugars .....	76
3.8	Swelling of <i>BpsOmp38</i> proteoliposomes induced by cephalosporins and carbapenems .....	77
3.9	Purification and crystallisation of <i>BpsOmp38</i> .....	79
3.10	X-ray crystal structure of <i>BpsOmp38</i> .....	81
3.11	CD spectra and thermal unfolding curves of <i>BpsOmp38</i> .....	83

## LIST OF FIGURES (Continued)

Figure		Page
3.12	Fluorescence spectra and thermal unfolding curves of <i>Bps</i> Omp38.....	85
3.13	Tryptophan quenching fluorescence spectra of <i>Bps</i> Omp38-antibiotic interactions .....	87
3.14	Binding curves of <i>Bps</i> Omp38 with antibiotics .....	88
3.15	Tryptophan quenching fluorescence spectra of <i>Bps</i> Omp38-ceftazidime interactions .....	90
3.16	Tryptophan quenching fluorescence spectra of <i>Bps</i> Omp38-cefoxitin interactions .....	91
3.17	Tryptophan quenching fluorescence spectra of <i>Bps</i> Omp38-meropenem interactions .....	92
3.18	Tryptophan quenching fluorescence spectra of <i>Bps</i> Omp38-doripenem interactions .....	93
3.19	Plots of thermodynamic parameters of <i>Bps</i> Omp38-antibiotics interactions obtained by fluorescence quenching technique.....	94
3.20	Thermodynamic parameters of <i>Bps</i> Omp38-antibiotic interactions determined by fluorescence quenching technique .....	95
3.21	The BLM traces of ion conductance through the single trimeric <i>Bps</i> Omp38 channel reconstituted into planar lipid membranes in the presence of sensitive drugs .....	97
3.22	Binding curve plots of <i>Bps</i> Omp38-antibiotics interactions .....	98

## LIST OF FIGURES (Continued)

Figure	Page
3.23	The BLM traces of ion conductance through single trimeric <i>BpsOmp38</i> channels reconstituted into planar lipid membranes in the absence and presence of resistance drugs of <i>B. pseudomallei</i> .....99
3.24	Homology model of <i>VhChiP</i> (A) the monomeric <i>VhChiP</i> (WT) from <i>Vibrio harveyi</i> and mutants ..... 101
3.25	Protein expression, purification and immuno-blotting analysis of WT and its mutants ..... 103
3.26	CD spectra and thermal unfolding curves of the WT and mutants ..... 105
3.27	Amino acid sequence and a cross-section of the modelling structure of <i>V. harveyi</i> monomeric chitoporin ..... 107
3.28	Fluorescence spectra and thermal unfolding curves of the WT and mutants ..... 108
3.29	Tryptophan fluorescence quenching spectra of <i>VhChiP</i> WT ..... 112
3.30	Tryptophan fluorescence quenching spectra of <i>VhChiP</i> W136F ..... 113
3.31	Tryptophan fluorescence quenching spectra of <i>VhChiP</i> W136A ..... 114
3.32	Binding curve plots of WT and its mutants with chitooligosaccharides ..... 115
3.33	Comparison of protein-chitooligosaccharide binding constants ..... 116
3.34	Tryptophan fluorescence quenching spectra of <i>VhChiP</i> WT ..... 119
3.35	Tryptophan fluorescence quenching spectra of <i>VhChiP</i> W136F ..... 120

## LIST OF FIGURES (Continued)

Figure		Page
3.36	Tryptophan fluorescence quenching spectra of <i>VhChiP</i> W136A .....	121
3.37	Thermodynamic parameter plots of <i>VhChiP</i> - chitohexaose interaction assayed by the fluorescence quenching technique .....	122
3.38	X-ray crystal structure of <i>in vitro</i> folded <i>VhChiP</i> .....	126
3.39	Outer membrane expressed <i>VhChiP</i> .....	128
3.40	Single channel electrophysiology of <i>VhChiP</i> .....	130
3.41	Chitohexaose binding to <i>VhChiP</i> .....	132
3.42	Alignment of <i>VhChiP</i> orthologs from <i>Vibrio</i> species .....	133
3.43	Chitotetraose binding to natively-expressed <i>VhChiP</i> .....	135
3.44	Substrate binding to <i>VhChiP</i> probed by single-channel electrophysiology .....	137
3.45	Importance of the <i>N</i> -terminus for substrate transport.....	139
4.1	Structural comparison of OmpF and <i>BpsOmp38</i> .....	146
4.2	Comparison of sugar binding in LamB and <i>VhChiP</i> .....	158



## LIST OF ABBREVIATIONS

A/D	Analog-to-digital
BCA	Bicinchoninic acid
BLM	Black lipid membrane
<i>BpsOmp38</i>	<i>Burkholderia pseudomallei</i> outer membrane protein 38
BSA	Bovine serum albumin
<i>BthOmp38</i>	<i>Burkholderia thailandensis</i> outer membrane protein 38
CD	Circular dichroism
cDNA	Complementary DNA
ChiP	Chitoporin
DNA	Deoxyribonucleic acid
DPhPC	Diphytanoyl-phosphatidylcholine
ECL	Enhanced chemiluminescence
EDTA	Ethylenediaminetetraacetic
ESI	Electrospray ionisation
FL	Fluorescence
FPLC	Fast protein liquid chromatography
<i>G</i>	Conductance
GlcNAc	<i>N</i> -acetyl-glucosamine
(GlcNAc) <sub>2</sub>	Chitobiose
(GlcNAc) <sub>3</sub>	Chitotriose

**LIST OF ABBREVIATIONS (Continued)**

(GlcNAc) <sub>4</sub>	Chitotetraose
(GlcNAc) <sub>5</sub>	Chitopentaose
(GlcNAc) <sub>6</sub>	Chitohexaose
HRP	Horseradish peroxidase
<i>I</i>	Current
<i>I<sub>m</sub></i>	Membrane current
IPTG	Isopropyl- $\beta$ -D-thiogalactopyranoside
<i>K</i>	Binding constant
kbp	kilobase-pair
KCl	Potassium chloride
<i>K<sub>d</sub></i>	Dissociation constant
LamB	Maltose-specific porin
LB	Luria-Bertani
LC	Liquid chromatography
LDAO	Lauryldimethylamine-oxide
MR	Molecular replacement
MS	Mass spectrometry
Octyl-POE	<i>n</i> -Octylpolyoxyethylene
OH	hydroxyl
OM	Outer membrane
Omp	Outer membrane proteins

**LIST OF ABBREVIATIONS (Continued)**

OmpF	Outer membrane protein F
OmpN	Outer membrane protein N
OprB	Carbohydrate-selective porin <i>Pseudomonas aeruginosa</i>
PB	Phosphate buffer
PBS	Phosphate buffered saline
PCR	Polymerase chain reaction
PDB	Protein data bank
<i>Pst</i>	<i>Providencia stuartii</i>
r.m.s.d	Root-mean-square deviation
rpm	Revolutions per minute
SAD	Single-wavelength anomalous diffraction
ScrY	Sucrose-specific porin
SDS	Sodium dodecyl sulphate
SDS-PAGE	Polyacrylamide gel electrophoresis
SeMet	Selenomethionine
TBS	Tris-buffered saline
$T_m$	Midpoint temperature of thermal unfolding
U/L	Units per litre
$V$	Potential
VhChiP	<i>Vibrio harveyi</i> chitoporin
WT	Wild-type

**LIST OF ABBREVIATIONS (Continued)**

$\Delta G$	Gibbs free energy
$\Delta H$	Enthalpy change
$\Delta S$	Entropy change



# CHAPTER I

## INTRODUCTION

### 1.1 Gram-negative bacteria and their outer membrane proteins

#### 1.1.1 Gram-negative bacteria

Bacteria are tiny single-cell and widespread microorganisms that, in contrast to eukaryotic cells, do not have a membrane-bound nucleus or other membrane-surrounded intracellular organelles like mitochondria and endoplasmic reticulum (Adl *et al.*, 2005). In general, bacteria can be classified into Gram-positive and Gram-negative, depending on the structural components of their outer membrane layers. For Gram-positive bacteria, their plasma membrane is covered with a thick wall of peptidoglycan. In contrast, the cell envelope of Gram-negative bacteria is composed of two membranes enclosing the peptidoglycan-containing periplasm (Figure 1.1).

The outer membrane of Gram-negative bacteria is an asymmetrical bilayer containing phospholipids and lipopolysaccharides. The lipopolysaccharide molecules can be found exclusively in the outer leaflet of the outer membrane (Huijbregts *et al.*, 2000). They are composed of: i) lipid A which forms the hydrophobic membrane anchor; ii) the core region, which consists of a phosphorylated non-repeating oligosaccharide that is linked to lipid A; and iii) the O-antigen, which contains repeating oligosaccharides. Some Gram-negative bacteria lack the O-antigen (Raetz and Whitfield, 2002), and therefore their lipopolysaccharides are more rough. Like the inner membrane, the periplasmic leaflet of the outer membrane contains phospholipids that

consist of a glycerol backbone with two esterified fatty acid chains and a phosphate containing head group (Huijbregts *et al.*, 2000).

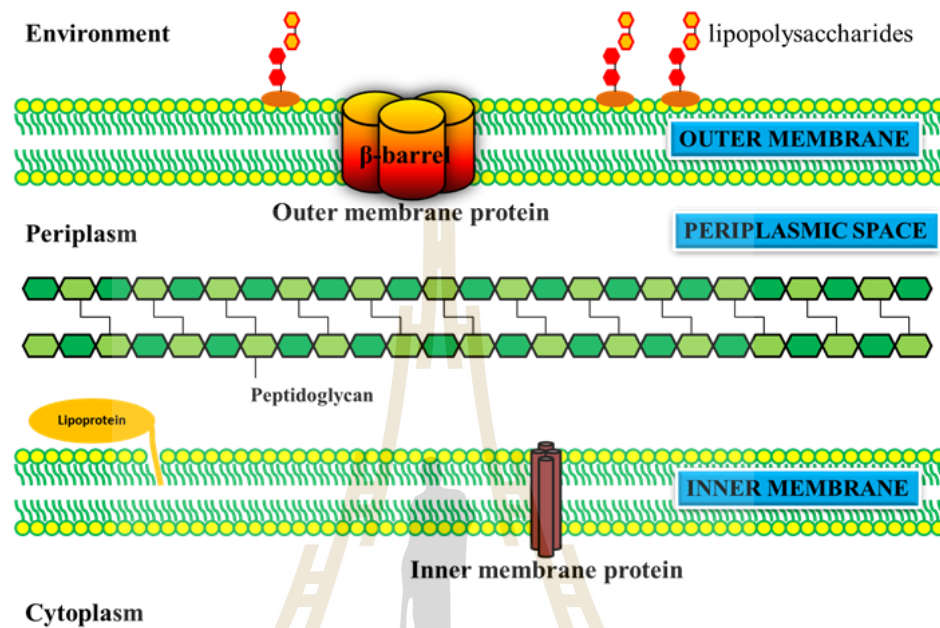


**Figure 1.1** A segment of cell envelope of Gram-negative bacteria composed of inner membrane and outer membrane enclosing the peptidoglycan (Huijbregts *et al.*, 2000).

Both outer and inner membranes include proteins that are inserted or anchored in the lipid bilayers. These proteins are synthesised in the cytoplasm and are guided towards the cell envelope, where many of them have to cross at least the inner membrane. After direction to their designated locations, these proteins fulfil various biological functions. For example, lipoproteins are acylated and anchored in the inner membrane or outer membrane via an amino-terminal *N*-acyl-diacylglyceryl-cysteine (Ichihara *et al.*, 1981). The major outer membrane lipoprotein, forms the connection of the outer membrane to the peptidoglycan layer via a peptide (Braun and Rehn, 1969;

Braun and Wolff, 1970). Integral membrane proteins are inserted into the lipid bilayer with unique structural arrangements. Inner membrane proteins are usually composed of  $\alpha$ -helices, while outer membrane proteins are usually composed of  $\beta$ -strands, forming a cylindrical or barrel structure of either one or three units. These barrels are referred to as porins (Nikaido and Vaara, 1985; Wimley, 2003).

### 1.1.2 Classification of outer membrane proteins

Membrane proteins are divided into five classes (Evans and Graham, 1989) as shown in Figure 1.2.

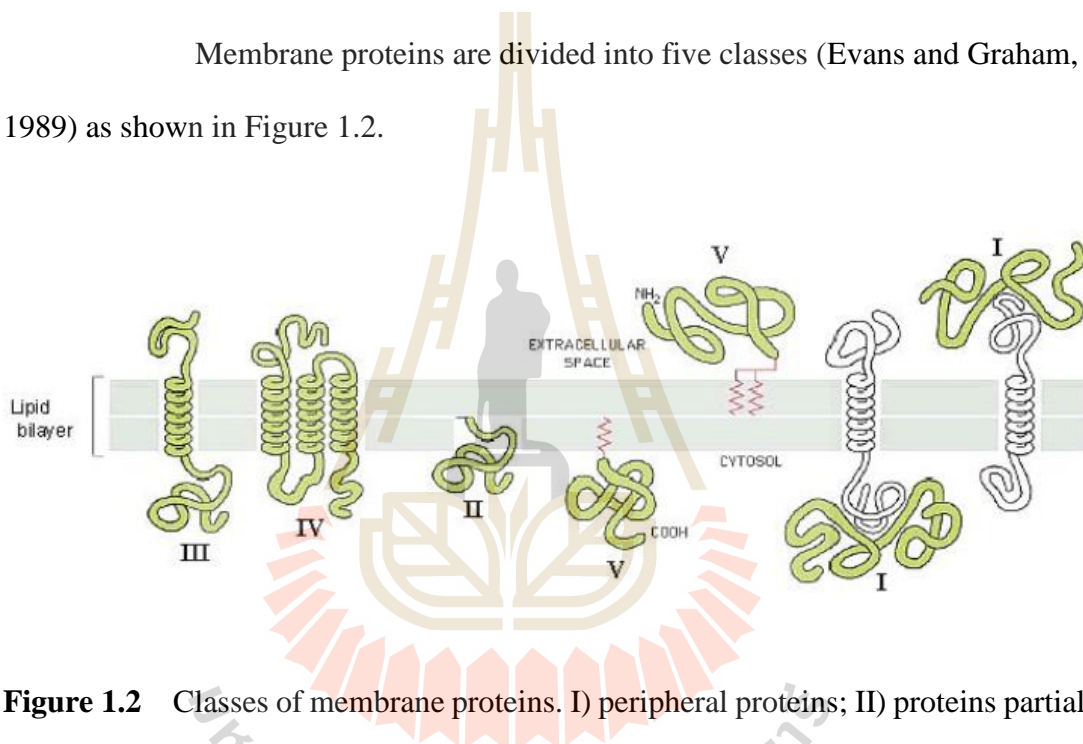


**Figure 1.2** Classes of membrane proteins. I) peripheral proteins; II) proteins partially inserted into lipid bilayer; III) integral proteins with one transmembrane domain; IV) integral proteins with multiple transmembrane domains; V) lipid-anchored peripheral proteins (Evans and Graham, 1989).

**Class I:** Peripheral or extrinsic proteins are bound mainly by ionic force to polar head groups of phospholipids or to other proteins. Example of class I protein is F<sub>1</sub> subunit of the ATP-synthase and cytochrome *c*.

**Class II:** Membrane proteins are anchored into a part of lipid bilayer by a hydrophobic peptide. These proteins may be inserted partially into the extracellular face of the membrane.

**Classes III and IV:** These classes are integral or transmembrane proteins, which contain polar amino acid sequences located at the external and cytoplasmic lesion of the membrane. They usually interact with phospholipid head groups in the extracellular and intracellular environments.

**Class V:** These peripheral proteins contain at least a domain which is anchored to the lipid bilayers by covalently attaching to glycolipids. Plasma membrane receptors of protozoa and mammalian cells are members of this class. Proteins anchored by a fatty acid via a thio-ester bond are also included in this class (Evans and Graham, 1989).

### 1.1.3 Classification of integral or transmembrane proteins (porins)

The outer membrane proteins of Gram-negative bacteria are peripheral to the periplasmic and peptidoglycan regions. These proteins are classified in classes III and IV (Evans and Graham, 1989) as shown in Figure 1.2. The proteins in these two classes are divided into three sub-groups, which are i) non-porin transporters, ii) general-diffusion porins, and iii) substrate-specific porins (Nikaido, 2003). In this context, only the last two sub-groups are described.

#### 1.1.3.1 General diffusion porins

All currently known outer membrane proteins with  $\beta$ -sheet secondary structure in the transmembrane region and no transmembrane helices facing the lipid bilayer are referred to “porins” (Schulz, 2002). The transmembrane strands of outer membrane porins are connected by short periplasmic  $\beta$ -turns and by long loops facing the polysaccharide region and the space outside the cell. The geometry of the  $\beta$ -



strands are arranged in the barrel structures, in which neighbouring strands are connected with each other by hydrogen bonds. The outer membrane proteins of bacteria of known crystal structures form transmembrane  $\beta$ -barrels with even numbers of  $\beta$ -strands ranging from 8 to 22 (Schulz, 2002).

*E. coli* express two major general diffusion porins, OmpF and OmpC. (Nikaido, 2003; Nikaido and Rosenberg, 1983). *E. coli* OmpF (Figures 1.3) is considered as a non-specific pore for the diffusion of small polar molecules across the hydrophobic insulating bilayer structure of the outer membrane. Spherical species with a molecular weight up to 600 Da can pass through the OmpF pores and enter the bacterial cytoplasm. The transported molecules include small ions (e.g.  $K^+$ ,  $Na^+$ ,  $Ca^{2+}$ ,  $Cl^-$  etc.), glucose, ascorbate, amino acids and other nutrients as well as metabolic waste products (Berkane *et al.*, 2005; Cowan *et al.*, 1995; Prashant S. Phale *et al.*, 2001). OmpF is the first integral membrane protein for which crystals were obtained at resolution less than 4 Å (Garavito and Rosenbusch, 1980). OmpF and OmpC are found as trimers that are held together by hydrophobic interactions between the barrel surfaces and the loop L2. Each of the L2 loops in the trimer reaches into the adjacent monomer forming a conserved salt bridge between L2's glutamic acid and an arginine inside the barrel (Baslé *et al.*, 2006; Cowan *et al.*, 1992; Prashant S Phale *et al.*, 1998). Each monomer in the *E. coli* OmpF and OmpC trimer consists of a  $\beta$ -barrel made up of 16  $\beta$ -strands (Cowan *et al.*, 1992), which define an aqueous channel that spans the outer membrane, with eight extended loops L1 – L8 on the extracellular side of the barrel monomer, and eight tight turns on the periplasmic side. The stave of the barrel surrounding a water-filled pore has a narrow elliptically shaped ( $7 \times 11$  Å) selectivity

filter with a solvent accessible area of 30-40 Å<sup>2</sup> (Cowan *et al.*, 1992; Varma *et al.*, 2006).

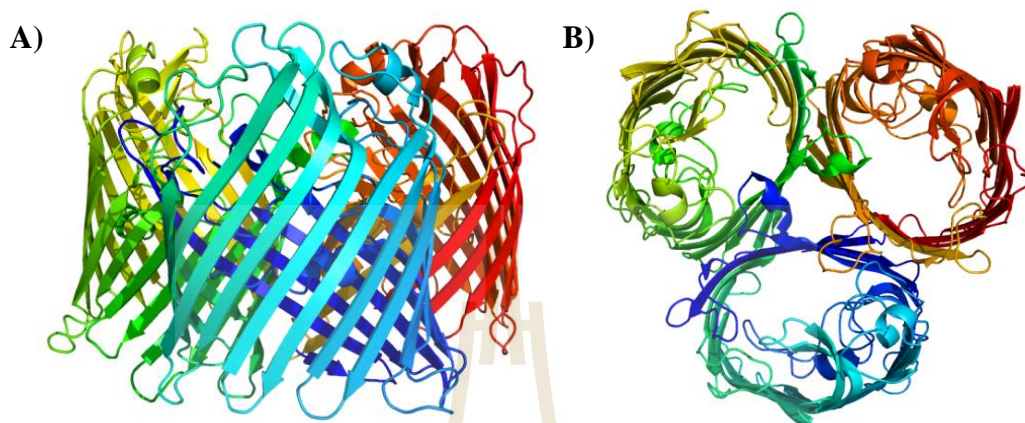


**Figure 1.3** The 3D structure of general diffusion porin OmpF (A) Side view structure of the trimer. (B) Top view structure (PDB code, 4JFB).

### 1.1.3.2 Substrate-specific porins

Maltoporin (also called LamB) is the best characterised substrate-specific porin from *E. coli* (Szmecman and Hofnung, 1975). Maltoporin is expressed as part of the mal regulon upon induction by maltose or maltodextrins (Szmecman and Hofnung, 1975; Szmecman *et al.*, 1976) and serves as the receptor for bacteriophage lambda (Randall-Hazelbauer and Schwartz, 1973). Liposome swelling assays showed that maltoporin had high permeation rate for maltose and maltodextrins, whereas uptake of sucrose was hardly detectable (Hardesty *et al.*, 1991; Luckey and Nikaido, 1980). Nevertheless, both maltose and sucrose exhibit similar binding affinities ( $K = 10$  mM for maltose and  $K = 6 - 15$  mM for sucrose) to the maltoporin channel as determined by inhibition of ion flow in planar lipid bilayers (Andersen *et al.*, 1995; Schülein *et al.*, 1991). The crystal structures of the apo form of

maltoporin (Schirmer *et al.*, 1995) and of several maltoporin-sugar complexes are shown in Figure 1.4 (Dutzler *et al.*, 1996; Wang *et al.*, 1997).

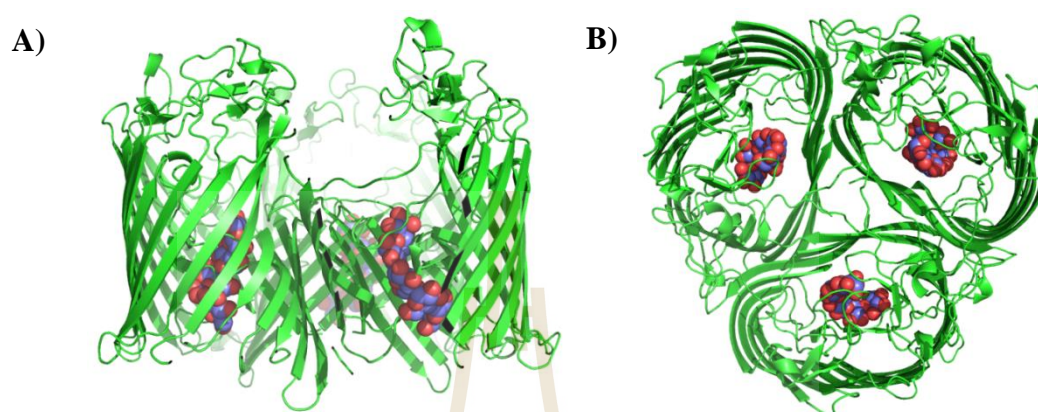


**Figure 1.4** The 3D structure of substrate-specific porins (A) Side view structure of LamB trimer (PDB code, 3NSG). (B) Top view structure of maltooligosaccharides bound to maltoporin (PDB code, 1MPM).

In general, the maltoporin monomer comprises an 18 stranded  $\beta$ -barrel with short turns at the periplasmic side and large irregular loops at the extracellular side. Loops L1 and L6 are located inside the channel. The third loop, L3, folds inside the  $\beta$ -barrel, thereby forming a constriction at the middle of the channel. An elongated non-polar patch, composed of several aromatic residues, extends from the extracellular entrance to the periplasmic exit. Maltodextrins (Dutzler *et al.*, 1996) and the glucosyl units of sucrose (Wang *et al.*, 1997) were found to make hydrophobic interactions with such residues that are part of the greasy slide. Additionally, the sugar hydroxyls interact with several ionic residues, which are not part of the greasy slide but located nearby (Dumas *et al.*, 2000). While maltodextrins bind to the middle of the channel, sucrose appears to be stuck above the channel constriction owing to its bulky

fructosyl residue. This observation explains how sucrose inhibits ion flow, but does not permeate. The crystal structure of LamB shows a sequence of aromatic residues including Trp74, Tyr41, Tyr6, Trp420, Trp358, Phe227 lining inside the channel along a left-handed helical path. This stretch of aromatic residues was named the “greasy slide” and actually is believed to be the structural element responsible for substrate binding and specificity as shown in Figure 1.5. A chain of polar residues (namely, Arg8, Arg33, Glu43, Arg82, Arg109, Asp111, Asp116), the so called polar track, is also situated around the constriction site and plays an important role in maltose and maltodextrin translocation (Ranquin and Van Gelder, 2004).

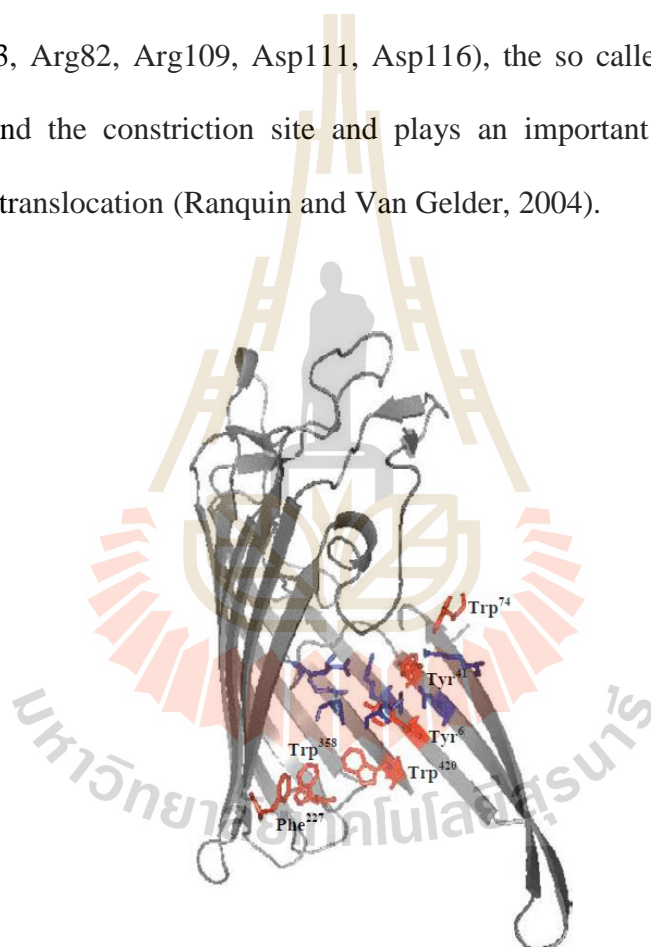


**Figure 1.5** Cross-section of maltoporin monomer. The greasy slide residues are shown in red with the following sequence: Trp74 (at the top), Tyr41, Tyr6, Trp420, Trp358 and Phe227. The polar tracks are shown in blue, comprising the residues: Arg8, Arg33, Glu43, Arg82, Arg109, Asp111, and Asp116 (Ranquin and Van Gelder, 2004).

A sucrose-specific porin (ScrY) from *Salmonella typhimurium*, is the subsequently identified sugar-specific porin. It was found as part of a plasmid encoded regulon, and was homologous to maltoporin (Hardesty *et al.*, 1991; Schmid *et al.*, 1988). Cells containing this plasmid are able to utilise sucrose as the sole carbon source (Hardesty *et al.*, 1991; Schmid *et al.*, 1991). ScrY reconstituted into vesicles showed a high permeation rate for sucrose, but no permeation for maltose (Hardesty *et al.*, 1991). *In vivo* study using <sup>14</sup>C-labelled maltopentaose showed that this radioactively-labelled compound was taken up slowly by cells expressing only ScrY (Schülein *et al.*, 1995), whereas higher ScrY growth was observed when the cells were grown on maltotetraose (Schmid *et al.*, 1991). The crystal structure of ScrY had been elucidated by Forst *et al.* (1998). Although its sequence identity is only 20% to maltoporin, their trimeric structures are highly similar. In particular, the greasy slide and other residues of the channel lining are largely conserved. There are, however, three substitutions at the pore constriction residues: R109, Y118, and D121 in maltoporin were found as N192, D201 and F204 in ScrY. These residues were shown to interact with their respective substrates in both maltoporin and ScrY (Dutzler *et al.*, 1996; Forst *et al.*, 1998).

## 1.2 *Vibrio harveyi* and *Burkholderia pseudomallei*

### 1.2.1 *Vibrio harveyi*

*Vibrio harveyi* (*V. harveyi*) is a Gram-negative, bioluminescent (Figure 1.6A), marine bacterium in the genus *Vibrio*. *V. harveyi* is rod-shaped, motile, facultatively anaerobic, halophilic, and competent for both fermentative and respiratory metabolism (Owens and Busico-Salcedo, 2006). *V. harveyi* is a pathogen that infects

sharks, seabass, seahorses, lobsters and shrimps, causing eye-lesions, gastro-enteritis, vasculitis, and luminous *Vibriosis* (Figure 1.6B). Especially, luminous *Vibriosis* is a leading cause of death among commercially farmed shrimp and other aquaculture and a subject of economic loss world-wide (Lightner, 1993).

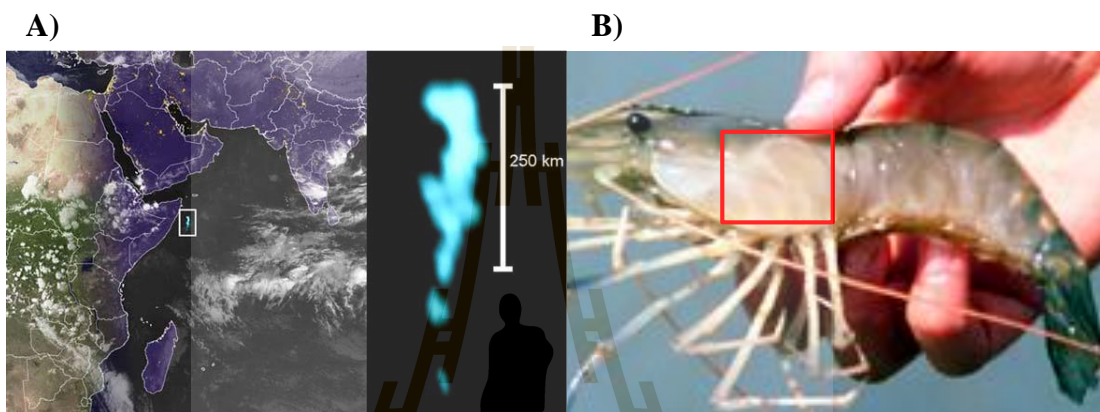


**Figure 1.6** A) Milky seas, or mareel, is a condition on the ocean where large areas of seawater (up to 6,000 sq mi or 16,000 km<sup>2</sup>) appear to glow brilliantly enough at night to be seen by satellites orbiting Earth. B) *Vibriosis* is also known as Sea Gull Syndrome due to shrimp swimming at the surface of the pond.

*V. harveyi* is mainly responsible for the rapid turnover of chitin biomass in open oceans, as they can efficiently utilise chitin as their sole source of cellular energy. The energy production in *V. harveyi* follows the pathway of chitin catabolism as shown in Figure 1.7. The initial steps in this pathway involves chitin attachment and degradation, generating chitooligosaccharides which are taken up through the bacterial cell wall, and finally catabolism of the transport products as carbon and nitrogen sources (Bassler *et al.*, 1991; Hunt *et al.*, 2008; Jung *et al.*, 2008). After chitin fragments

are transported through the outer membrane by chitoporin, further enzymatic degradation takes place in the periplasm, producing GlcNAc and (GlcNAc)<sub>2</sub>. Binding of (GlcNAc)<sub>2</sub> to CBD activates the ChiS sensor, producing transcription of the genes under control of the (GlcNAc)<sub>2</sub> catabolic operon. GlcNAc is translocated to the cytoplasm by the GlcNAc PTS system, while (GlcNAc)<sub>2</sub> is transported through the inner membrane by the (GlcNAc)<sub>2</sub> ABC permease. Both products are phosphorylated, and finally converted to Fructose- 6-P, acetate and NH<sub>3</sub>.

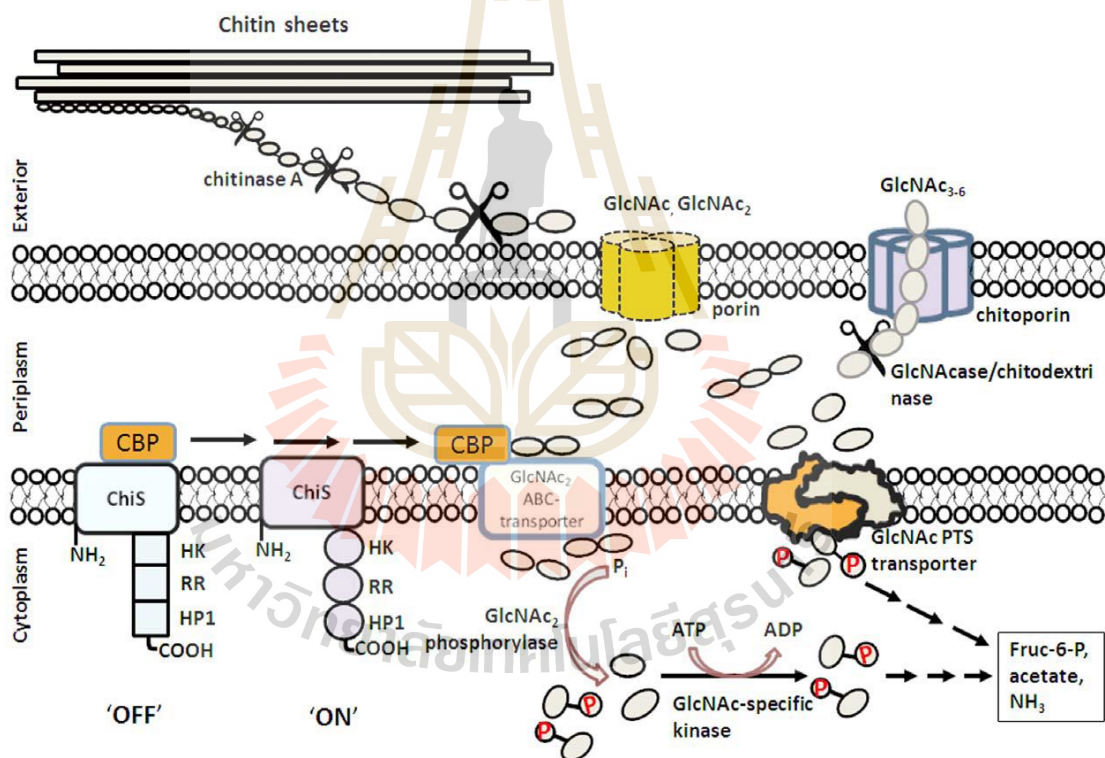


**Figure 1.7** Model of the chitin degradation cascade of the marine bacterium *Vibrio harveyi*. The model was reconstructed from the chitinolytic cascade proposed by Li and Roseman (2004) and modified by Suginta *et al.* (2013a).

### 1.2.2 *Burkholderia pseudomallei*

*Burkholderia pseudomallei* (*B. pseudomallei* or *Bps*) is a soil-dwelling Gram-negative bacterium (Figure 1.8), commonly found in Southeast Asia and Northern Australia. *Bps* causes melioidosis, a potentially fatal disease in humans and other animals, including dolphins, sheep, pigs and goats (Currie *et al.*, 1994; Dance, 1991; Vedros *et al.*, 1988).

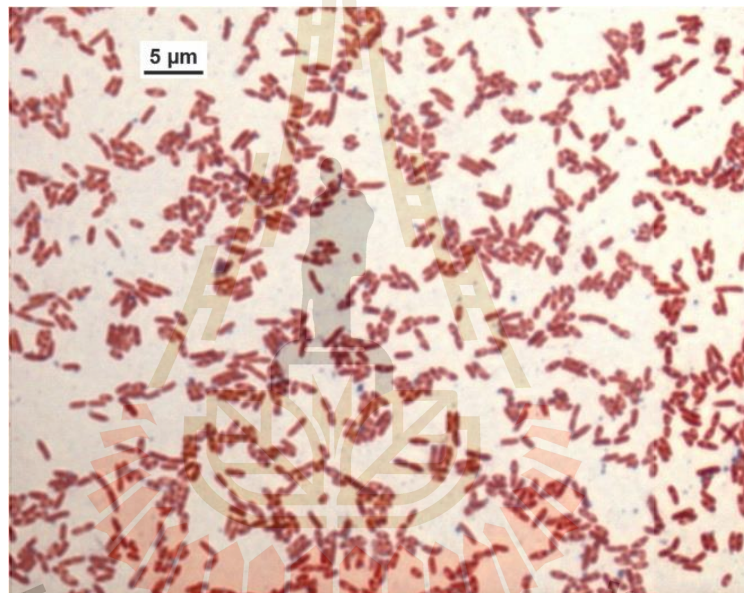


**Figure 1.8** Gram-stain of *B. pseudomallei* isolate VB976100 (Elschner *et al.*, 2014).

Thailand has the highest recorded incidence of melioidosis in the world, with an average 21.3 cases per 100,000 people per year (Limmathurotsakul *et al.*, 2010). Especially, in the north-eastern region, 80% of children are positive for antibodies against *Bps* by the age of 4 (Kanaphun *et al.*, 1993). Patients infected with *B. pseudomallei* usually develop skin ulcers, visceral abscesses, pneumonia, and septicemia that imperatively require immediate antimicrobial treatment to avoid fatal



progression of the disease (Figure 1.9). Very often, antimicrobial treatment is difficult due to high intrinsic resistance that most *B. pseudomallei* strains exhibit towards a broad spectrum of antimicrobial agents, including  $\beta$ -lactam antibiotics, aminoglycosides, macrolides, and cephalosporins (Aldhous, 2005; Cheng and Currie, 2005; Peacock, 2006; Wiersinga *et al.*, 2006).

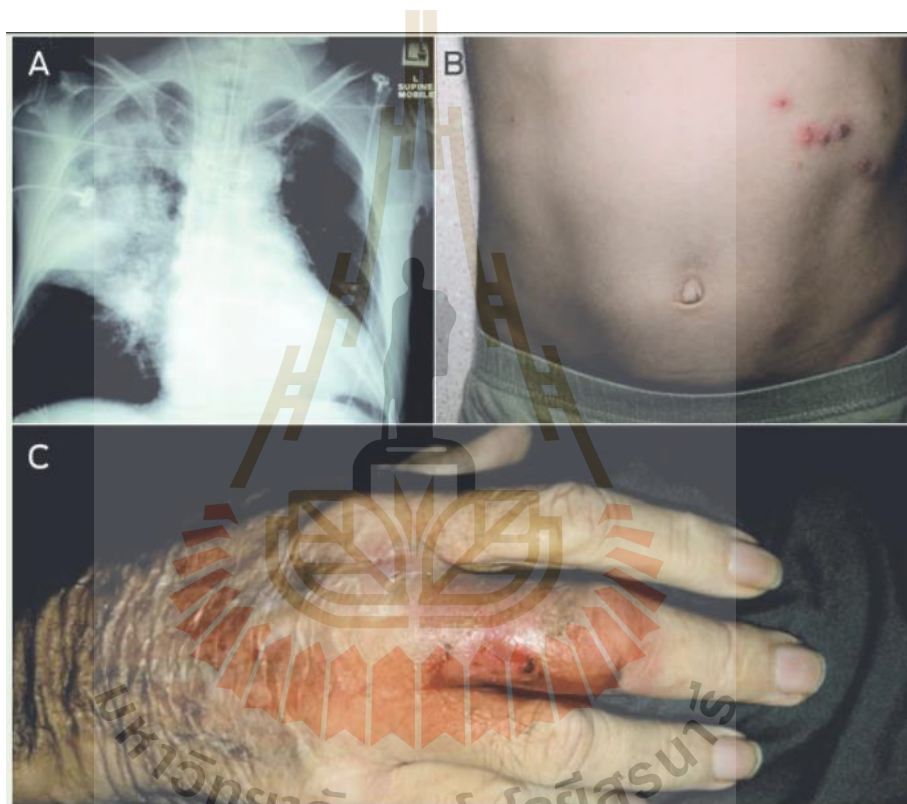


**Figure 1.9** The symptoms of melioidosis. A) Chest X-ray of a melioidosis patient; B) Cutaneous melioidosis; and C) Soft tissue abscess of right middle finger (Parameswaran *et al.*, 2012).

Melioidosis patients are usually treated with a broad-spectrum antibiotic cocktail, including ceftazidime, meropenem, and imipenem. In more severe cases, a combination of cefoperazone and sulbactam may be administered, but the survival rate

is relatively low at 60%. A combination of ceftazidime and cotrimoxazole may help to increase the survival rate to 70 – 75% (Cheng *et al.*, 2004; Chetchotisakd *et al.*, 2001; Simpson *et al.*, 1999; Wuthiekanun and Peacock, 2006). *B. pseudomallei* is regarded as a Tier 1 Select Agent (Woods, 2005) and has been listed by the US Centre for Disease Control and Prevention as a category B health hazard (2012). The severe biosafety concerns associated with *B. pseudomallei* have prompted biomedical research into drug resistance mechanisms during melioidosis infection, the ultimate goal being the development of effective anti-*Bps* agents.

### **1.3 Porins involved in antibiotic resistance of pathogenic bacteria**

Treatment of bacterial infections is increasingly complicated by the ability of bacteria to develop resistance to most antimicrobial agents (Tenover, 2006). Although the manner of acquisition of resistance may vary among bacterial species, resistance is created by a few mechanisms. As shown in Figure 1.10, (1) the membrane barrier limits the intracellular access of antibiotic (Pagès *et al.*, 2008); (2) antibiotic inactivation: direct inactivation of the active antibiotic molecule; (3) target modification: alteration of the sensitivity to the antibiotic by modification of the target; (4) efflux pumps and outer membrane permeability changes: reduction of the concentration of drug without modification of the compound itself; and (5) target bypass: some bacteria become refractory to specific antibiotics by bypassing the inactivation of a given enzyme (Džidić *et al.*, 2008).

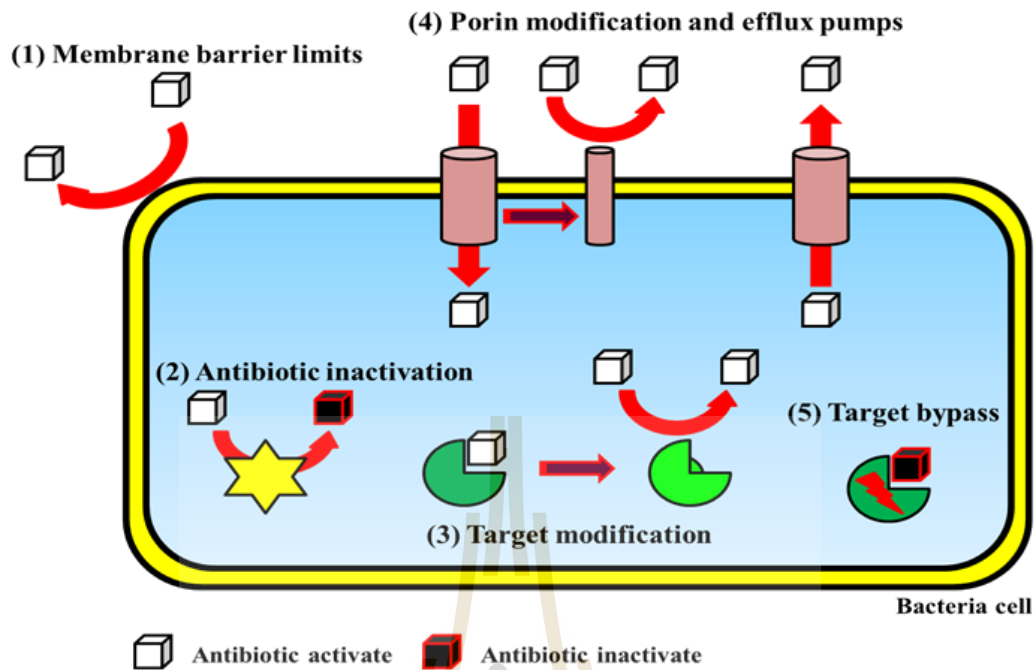


**Figure 1.10** Mechanisms of antibiotic resistance (Tenover, 2006).

The major bacterial strategies have emerged for the development of drug resistance: the enzymatic barrier produces detoxifying enzymes that degrade or modify the antibiotic, and the target protection barrier impairs target recognition and thus antimicrobial activity. These mechanisms can act simultaneously in clinical isolates, generating a high level of resistance. Also, there are two different aspects of the transport systems across the bacterial membrane: influx and efflux, which involve in drug resistance of pathogenic bacteria (Pagès *et al.*, 2008).

As for influx of antibiotics, recent clinical evidence for distinct bacterial strategies of porin modification to limit antibiotic uptake is shown in Figure 1.11. Changes in levels of porin expression and mutation or modification impairs the functional properties of porin channel (Pagès *et al.*, 2008).

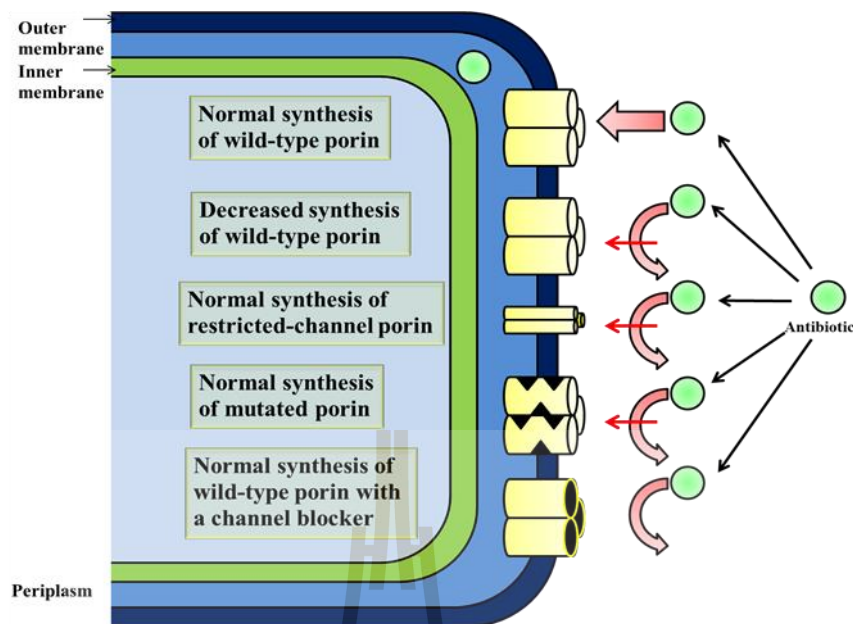


**Figure 1.11** Multidrug resistance mechanisms associated with porin modification (Pagès *et al.*, 2008).

### 1.3.1 Porins involved in membrane susceptibility

Genetic modifications of porins that contribute to membrane permeability have been reported in *Providencia stuartii*. *P. stuartii* is an opportunistic pathogen seen in patients with severe burns or long-term indwelling urinary catheters (Stock and Wiedemann, 1998). In animals, *P. stuartii* infections can cause neonatal diarrhea. In humans, *P. stuartii* can be isolated from urine, stool, and blood, as well as from sputum, skin, and wound cultures. Membrane permeability of *P. stuartii* toward antibiotics takes place through two major outer membrane porins, namely OmpPst1 and OmpPst2. An approach combining microbiology and electrophysiology was used to analyse the selectivity of the *Providencia* porins toward different  $\beta$ -lactams. *P. stuartii* lacking OmpPst porins showed significant decrease of susceptibility to  $\beta$ -lactam antibiotics. Determination of  $\beta$ -lactam translocation through OmpPst1 and

OmpPst2 indicated that the strength of interaction decreased in the order of ertapenem, followed by cefepime and ceftazidime, respectively. Moreover, the translocation of these antibiotics through OmpPst1 was more efficient than through OmpPst2. Heterologous expression of OmpPst1 in the porin-deficient *E. coli* strain BL21 (DE3) omp8 was associated with a higher antibiotic susceptibility of the *E. coli* cells to  $\beta$ -lactams compared with expression of OmpPst2 (Tran *et al.*, 2010).

### 1.3.2 Antibiotic resistance of *B. pseudomallei*

Currently, the antibiotic of choice for melioidosis treatment is a ceftazidime, meropenem, imipenem and ceftazidime-sulbactam combination (Sulperazone) (Cheng *et al.*, 2004; Chetchotisakd *et al.*, 2001; Simpson *et al.*, 1999; Wuthiekanun and Peacock, 2006). While various antibiotics are active *in vitro* (e.g., chloramphenicol, doxycycline, co-trimoxazole), they have been found to be ineffective *in vivo* for the treatment of acute melioidosis (White *et al.*, 1989). The actions of co-trimoxazole and doxycycline are antagonistic, which suggests that these two drugs should not to be used together (Saraya *et al.*, 2009). The organism is also resistant to gentamicin (Trunck *et al.*, 2009) and colistin, and this intrinsic property is used in the identification of the organism (Ashdown, 1979).

Kanamycin is used to kill *B. pseudomallei* in the laboratory, but the concentrations used are much higher than those achievable in humans (Kespichayawattana *et al.*, 2004). The mechanism underlying antimicrobial resistance of *B. pseudomallei* is not clear. The bacterium is thought to be able to pump drugs out of the cell, as well as develop low permeability for the antibiotic to pass into the cell, thus mediating resistance to aminoglycosides, tetracyclines, fluoroquinolones and

macrolides (Harris *et al.*, 2011; Mima and Schweizer, 2010; Shih *et al.*, 2008; Thamlikitkul and Trakulsomboon, 2010).

## 1.4 Previous studies on porins from *B. pseudomallei* and *V. harveyi*

### 1.4.1 Liposome-swelling assays of outer membrane proteins from *B. pseudomallei*

*B. pseudomallei* and *B. thailandensis* have the same outer membrane protein sequence and have highly antibiotic resistant strains. The outer membrane proteins of the two *Burkholderia* species were found to have a trimeric form with molecular weight of approximately 110 kDa. Topology prediction and molecular modeling suggested that *BpsOmp38* and *BthOmp38* porins are 16-stranded  $\beta$ -barrels with the 8 long loops and 7 short turn, compatible with a pore diameter of between 1.2 and 1.6 nm (Siritapetawee *et al.*, 2004a). The gene corresponding to an outer membrane *BpsOmp38* was isolated from the genome of *B. pseudomallei*. This porin was expressed in *E. coli* as insoluble inclusion bodies and refolded. In functional liposome-swelling assays, both proteins showed similar permeabilities for small sugar molecules. As expected, *L*-arabinose ( $M_r$  150), which is the smallest sugar tested, gave the highest rate of diffusion through the *BpsOmp38* pore, followed by the diffusion rates of *D*-glucose, *D*-mannose and *D*-galactose ( $M_r$  180), *D*-GlcNAc ( $M_r$  221), and *D*-sucrose ( $M_r$  342). *D*-stachyose ( $M_r$  667) showed the slowest diffusion rate, as it has the highest molecular weight compared with the other sugars shown in Figure 1.12 (Siritapetawee *et al.*, 2004b).

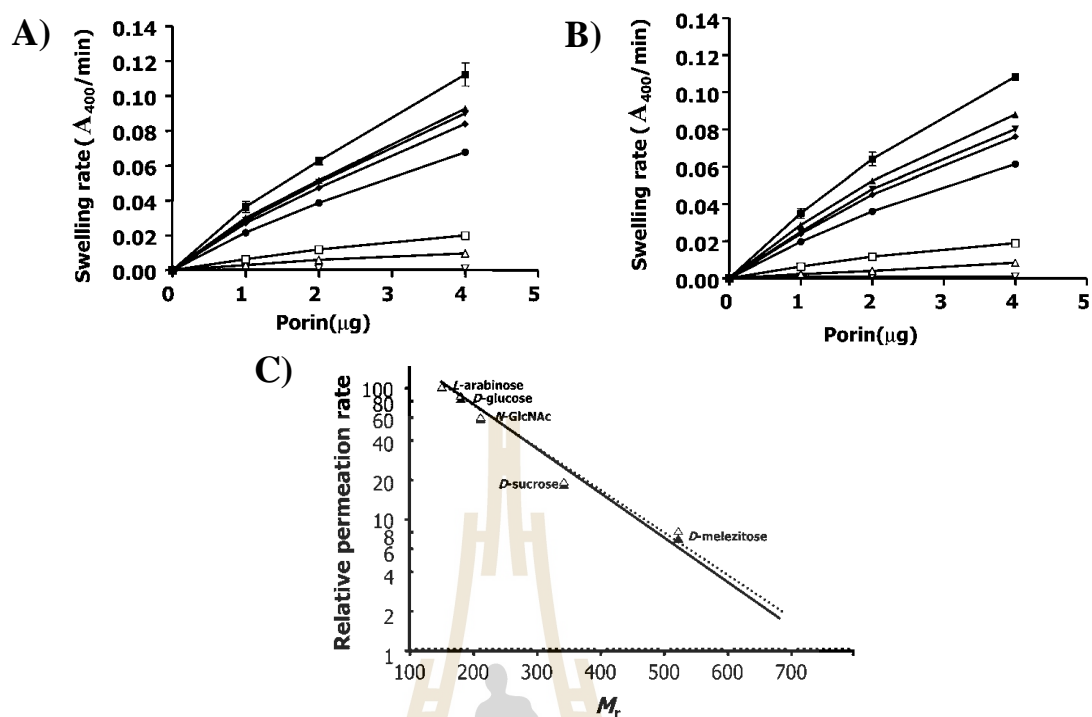


**Figure 1.12** Liposome-swelling assays of refolded Omp38. Diffusion rates for neutral saccharides were determined by liposome-swelling assays using proteoliposomes reconstituted with the native (A) and refolded (B) *BpsOmp38*. The following symbols represent *L*-arabinose ( $\blacktriangle$ ); *D*-glucose ( $\blacktriangle$ ); *D*-mannose ( $\blacktriangledown$ ); *D*-galactose ( $\blacklozenge$ ); GlcNAc ( $\bullet$ ); *D*-sucrose ( $\square$ ); *D*-melezitose ( $\triangle$ ) and *D*-stachyose ( $\triangle$ ). (C) Relative permeation rates of sugars through liposomes reconstituted with native ( $\cdots$ ) or refolded ( $-$ ) *BpsOmp38*. The values are normalised to the permeation rate of *L*-arabinose and plotted on a logarithmic scale.

#### **1.4.2 Pore-forming properties and translocation of antibiotics through single channel of *BpsOmp38* by black lipid membrane (BLM) technique**

Porins are inserted into the outer membrane lipid bilayer of the bacterial cell wall to form pores through which molecules can diffuse and access the periplasmic space and cytosol (Galdiero *et al.*, 2007; Nikaido, 2003; Schulz, 2002). Translocation and membrane permeability via porins have been measured using the black lipid membrane (BLM) technique (Tien and Ottova, 2001; Weingart *et al.*, 2008; Winterhalter, 2000).

BLM reconstitution was used to demonstrate the single-channel conductance of the trimeric *BpsOmp38*. High-time resolution BLM measurements displayed ion current blockages of seven antimicrobial agents in a concentration-dependent manner with the binding constant ( $M^{-1}$ ) following the order: norfloxacin > ertapenem > ceftazidime > cefepime > imipenem > meropenem > penicillin G. The BLM data provide the first insight into antimicrobial agent translocation through the *BpsOmp38* channel. The blockage event of ertapenem is shown in Figure 1.13 (Suginta *et al.*, 2011).



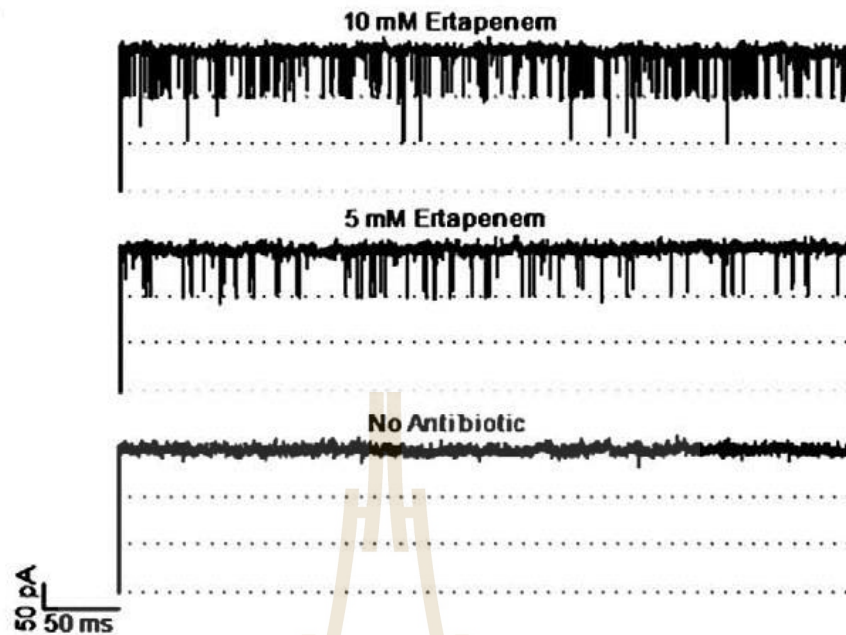


**Figure 1.13** Kinetic analysis of antimicrobial agent translocation through *BpsOmp38*. Effect of ertapenem concentrations. No blockage event was detected when the electrophysiological activity of a single trimeric channel was recorded in the absence of antimicrobial agents, whereas complete blockage events were observed with frequency directly proportional to the concentrations of ertapenem from 2.5, 5, 7.5, and 10 mM. Here, only the traces for 5 and 10 mM concentrations are presented.

#### 1.4.3 Characterisation of chitooligosaccharide-specific porins from *V. harveyi*

Recently, the gene corresponding to chitoporin (so called *VhChiP*) was isolated from the genome of *V. harveyi*. *VhChiP* was expressed in *E. coli* and the specific function of *VhChiP* was investigated using BLM technique. *VhChiP* was found to be able to insert into artificial membranes and formed stable, trimeric channels with

average single conductance of  $1.86 \pm 0.3$  nS. Single channel recordings at microsecond-time resolution resolved translocation of chitooligosaccharides, with the greatest rate being observed for chitohexaose. The BLM trace for chitohexaose is shown in Figure 1.14.

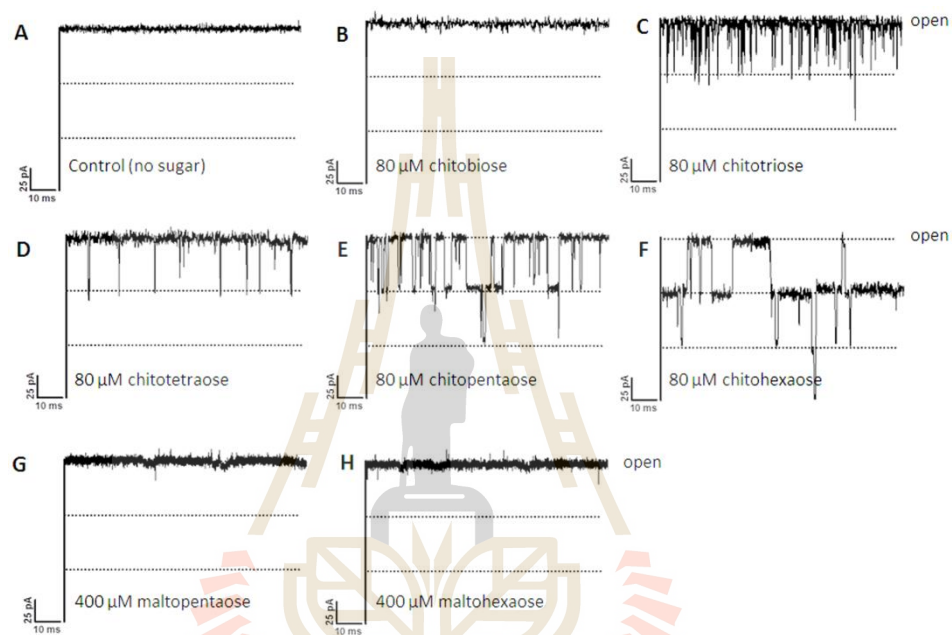


**Figure 1.14** Effect of chitooligosaccharides on chitoporin ion currents. A single channel of *VhChiP* was inserted in the artificial membrane in A). A fully open state. Then, chitooligosaccharide: B) chitobiose, C) -triose, D) -tetraose, E) -pentaose, and F) -hexaose were added on the cis side of the chamber to a final concentration of 80  $\mu$ M. Control recordings were made with G) maltopentaose and H) maltohexaose at a concentration of 400  $\mu$ M. Ion current fluctuations were monitored for 120 s at applied voltages of +100 mV (Suginta *et al.*, 2013a).

Liposome swelling assays showed no permeation of other oligosaccharides, including maltose, sucrose, maltopentaose, maltohexaose and raffinose, indicating that *VhChiP* is a highly specific channel for chitooligosaccharides, as shown in Figure 1.15 (Suginta *et al.*, 2013a; Suginta *et al.*, 2013b).

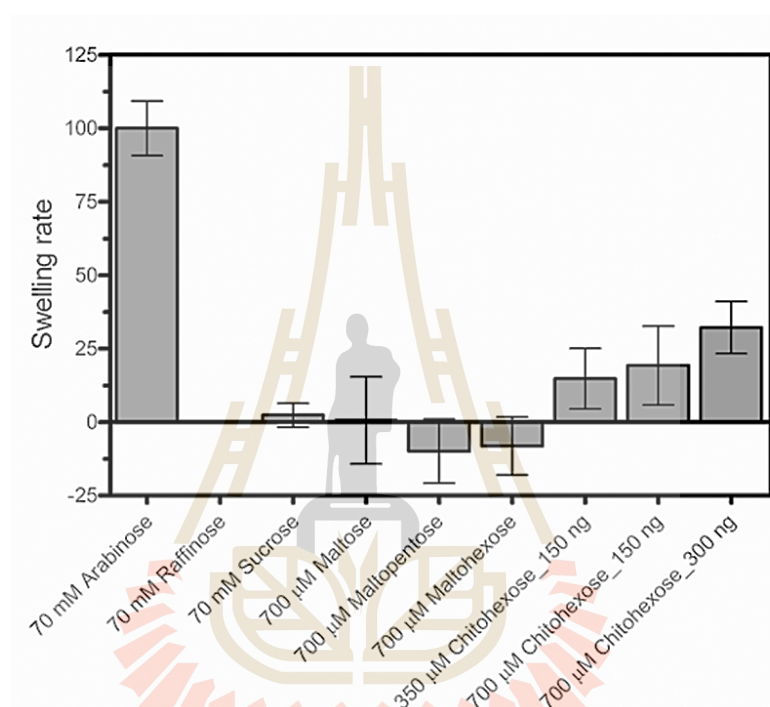


**Figure 1.15** Liposome swelling assays. Multilamellar liposomes were reconstituted with purified *VhChiP* (150 or 300 ng). The isotonic concentration was defined as the concentration of raffinose added into the proteoliposome suspension that did not cause change in absorbance at 500 nm for a period of 60 s. Permeation of different types of sugars through *VhChiP* reconstituted liposomes were then tested. The swelling rates were normalised, with the rate of swelling in arabinose set to 100% (Suginta *et al.*, 2013a).

#### **1.4.4 Mutational effects on chitooligosaccharide permeability through *VhChiP* from *V. harveyi***

Previous study showed that Trp136, located at the mouth of the *VhChiP* pore, plays an essential role in controlling the channel's ion conductivity, chitin affinity and permeability. Kinetic analysis of sugar translocation obtained from single channel recordings indicated that the Trp136 mutations W136A, W136D, W136R, and W136F considerably reduced the binding affinity of the protein channel for its best substrate, chitohexaose. The sugar blocking events were observed to be much more irregular, indicating incomplete subunit blocking.

The chitohexaose at a very low concentration (0.25  $\mu\text{M}$ ) blocked one protein monomer, and occasionally blocked a second monomer. In case of the W136 mutants, only one channel subunit of the mutants W136A/F/D/R was partially blocked. At a high concentration (5.0  $\mu\text{M}$ ) of chitohexaose, monomeric, dimeric and even trimeric blockages occurred in the case of wild type *VhChiP* (Figure 1.16A) and W136F mutant (Figure 1.16D). However, at the same sugar concentration, only one subunit of the mutant W136A (Figure 1.16B) was blocked and dimeric blockages were infrequently seen with the W136R (Figure 1.16C) and W136D (Figure 1.16E) mutants. W136 is in the position to act as the main binding site and has an important role in the translocation of sugar molecule through the *VhChiP* channel (Chumjan *et al.*, 2015).

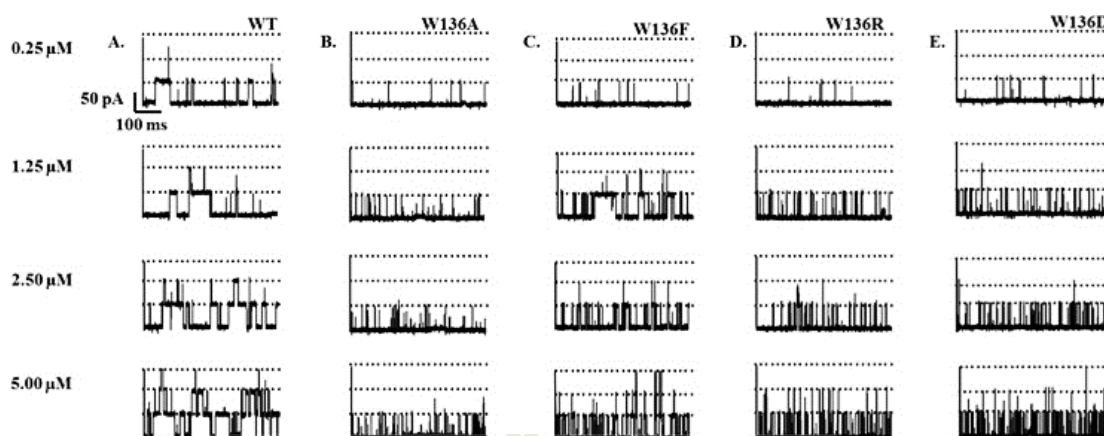


**Figure 1.16** The effect of transmembrane potentials at various concentrations of chitohexaose on the single channel conductance of trimeric *VhChiP* (WT) and its mutants. The single channel insertion of WT (A) and its mutants (B – E) were reconstituted into solvent-free lipid membrane in 1 M KCl, 20 mM HEPES (pH 7.5) and exposed to various concentrations of chitohexaose (0.25, 1.25, 2.5, and 5  $\mu$ M) on the cis side at a transmembrane potential of  $-100$  mV (Chumjan *et al.*, 2015).

## 1.5 Research objectives

This PhD research project aims to address some research gaps in the crystal structures and some physiological functions of *BpsOmp38* and *VhChiP*. This project is divided into two parts. The first part focuses on the functional characterisation to determine the effects of mutation on the permeability of antibiotic through *BpsOmp38*. Later, the crystal structure of the *BpsOmp38* porin was determined in collaboration with Prof. Dr. Bert van den Berg, Institute for Cellular and Molecular Biosciences, Newcastle University, UK. In the second part of this study, the crystal structures of

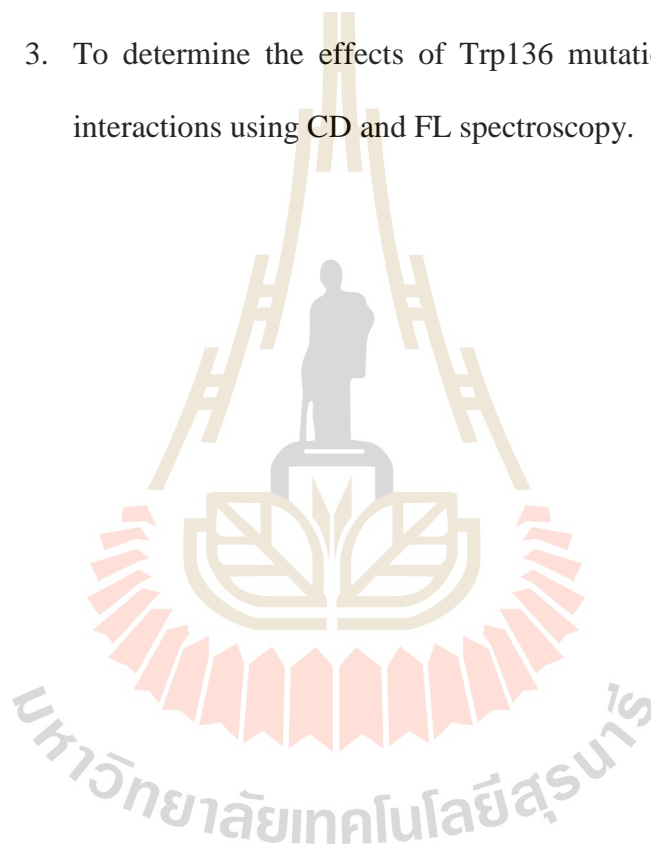
VhChiP in absence and presence of chitohehexose substrate are presented. In addition, the channel specificity has been investigated using circular dichroism and fluorescence spectroscopy. The objectives of this project include:

### 1.5.1 Outer membrane protein from *B. pseudomallei* (*BpsOmp38*)

1. To clone, express, and purify *BpsOmp38* with His<sub>6</sub>-tag from *B. pseudomallei*.
2. To study effects of mutation of Tyr119 on antimicrobial susceptibility involving *BpsOmp38*.
3. To solve the 3D-structure of *BpsOmp38*.
4. To determine MIC values of the *E. coli* harbouring pET23d(+)/*BpsOmp38* wild type, Y119A and Y119F recombinant plasmids in comparison with the MIC values of *B. pseudomallei* native strain.
5. To carry out sugar and antibiotic permeation of the recombinant *BpsOmp38* expressed with *E. coli* BL21 (DE3) Omp8 Rosetta strain using liposome swelling assays.
6. To determine the secondary structure and thermal unfolding of *BpsOmp38* in the presence of selected antibiotics using circular dichroism (CD) spectroscopy.
7. To determine the 3D structures, thermal unfolding, and binding kinetics of *BpsOmp38* with antibiotic using fluorescence (FL) spectroscopy.

### 1.5.2 Outer membrane protein from *V. harveyi* (VhChiP)

1. To solve the 3D-structures of VhChiP WT, refolded and truncated proteins.
2. To carry out sugar permeation of the recombinant VhChiP expressed with *E. coli* BL21 (DE3) Omp8 Rosetta strain using liposome swelling assays.
3. To determine the effects of Trp136 mutations on sugar-channel interactions using CD and FL spectroscopy.



## CHAPTER II

### MATERIALS AND METHODS

#### 2.1 Design of oligonucleotide primers

##### 2.1.1 *BpsOmp38* from *Burkholderia pseudomallei*

The primers used for the generation of recombinant *BpsOmp38* with His<sub>6</sub>-tag and signal peptide are shown below. Sequences underlined are the cloning sites.

Forward primer (*Nco*I) = 5' TACCATGGCAAATAAGACTGATTGTTG 3'

Reverse primer (*Xho*I) = 5' TACTCGAGGAAACGTGACGCAGACC 3'

The primers used for the generation of recombinant *BpsOmp38* without His<sub>6</sub>-tag but with signal peptide are shown below. Sequences underlined are the cloning sites.

Forward primer (*Nco*I) = 5' TACCATGGCAAATAAGACTCTGATTGTTG 3'

Reverse primer (*Xho*I) = 5' AATCTCGAGTTAGAAGCGGTGACGCAGAC 3'

The primers used for the generation of recombinant *BpsOmp38* without His<sub>6</sub>-tag and without signal peptide are shown below. Sequences underlined are the cloning sites.

Forward primer (*Nco*I) = 5' GCGCCATGGGCCAAAGCAGCGTCACG 3'

Reverse primer (*Xho*I) = 5' GCGCTCGAG GAAGCGGTGACGCAG 3'



The primers for designed mutation of *BpsOmp38* Tyr119 → Ala (mutant Y119A) and *BpsOmp38* Tyr119 → Phe (mutant Y119F) are shown below. Sequences underlined indicate the mutated codons.

Mutation: Tyr119 → Ala (Y119A)

Forward primer = 5' CTGGGCCGTCAGGCCGACGCAACCCAAGAC 3'

Reverse primer = 5' GTCTTGGGTTGCGTCGCCTGACGGCCCCAG 3'

Mutation: Tyr119 → Phe (Y119F)

Forward primer = 5' GGGCCGTCAGTTCGACGCAACCCAAG 3'

Reverse primer = 5' CTTGGGTTGCGTCGAACTGACGGCCCC 3'

### 2.1.2 *VhChiP* from *Vibrio harveyi*

The primers used for the generation of recombinant *VhChiP* (folded protein) without signal peptide are shown below. Sequences underlined are the cloning sites.

Forward primer (NcoI) = 5' GCGCCATGGGCGATGGTGCAAACAGTG 3'

Reverse primer (XhoI) = 5' GCGCTCGAGTTAGAAGTAGTATTCAAC 3'

## 2.2 Expression vectors and bacterial host cells

The expression vector pET23d(+) was used for expression of outer membrane protein (*BpsOmp38* and *VhChiP*) with a signal peptide. The expression vector pET28a(+) was used for expression of outer membrane protein (*VhChiP* refolded) without signal peptide. *E. coli* DH5 $\alpha$  strain was used as a routine host for cloning, subcloning and preparation of recombinant plasmid. *E. coli* XL1-Blue supercompetent cells were used as the host for transformation of the recombinant plasmid harboring the desired mutated DNAs. *E. coli* BL21 (DE3) omp8 Rosetta mutant strain lacking OmpF,

OmpA, OmpC and LamB was used as the expression host for all outer membrane proteins with signal peptide. *E. coli* BL21 (DE3) was used as the expression host for outer membrane protein without signal peptide.

**Table 2.1** Bacterium strain, the plasmids and the recombinant plasmids.

Strains , plasmids	Description	Source
<b>Strains</b>		
<i>E. coli</i> DH5 $\alpha$	Cloning host	Promega, Singapore
<i>E. coli</i> XL1-Blue	Desired mutant DNAs	Promega, Singapore
<i>E. coli</i> BL21 (DE3) Omp8 rosetta	Expression host	A gift from Professor Roland Benz, Jacob University Bremen, Germany
<i>E. coli</i> BL21 (DE3)	Expression host	From Professor Bert van den Berg's laboratory, Newcastle University, UK
<b>Plasmids</b>		
pGEM - T easy	Cloning vector	Promega, Singapore
pET23d (+)	Expression vector	Novagen, Germany
pET28a (+)	Expression vector	From Professor Bert van den Berg's laboratory, Newcastle University, UK
pGEM - T easy/ <i>Bps</i> Omp38	Cloning vector	In-house prepared
<b>Recombinant plasmids</b>		
pET23d(+)/ <i>VhChiP</i>	Wild type and Cloning vector	In-house prepared
pET23d(+)/ <i>VhChiP</i> Y136A	Mutant Trp136 $\rightarrow$ Ala	In-house prepared
pET23d(+)/ <i>VhChiP</i> Y136F	Mutant Trp136 $\rightarrow$ Phe	In-house prepared

### 2.3 Chemicals and reagents

Chemicals and reagents for cloning, expression and crystallisation of outer membrane proteins were analytical grade unless otherwise stated. *Pfu* DNA

polymerase, dNTP mix, *Pfu* polymerase buffer, magnesium chloride, *DpnI*, *NcoI*, *XhoI* restriction enzymes are products of Promega. QIA prep spin Mini prep kit , Ni-NTA superflow, bovine serum albumin (BSA), isopropyl- $\beta$ -D-thiogalactopyranoside (IPTG), bacto tryptone, bacto yeast extract, agar, calcium chloride, potassium chloride, sodium chloride, sodium tetraborate, sodium acetate, sodium hydroxyl disodium ethylenediaminetetraacetic (EDTA), glycerol, lysozyme, glycine, imidazole, tris base, sodium dodecyl sulphate (SDS), acrylamide, *N,N'*-methylene bisacrylamide, TEMED, ammonium persulfate, coomassie brilliant blue R-250, and 2-mercaptoethanol are products of Sigma-Aldrich (St. Louis, MO, USA). DNaseI and RNaseA were purchased from Pacific Science Co., LTD. Ampicillin and kanamycin were products of USB Corporation (Cleveland, OH, USA). Micro-Bridge, Imp@ct Plate, Cryschem Plate<sup>TM</sup>, Limbro Plate<sup>®</sup>, VDX Plate Greased<sup>TM</sup>, 20 and 18 mm Siliconised glass cover, Crystal Screen HR114 (Hampton research) and JBS Screen Kits (JBS), SaltRx HT, Index HT, 2,4-dimethyl-5-pentenediol (MPD), A's oil and Crystal Clear sealing tape and 96 well CrystalQuick<sup>TM</sup> plates were products of Hampton Research.

## 2.4 Instrumentation

Instruments used in this study included a Sonopuls Ultrasonic homogeniser with a 6-mm diameter probe (Sonics, Connecticut, USA), a PCR thermocycler (Perkin Elmer, Massachusetts, USA), a DNA gel apparatus (Myrun<sup>nc</sup>, Ontario, Canada), protein gel apparatus plus with a compatible power supply (BIO-RAD, California, USA), Genway UV-VIS spectrophotometer (Thermo Scientific, Dreieich, Germany), Gel Document system (BIO-RAD, Milan, Italy), microtiter plate reader (Anthos,

Cambridge, UK), AKTA prime purification system (GE Healthcare, Uppsala, Sweden), and Stereo Microscope mounted with a video camera (ZEISS, Oberkochen, Germany).

## 2.5 Methodology

### Part I: Outer membrane protein (*BpsOmp38*) from *Burkholderia pseudomallei*

#### 2.5.1 Structural and functional characterisation of *BpsOmp38* from *B. pseudomallei*

##### 2.5.1.1 Antimicrobial susceptibility assay

MIC values were determined from 4 – 6 trials (the reaction was set up in triplicate for each trial) by the Mueller-Hinton (MH) two-fold dilution method, following the Clinical and Laboratory Standards Institute (CLSI) guidelines (Wikler, 2006). Different classes of antimicrobial agents were used for the susceptibility tests, which include: class 1 (penicillins): penicillin G and amoxicillin; class 2 (cephalosporins): ceftazidime, cefoxitin and cefepime; class 3 (carbapenems): meropenem, imipenem and doripenem; class 4 (fluoroquinolones): norfloxacin and ciprofloxacin; class 5 (quinolone carboxylic acid): enrofloxacin; class 6 (sulfonamide-trimethoprim): co-trimoxazole; and class 7 kanamycin and gentamicin. MIC values were evaluated with the cells grown in the presence of 50  $\mu\text{g mL}^{-1}$  phenylarginine- $\beta$ -naphthylamide (PA $\beta$ N), an inhibitor of RND-type multidrug efflux pumps (Kern *et al.*, 2006; Tran *et al.*, 2010). *B. pseudomallei* or *E. coli* BL21 (DE3) Omp8 Rosetta cells, transformed with an empty pET23d(+) vector or with the recombinant vector pET23d(+)/*BpsOmp38*, were streaked onto LB agar plates and incubated at 37 °C for

16 h. Single colonies of the bacteria were grown in 5 mL of MH medium and incubated at 37 °C for an additional 16 h.

To assess the effect of the plasmid-derived  $\beta$ -lactamases on penicillin antimicrobial agents, 10  $\mu$ L aliquots of the cell culture (diluted to OD<sub>600</sub> of 0.1 or equivalent to  $10^4 - 10^5$  CFU mL<sup>-1</sup>) were transferred into a 96-well plate, each well containing 90  $\mu$ L LB medium and two-fold dilutions of penicillin G or amoxicillin mixed with clavulanic acid in a ratio of 2:1. After incubation at 37 °C for 24 h, MIC values were evaluated in comparison with the breakpoints for *Pseudomonas spp.* as recommended by the European Committee on Antimicrobial Susceptibility Testing-EUCAST (<http://www.eucast.org/>).

#### 2.5.1.2 Topology structure prediction

The structural model of *BpsOmp38* was automatically built by the program Modeller suite. Initially, several iterations of the PSI-BLAST protein sequence search program in the PDB database were performed to allow detection of remote homologues of the *BpsOmp38* porin. Only the templates with non-redundant structures were kept and further used for building the homology model. The template included the PDB codes 3K1B (OmpF from *E. coli*). Sequence alignment revealed a complete coverage of the homology sequence, although only about 20% sequence identity was observed between the *BpsOmp38* and the template amino acid residues. The structural model of the *BpsOmp38* trimers was further generated by the Modeller program (Eswar *et al.*, 2008), from which the representative model was defined as the one that minimised both the overall Modeller objective function and the Dope score evaluation function.

Finally, the final best model was assessed with the energetic-based validation suite ProQ (Wallner and Elofsson, 2003) and the geometric based PROCHECK, with the latter showing only 2.8% of Ramachandran disallowed regions and absence of close (or “bad”) contacts. The mutated structures of *BpsOmp38Y119A* and *BpsOmp38Y119F* were created using the program WinCoot (version 0.8.6.1) (<http://www.yysbl.york.ac.uk/~lohkamp/coot/>) and displayed by PyMol (version 1.8.6.1) (<https://sourceforge.net/projects/pymol/>).

### 2.5.1.3 PCR amplification of the cDNA encoding *BpsOmp38*

Previously a technique demonstrated by Siritapetawee *et al.* (2004b) has successfully expressed *BpsOmp38* porin using cDNA construct without signal peptide and His<sub>6</sub>-tag. In this study, the purity of porin was further improved with the use of a new *BpsOmp38* DNA construct with signal peptide and His<sub>6</sub>-tag. The introduction of His<sub>6</sub>-tag in the cDNA also improved the ease of purification of *BpsOmp38*, while the signal peptide enabled the folding of protein according to the structure of native protein expressed in the outer membrane. More importantly, porin expressed with this new cDNA construct enabled the BLM analyses with its ability to insert into lipid bilayer. The full-length cDNA encoding *BpsOmp38* was amplified by PCR reaction using the pGEM-T easy/*BpsOmp38* as DNA template (Siritapetawee *et al.*, 2004b).

The PCR reaction comprises DNA template, 10x *Pfu* buffer, 10 mM dNTP mix, 10 μM primer, 25 mM MgCl<sub>2</sub>, and 1 unit of *Pfu* DNA polymerase. The reaction was amplified in GeneAmp® PCR system 9700 thermocycler. The DNA template was initially denatured for 2 min at 98 °C, then denatured for 1 min at 98 °C and subjected to 30 cycles of annealing at 50 °C, for 30 sec and extension at 72 °C for

3 min , followed by a final extension for 5 min at 72 °C. PCR products were resolved on 1% agarose gel. The DNA insert of expected size (about 1.12 kbp) was excised, and then ligated into pGEM-T cloning vector, according to the Promega Manufacturer's instruction.

For addition of A-tailing into PCR products, (reaction comprises purified PCR, 10x buffer, 2 mM MgCl<sub>2</sub>, 10 mM ATP and Taq DNA polymerase). Deionised water was added to make up a final volume of 10 µL. The reaction mixture was then incubated at 70 °C for 15 – 30 min. The amounts of DNA insert used for ligation are calculated as follows:

$$\frac{(\text{ng of vector} \times \text{kb size of insert})}{\text{kb size of vector}} \times (\text{insert} : \text{vector molar ratio}) = \text{ng of insert}$$

Ligation reaction mixture was made by mixing 2x T4 DNA ligase buffer, 50 ng of pGEM-T easy vector (3 kbp), PCR products and 0.3 unit of T4 DNA ligase. Deionised water was added to make up a final volume of 25 µL. The reaction mixture was then incubated overnight at 4 °C.

#### **2.5.1.4 Cloning of DNA encoding *BpsOmp38* into pET23d(+) and confirmation of DNA insert**

Five microliters of the ligated products were transformed into 100 µL of *E. coli* DH5α competent cells, using a standard protocol. Single colonies, which carried the plasmid containing the *BpsOmp38* DNA insert, were subjected to plasmid extraction using High-Speed plasmid mini kit (Geneaid Biotech Ltd., USA) and analysed by 1% agarose gel electrophoresis.

The purified plasmids (pGEM-T easy/*BpsOmp38*) were further digested with the restriction enzymes *XhoI* and *NcoI* to obtain cohesive ends for further ligation. Double digestion reactions comprised 10 µg DNA insert, 2 µL of 10x NEB buffer, 10 units of *XhoI* and 10 units of *NcoI*. Sterilised H<sub>2</sub>O was added to a final volume of 20 µL. The reaction mixture was then incubated at 37 °C for 3 h and the reaction was inactivated at 65 °C for 15 min. The digestion products were separated by agarose gel electrophoresis and purified by the QIAQuick gel extraction kit (QIAGEN, USA).

The purified *BpsOmp38* cDNA was then ligated into pET23d(+) vector. The reaction mixture was made up of 1 µL of 10x rapid ligation buffer, 50 ng purified pET23d(+) vector, 45 ng DNA insert of the *BpsOmp38* DNA, 1 unit T4 DNA ligase, and sterile distilled water to bring the volume up to 20 µL. The ligation reaction mixture was then incubated at 4 °C overnight. The total reaction mixture was transformed into *E. coli* DH5α strain. The bacterial cells were grown in LB broth contained 100 µg mL<sup>-1</sup> ampicillin and the recombinant plasmid was isolated by using the QIAprep Spin Miniprep kit (QIAGEN, USA).

#### **2.5.1.5 Mutation design and site-directed mutagenesis of pET23d(+)/*BpsOmp38***

Amino acid alignment revealed that Tyr119 located at the centre of the *BpsOmp38* pore may be important for pore size restriction. To demonstrate the functional role of Tyr119, this residue was mutated by site-directed mutagenesis. The pET23d(+) plasmid harboring *BpsOmp38* was used as the DNA template. Mutations of the desired nucleotides were carried out using PCR-based strategy, employing the mutagenic primers as described in Section 2.1.1. The PCR



reaction mixtures were made of DNA template, 10x *Pfu* buffer, 10 mM dNTP mix, 10  $\mu$ L primer, 25 mM MgCl<sub>2</sub>, and 1 unit of *Pfu* DNA polymerase. These reaction mixtures were amplified at optimal conditions in GeneAmp<sup>®</sup> PCR system 9700 thermocycler. The success of PCR amplification was verified by agarose gel electrophoresis.

The PCR products were then digested with *DpnI* restriction enzyme to remove the non-mutated parental strand. The *DpnI*-treated DNA was transformed into XL1-Blue supercompetent cells. Then, the transformed cells were spread on LB agar 100  $\mu$ g mL<sup>-1</sup> ampicillin. The recombinant plasmids obtained from the positive colonies were extracted using Qiagen Plasmid Miniprep. After correct mutations were confirmed by automatic DNA sequencing, the plasmids carrying the mutated gene were transformed into *E. coli* BL21 (DE3) Omp8 Rosetta cell for protein expression.

#### **2.5.1.6 Native protein expression and purification of *BpsOmp38***

For expression and purification of the recombinant *BpsOmp38* variants, transformed cells were grown at 37 °C in Luria-Bertani (LB) liquid medium containing 100  $\mu$ g mL<sup>-1</sup> ampicillin and 25  $\mu$ g mL<sup>-1</sup> kanamycin. At an OD<sub>600</sub> reading of 0.5, IPTG (isopropyl  $\beta$ -D-thiogalactoside) was added to a final concentration of 0.4 mM. Cell growth was continued for another 6 h and cells were then harvested by centrifugation at 4,500 rpm for 10 min. The cell pellet was re-suspended in buffer containing 20 mM Tris-HCl, pH 8.0, 2.5 mM MgCl<sub>2</sub>, 0.1 mM CaCl<sub>2</sub>, 10  $\mu$ g mL<sup>-1</sup> DNase I and 10  $\mu$ g mL<sup>-1</sup> RNase A and then disrupted using a high-pressure homogeniser (EmulsiFlex-C3, Avestin Europe, Mannheim, Germany).

The recombinant *BpsOmp38* was further extracted from the peptidoglycan layer using sodium dodecyl sulfate (SDS)-containing solutions, based on

a procedure reported by Lugtenberg and Van Alphen (1983). Briefly, SDS was added to the cell suspension to a final concentration of 2% (w/v) and incubation was carried out for 1 h at 50 °C with gentle shaking. The crude extract was then centrifuged at 22,000 rpm for 60 min at 4 °C. The pellet, which at this stage including the cell envelopes, was re-suspended in 20 mM phosphate buffer saline (PBS), pH 7.4, containing 0.125% (v/v) octyl-POE (*N*-octyl-polyoxyethylene; ALEXIS Biochemicals, Lausanne, Switzerland). The suspension was incubated at 37 °C with gentle shaking for 60 min and then centrifuged at 40,000 rpm at 4 °C for 40 min. The new pellet, enriched in outer membranes, was re-suspended in 20 mM PBS, pH 7.4 containing 3% (v/v) octyl-POE and the suspension was incubated at 37 °C with gentle shaking for 1 h to solubilise the porin. Insoluble material was removed by centrifugation at 40,000 rpm at 20 °C for 40 min and the porin-rich supernatant was concentrated and exchanged into a new buffer containing 0.2% (v/v) LDAO (lauryldimethylamine oxide) using Amicon Ultra-15 centrifugal filter devices with a MW limit of 30 kDa (Millipore, Schwalbach, Germany).

*BpsOmp38* was further purified by cation exchange chromatography using a Hitrap SP HP column (5 × 1 mL) connected to an ÄKTA Prime plus FPLC system (GE Healthcare Life Sciences). The chromatography was performed at 25 °C with a constant flow rate of 1.0 ml min<sup>-1</sup>. *BpsOmp38* was eluted with a linear gradient of 0 – 1 M KCl in 20 mM Tris-HCl, pH 8.0 containing 0.2% (v/v) LDAO. The purity of the eluted proteins was confirmed by SDS-PAGE. Fractions containing only the *BpsOmp38* were pooled and the protein concentration was determined using the Pierce BCA protein assay kit (Bio-Active Co., Ltd., Bangkok, Thailand).

### 2.5.1.7 Immunological analysis

Immunoblotting was performed following the standard ECL protocol. Purified *BpsOmp38* (5 µg) was resolved on a 10% SDS-PAGE gel, and after electrophoresis, the protein was transferred to a nitrocellulose membrane using a Trans-Blot SD semi-dry electrophoretic transfer cell (Bio-Rad Laboratories Ltd., Bangkok, Thailand). Cross-reactivity of different porins was tested using specific antibodies against *BpsOmp38*, *E. coli* OmpF, *E. coli* OmpN, and *Vibrio harveyi* VhChiP. Signals representing antibody-antigen interaction were detected with HRP-conjugated IgG, using the enhanced chemiluminescence method (ECL, Amersham, UK). Rabbit anti-*BpsOmp38* serum was prepared in our laboratory as described by Siritapetawee *et al.* (2004a). Immunoblotting was performed using a 1:10,000 dilution of anti-*BpsOmp38* antiserum and 1:20,000 dilution of goat anti-rabbit HRP antiserum in PBS, pH 7.4, containing 2% (w/v) fat free dried milk.

### 2.5.1.8 Pore conductance analysis

Black lipid membrane (BLM) reconstitution technique was used to demonstrate the pore-forming properties of the *BpsOmp38* variants. Ion channel measurements were performed as described by Schulte *et al.* (2009). The BLM setup included a patch clamp amplifier with a two-electrode bilayer head-stage (PC-ONE plus PC-ONE-50, Dagan Corporation, Minneapolis, MN, USA), a Faraday cage placed on a vibration-dampening table, an A/D converter and software for computer-controlled operation (PULSE program, HEKA Elektronik, Lambrecht, D).

In the BLM setup, a 1.5 mL Delrin cup with a 200-µm hole was fitted tightly into one of the two wells of a polymer bilayer chamber. The interior of the cup (*cis*) and the vacant well (*trans*) were filled with the 1M KCl electrolyte

solution into which the two Ag/AgCl electrodes, connected to the amplifier's headstage, were immersed. Routinely, the *trans* electrode was voltage-clamped with respect to the *cis* electrode, which was connected to the ground pin of the amplifier headstage. BLM recordings were formed by painting *L*- $\alpha$ -phosphatidylcholine (azolectin) dissolved in hexane (50 mg mL<sup>-1</sup>) over a cup aperture that had been treated earlier with a few microliters of hexadecane/hexane (1:100 v/v), and allowed to air-dry. For *BpsOmp38* experiments the BLM had to display a capacitance of about 100 pF and give a stable, virtually leak-free current signal throughout minute-long recordings at constant potentials. After electrolyte (1 M KCl) was added to both sides of the BLM chamber, a stock solution of the purified *BpsOmp38* (100  $\mu$ g mL<sup>-1</sup>) in 20 mM phosphate buffer, pH 7.5 and 0.2% (v/v) LDAO) was added into the *cis* chamber. *BpsOmp38* insertions were induced when an external transmembrane potential of +200 or -200 mV was applied. Membrane current ( $I_m$ ) recordings were made at 25 °C with the membrane potential across the phospholipid bilayer kept at defined constant values between  $\pm 25$  and  $\pm 150$  mV.

The acquired data were filtered with a 3-pole low-pass Bessel filter at 1 kHz and saved into the computer memory with a 1 ms (1 kHz) sampling interval. The membrane activity in terms of current flow was analysed directly with PULSE acquisition software. Stored traces were handled with Microsoft Office Excel 2010 and GraphPad Prism v.5.0 (GraphPad Software Inc., San Diego, CA).

### 2.5.1.9 Liposome Swelling Assays

The trimeric *BpsOmp38* channel was reconstituted into liposomes as described previously (Luckey and Nikaido, 1980; Yoshimura and Nikaido, 1985). Soybean *L*- $\alpha$ -phosphatidylcholine (Sigma-Aldrich) (20 mg mL<sup>-1</sup>,

freshly prepared in chloroform) was used to form multi-lamellar liposomes. For proteoliposome preparation, 200 ng of *BpsOmp38* was reconstituted into the liposomes by brief sonication, and 15% (w/v) dextran ( $M_r$  40,000) was subsequently entrapped in the proteoliposomes. The isotonic solute concentration was determined by mixing different concentrations of *D*-raffinose (prepared in 20 mM HEPES buffer, pH 7.5) with the liposome suspension. The concentration of *D*-raffinose that produced no liposome swelling or shrinking was the 'isotonic concentration'. This value was used for the adjustment of isotonic concentrations of other solutes.

Twenty microliters of liposome or proteoliposome solution was diluted into 600  $\mu$ L of the isotonic test solution in a 1-mL cuvette and mixed manually. The initial rate of swelling upon addition of the isotonic sugar solutions was monitored using a spectrophotometer with the wavelength set at 500 nm. The apparent absorbance change over the first 60 sec was used to estimate the swelling rate ( $s^{-1}$ ) using the equation:  $\Phi=(1/A_i)dA/dt$ , in which  $\Phi$  is the swelling rate,  $A_i$  the initial absorbance, and  $dA/dt$  the rate of absorbance change during the first 60 s. The swelling rate for each sugar was normalised by setting the rate with the smallest sugar, *L*-arabinose ( $M_r$  150), to 100%. The values were shown as the averages obtained from four to six determinations. Protein-free liposomes and proteoliposomes without sugars or antimicrobial agents were used as negative controls.

The sugars tested were *D*-glucose ( $M_r$  180), *D*-mannose ( $M_r$  180), *D*-galactose ( $M_r$  180), *N*-acetylglucosamine (GlcNAc,  $M_r$  221), *D*-sucrose ( $M_r$  342) and *D*-melezitose ( $M_r$  522). Antimicrobial agents used in liposome swelling assays were meropenem ( $M_r$  383), imipenen ( $M_r$  299), doripenem ( $M_r$  421), ceftoxitin ( $M_r$  428), cefepime ( $M_r$  481) and ceftazidime ( $M_r$  637).

#### 2.5.1.10 Statistical analysis

The significance of antimicrobial susceptibility tests for *Bps* and for *E. coli* expressing *BpsOmp38* variants against 14 antimicrobial agents was evaluated using  $\pm\log_2$  dilution analysis, following the description in previous reports (Amsler *et al.*, 2010; Lubber *et al.*, 2003), and one-way ANOVA, available in GraphPad Prism v. 5.0. The statistical significance of ion conductances and relative permeability rate of sugars and antimicrobial agents of the three *BpsOmp38* variants was evaluated by one-way ANOVA.

#### 2.5.1.11 Binding studies using BLM technique

The antibiotic diffusion through single channel conductance was carried out following Chumjan *et al.* (2015). Briefly, the small aperture of 40 – 60  $\mu\text{m}$  on a 25- $\mu\text{m}$ -thick Teflon partition separating two cell chambers was pre-treated with three times 2  $\mu\text{L}$  1% (v/v) hexadecane in hexane (Sigma-Aldrich) by simple drop-loading on both sides of the film. The partition film was then left to dry for 10 min. Then, the chambers were filled with 1 M KCl with 20 mM HEPES (adjusted to pH 7.5) as the electrolyte solution and Ag/AgCl electrode was immersed into both sides of the Teflon film. One of the electrodes was used as ground (cis) whereas the other electrode was connected (trans) to the headstage.

Then, lipid bilayer was formed by adding 2-5  $\mu\text{L}$  5  $\text{mg mL}^{-1}$  DPhPC (1,2-Diphytanoyl-sn-glycero-3-phosphatidyl-choline) lipid in pentane into each side of the chamber followed by raising and lowering the solution. After the establishment of a stable planar lipid bilayer, the concentration of *BpsOmp38* in the cis chamber was gradually increased by adding 1 – 10  $\mu\text{L}$  of 100  $\mu\text{g mL}^{-1}$  protein. This was done until a single trimeric channel insertion into the lipid bilayer was achieved.

To prevent multiple-channel insertion, the protein solution was then gently diluted with 1 M KCl in 20 mM HEPES (pH 7.5).

The current of the single channel was recorded for 2 min with a  $\pm 100$  mV applied voltage and 10 kHz low filter on a HAKA instrument. After that, antibiotics under study, i.e. meropenem ( $M_r$  383), imipenem ( $M_r$  299), doripenem ( $M_r$  421), ceftazidime ( $M_r$  428), cefepime ( $M_r$  481) and ceftazidime ( $M_r$  637) were added into the chamber, respectively. The current trace was then recorded for 2 min, each for voltage at +100 and -100 mV.

The equilibrium binding constant  $K$  ( $M^{-1}$ ) was estimated from the decrease in the ion conductance in the presence of increasing concentrations of antibiotics using the following equation 1 (Benz and Hancock, 1987):

$$G_{\max} - G_c / G_{\max} = I_{\max} - I_c / I_{\max} = K[c] / (K[c] + 1) \quad \text{Eq. 1}$$

$G_{\max}$  is the average conductance of the fully open *BpsOmp38* channel, and  $G_c$  is the average conductance at a given concentration  $[c]$  of antibiotic.  $I_{\max}$  is the initial current through the fully open channel in the absence of antibiotics, and  $I_c$  is the current at a particular antibiotics concentration. The titration experiments could also be analysed using double reciprocal plots.

#### 2.5.1.12 Thermal unfolding using circular dichroism (CD) spectroscopy

CD spectra were obtained with a JASCO J-815 CD Spectrometer. Far ultraviolet CD spectra of the *BpsOmp38* were obtained in 20 mM phosphate buffer, pH 7.5 and 0.2% LDAO. For the thermal unfolding curves of *BpsOmp38*, the CD value at 218 nm was monitored while raising the solution

temperature at a rate of  $1\text{ }^{\circ}\text{C min}^{-1}$  by a temperature controller (PTC-423L, Jesco). Protein and antibiotics (meropenem ( $M_r$  383), imipenen ( $M_r$  299), doripenem ( $M_r$  421), ceftoxitin ( $M_r$  428), cefepime ( $M_r$  481) and ceftazidime ( $M_r$  637)) at final concentrations of  $10\text{ }\mu\text{M}$  and  $10\text{ mM}$  were respectively added to a  $200\text{ }\mu\text{L}$  quartz cuvette. The fraction of unfolded protein was calculated from the CD intensity difference between folded and fully unfolded protein. This fraction was then plotted against temperature. The theoretical curve was fitted to the experimental data obtained by non-linear least square fitting procedure.  $T_m$  values for each unfolding process were obtained by directly fitting to the sigmoidal curve function Boltzman in Origin Pro8 (OriginLab Software, MA, USA) (Charalambous *et al.*, 2009).

#### 2.5.1.13 Thermal unfolding using fluorescence spectroscopy

Initial unfolding experiments with *BpsOmp38* were carried out in a JASCO FP-6200 fluorescence spectroscopy. The excitation wavelength of  $295\text{ nm}$  was set, while the emission wavelength was scanned from  $190$  to  $260\text{ nm}$  at  $25\text{ }^{\circ}\text{C}$ . For thermal unfolding experiment, the fluorescence intensity at  $F_{\text{max}}$  of  $340\text{ nm}$  was monitored raising the solution temperature at a rate of  $1\text{ }^{\circ}\text{C min}^{-1}$  by a temperature controller (PTC-423L, Jesco) to cover the temperature range of  $25$  to  $115\text{ }^{\circ}\text{C}$ , with excitation and emission slit widths set at  $10$  and  $20\text{ nm}$ , respectively. Protein and antibiotics at final concentrations of  $1\text{ }\mu\text{M}$  and  $1\text{ mM}$  were respectively added to a  $500\text{ }\mu\text{L}$  quartz cuvette. The antibiotics tested were meropenem ( $M_r$  383), imipenen ( $M_r$  299), doripenem ( $M_r$  421), ceftoxitin ( $M_r$  428), cefepime ( $M_r$  481) and ceftazidime ( $M_r$  637). The fraction of unfolded protein was calculated from the fluorescence intensity difference between folded and fully unfolded proteins. This fraction was then and plotted against temperature. The theoretical curve was fitted to the experimental data



by non-linear least square fitting procedure.  $T_m$  values for each unfolding process were obtained by directly fitting to the sigmoidal curve function Boltzman in Origin Pro8 (OriginLab Software, MA, USA) (Charalambous *et al.*, 2009). The equation is given in Eq 2.

$$y = [(A_i - A_f) / ((1 / (1 + e^{(x - T_m) / dx})))] + A_f \quad \text{Eq. 2}$$

$A_i$  and  $A_f$  are initial and final values of unfolding fraction;  $T_m$  refers to values for unfolding process ( $^{\circ}\text{C}$ ) and  $x$  is the temperatures ( $^{\circ}\text{C}$ ) at a given the values of unfolding fractions ( $y$ ).

#### 2.5.1.14 Binding studies using fluorescence quenching

The purified *BpsOmp38* (200 ng  $\mu\text{L}^{-1}$ , in 20 mM phosphate buffer, pH 7.4 and 0.2% (v/v) LDAO) was titrated with antibiotic at  $25 \pm 3$   $^{\circ}\text{C}$ . Changes in the intrinsic tryptophan fluorescence intensity were monitored directly with an LS-50 fluorescence spectrometer (Perkin-Elmer Limited, Thailand). The excitation wavelength was set to 295 nm and emission spectra were collected over the range 300-550 nm, with excitation and emission slit widths set at 5 and 10 nm, respectively. The spectrum of each protein was corrected for the blank spectrum. Binding curves were evaluated with a nonlinear regression function available in Prism version 6.0 (GraphPad Software, California, USA) using a model based on a single binding-site. To estimate the dissociation constant, relative fluorescence  $\Delta F = (F_0 - F_c)$  was plotted as a function of antibiotic concentration, yielding a rectangular hyperbolic curve. This curve allows the calculation of the dissociation constant for the antibiotics using a single-site binding model, according to Eq. 3 (Neves *et al.*, 2005; Songsiriritthigul *et al.*, 2008; Srivastava *et al.*, 2006):

$$\Delta F = F_0 - F_c = (F_0 - F_{\min})K[c]/(1 + K[c]) \quad \text{Eq. 3}$$

$\Delta F$  is the difference between fluorescence intensity before and after addition of the antibiotic (ligand);  $F_0$  refers to the maximum emission intensity in the absence of antibiotic;  $F_{\min}$  is the minimum emission intensity;  $F_c$  is the emission intensity at a given concentration of ligand;  $[c]$  is the concentration of ligand; and  $K$  is the equilibrium binding constant (M) (Kullman *et al.*, 2002). The free energy binding ( $\Delta G_{\text{binding}}$ ) can be estimated from the following relationship to Eq. 4:

$$\Delta G^\circ = -RT \ln K_B \quad \text{Eq. 4}$$

At equilibrium under conditions of constant pressure, the binding constant  $K$  is related to the standard Gibbs free-energy change ( $\Delta G^\circ$ ) of the reaction through, where  $R$  is the gas constant (8.314472 J mol<sup>-1</sup> K<sup>-1</sup>) and  $T$  is the temperature (in Kelvin).

#### **2.5.1.15 Thermodynamic parameters and the binding using fluorescence quenching**

The experiment is similar to the binding studies using fluorescence quenching with exception that the temperatures applied were 25, 30, 35, 40, and 45 °C. The thermodynamic parameters were calculated in order to elucidate the interaction between the *BpsOmp38* and antibiotics. The thermodynamic parameters were determined from the Van't Hoff equation to Eq. 5:

$$\ln K_a = - (\Delta H/RT) + (\Delta S/R) \quad \text{Eq. 5}$$

Where  $\Delta S$  is the entropy change; constants  $K_a$  are equilibrium binding quenching constant at the corresponding temperature.  $R$  is the gas constant (8.314472 J mol<sup>-1</sup> K<sup>-1</sup>).

The enthalpy change ( $\Delta H$ ) and the entropy change ( $\Delta S$ ) can be determined from the slope and y-intercept of the fitted curve of  $\ln K_a$  against  $1/T$  respectively. The free energy change ( $\Delta G$ ) was estimated from the following relationship Eq. 6:

$$\Delta G = \Delta H - T\Delta S \quad \text{Eq. 6}$$

The Binding and Van't Hoff curves were plotted in Prism version 6.0 (GraphPad Software, California, USA) (Sun *et al.*, 2006).

#### 2.5.1.16 Crystallisation and structure solution of *BpsOmp38*

Initial crystallisation trials for *BpsOmp38* were performed at 22 °C by sitting-drop vapour diffusion using MemGold1- and MemGold2-Screen from Molecular Dimensions (Molecular Dimensions Limited, Suffolk, UK) with a mosquito robot (TTP Labtech Ltd, Hertfordshire, UK). The initial hits were optimised by fine-screening with larger drops by hanging drop vapour diffusion. Crystals in space group  $P2_12_12_1$  were grown in 33% (v/v) PEG 400, 0.1 M magnesium chloride, 0.1 M sodium chloride 0.1 M Tris pH 8.5 and 5% water. Crystals were directly flash-frozen in liquid nitrogen. A data set was collected at IO2 at the Diamond Light Source (DLS), UK. The crystals, derived from *in vitro* folded *BpsOmp38*. The protein model was refined with REFMAC. Phases for *BpsOmp38* was obtained by molecular replacement using MOLREP with the refined structure of Omp32 from *Delftia acidovorans* (PDB ID 2FGR) as a search model. Model building was performed using WinCOOT and the structure was refined with PHENIX. The programs MolProbity and PROCHECK were used to evaluate the final model and PyMOL (Schrödinger, LLC) was used for the visualisation of the protein structures.

## Part II: Chitoporin (*VhChiP*) from *Vibrio harveyi*

### 2.5.2 Structure and functional properties of outer membrane protein (*VhChiP*) from *Vibrio harveyi*

#### 2.5.2.1 Structure Prediction of *VhChiP*

The structural model of *VhChiP* was built by the automated Modeller. The structures of *VhChiP* and its mutants were modelled using the X-ray structure of PorB (PDB 3VY9) from *Neisseria meningitidis* as structure template (Kattner *et al.*, 2013). The mutated structures of *VhChiP* W136F and *VhChiP* W136A were created using the program WinCoot (version 0.8.6.1) (<http://www.ytbl.york.ac.uk/~lohkamp/coot/>) and displayed with PyMol (version 1.8.6.1) (<https://sourceforge.net/projects/pymol/>).

#### 2.5.2.2 Expression and purification of *VhChiP* variants

Production of wild type and mutated *VhChiP* with *V. harveyi* clones was done as described previously by Chumjan *et al.* (2015). Recombinant wild-type *VhChiP* and the W136A and W136F mutants were expressed and purified, following the protocol originally described by Garavito and Rosenbusch (1986). In brief, transformed cells were grown at 37 °C in Luria-Bertani (LB) liquid medium containing 100 µg mL<sup>-1</sup> ampicillin, 25 µg mL<sup>-1</sup> kanamycin and 1% (w/v) glucose. At an OD<sub>600</sub> of 0.6 – 0.8, isopropyl β-D-thiogalactoside (*IPTG*) was added to a final concentration of 0.5 mM. Cell growth was continued for further 6 h and cells were then harvested by centrifugation at 4,500 × g at 4 °C for 20 min. The cell pellet was resuspended in a buffer containing 20 mM Tris-HCl, pH 8.0, 2.5 mM MgCl<sub>2</sub>, 0.1 mM CaCl<sub>2</sub>, 10 µg mL<sup>-1</sup> DNaseI and 10 µg mL<sup>-1</sup> RNaseA. Cells were lysed by sonication on ice for 10 min (30% duty cycle; amplitude setting 20%) using a Sonopuls Ultrasonic

homogeniser with a 6 mm diameter probe. The *VhChiP* was extracted with sodium dodecyl sulphate (SDS), based on the method of Lugtenberg and Alphen (1983). 20% (w/v) SDS stock solution was added into the lysed cell suspension to obtain a 2% (w/v) final concentration, followed by incubation at 50 °C for 1 h with gentle stirring, and centrifugation at  $40,000 \times g$  at 4 °C for 60 min. WT and mutant *VhChiPs* were extracted from the pellets, which were enriched in outer membranes, in two steps. In a pre-extraction step, the pellet was washed with 15 ml of 0.125% noctyl POE (*N*-octylpolyoxyethylene) in 20 mM phosphate buffer pH 7.4 (ALEXIS Biochemicals, Lausen, Switzerland), homogenised with a Potter-Elvehjem homogeniser, incubated at 37 °C for 60 min then centrifuged at  $100,000 \times g$ , 4 °C for 40 min. In the second step, the pellet from centrifugation at  $100,000 \times g$  was resuspended in 10 – 15 ml of 3% (v/v) *N*-octyl POE in 20 mM phosphate buffer pH 7.4, then homogenised with a Potter-Elvehjem homogeniser and incubated at 37 °C for 60 min, followed by further centrifugation at  $100,000 \times g$ , 4 °C for 40 min. The detergent was then exchanged with 0.2% (v/v) LDAO (lauryldimethylamine oxide, Sigma-Aldrich) through dialysis. The supernatant obtained was subjected to ion exchange chromatography on a HiTrap Q HP prepacked column ( $5 \times 1$  ml), connected to an ÄKTA Prime plus FPLC system (GE Healthcare Life Sciences, Life Sciences Instruments, ITS (Thailand) Co., Ltd., Bangkok, Thailand). Bound proteins were eluted with a linear gradient of 0 – 1 M KCl in 20 mM phosphate buffer, pH 7.4 containing 0.2% (v/v) LDAO. The purity of the eluted proteins was checked by SDS-PAGE and verified immunoblotting. Fractions containing only *VhChiP* were pooled and the protein concentration was determined using the Pierce BCA protein assay kit (Bio-Active Co., Ltd., Bangkok, Thailand).

### 2.5.2.3 Confirmation of *VhChiP* expression by immunoblotting

Purified *VhChiP* (5  $\mu\text{g}$ ) was resolved on a 10% polyacrylamide-SDS gel. After electrophoresis, the protein was transferred to a nitrocellulose membrane using a Trans-Blot SD semidry electrophoretic transfer cell (Bio-Rad Laboratories Ltd., Bangkok, Thailand). Cross-reactivity of different porins was tested using specific antisera against *E. coli* OmpN and *V. harveyi* ChiP. Antibody-antigen interaction was detected with HRP-conjugated IgG, using the ECL method (Amersham, UK). Rabbit anti-*VhChiP* antiserum was prepared in our laboratory as described by Suginta *et al.* (2013a). Immunoblotting was performed using a 1:40,000 dilution of anti-*VhChiP* antiserum and 1:20,000 dilution of goat anti-rabbit HRP antiserum in PBS, pH 7.4, containing 2% (w/v) fat free dried milk.

### 2.5.2.4 Thermal unfolding assay using circular dichroism (CD)

CD measurements were carried out using a JASCO J-815 CD Spectrometer. Far ultraviolet CD spectra of the *VhChiP* were obtained in 20 mM phosphate buffer, pH 7.5 and 0.2% LDAO. Thermal unfolding curves of the *VhChiP* were plotted by monitoring the CD value increment at 220 nm while raising the solution temperature at a rate of  $1\text{ }^{\circ}\text{C min}^{-1}$  by a temperature controller (PTC-423L, Jasco) and temperature range of 25 to 100  $^{\circ}\text{C}$  were recorded. *VhChiP* and substrate (chitooligosaccharides ((GlcNAc)<sub>n</sub>, n = 1, 2, 3, 4, 5, and 6)) were added into a 200  $\mu\text{L}$  quartz cuvette creating a mixture with final concentration of protein and substrate at 10  $\mu\text{M}$  and 10 mM, respectively. The fraction of unfolded protein was calculated from the CD intensity difference between folded and fully unfolded protein. This fraction was then plotted against temperature. The theoretical curve was fitted to the experimental data obtained by a non-linear least square fitting procedure based on equation 2.  $T_m$

values for each unfolding process were obtained by directly fitting to the sigmoidal curve function Boltzman in Origin Pro8 (OriginLab Software, MA, USA) (Charalambous *et al.*, 2009).

#### **2.5.2.5 Thermal unfolding assay using fluorescence spectroscopy**

Fluorescence measurements were obtained by JASCO FP-6200 spectroscopy. *VhChiP* in 20 mM phosphate buffer, pH 7.5 and 0.2% LDAO was excited with wavelength 295 nm. The maximum fluorescence intensity at the emission wavelength 340 nm was monitored while raising the solution temperature at a rate of 1 °C min<sup>-1</sup> by a temperature controller (PTC-423L, Jasco). The excitation and emission slit widths were 10 and 20 nm, respectively. Protein and substrate (chitooligosaccharides ((GlcNAc)<sub>n</sub>, n = 1, 2, 3, 4, 5, and 6)) were added into a 200 µL quartz cuvette forming a mixture with final concentrations of protein and substrate at 10 µM and 10 mM, respectively. The fraction of unfolded protein was calculated from the fluorescence intensity difference between folded and fully unfolded proteins. This fraction was then and plotted against temperature. The theoretical curve was fitted to the experimental data by non-linear least square fitting procedure. *T<sub>m</sub>* values for each unfolding process were obtained by directly fitting to the sigmoidal curve function Boltzman in Origin Pro8 (OriginLab Software, MA, USA) (Charalambous *et al.*, 2009).

#### **2.5.2.6 Binding studies using fluorescence quenching**

The purified *VhChiP* (80 ng µL<sup>-1</sup>, in 20 mM phosphate buffer, pH 7.4 and 0.2% (v/v) LDAO) was titrated with chitooligosaccharides at 25±3 °C. Changes in the intrinsic tryptophan fluorescence intensity were monitored directly with a LS-50 fluorescence spectrometer (Perkin-Elmer Limited, Thailand). The excitation wavelength was set to 295 nm and emission spectra were collected over the range 300

– 550 nm, with excitation and emission slit widths of 5 and 10 nm, respectively. The spectrum of each protein was corrected for the blank. Binding curves were evaluated with a nonlinear regression function available in Prism version 6.0 (GraphPad Software, California, USA) using a model based on a single binding-site. To estimate the dissociation constant, relative fluorescence  $\Delta F = (F_0 - F_c)$  was plotted as a function of sugar concentration, yielding a rectangular hyperbolic curve. This curve allows the calculation of the dissociation constant for the chitoooligosaccharides using a single-site binding model, according to Eq. 2. Meanwhile, the free energy binding ( $\Delta G_{\text{binding}}$ ) can be estimated with Eq. 4.

#### **2.5.2.7 Thermodynamic parameters and binding assay using fluorescence quenching**

This experiment was similar to the binding studies using fluorescence quenching except that the temperatures used were 25, 30, 35, 40 and 45 °C. The thermodynamic parameters were calculated in order to elucidate the interaction between the *VhChiP* and chitohexaose. The thermodynamic parameters were determined from the Van't Hoff equation to Eq. 5. Meanwhile, the free energy ( $\Delta G$ ) can be estimated with Eq. 6.

#### **2.5.2.8 Cloning and expression of OM-expressed *VhChiP***

Cloning, expression and purification of the native *VhChiP* were carried out following the protocol reported previously by Suginta *et al.* (2013b) with some modifications in the gel filtration step. Briefly, The *chip* gene with its native signal sequence was cloned into pET23d(+). The plasmid was transformed into the porin-deficient omp8 strain (*E. coli* BL21 DE3 Omp8 rosetta). The expression was induced by adding 0.4 mM IPTG at an OD<sub>600</sub> ~ 0.6 and the cells were incubated for 6



hours at 37 °C. After cell disruption, the membranes were spun down and incubated with 2% (w/v) SDS for one hour at 50 °C. Afterwards, the membranes were washed with 0.125% (v/v) octyl-POE and finally extracted with 3% (v/v) octyl-POE. Insoluble particles were centrifuged for 30 min at 45,000 rpm and the supernatant was loaded onto a HiPrep Mono Q anion exchange column. The column was washed with 10 column volumes (CV) 20 mM (Phosphate buffer) sodium phosphate and 0.2% (v/v) LDAO at pH 7.4. The protein was then eluted with a linear gradient of 0 – 1 M KCl. Fractions containing *VhChiP* were pooled and subjected to size exclusion chromatography using a HiLoad 16/600 Superdex 200 (GE Healthcare) using a constant flow rate of 0.5 mL min<sup>-1</sup>. The mobile phase used was made of 10 mM HEPES, 100 mM LiCl, and 0.4% (v/v) C<sub>8</sub>E<sub>4</sub>, with pH 7.5. The purified protein was concentrated to about 10 mg mL<sup>-1</sup> and directly flash-frozen into liquid nitrogen.

#### **2.5.2.9 Inclusion body expression of SeMet-labelled *VhChiP* and *in vitro* folding**

For expression of *VhChiP* into inclusion bodies, the gene without signal sequence and His-tag was cloned into pET28a via *NcoI* and *XhoI*. The plasmid was transformed into BL21 (DE3) cells. The cells were then grown in the minimal medium (LeMasters-Richards) to OD<sub>600</sub> ~0.6 at 37°C before SeMet in combination with lysine, phenylalanine, threonine, leucine, isoleucine and valine were added. Half an hour later the cells were induced with 1 mM IPTG at 37 °C for three hours. Cells were harvested by centrifugation at 4,000 rpm for 30 min (Beckman Coulter). After cell disruption, inclusion bodies were obtained by centrifugation at 20,000 rpm for 20 min (45 Ti rotor, Beckman). The inclusion bodies were then washed once in TBS including 1% TritonX-100 for 30 min and twice afterwards without Triton

X-100 at room temperature, followed by centrifugation for 20 min at 20,000 rpm after each step. Inclusion bodies were then solubilised in ~25 ml TBS including 8M urea for 2 hours at room temperature. Unsolubilised pellet was removed by centrifugation at 45,000 rpm for 30 min. For refolding, the supernatant was added dropwise with a syringe (~ 5 mL) to 200 ml of TBS including 3% Elugent (Calbiochem) and the folding reaction was incubated at room temperature overnight. The next morning, the refolded protein was loaded onto a 10 mL anion exchange column and purified as described above for the OM-expressed protein.

#### 2.5.2.10 Crystallisation and structure solution of *VhChiP*

Initial crystallisation trials for OM-expressed *VhChiP* were performed at 295 K by sitting-drop vapour diffusion using MemGold1- and MemGold2-Screen kits from Molecular Dimensions with a mosquito robot (TTP Labtech). The initial hits were optimised by fine-screening with larger drops by hanging drop vapour diffusion. Crystals in space group C2 were grown in 28% (w/v) PEG 400, 0.2 M sodium acetate and 0.1 M MES pH 6.5. Crystals were directly flash-frozen in liquid nitrogen. A data set was collected at IO2 at the Diamond Light Source (DLS), UK. SeMet crystals, derived from *in vitro* folded *VhChiP*, were obtained in two different crystal forms. Crystal form I in space group P2<sub>1</sub> was crystallised in 30% (w/v) PEG 400, 0.05 M NaCl and 0.1 M sodium citrate pH 5.5. Crystals in crystal form II were grown in 28% (w/v) PEG 400, 0.5 M potassium iodide and 0.1 M Tris pH 8.5. A SAD data set for crystal form I was collected to 1.95 Å at beamline IO2 at the Diamond Light Source (DLS), UK. Data were integrated and scaled with XDS. Initial phasing and modelling was done using AUTOSOL within PHENIX. Further model building was performed using WinCOOT. The protein model was refined with REFMAC.

Phases for OM-expressed *VhChiP* and *in vitro* folded *VhChiP* in crystal form II were obtained by molecular replacement using MOLREP with the refined structure of SeMet-*VhChiP* as a search model. Model building was performed using WinCOOT and the structure was refined with REFMAC. The programs MolProbity and PROCHECK were used to evaluate the final model and PyMOL (Schrödinger, LLC) for the visualisation of the protein structures.

For *VhChiP* complex structures, *in vitro* folded protein was co-crystallised with 10 mM chitohexaose in 34% (w/v) PEG 400, 0.05 M NaCl and 0.1 M sodium citrate pH 5.5. Accordingly, native expressed protein was co-crystallised with 10 mM chitohexaose in 18% (w/v) PEG 400, 0.2 M sodium acetate and 0.1 M MES pH 6.5. The structures were solved via MR as described above for the apo proteins.

#### **2.5.2.11 Single channel electrophysiology of *VhChiP***

Black lipid membrane (BLM) reconstitution was carried out in electrolyte containing 1 M KCl and 20 mM HEPES pH 7.5, at 25 °C following the protocol described elsewhere (Chumjan *et al.*, 2015; Schulte *et al.*, 2009). Solvent-free bilayer (Montal-Mueller type) formation was performed using 1, 2-diphytanoyl-sn-glycero-3-phosphatidylcholine (DPhPC; Avanti Polar Lipids, Alabaster, AL). First, the aperture was pre-painted with a few microliters of 1% (v/v) hexadecane in hexane, then a planar bilayer was formed across the aperture by lowering and raising the liquid level. Ionic currents were detected using Ag/AgCl electrodes with a patch-clamp amplifier connected to a two-electrode bilayer head-stage (PC-ONE plus PC-ONE-50; Dagan Corp., Minneapolis, MN, USA). The BLM setup was operated within a Faraday cage on a vibration-dampening table, with an A/D converter (LIH 1600, HEKA Elektronik,

Lambrecht, Germany) and was operated using the software PULSE program (HEKA Elektronik, Lambrecht, Germany). The electrodes immersed in 1M KCl electrolyte on the *cis* side of the cuvette were connected to ground, while the other electrode on the *trans* side was connected to the amplifier head-stage. *VhChiP* was always added to the *cis* side of the cuvette. Conductance values were extracted from the *I-V* curve obtained from the current flow of single channel insertion at different voltages.

To investigate sugar translocation, single channels of the *VhChiP* variants were reconstituted in the artificial lipid membrane as described earlier in Section 2.5.1.12. To prevent multiple insertions during data acquisition, the protein solution in the chamber was gently diluted after the first insertion by sequential additions of the working electrolyte. Then the fully open channel was titrated with distinct concentrations from 0.1 – 10  $\mu\text{M}$  of chitohexaose. Each sugar was added to the *cis* side of the chamber. Fluctuations of ion flow were observed as a result of sugar diffusion through the reconstituted channel. This fluctuation traces were usually recorded for 2 min at different transmembrane potentials. The equilibrium binding constant  $K$  ( $\text{M}^{-1}$ ) was estimated from the decrease in the ion conductance in the presence of increasing concentrations of sugar using the following equation 1.

#### 2.5.2.12 Liposome swelling experiments

*VhChiP*-reconstituted proteoliposomes were prepared as described elsewhere (Suginta *et al.*, 2013a). Soybean *L*- $\alpha$ -phosphatidylcholine (20 mg  $\text{mL}^{-1}$ , freshly prepared in chloroform) (Sigma-Aldrich) was used to form multi-lamellar liposomes. For the preparation of proteoliposomes, 200 ng of *VhChiP* was reconstituted into 200  $\mu\text{L}$  of the liposome suspension by sonication, and then 17% (w/v) dextran (40 kDa) was entrapped in the proteoliposomes. *D*-Raffinose solutions were prepared in

phosphate buffer to obtain concentrations of 40, 50, 60, and 70 mM, for the determination of isotonic solute concentration. This value was then used for the adjustment of the isotonic concentration for other solutes. To carry out a liposome-swelling assay, 25  $\mu\text{L}$  of the proteoliposome suspension was added to 600  $\mu\text{L}$  of sugar solution and changes in absorbance at 500 nm were monitored immediately. The apparent absorbance change over the first 60 s was used to estimate the swelling rate ( $\text{s}^{-1}$ ) following the Eq. 7:

$$\phi = (1/A_i)dA/dt \quad \text{Eq. 7}$$

In which  $\phi$  is the swelling rate,  $A_i$  the initial absorbance, and  $dA/dt$  the rate of absorbance change during the first 60 s. The swelling rate for each sugar was normalised by setting the rate of *L*-arabinose (150 Da), the smallest sugar, to 100%. The values were presented as the averages from three to five independent determinations. Protein-free liposomes and proteoliposomes without sugars were used as negative controls. The sugars tested were *D*-glucose (180 Da), *D*-mannose (180 Da), *D*-galactose (180 Da), *N*-acetylglucosamine (GlcNAc) (221 Da), *D*-sucrose (342 Da), *D*-melezitose (522 Da), (GlcNAc)<sub>2</sub> (424 Da), (GlcNAc)<sub>3</sub> (628 Da), (GlcNAc)<sub>4</sub> (830 Da), (GlcNAc)<sub>5</sub> (1034 Da), (GlcNAc)<sub>6</sub> (1237 Da) and maltodextrins.

## CHAPTER III

### RESULTS

#### **Part I: Outer membrane protein (*BpsOmp38*) from *Burkholderia pseudomallei***

##### **3.1 Functional and mutational effects of Tyr119 *BpsOmp38***

###### **3.1.1 Antimicrobial susceptibility of *Burkholderia pseudomallei***

Levels of antibiotic resistance of a clinically-derived *B. pseudomallei* strain were investigated using the twofold serial broth microdilution method. When compared with the most recently updated breakpoints recommended for *Pseudomonas spp.* by EUCAST (Table 3.1), most antimicrobial agents tested against *B. pseudomallei* had MIC (minimum inhibitory concentration) values higher than the breakpoint values for resistance. Ceftazidime and meropenem are the only two antibiotics with MIC values lower than the breakpoint values, indicating that this *B. pseudomallei* strain is sensitive to these two antibiotics.

**Table 3.1 Antibiotic susceptibility of a clinically derived strain of *Burkholderia pseudomallei*.**

Antibiotic	Breakpoint for resistance <sup>a</sup>		MIC value( $\mu\text{g mL}^{-1}$ )	
	S $\leq$	R $>$	-PA $\beta$ N	+PA $\beta$ N
<b><i>Penicillin</i></b>				
Penicillin G	$\leq 16$	$> 16$	1024 <sup>R</sup>	1024 <sup>R</sup>
Amoxicillin	-	-	256	256
<b><i>Cephalosporin</i></b>				
Cefoxitin	NA	NA	1024	1024
Ceftazidime	$\leq 8$	$> 8$	2 <sup>S</sup>	2 <sup>S</sup>
Cefepime	$\leq 8$	$> 8$	512 <sup>R</sup>	512 <sup>R</sup>
<b><i>Carbapenem</i></b>				
Meropenem	$\leq 2$	$> 8$	4 <sup>S</sup>	4 <sup>S</sup>
Imipenem	$\leq 4$	$> 8$	8	8
Doripenem	$\leq 1$	$> 2$	$> 2048^{\text{R}}$	$> 2048^{\text{R}}$
<b><i>Fluoroquinolone</i></b>				
Norfloxacin	-	-	8	8
Ciprofloxacin	$\leq 0.5$	$> 1$	4 <sup>R</sup>	4 <sup>R</sup>
<b><i>Quinolone carboxylic acid</i></b>				
Enrofloxacin	-	-	4	4
<b><i>Sulfonamide-trimethoprim</i></b>				
Co-trimoxazole	4	4	128 <sup>R</sup>	128 <sup>R</sup>
<b><i>Aminoglycoside</i></b>				
Kanamycin	-	-	16	16
Gentamicin	$\leq 4$	$> 4$	32 <sup>R</sup>	32 <sup>R</sup>

The values presented are obtained from the experiments performed 4 – 6 times.

<sup>a</sup>Breakpoints defined for *Pseudomonas spp.* follow the EUCAST Clinical Breakpoint Table v. 4.0, valid from 2014-01-01 (Wikler, 2006). R, Resistant; S, Sensitive; NA, Not applicable; -, No breakpoints. Susceptibility testing is not recommended. In order to simplify the EUCAST tables, the intermediate category is not listed.

Statistical analysis of the data in Table 3.1 was carried out as shown in Table 3.2. Log<sub>2</sub> dilution analysis for each antimicrobial agent in the absence and presence of PAβN gave MIC values that are in complete agreement within  $\pm 2$  log<sub>2</sub> dilution, and with  $\geq 92\%$  agreement within  $\pm 1$  log<sub>2</sub> dilution. For most antimicrobial agents, 67 – 100% of MIC values are the same (log<sub>2</sub> dilution difference = 0). The only exceptions are imipenem and ciprofloxacin, where their essential agreements within the same concentration are 50%, and 58%, respectively. Additionally, the significance of antimicrobial susceptibility of *B. pseudomallei* was evaluated using one-way ANOVA. The results of analysis showed *p*-values  $> 0.05$  with all the tested antimicrobial agents, showing that there is no significant difference between MIC values determined in the presence and absence of PAβN.

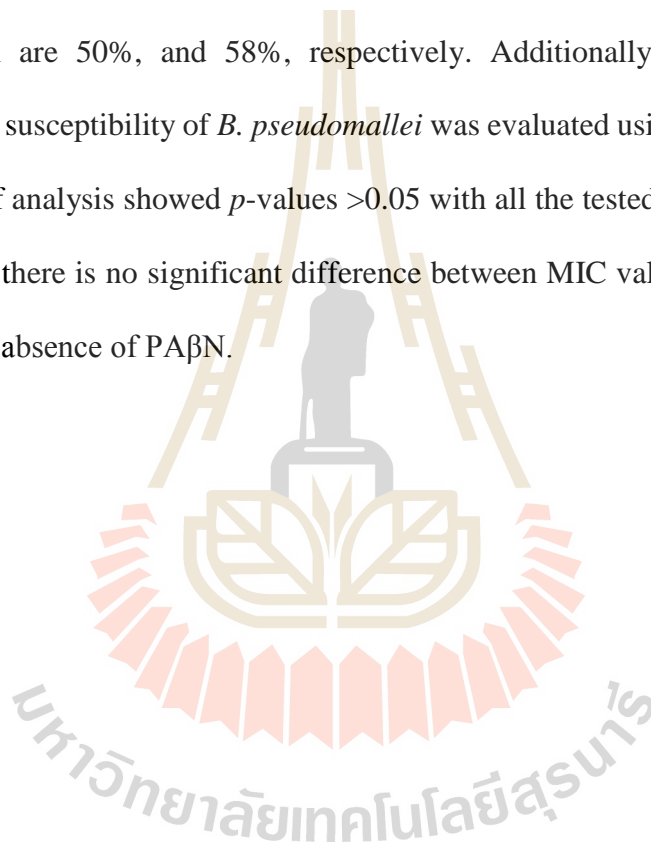




**Table 3.2** Statistical analysis of MIC values of *Burkholderia pseudomallei* by one-way ANOVA and log<sub>2</sub> dilution methods.

Antibiotic	N <sup>a</sup>	ANOVA analysis	Log <sub>2</sub> dilution analysis					% Agreement <sup>c</sup>		
			Distribution of MIC values Within ±log <sub>2</sub> dilution					Same	±1	±2
		p-value	-2	-1	0	1	2			
<b>Penicillin</b>										
Penicillin G	12	0.673(NS) <sup>b</sup>	0	1	11	0	0	92	100(NS)	100(NS)
Amoxycillin	12	1.000(NS)	0	1	9	2	0	75	100(NS)	100(NS)
<b>Cephalosporin</b>										
Cefoxitin	12	0.7728(NS)	0	3	9	0	0	75	100(NS)	100(NS)
Ceftazidime	12	1.000(NS)	0	3	8	1	0	67	100(NS)	100(NS)
Cefepime	12	0.5862(NS)	0	2	9	1	0	75	100(NS)	100(NS)
<b>Carbapenem</b>										
Meropenem	12	0.7728(NS)	0	0	9	3	0	75	100(NS)	100(NS)
Imipenem	12	0.1736(NS)	1	2	6	3	0	50	92(NS)	100(NS)
Doripenem	12	0.7728(NS)	0	3	9	0	0	75	100(NS)	100(NS)
<b>Fluoroquinolone</b>										
Norfloxacin	12	1.000(NS)	1	2	8	1	0	67	92(NS)	100(NS)
Ciprofoxacin	12	0.1250(NS)	1	2	7	2	0	58	92(NS)	100(NS)
<b>Quinolone carboxylic acid</b>										
Enrofloxacin	12	1.000(NS)	1	3	8	0	0	67	92(NS)	100(NS)
<b>Sulfonamide-trimethoprim</b>										
Cotrimoxazol	12	0.7728(NS)	0	0	9	3	0	75	100(NS)	100(NS)
<b>Aminoglycoside</b>										
Kanamycin	12	1.000(NS)	1	3	8	0	0	67	92(NS)	100(NS)
Gentamicin	12	0.7500(NS)	1	1	9	1	0	75	92(NS)	100(NS)

<sup>a</sup>N is the total number of samples used for both analyses. Two equal-sized sampling groups (each group, n = 6) were used, in the absence and presence of PABN.

<sup>b</sup>NS represents non-significant difference between the two studied groups at  $p < 0.05$ .

<sup>c</sup>NS represents non-significant difference between the two studied groups at essential agreement  $\geq 85\%$  (Marley *et al.*, 1995).

### 3.1.2 Recombinant expression, purification and protein identification of *BpsOmp38*

The *omp38* gene, previously cloned in our lab with signal sequence in pGEM-T easy vector, namely pGEM-T easy/*BpsOmp38*, was used as the DNA template for PCR amplification. Both the oligonucleotides 5' TACCATGGCAAATAAGACTGATTGTTG 3' (forward primer) and 5' TACTCGAGGAAACGTGACGCAGACC 3' (reverse primer) were used for PCR amplification. The PCR product was of the expected size, about 1.12 kbp (Figure 3.1A), and was then cloned into pET23d(+) vector using *NcoI* and *XhoI* cloning sites (sequences underlined) following the protocol supplied by the manufacturer. After that, the success of gene cloning was checked by PCR amplification using the same set of oligonucleotides as shown above (Figure 3.1B) and by enzyme double digestion with *NcoI* and *XhoI* restriction enzymes (Figure 3.1C). Nucleotide sequences of sense and anti-sense strands of the cloned fragment were also determined by automated sequencing (First BASE Laboratories Sdn Bhd, Selangor Darul Ehsan, Malaysia).

After the correct nucleotide sequence was confirmed, the full-length *BpsOmp38* DNA obtained from PCR amplification was cloned into pET23d(+) expression vector, which was ready to be expressed in *E. coli* BL21(DE3) Omp8 Rosetta strain. The recombinant protein was expressed with the 20-amino acid signal sequence attached, to aid protein targeting to the bacterial cell wall and with the His<sub>6</sub>-tag at C-terminus to aid protein purification. After proteolytic removal of the signal sequence, the mature *BpsOmp38* contains 360 amino acid residues and has a predicted MW of 37,986.38 Da.

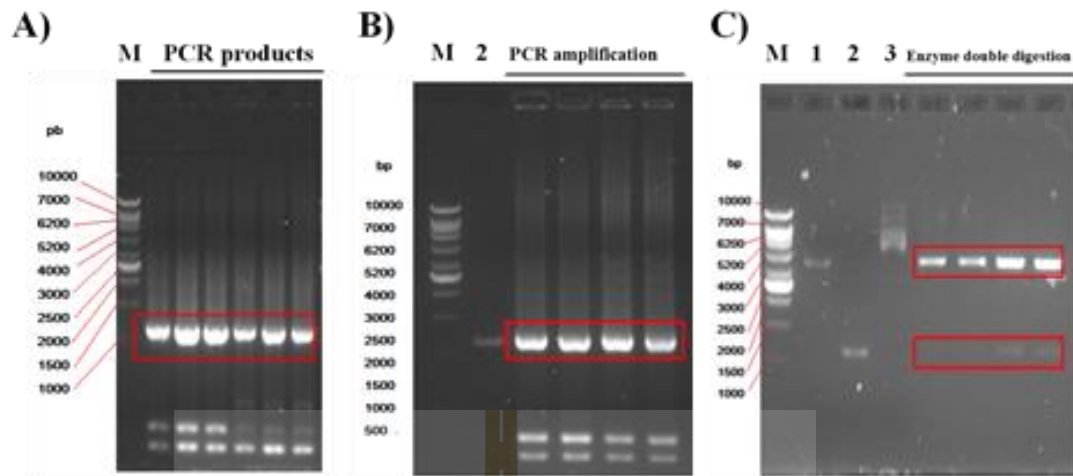


**Figure 3.1** Agarose gel electrophoresis of recombinant DNA and SDS-PAGE of *BpsOmp38* protein (A) PCR products amplified from pGEM-T easy/*BpsOmp38*. (B) Check of ligation by DNA amplification: pET23d(+)/*BpsOmp38* recombinant plasmid. (C) Check of ligation by enzyme double digestion (*NcoI* and *XhoI*) pET23d(+)/*BpsOmp38* recombinant plasmid. DNA marker (M), pET23d(+) vector (1), *BpsOmp38* DNA fragment (2) and pET23d(+)/*BpsOmp38* recombinant non-digest (3).

The SDS-PAGE analysis displayed the corresponding protein band migrating to between 35 and 45 kDa. Figure 3.2A shows further cell induction by 0.5 mM IPTG for 6 h, the fraction containing enriched *BpsOmp38* and Figure 3.2B following 2% (v/v) SDS, 0.125% (v/v), and then 3% (v/v) octyl-POE in 20 mM phosphate buffer (pH 7.4), the solubilised fraction containing enriched *BpsOmp38*.

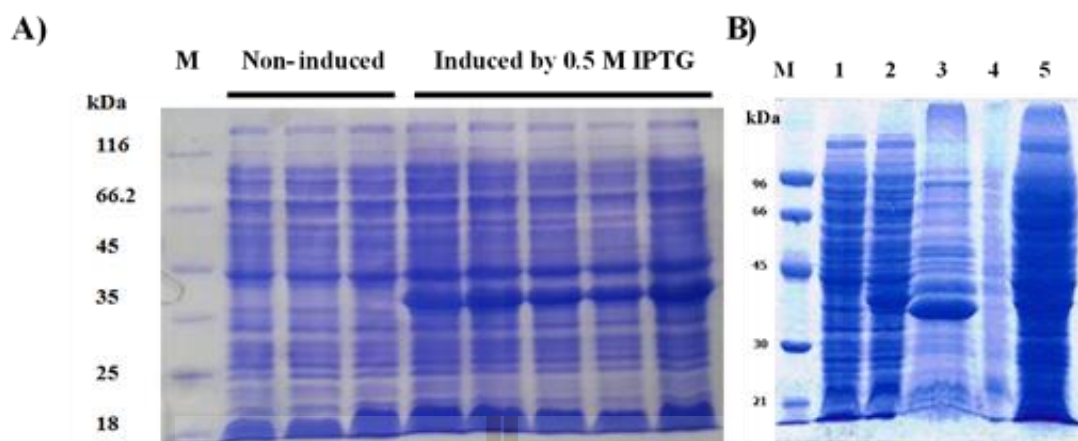


**Figure 3.2** (A) SDS-PAGE of cell non-induction and cell induction by 0.5% IPTG. (B) Outer membrane proteins extracted with 2% (w/v) SDS (lane 5), followed by 3% (v/v) octyl-POE (lane 3), the pellet after 3% octyl-POE extraction (lane 4), compared with cell non-induction (lane 1) and cell induction (lane 2).

In this work, the *BpsOmp38* expression system was improved by re-cloning the gene encoding *BpsOmp38*, including the endogenous signal sequence to allow the recombinant protein to insert into the *E. coli* cell wall. The protein was then purified from the membrane fraction of the disrupted cells. Site-directed mutagenesis was carried out to investigate the importance of Tyr119 in regulating channel permeability. In the modelled 3D-structure, this residue is part of a short right-handed  $\alpha$ -helix (Tyr119→Leu126) that precedes the longest loop 3 (L3) and its side chain is situated in the lumen of *BpsOmp38*. Tyr119 may therefore be involved in controlling the passage of hydrophilic molecules through the *BpsOmp38* pore. Figure 3.3 is a ribbon model of *BpsOmp38*<sup>WT</sup>, showing the sidechain of Tyr119 protruding into the centre of the pore (Figure 3.3A). Figures 3.3B and 3.3C show the same view of the

*BpsOmp38*WT pore, with Y119 virtually mutated to alanine and phenylalanine, respectively. Amino acid substitution of *BpsOmp38* generated two single mutants, *BpsOmp38*Y119A and *BpsOmp38*Y119F, which differed in the properties of the sidechains at position 119. Alanine is small and non-polar, whereas phenylalanine is aromatic and hydrophobic.

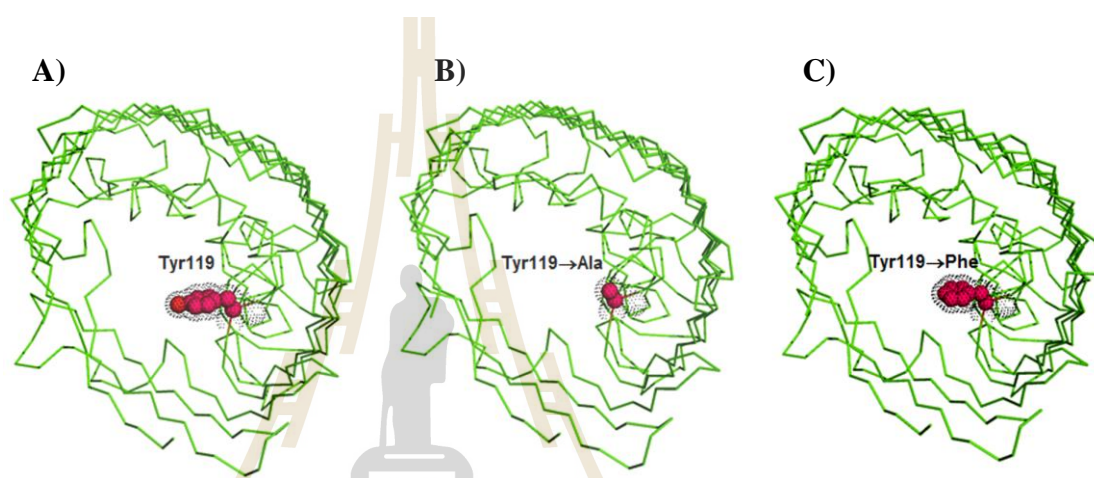


**Figure 3.3** A ribbon representation of the homology model of *BpsOmp38*. The modeled structure of *BpsOmp38*WT (A) shows the key residue Y119 (red) protruding into the channel lumen (top view). This residue was mutated to Ala or Phe, generating two single mutants, *BpsOmp38*Y119A (B) and *BpsOmp38*Y119F (C).

The recombinant *BpsOmp38* was expressed as a His<sub>6</sub>-tagged polypeptide, which accumulated in the cell walls of the *E. coli* host. For purification, the peptidoglycan fraction was first extracted with the detergent octyl-POE and the soluble extract, containing *BpsOmp38*, was subjected to affinity chromatography, and then to ion exchange chromatography as described in Materials and Methods. Bound

*BpsOmp38* was eluted from the Hitrap SP HP ion exchange column with an applied gradient of 0 – 1 M KCl. The elution profile of the recombinant *BpsOmp38*WT is shown in Figure 3.4A. Figure 3.4B shows a Coomassie blue-stained SDS-polyacrylamide gel, in which purified *BpsOmp38* variants migrated as single bands to slightly below 42 kDa. Figure 3.4C shows an immunoblot of the corresponding protein bands, detected with anti-*BpsOmp38* polyclonal antiserum. Only *BpsOmp38*WT (lane 1), *BpsOmp38*Y119A (lane 2), *BpsOmp38*Y119F (lane 3) and the refolded *BpsOmp38* from our previous expression and purification protocol (lane 4) reacted strongly with the *BpsOmp38* antiserum. Note that the *BpsOmp38* antiserum also cross-reacted with a protein band identified as *E. coli* OmpN (lane 6), but not with *E. coli* OmpF (lane 5) or *V. harveyi* chitoporin or ChiP (lane 7). When an immunoblot identical to that in Figure 3.4B was probed with anti-His<sub>6</sub> monoclonal antibody (Figure 3.4D), only the protein bands in the first three lanes were labeled, while the other proteins, which lack His<sub>6</sub>-tags, failed to react with the antibody. These results confirmed that the proteins expressed by the Omp-deficient *E. coli* host are *BpsOmp38*.

To confirm that the expressed and purified protein was *BpsOmp38*, tryptic peptides were generated from the purified fraction and analysed by mass spectrometry (First BASE Laboratories Sdn Bhd, Selangor Darul Ehsan, Malaysia). A MASCOT database search identified 11 peptides (three of which were redundant) that were identical to the internal sequences of an outer membrane porin from *B. pseudomallei* type strain 1655 (gene id. BURPS1655\_I0506) (Table 3.3). These internal peptide sequences, labelled P1 – P8, are shown in Figure 3.3E and provide 25% coverage of the putative *BpsOmp38* sequence identified previously (Siritapetawee *et al.*, 2004b).

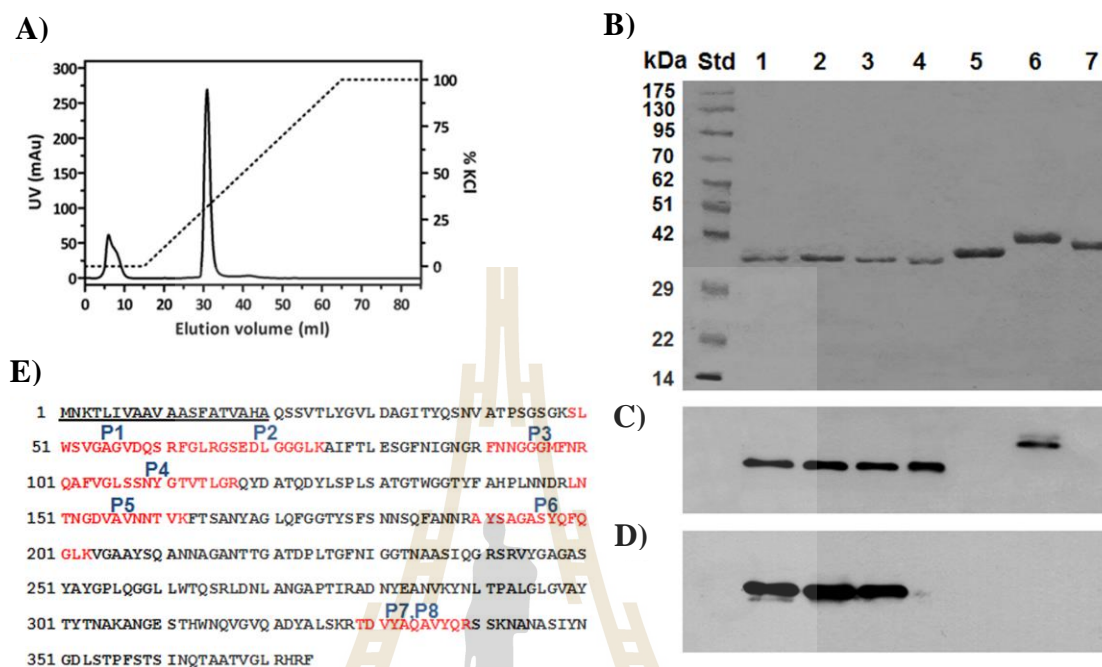


**Figure 3.4** Purification, immunodetection, and mass analysis of the *BpsOmp38* variants, expressed in *E. coli*. (A) Chromatographic profile of *BpsOmp38* purification with a Hitrap SP HP column. The protein was eluted with a linear gradient of 0 – 1 M KCl; (B) SDS/PAGE followed by Coomassie Blue staining; (C) immunoblot analysis of the same samples as in panel B, using polyclonal anti-*BpsOmp38* serum; (D) immunoblot analysis using anti-His<sub>6</sub> monoclonal antibody; and (E) identification of tryptic digests of the expressed proteins by nanoLC/ESI MS. Eight peptides, designated P1 – P8 and shown in red, were unambiguously identified by MASCOT as identical to internal sequences of *BpsOmp38*. The 20-amino acid signal peptide is underlined. Lanes: Std, standard proteins; 1, *BpsOmp38*WT; 2, *BpsOmp38*Y119A; 3, *BpsOmp38* mY119F; 4, refolded *BpsOmp38*; 5, *E. coli* OmpF; 6, *E. coli* OmpN; and 7, *V. harveyi* ChiP.

**Table 3.3 Identification of tryptic peptides by nano LC/ESIMS.**

After submission of the isotopic masses to a MASCOT database search, eight peptides were identified to be unambiguously compatible with the internal peptides of an outer membrane porin from *Burkholderia pseudomallei* 1655 (gene id. BURPS1655\_I0506).

Peptide no*	Start	–	End	Observed	Charge	$M_r$ (expt)	$M_r$ (calc)	Peptide
1	49	–	61	454.4741	+3	1360.4003	1360.6735	K.SLWSVGAGVDQSR.F
1	49	–	61	1362.1779	+1	1361.1706	1360.6735	K.SLWSVGAGVDQSR.F
2	62	–	75	469.4582	+3	1405.3528	1404.7361	R.FGLRGSEDLGGGLK.A
3	91	–	100	565.2778	+2	1128.5410	1128.4771	R.FNNGGGMFNR.Q + Oxidation (M)
4	101	–	117	590.5537	+3	1768.6394	1768.9108	R.QAFVGLSSNYGTVTLGR.Q
5	149	–	162	730.2538	+2	1458.4930	1457.7474	R.LNTNGDVAVNNTVK.F
5	149	–	162	1459.8120	+1	1458.8047	1457.7474	R.LNTNGDVAVNNTVK.F
6	190	–	203	745.9739	+2	1489.9333	1489.7201	R.AYSAGASYQFQGLK.V
7	328	–	339	735.4683	+2	1468.9220	1468.7423	K.RTDVYAQAVYQR.S
7	328	–	339	735.5847	+2	1469.1548	1468.7423	K.RTDVYAQAVYQR.S
7	328	–	339	490.9310	+3	1469.7713	1468.7423	K.RTDVYAQAVYQR.S
8	329	–	339	657.4061	+2	1312.7977	1312.6412	R.TDVYAQAVYQR.S

\*Numbers of peptides identified by MS/MS are labeled. Peptides with identical sequences are assigned the same number.



### 3.1.3 Effects of Tyr119 mutations on antimicrobial properties

Susceptibility of the *E. coli* expressing *BpsOmp38* MIC values, of the *E. coli* (Omp8) Rosetta strain expressing *BpsOmp38*WT and of the *E. coli* strain harboring an empty pET23d(+) vector (control *E. coli*) were compared. Table 3.4 shows that *E. coli* harboring pET23d(+) with and without *BpsOmp38* DNA insert had very high MIC values for penicillin G and amoxicillin ( $>2,048 \mu\text{g mL}^{-1}$ ). However, when clavulanic acid, a known suicide inhibitor of  $\beta$ -lactamases (<http://www.drugbank.ca/drugs/DB00766>), was included in the culture medium, their MIC values were dramatically reduced to  $32 \mu\text{g mL}^{-1}$  (Table 3.4, values in brackets). Apart from the penicillin class, for most antimicrobial agents, the MIC values against *E. coli* expressing *BpsOmp38* were one dilution higher than MIC values against control *E. coli*. Comparing the three *E. coli* expressing *BpsOmp38* variants, MIC values for the *BpsOmp38*Y119A mutant were significantly lower than the WT values, particularly for the cephalosporins (ceftazidime and cefoxitin), and the carbapenems (meropenem and imipenem). For the *E. coli* expressing *BpsOmp38*Y119F mutant, MIC values were significantly decreased for ceftazidime and gentamicin, while an increase in MIC value was seen only with doripenem. For the other agents, their MIC values for *BpsOmp38*Y119F and WT were equal.

**Table 3.4** Antimicrobial susceptibility of Omp-deficient *E. coli* expressing *BpsOmp38* variants.

Antibiotic	N	MIC( $\mu\text{g mL}^{-1}$ )				% Agreement within $\pm 1 \log_2$ dilution		
		Control	WT	Y119A	Y119F	Control vs. WT	WT vs. Y119A	WT vs. Y119F
<b>Penicillin</b>								
Penicillin G	10	>2048(16) <sup>a</sup>	>2048(32)*	>2048(16)**	>2048(16)**	100	80**	80**
Amoxicillin	10	>2048(32)	>2048(32)	>2048(32)	>2048(32)	100	90	100
<b>Cephalosporin</b>								
Ceftazidime	10	0.5	1*	0.5**	0.5**	80*	80**	80**
Cefoxitin	10	2	4**	2**	4	90	100	100
Cefepime	10	0.125	0.125	0.25	0.125	100	100	100
<b>Cabepenem</b>								
Meropenem	10	0.25	0.25	0.125**	0.25	100	100	100
Imipenem	10	2	4*	2**	2	90	100	100
Doripenem	10	128	256*	512	512**	100	100	90
<b>Fluoroquinolone</b>								
Norfloxacin	10	0.0625	0.125	0.125	0.125	100	100	100
Ciprofloxacin	10	$\leq 0.03125$	$\leq 0.03125$	$\leq 0.03125$	$\leq 0.03125$	100	100	100
<b>Quinolone carboxylic acid</b>								
Enrofloxacin	10	$\leq 0.03125$	$\leq 0.03125$	$\leq 0.03125$	$\leq 0.03125$	100	100	100
<b>Sulfonamide-trimethoprim</b>								
Co-trimoxazol	10	1	2	2	1	100	100	100
<b>Aminoglycoside</b>								
Kanamycin	10	256	512	512	256	100	100	100
Gentamicin	10	0.25	2**	1	0.5**	50**	80**	70**

Two statistical methods (ANOVA and  $\log_2$  dilution) were used to evaluate the significance of their MIC values. Difference between the two studied groups is statistically significant with  $p < 0.05$  using ANOVA analysis or with  $\geq 85\%$  essential agreement using  $\log_2$  dilution analysis.

<sup>a</sup>Value in brackets is the MIC value when grown in the presence of antibiotic and clavulanic acid, a  $\beta$ -lactamase inhibitor.

\*Significantly different MIC values for *E. coli* expressing *BpsOmp38* WT and control *E. coli*.

\*\*Significantly different MIC values for *E. coli* expressing *BpsOmp38* WT and *E. coli* expressing *BpsOmp38*Y119A or *BpsOmp38*Y119F.

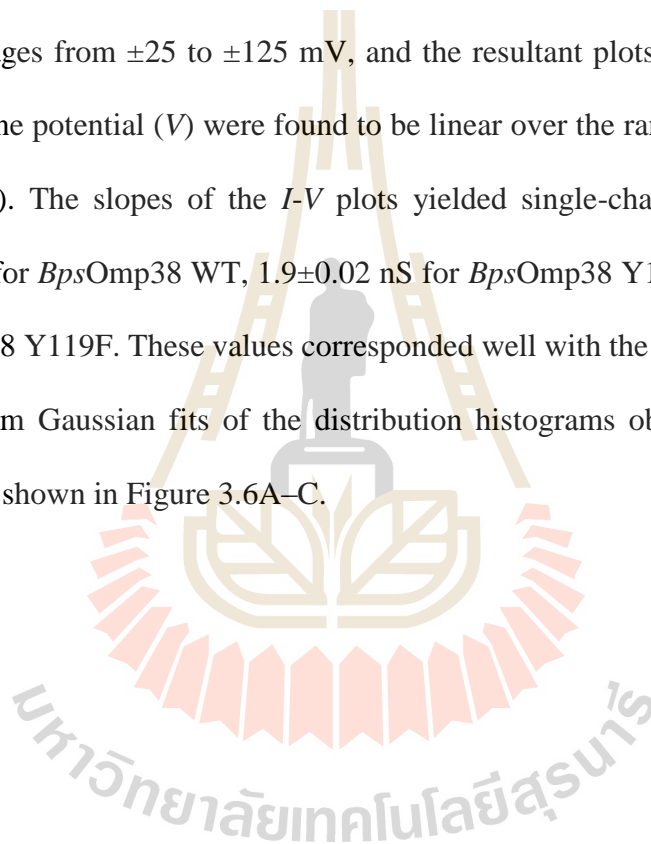
### 3.1.4 Effects of Tyr119 mutations on the pore conductance of the *BpsOmp38* channel

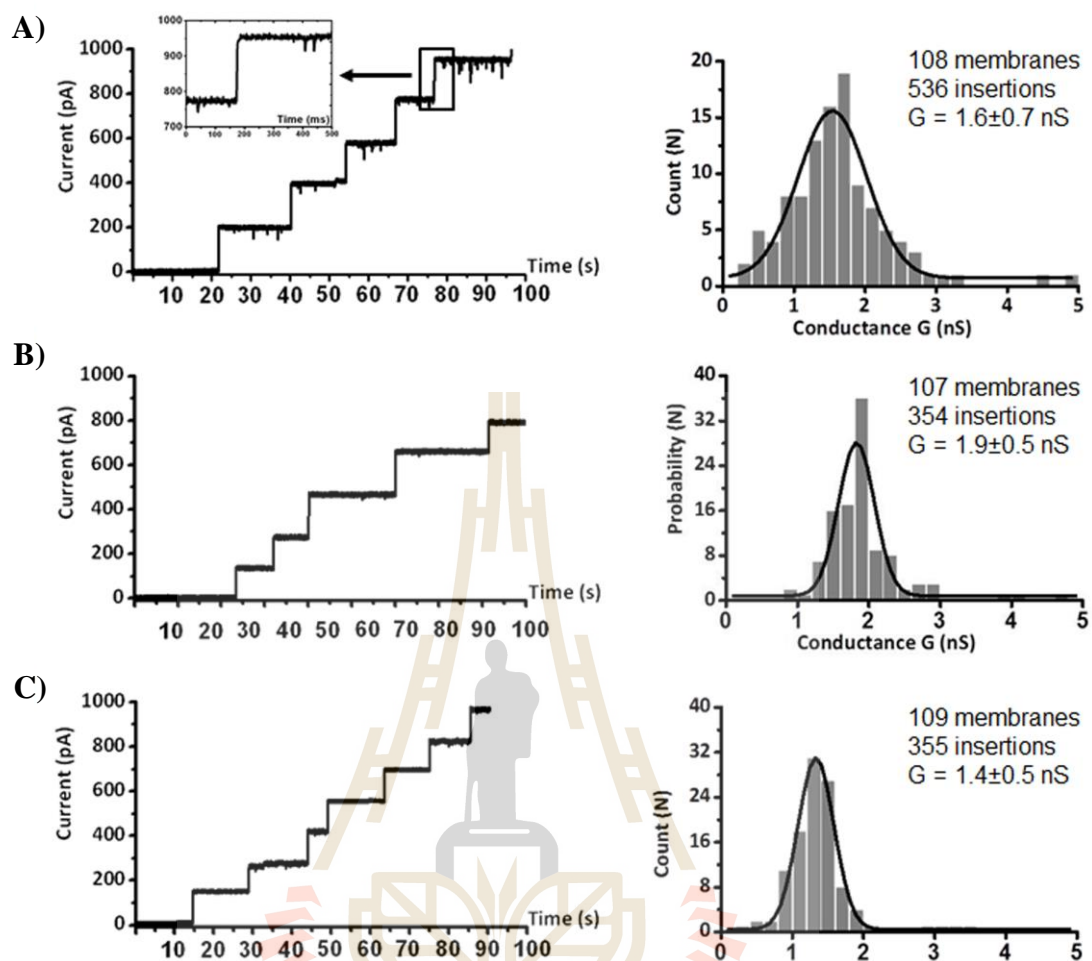
The channel-forming properties of the recombinant *BpsOmp38* was further investigated using the black lipid membrane (BLM) reconstitution technique. The purified protein was reconstituted into a freshly-formed phospholipid (azolectin) bilayer following addition on the cis (ground) side, the two sides of the chamber were filled with equal volumes of 1M KCl, 20 mM pH 7.5 phosphate buffer. Insertions of *BpsOmp38* channel were induced by applying potentials of  $\pm 200$  mV across the 200  $\mu\text{m}$  diameter aperture. Employing the solvent-containing (so-called 'painting') BLM technique, multiple channels of the wild-type *BpsOmp38* were frequently inserted (Figure 3.5A, left panel) in a stepwise fashion until the ionic current reached 1 nA, beyond which current signals exceeded the limit of detection by the Dagan amplifier of the BLM setup.

Figure 3.5A (right panel) is a histogram analysis, showing the statistical distribution of pore conductance averaged over 108 membranes and 535 channel insertions at +100 mV. For the wild-type channel (*BpsOmp38* WT), the average conductance was estimated to be  $1.6 \pm 0.7$  nS. Figure 3.4B (left panel) shows a typical insertion profile of the *BpsOmp38* Y119A mutant. Substitution of Tyr119 with alanine increased the ionic conductance of the *BpsOmp38* channel to  $1.9 \pm 0.5$  nS (Figure 3.4B, right panel), whereas substitution with phenylalanine (*BpsOmp38* Y119F mutant, Figure 3.5C, left panel) decreased it to  $1.4 \pm 0.5$  nS (Figure 3.5C, right panel). Although the Dagan BLM set up was not convenient for single channel measurement, insertion of a single *BpsOmp38* molecule into the lipid bilayer could be achieved when

protein at a very low concentration ( $<20 \text{ ng mL}^{-1}$ ) was added into the cis chamber, allowing data acquisition from a single channel.

Figure 3.6A shows the data traces from the insertion of single *BpsOmp38* WT, *BpsOmp38* Y119A and *BpsOmp38* Y119F channels. The results confirmed that the conductance of the WT channel was lower than that of the Ala mutant, but higher than that of the Phe mutant. Ionic currents were also recorded at discrete voltages from  $\pm 25$  to  $\pm 125$  mV, and the resultant plots of ion current ( $I$ ) vs. transmembrane potential ( $V$ ) were found to be linear over the range  $-100$  to  $+125$  mV (Figure 3.6B). The slopes of the  $I$ - $V$  plots yielded single-channel conductances of  $1.6 \pm 0.03$  nS for *BpsOmp38* WT,  $1.9 \pm 0.02$  nS for *BpsOmp38* Y119A and  $1.4 \pm 0.05$  nS for *BpsOmp38* Y119F. These values corresponded well with the average conductances estimated from Gaussian fits of the distribution histograms obtained from multiple insertions, as shown in Figure 3.6A–C.





**Figure 3.5** Ion current recordings obtained by the black lipid membrane (BLM) reconstitution technique. BLM measurements of successive insertions of *BpsOmp38* trimers was conducted at a transmembrane potential of +100 mV. Lipid bilayers were formed across a 200- $\mu$ m aperture by the ‘painting’ technique using 50 mg mL<sup>-1</sup> azolectin in *n*-hexane and bathed on either side in 1 M KCl. *BpsOmp38* (1  $\mu$ g mL<sup>-1</sup>) was added on the cis side. (A) *BpsOmp38* WT, (B) *BpsOmp38* Y119A, and (C) *BpsOmp38* Y119F. Left panels are ion current traces acquired for 100 s. Fast insertion of one *BpsOmp38* WT channel, occurring within millisecond

time-resolution, was captured and shown as an inset. The traces represent multiple insertions of *BpsOmp38* variants produced by an applied membrane potential of +100 mV. Right panels are the histogram representations of the corresponding traces, giving the probability of a pore conductance ( $G$ ) averaged over several hundred inserting channels as indicated. The black line represents a single Gaussian fit.

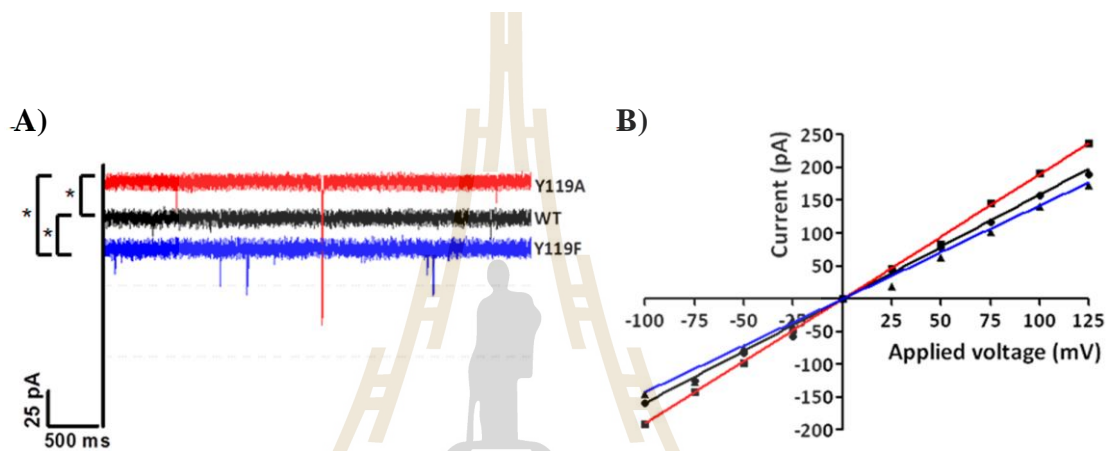


**Figure 3.6** Single channel recordings of *BpsOmp38* porin in artificial lipid membrane. A) Typical ion current traces of single *BpsOmp38* variant channels in a fully open state at a transmembrane potential of +100 mV, (B) Current-voltage relationship of *BpsOmp38* WT in comparison with its two mutants. The current through a single open *BpsOmp38* channel was monitored in 1 M KCl, followed by discrete changes in the voltage across the phospholipid membrane, from  $-100$  to  $+125$  mV. The slopes of a linear fit yielded the single channel conductances of individual *BpsOmp38* channels. Differences in the three data sets were evaluated using one-way ANOVA. Statistically significant difference ( $p < 0.05$ ) is shown with an asterisk (\*).

### 3.1.5 Effects of Tyr119 mutation of sugar and antibiotic permeability of *BpsOmp38*

The involvement of the Tyr119 residue in sugar permeability was further demonstrated (Figure 3.7). The liposome swelling assay showed that the rate of swelling of *BspOmp38*-reconstituted liposomes, a measure of the rate of sugar permeation, decreased as the molecular size of sugar increased (Figure 3.7A). The rates are presented relative to that of the smallest sugar (*L*-arabinose). The permeation rates of the selected neutral sugars were in the order: *L*-arabinose (MW 150) > *D*-galactose  $\approx$  *D*-glucose  $\approx$  *D*-mannose (MW 180) > *D*-GlcNAc (MW 221) > *D*-sucrose (MW 342). Low permeation was observed in the case of *D*-melezitose (MW 522) or *D*-raffinose (MW 504) which have molecular sizes close to the exclusion limit of *BpsOmp38*. Figure 3.6B shows that the logarithm of the permeation rate was linearly proportional to the molecular weight of the sugars. Figures 3.6A and B show that the permeation rates with *BpsOmp38* Y119A were significantly higher, while the rates with *BpsOmp38* Y119F were lower than those with the wild-type.

Since expression of *BpsOmp38* has affected the susceptibility of *E. coli* to cephalosporins and carbapenems, the permeability of these antibiotics through the three *BpsOmp38* variants were also investigated. For cephalosporins, the permeation rates of ceftazidime, to which *B. pseudomallei* is sensitive, and those of cefoxitin and cefepime, to which *B. pseudomallei* is resistant were compared. Similarly for carbapenems, the penetration rates of imipenem and meropenem, to which *B. pseudomallei* is sensitive, and that of doripenem, to which it is resistant were compared. The liposome swelling assays were performed at pH 7.5, to ensure that permeation occurred under physiological conditions. At this pH the net charge on the carbapenems

and one of the cephalosporins (cefepime) is 0, while ceftazidime and cefoxitin have a net charge of  $-1$  (Irwin *et al.*, 2012). Figure 3.8 shows a relatively high rate of permeation rate of ceftazidime and relatively lower permeation rates of meropenem and imipenem through *BpsOmp38* WT. On the other hand, the apparent permeation rates of cefoxitin, cefepime and doripenem are negative, indicating shrinkage of the liposomes, and therefore the antibiotics were impermeant. The permeation of cephalosporin and carbapenem antibiotics through *BpsOmp38* mutant channels was also investigated. The *BpsOmp38* Y119A mutant showed higher permeability than *BpsOmp38* WT towards the antimicrobial agents tested, while the permeability was dramatically decreased in case of the *BpsOmp38* Y119F mutant.

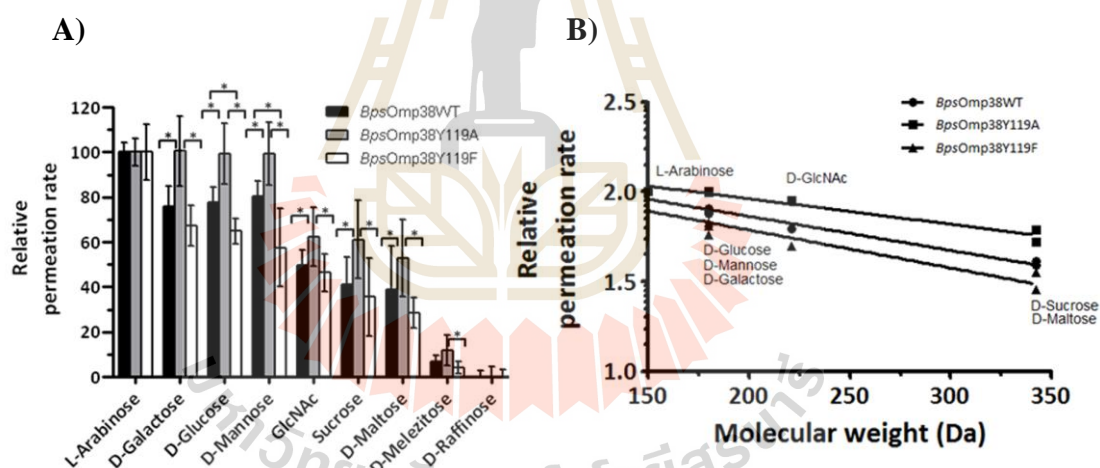


**Figure 3.7** Swelling of *BpsOmp38*-containing proteoliposomes, induced by neutral sugars. For each preparation, multilamellar liposomes were reconstituted with 200 ng of purified *BpsOmp38*. The isotonic concentration was defined as the concentration of *D*-raffinose that caused no change in the absorbance at 500 nm of the proteoliposome suspension, over a period of 60 s. (A) Permeation of different types of sugars through *BpsOmp38* reconstituted liposomes. Each swelling rate was normalised to the rate



of swelling in arabinose, which was set to 100%. (B) Semilogarithmic plot of relative permeation rates of sugars through the proteoliposomes reconstituted with *BpsOmp38* WT and other mutants. The logarithm of the permeation rate is plotted against the molecular weight of the sugar. Differences in the three data sets were evaluated using oneway ANOVA. Statistically significant differences ( $p < 0.05$ ) are marked with an asterisk (\*). Values are means  $\pm$ SD, obtained from 4 – 6 independent sets of experiments.

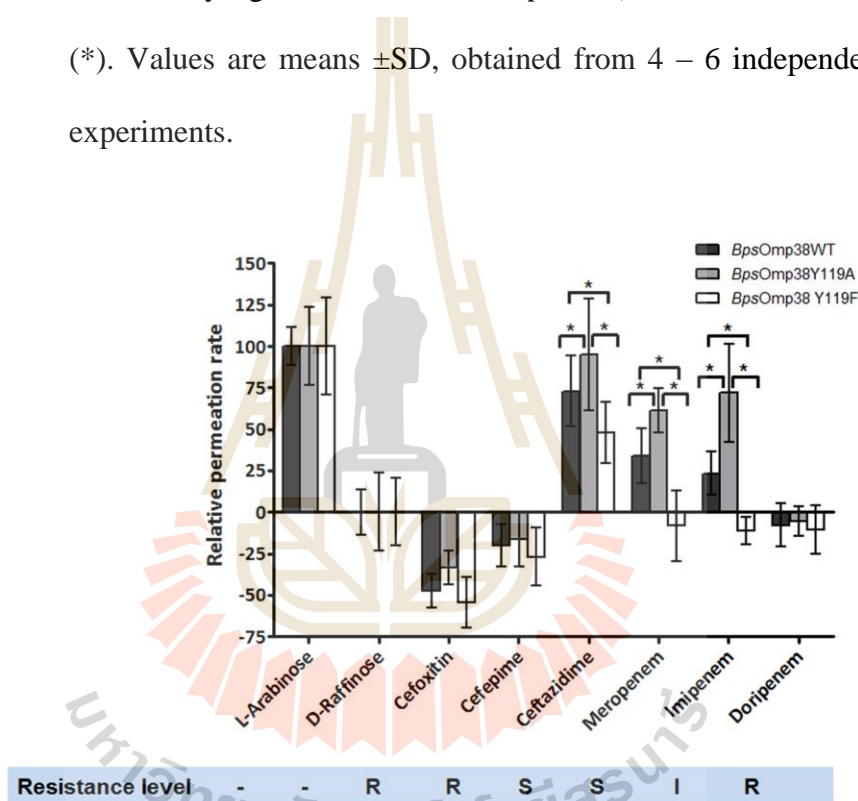


**Figure 3.8** Swelling of *BpsOmp38* proteoliposomes induced by cephalosporins and carbapenems. The proteoliposomes were prepared at pH 7.5. The swelling rate in a solution of each antimicrobial agent was normalised to the rate in *L*-arabinose. Values presented are the averages of 4 – 6 independent experiments. Levels of *Burkholderia pseudomallei* resistance were determined by a broth micro dilution assay as presented in Table 3.1. R, represents resistant; S, sensitive; and I, intermediate.

Differences in the three data sets were evaluated using one-way ANOVA. Statistically significant differences ( $p < 0.05$ ) are marked with an asterisk (\*). Values are means  $\pm$ SD, obtained from 4 – 6 independent sets of experiments.

## **3.2 Structure, thermal stability and thermodynamic parameters of outer membrane protein (*BpsOmp38*) from *Burkholderia pseudomallei***

### **3.2.1 X-ray crystal structure of *BpsOmp38***

*BpsOmp38* was expressed in the outer membrane of the porin-deficient *E. coli* BL21 DE3 Omp8 rosetta strain. Figure 3.9A shows that in contrast to many other outer membrane proteins, boiled and non-boiled SDS-PAGE samples have different mobilities, indicating that *BpsOmp38* is heat modifiable due to a lower stability of the barrel, when folded being a trimeric porin but when unfolded a monomeric porin. The size of the trimeric channel was about 110 – 120 kDa and the monomer about 35 – 40 kDa. The purified protein was crystallised in the presence of 0.4% C<sub>8</sub>E<sub>4</sub> in 100 mM LiCl and 10 mM HEPES at pH 7.5. The protein crystal (Figure 3.9B) was grown in the condition of 33% (v/v) PEG 400, 0.1 M magnesium chloride, 0.1 M sodium chloride, 0.1 M Tris pH 8.5 and 5% water. The obtained crystals of *BpsOmp38* in space group P2<sub>1</sub>2<sub>1</sub>2<sub>1</sub> diffracted to reasonable resolutions of 3.0 Å (Table 3.5).

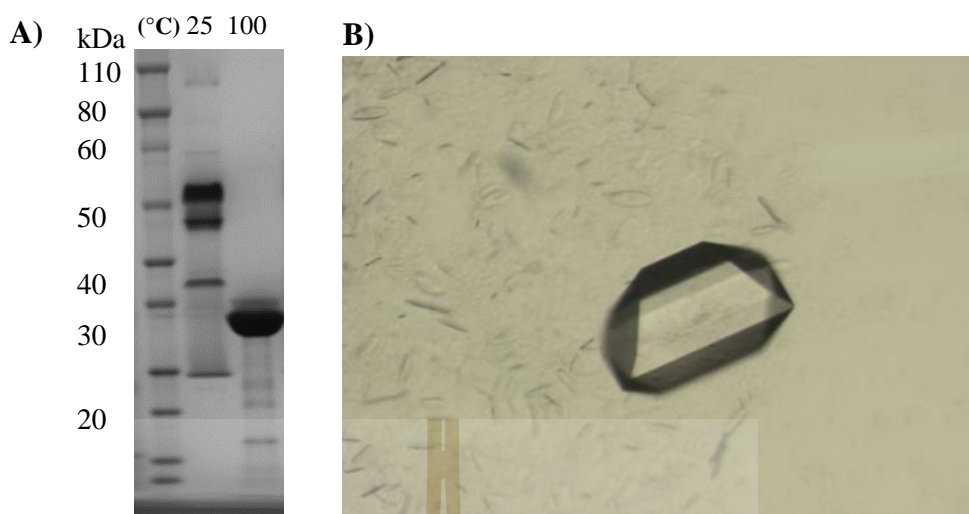


**Figure 3.9** Purification and crystallisation of *BpsOmp38* (A) SDS-PAGE gel of boiled (100 °C, 10 min) and non-boiled outer membrane protein expression samples. (B) *BpsOmp38* crystal obtained by hanging drop technique in condition of 33% (v/v) PEG 400, 0.1 M magnesium chloride, 0.1 M sodium chloride, 0.1 M Tris pH 8.5 and 5% water.

**Table 3.5** Structural data and refinement statistics.

Statistics	Value
<b>Data collection</b>	
Space group	P2 <sub>1</sub> 2 <sub>1</sub> 2 <sub>1</sub>
Cell dimensions	
a, b, c (Å)	89.6, 99.6, 145.7
$\alpha$ , $\beta$ , $\gamma$ (°)	90, 90, 90
Resolution (Å)	49.16 – 3.00 (3.18 – 3.00)
R <sub>merge</sub> (%)	9.0 (83.5)
I/ $\sigma$ (I)	14.5 (2.4)
Completeness (%)	100.0 (100.0)
Redundancy	7.0 (7.2)
<b>Refinement</b>	
R <sub>work</sub> /R <sub>free</sub>	22.2/28.6

Note: Values in parentheses are for the highest resolution shell.

The crystal structure of *BpsOmp38* was determined to a resolution of 3.0 Å using molecular replacement (MR). *Omp32* from *Delftia acidovorans* (PDB number: 2FGR) was the best homology model, which shared 28% sequence identity with *BpsOmp38*. Both structures are quite similar in their  $\beta$ -strands, but are different in their long loops (Figure 3.10C). The 3D structure of *BpsOmp38* shows that it is a trimeric protein, which consists of 16 antiparallel  $\beta$ -strands with eight extracellular long loops and seven turns at the periplasmic side (Figure 3.10A and B). The longest loop, designated Loop 3 (L3), which is situated inside the pore and may act as a pore-confining loop and hide the pore of *BpsOmp38* (Figure 3.10D), contains 28 amino acid residues (Ser127 to Asp154) and had two short antiparallel  $\beta$ -strands at the very beginning and the end. Loop 8 (L8), the second longest loop in the *BpsOmp38*, appeared to be folded into the barrel interior and was suggested to assist L3 to control the size exclusion limit of the *BpsOmp38* pore. The channel interior was found to be highly hydrophilic (Figure 3.10E).

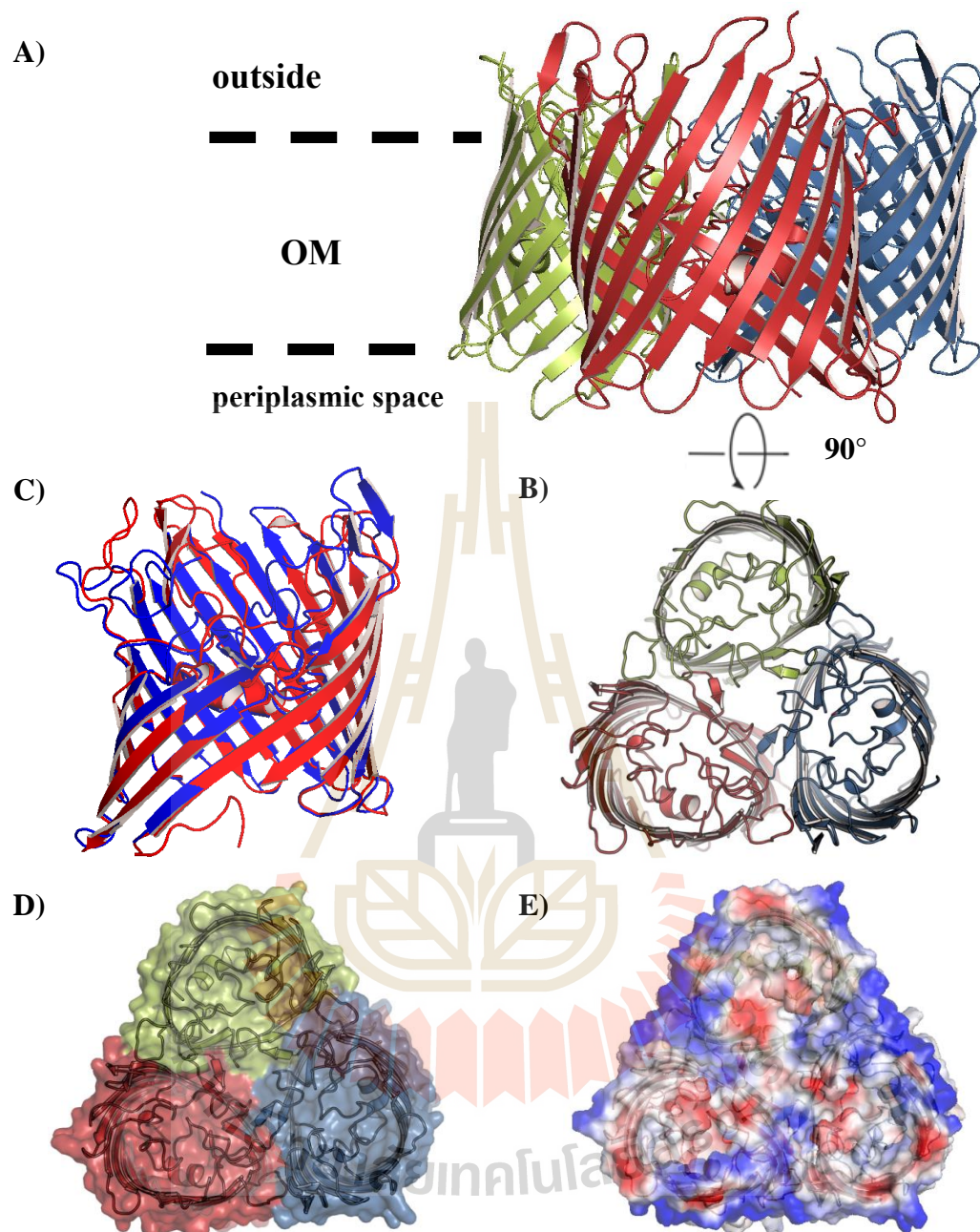


**Figure 3.10** X-ray crystal structure of *BpsOmp38*. A) Side view and B) top view cartoon presentations of the *BpsOmp38* trimer. C) Superposition of *BpsOmp38* (blue) with Omp32 (red) from *Delftia acidovorans* (PDB: 2FGR). D) The long loop (L3) hiding the pore of the *BpsOmp38* and E) electrostatic surfaces of the top view of *BpsOmp38* protein; (red) negatively charged and (blue) positively charged.

### 3.2.2 Thermal unfolding using circular dichroism (CD)

Circular dichroism (CD) is a method of determining the stability of the secondary structure of proteins. Scanning of *BpsOmp38* from 190 – 260 nm showed that different structural elements had different characteristic CD spectra (Figure 3.11A). *BpsOmp38* with well-defined antiparallel  $\beta$ -pleated sheets gave negative bands at 218 nm, while the denatured protein (boiled at 100 °C for 10 min) showed a decrease in negative molar ellipticity at this wavelength. In a further experiment, we tested the effects of certain antibiotics on the protein stability. The normalised unfolding curves of *BpsOmp38* with cephalosporin (Figure 3.11B) and carbapenem antibiotics (Figure 3.11C) were plotted with their data fitted to a Boltzman sigmoidal function. There is an overall increase in the intensity of all peaks with temperature. The value of  $T_m$  (Table 3.6) was extracted from the curves after fitting the data from all CD experiments for protein in the presence and absence of antibiotics. The  $T_m$  value of *BpsOmp38* increased upon the addition of ceftazidime, cefepime and ceftoxitin from the cephalosporin group. This phenomenon was also observed when carbapenems, i.e. meropenem, imipenem and doripenem, were added to the protein. The stabilisation effect induced by antibiotics seems to be derived from the specific binding and permeability of antibiotics to the *BpsOmp38*. The  $\Delta T_m$  (Table 3.6) is the difference in  $T_m$  values of the protein with and without antibiotics. The highest  $\Delta T_m$  was demonstrated by ceftazidime and meropenem with 10.5 and 10.0 °C, respectively. This indicates that ceftazidime and meropenem have the highest binding affinity for *BpsOmp38* among the antibiotics studied in this work.

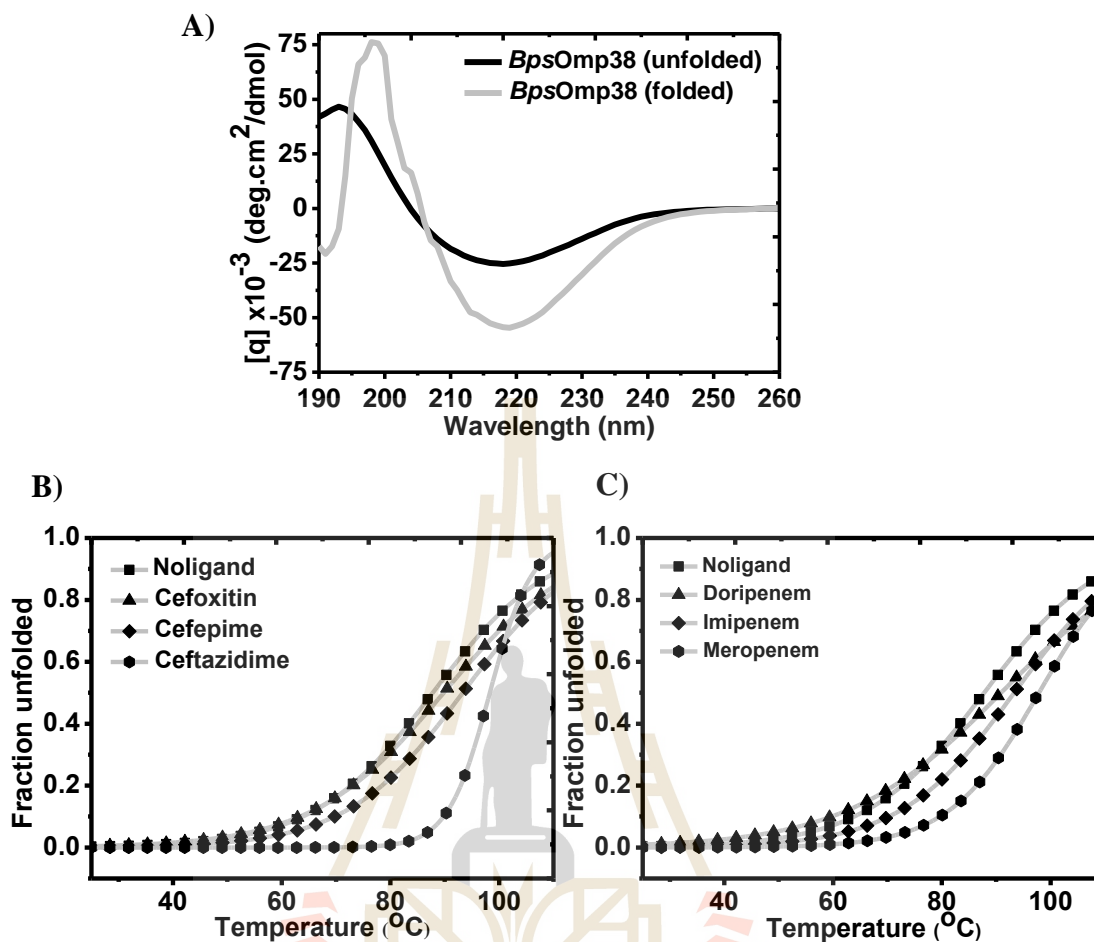


**Figure 3.11** CD spectra and thermal unfolding curves of *BpsOmp38*. CD spectra (A) of the folded and unfolded proteins were recorded with a solution of 10  $\mu$ M protein in 20 mM phosphate buffer pH 7.5 and 0.1% LDAO at 25  $^{\circ}$ C. The unfolded protein was obtained by boiling at 100  $^{\circ}$ C for 10 min. The normalised thermal unfolding curves of *BpsOmp38*-cephalosporins (B) and *BpsOmp38*-carbapenems (C) interactions were studied by monitoring the CD intensity at 218 nm while gradually increasing the temperature. The protein concentrations were 10  $\mu$ M with and without the 10 mM antibiotics concentrations.

### 3.2.3 Thermal unfolding using fluorescence

Fluorescence spectroscopy is a method for determining the stability of the tertiary structure of proteins. The fluorescence spectra from 310 to 450 nm were scanned with the application of wavelength 295 nm for the excitation of Trp. The fluorescence intensity at 340 nm of folded *BpsOmp38* is higher than that of denatured *BpsOmp38* (Figure 3.12A). In the absence of ligand, the *BpsOmp38* showed a low midpoint temperature ( $T_m$ ) of thermal unfolding at about 84.3 °C, when compared to that of the *BpsOmp38* with antibiotics. The normalised folding curves of *BpsOmp38* with cephalosporin group (Figure 3.12B) and *BpsOmp38* with carbapenem group (Figure 3.12C) were fitted to a Boltzman sigmoidal function. It was observed that there was an overall increase in  $T_m$  values after the application of antibiotics. The  $\Delta T_m$  values were the largest for ceftazidime (cephalosporin group) and meropenem (cabapenem group) which were reported at 8.6 and 6.5 °C, respectively. The values of  $T_m$  and  $\Delta T_m$  are presented in Table 3.6.



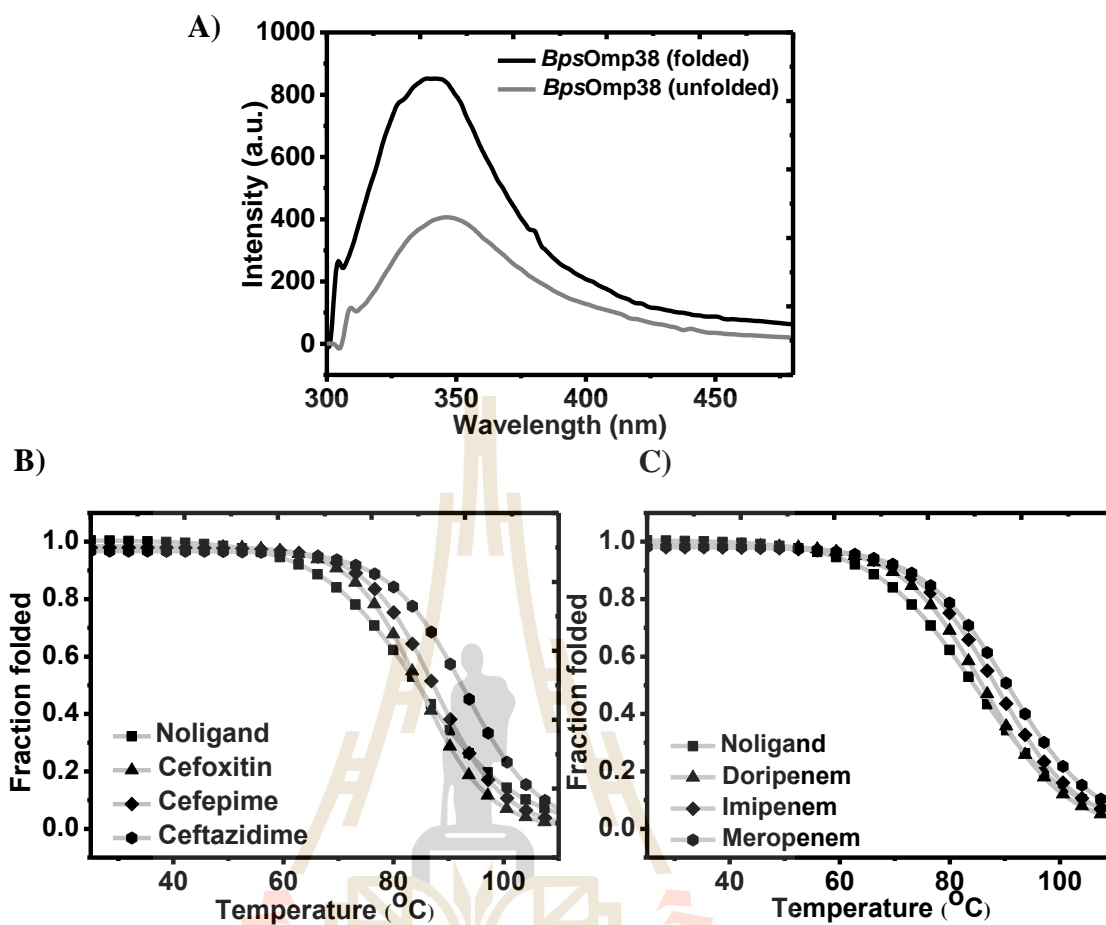


**Figure 3.12** Fluorescence spectra and thermal unfolding curves of *BpsOmp38*. Fluorescence spectra (A) of the folded and unfolded proteins were recorded with a solution of 1  $\mu\text{M}$  protein in 20 mM phosphate buffer pH 7.5 and 0.1% LDAO at 25  $^{\circ}\text{C}$ . The unfolded protein was obtained by boiling at 100  $^{\circ}\text{C}$  for 10 min. The normalised thermal unfolding curves of *BpsOmp38*-Cephalosporin (B) and *BpsOmp38*-Carbapenem (C) interactions were plotted by monitoring fluorescence intensity of emission at 340 nm with an excitation wavelength 295 nm while gradually increasing the temperature. The protein concentrations were 1  $\mu\text{M}$  with and without the 1 mM antibiotics concentrations.

**Table 3.6** Thermal unfolding of *BpsOmp38* with the antibiotics

Antibiotics	Circular Dichroism		Fluorescence Spectroscopy	
	$T_m$	$\Delta T_m$	$T_m$	$\Delta T_m$
No ligand	87.8	-	84.3	-
<b><i>Cephalosporin</i></b>				
Ceftazidime	98.3	10.5	92.9	8.6
Cefepime	93.3	5.5	87.5	3.2
Cefoxitin	89.8	2	84.8	0.5
<b><i>Carbapenem</i></b>				
Meropenem	97.8	10	90.8	6.5
Imipenem	93.3	5.5	88.6	4.3
Doripenem	90.9	3.1	86.1	1.8

$T_m$  is midpoint temperature of thermal unfolding in °C.

$\Delta T = T_m$  (with substrate) –  $T_m$  (without the substrate)

### 3.2.4 Binding studies using fluorescence quenching

Intrinsic fluorescence changes were used to assess the binding affinity of *BpsOmp38* for antibiotics. The *BpsOmp38* was titrated with cephalosporins and carbapenems. Plots of Trp fluorescence quenching are shown in Figure 3.13. All antibiotics suppressed the fluorescence intensity of *BpsOmp38* in a concentration-dependent manner. Plots of relative changes in fluorescence intensity as a function of antibiotics concentrations yielded the binding curves. The dissociation constant ( $K_d$ ) was extracted from non-linear regression fitted curve of the fluorescence intensity plotted against the antibiotic concentration (Figure 3.14) and was used to calculate the binding constants  $K$  ( $K = 1/K_d$ ). The  $K_d$  and  $K$  values for all six antibiotics are summarised in Table 3.7. The  $K$  value of cephalosporins decreased in the following

order: ceftazidime > ceftoxitin > cefepime, while that of carbapenems decreased in following order: meropenem > imipenem > doripenem.

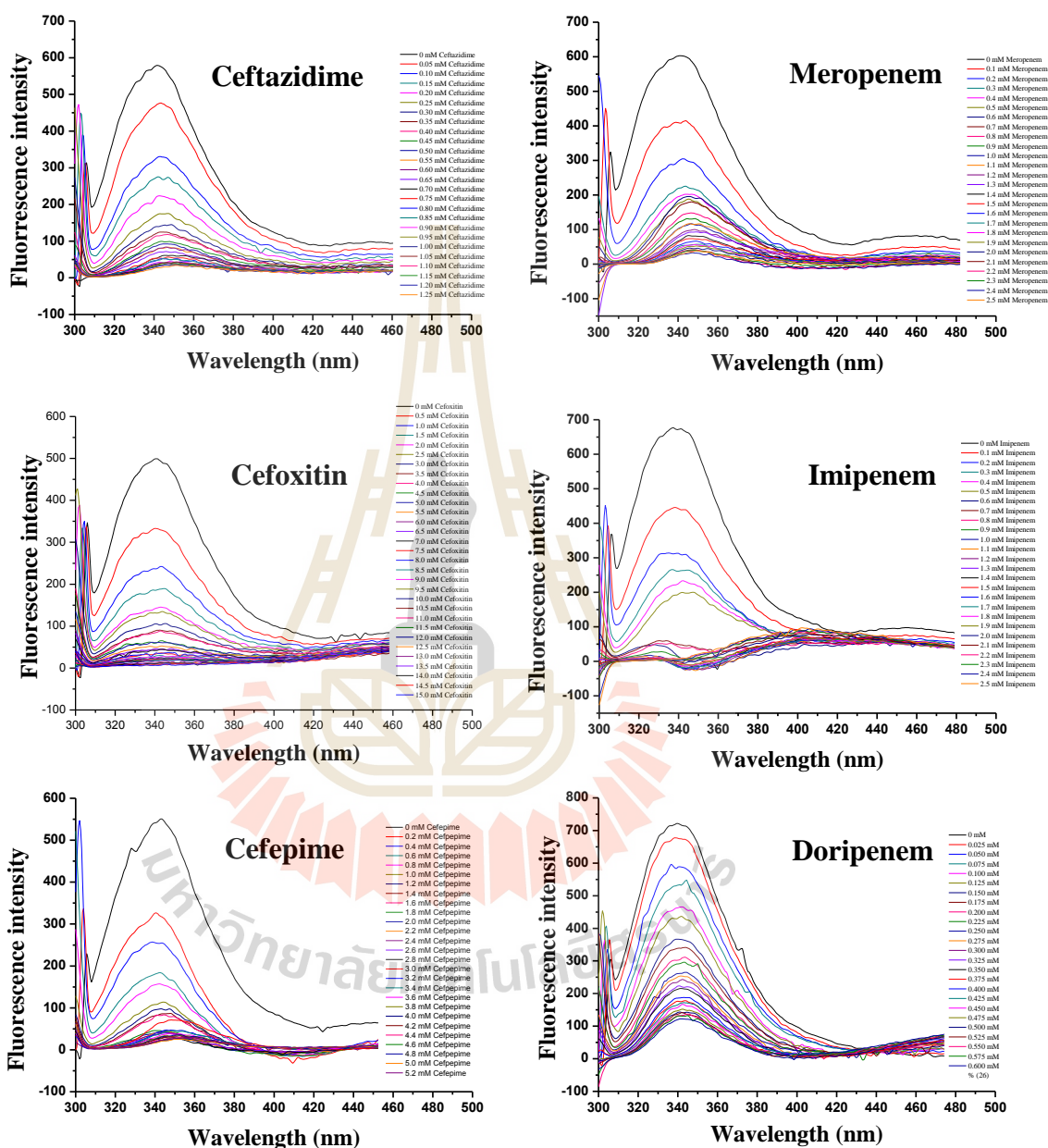


**Figure 3.13** Tryptophan quenching fluorescence spectra of *BpsOmp38*-antibiotic interactions. The titration curves show the changes in the fluorescence intensity (340 nm) with increasing concentration of antibiotics added to the protein solution.

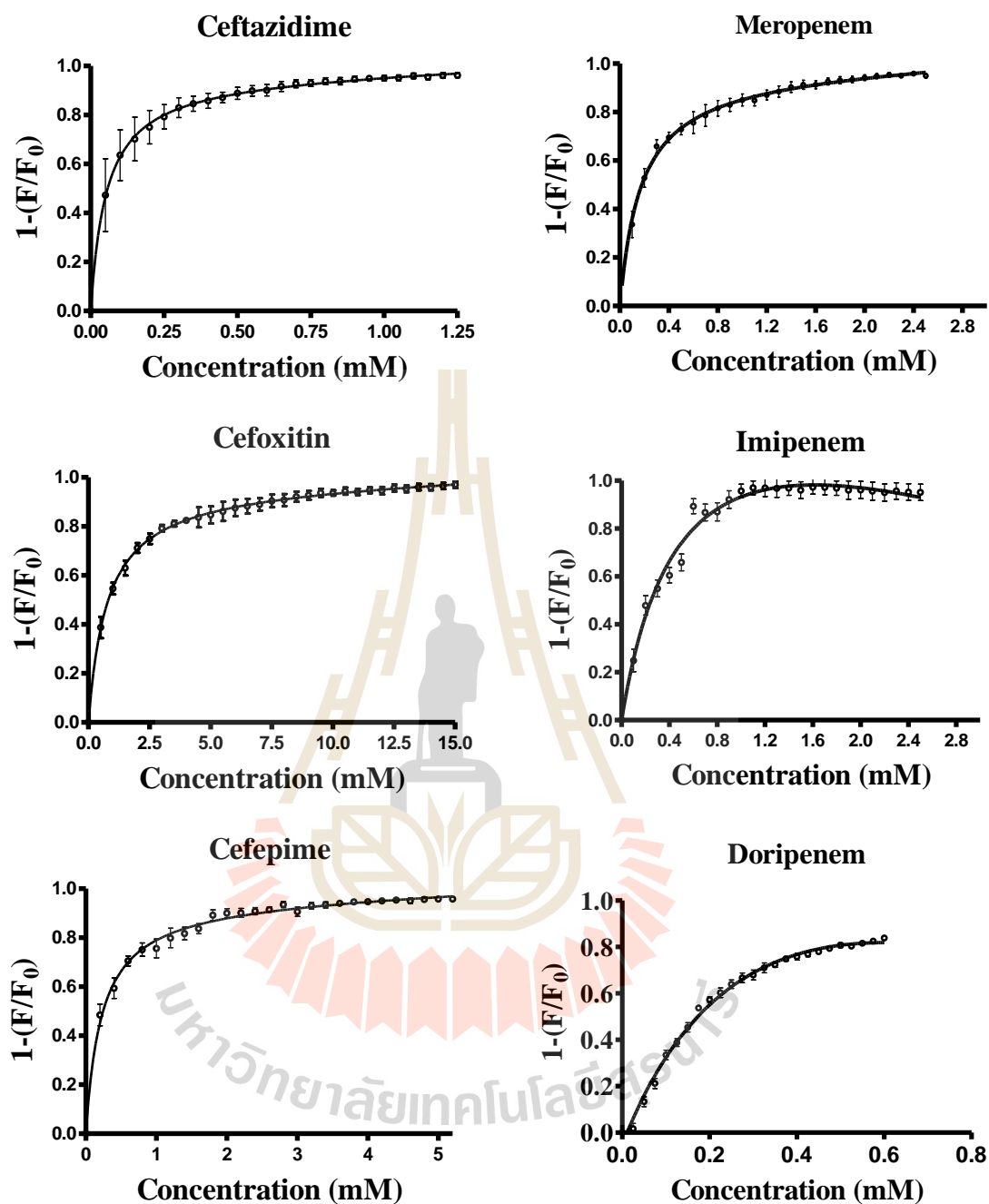


**Figure 3.14** Binding curves of *BpsOmp38* with antibiotics. The binding curve plots of  $1-(F/F_0)$  versus various concentrations of antibiotics were obtained from the data in Figure 3.13.

**Table 3.7** The stability constants of binding determined by fluorescence spectroscopy

Antibiotics	$K_d$ (mM)	$K$ ( $M^{-1}$ )	$\Delta G = -RT \ln K$ ( $kJ \text{ mol}^{-1}$ )
Cefoxitin	0.78±0.08	1282±133	-17.73±0.25
Cefepime	0.23±0.02	4347±381	-20.73±0.21
Ceftazidime	0.054±0.011	18518±3962	-24.34±0.51
Imipenem	0.54±0.10	1851±357	-18.64±0.46
Meropenem	0.17±0.02	5882±703	-21.50±0.29
Doripenem	0.46±0.11	2173±556	-19.03±0.60

$K_d$  is dissociation constant (M),  $K$  is binding constant ( $M^{-1}$ ),  $\Delta G^{\circ}$  = Gibbs free-energy change,  $R$  is the gas constant ( $8.314472 \text{ J mol}^{-1} \text{ K}^{-1}$ ) and  $T$  is the temperature (in Kelvin).

### 3.2.5 Thermodynamic parameters and the binding energy determined by fluorescence spectroscopy

Antibiotics with the highest and lowest binding constants in each group were selected for the evaluation of their thermodynamic parameters. The fluorescence spectra of *BpsOmp38* in the presence of various concentrations of cephalosporins (Figure 3.15 and 3.16) and carbapenems (Figure 3.17 and 3.18) were acquired with temperature set at 25, 30, 35, 40, and 45 °C. Then, the binding curves (Figure 3.19 – left panel) of *BpsOmp38* were evaluated with the binding curve plot to estimate their dissociation constants ( $K_d$ ), which were then converted into the binding constants ( $K$ ). The value of the enthalpy change ( $\Delta H$ ) and the entropy change ( $\Delta S$ ) of each antibiotic can then be estimated from their Van't Hoff plot of  $\log K$  against  $1/T$  (Temperature, Kelvin). The Van't Hoff linear equation (Figure 3.19 – right panel) of ceftazidime is  $y = 8,011x - 16.78$ , cefoxitin is  $y = 4,659x - 7.939$ , meropenem is  $y = 20,160x - 57.37$  and doripenem is  $y = 4,033x - 6.046$ . The gradient of the straight line gave the  $-\Delta H/R$

term, while y-intercept showed the  $\Delta S/R$  term. Gibbs free energy for binding can then be calculated with  $\Delta G = \Delta H - T\Delta S$ .

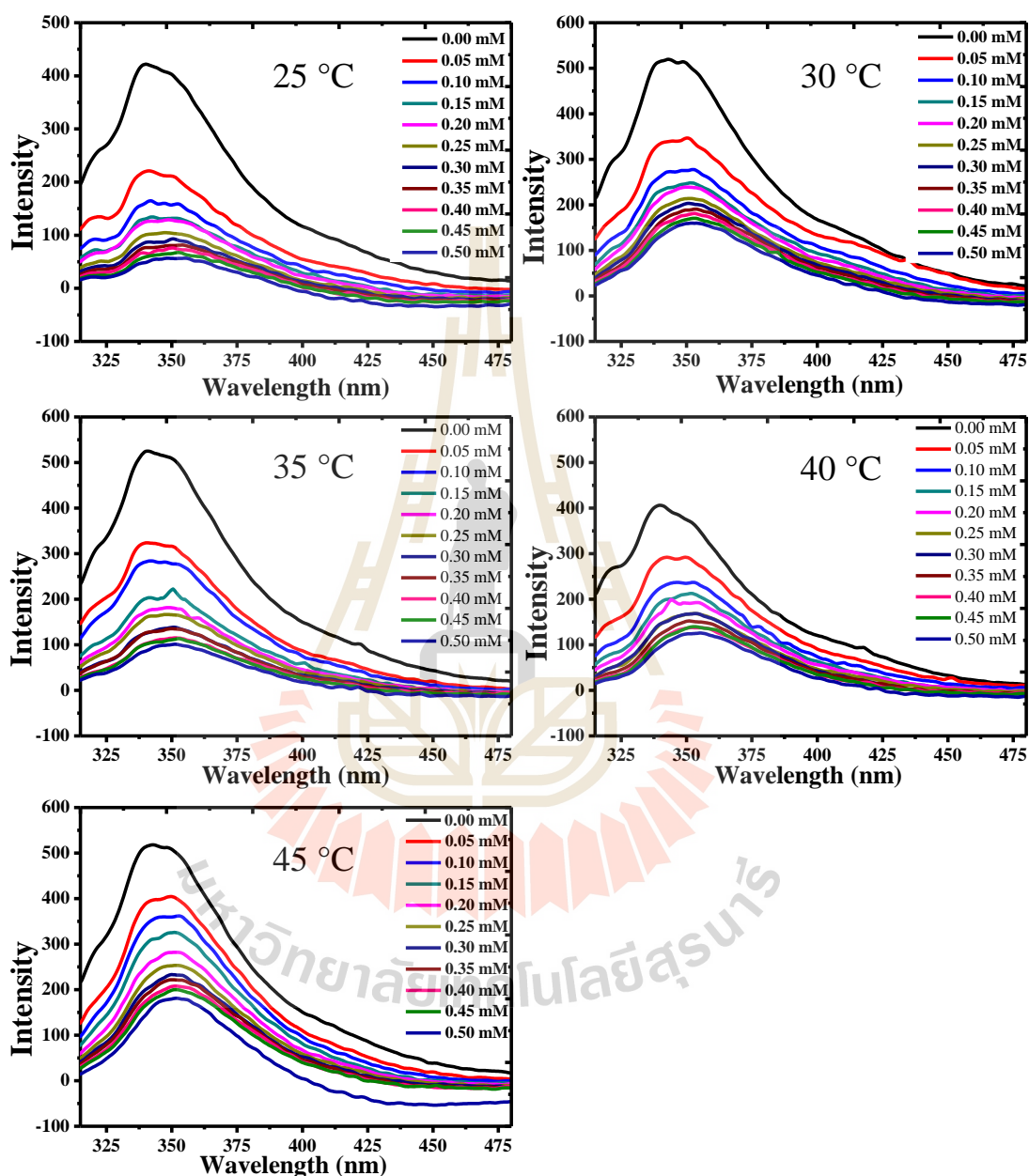


**Figure 3.15** Tryptophan quenching fluorescence spectra of *BpsOmp38*-ceftazidime interactions. The titration curves show the changes in the fluorescence intensity with increasing concentration of ceftazidime added to the protein solution at 25, 30, 35, 40, and 45 °C, respectively.

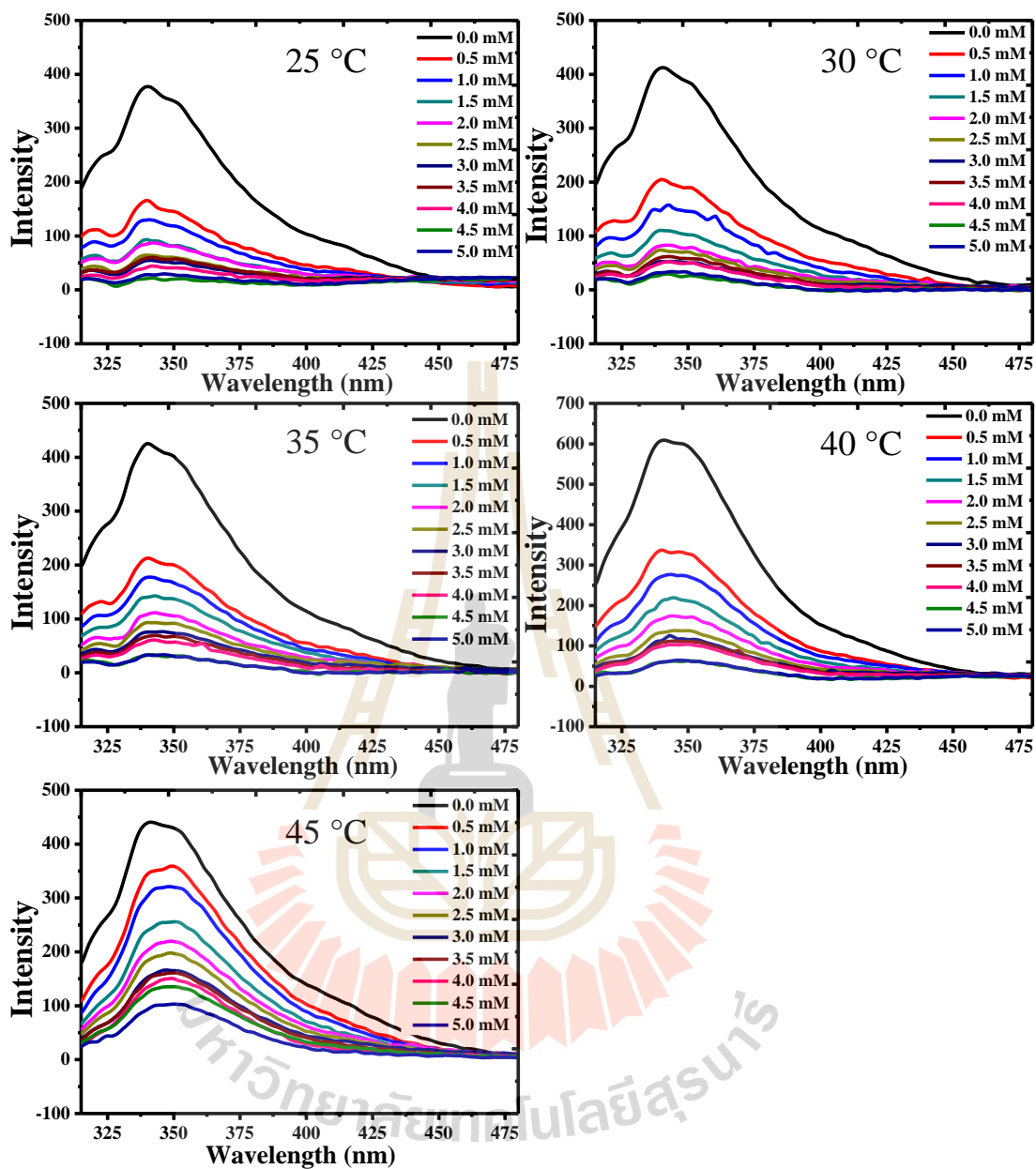


**Figure 3.16** Tryptophan quenching fluorescence spectra of *BpsOmp38*-cefoxitin interactions. The titration curves show the changes in the fluorescence intensity with increasing concentration of cefoxitin added to the protein solution at 25, 30, 35, 40, and 45 °C, respectively.

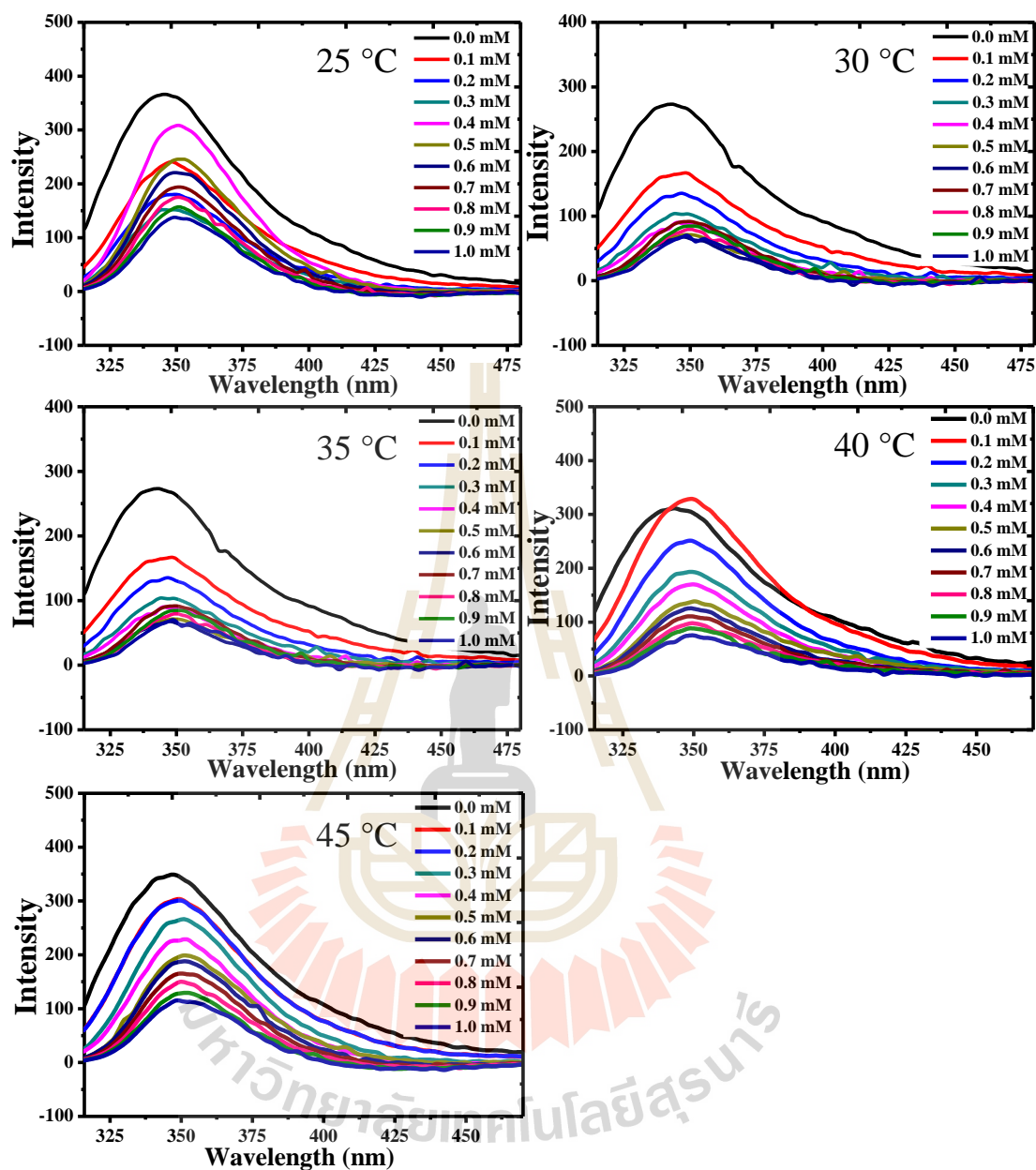


**Figure 3.17** Tryptophan quenching fluorescence spectra of *BpsOmp38*-meropenem interactions. The titration curves show the changes in the fluorescence intensity with increasing concentration of meropenem added to the protein solution at 25, 30, 35, 40, and 45 °C, respectively.



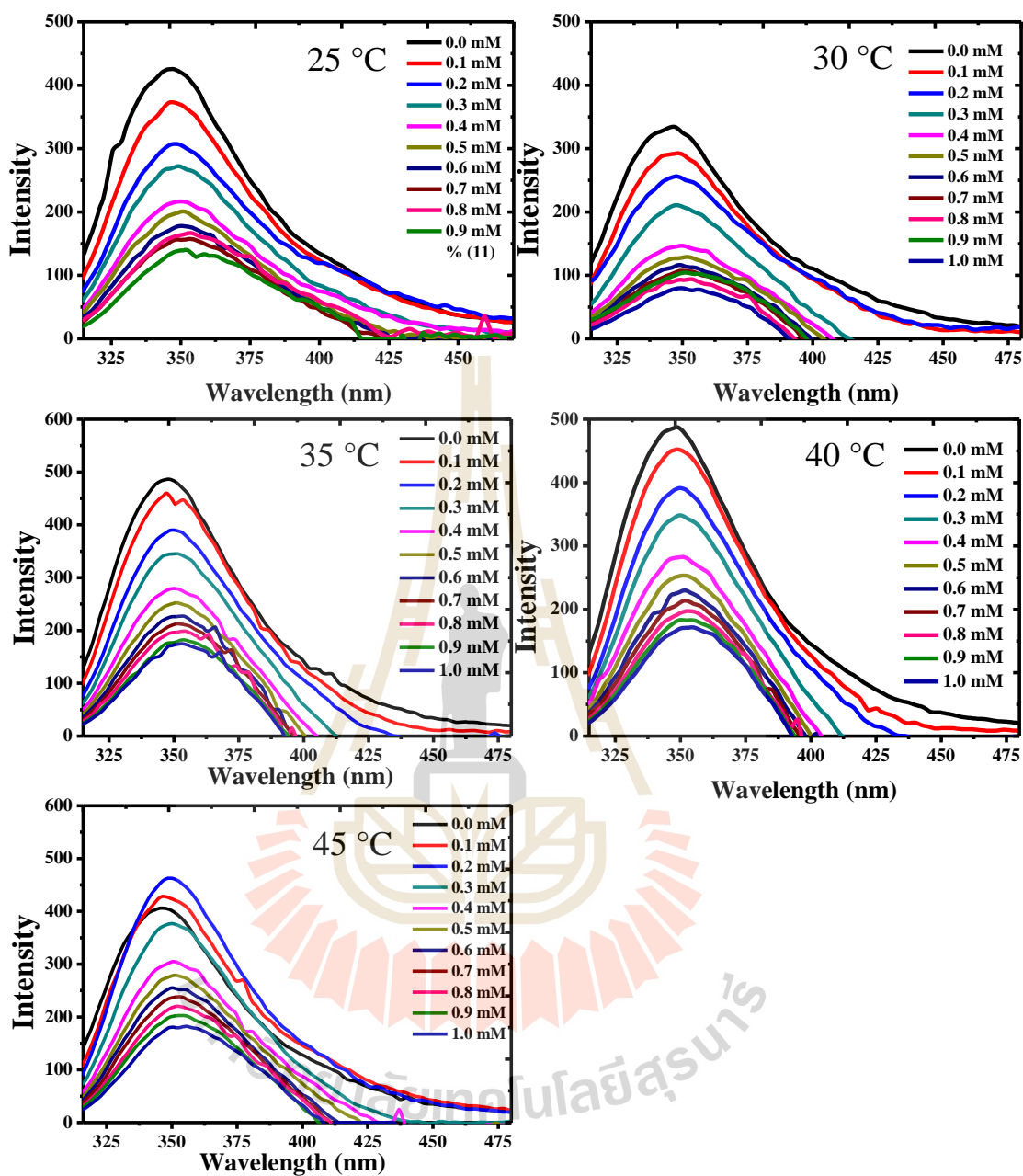


**Figure 3.18** Tryptophan quenching fluorescence spectra of *BpsOmp38*-doripenem interactions. The titration curves show the changes in the fluorescence intensity with increasing concentration of doripenem added to the protein solution at 25, 30, 35, 40, and 45 °C, respectively.

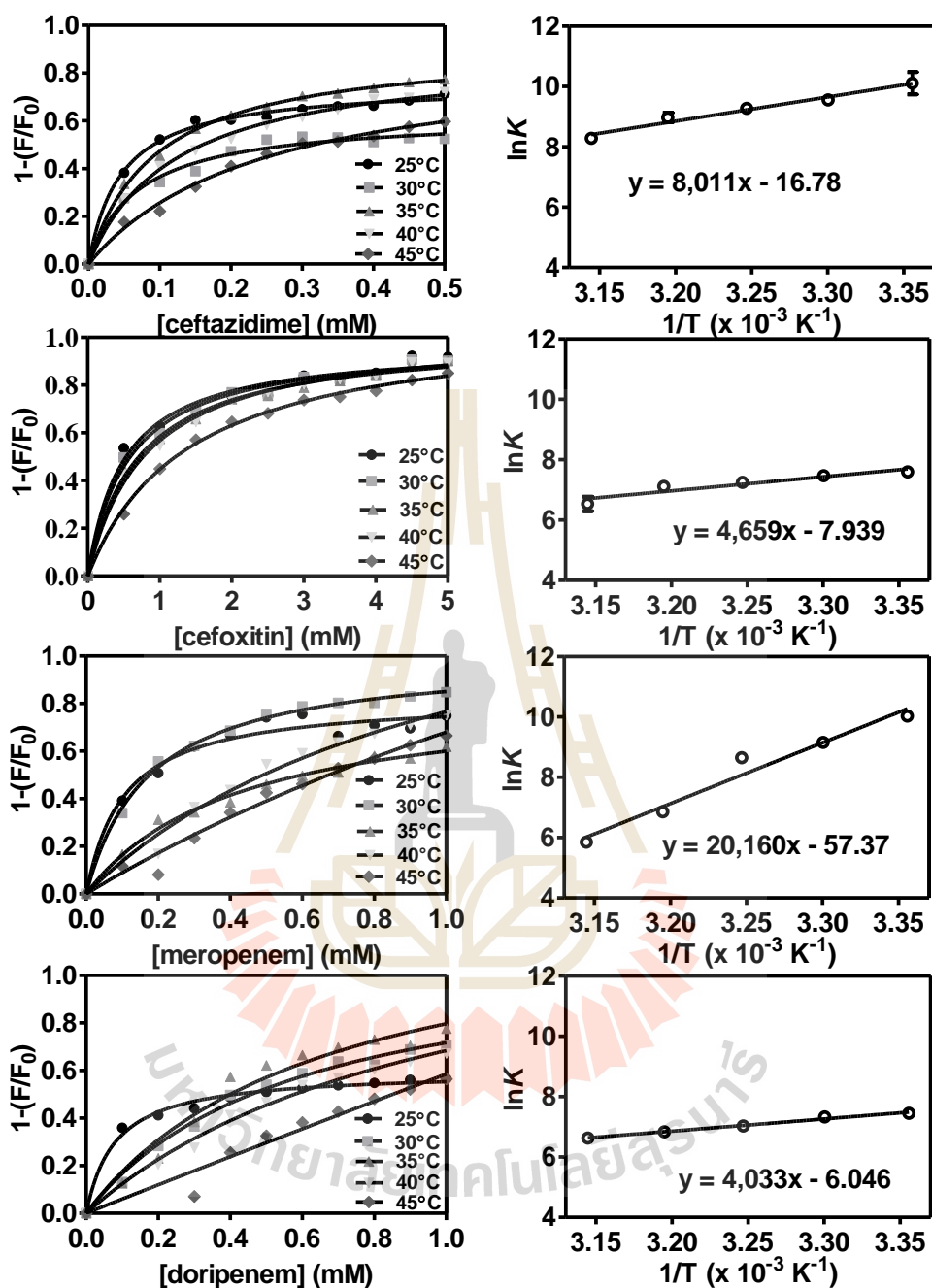


**Figure 3.19** Plots of thermodynamic parameters of *BpsOmp38*-antibiotics interactions obtained by fluorescence quenching technique. (A) ceftazidime, (B) cefoxitin, (C) meropenem and (D) doripenem. Top panel shows the binding curve plots of  $1-(F/F_0)$  versus concentration of antibiotics at each temperature: 25, 30, 35, 40, and 45 °C. The raw data

are given in Figure 3.15 – 3.18. Bottom panel shows the Van't Hoff plot of the logarithm of binding constants (from top panel) versus the reciprocal reaction temperatures.

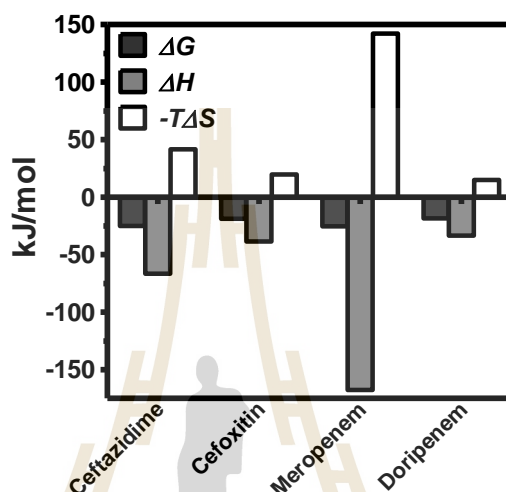


**Figure 3.20** Thermodynamic parameters of *BpsOmp38*-antibiotic interactions determined by fluorescence quenching technique. The bar chart illustrates the free energy ( $\Delta G$ ), enthalpy change ( $\Delta H$ ) and the entropy change ( $-T\Delta S$ ) of the binding of each antibiotic to *BpsOmp38*.

The thermodynamic parameters of these protein-antibiotic interactions are compiled in Figure 3.20 for easy comparison. The Gibbs free energies of antibiotic binding were found to be negative for ceftazidime ( $-25.03 \text{ kJ mol}^{-1}$ ), cefoxitin ( $-19.07 \text{ kJ mol}^{-1}$ ), meropenem ( $-25.47 \text{ kJ mol}^{-1}$ ) and doripenem ( $-18.55 \text{ kJ mol}^{-1}$ ). Meropenem released the most heat energy with enthalpy changes ( $\Delta H$ ) of  $-167.62 \text{ kJ mol}^{-1}$  followed by ceftazidime ( $-66.61 \text{ kJ mol}^{-1}$ ), cefoxitin ( $-38.74 \text{ kJ mol}^{-1}$ ) and doripenem ( $-33.53 \text{ kJ mol}^{-1}$ ). Meanwhile, the largest entropy change ( $\Delta S$ ) was demonstrated by

meropenem ( $-477.00 \text{ J mol}^{-1} \text{ K}^{-1}$ ), followed by ceftazidime ( $-139.52 \text{ J mol}^{-1} \text{ K}^{-1}$ ), cefoxitin ( $-66.01 \text{ J mol}^{-1} \text{ K}^{-1}$ ) and doripenem ( $-50.27 \text{ J mol}^{-1} \text{ K}^{-1}$ ).

### **3.2.6 Permeation of antibiotics through *BpsOmp38* studied by black lipid membrane (BLM) technique**

In this permeation study, the single channel conductance of *BpsOmp38* was shown to be 1.5 – 1.6 nS (in 1M KCl at  $-100\text{mV}$ ). Here, the permeability of the antibiotics, selected from the previously-described MIC assay for *BpsOmp38*, were compared. They were ceftazidime (sensitive) and cefepime (resistant) among cephalosporins; and meropenem (sensitive) and imipenem (intermediate) among carbapenems. Channel blockages were analysed after adding the selected antibiotics to the chamber. In the absence of antibiotic, ion current passing through the channels was stable with occasional fluctuations. Addition of antibiotics caused frequent fluctuations of the ion current, indicating strong interactions of the antibiotics with the channel.

Dimeric blocking events of the trimeric channel were clearly visible for ceftazidime at concentrations of 2.0 and 10 mM, while monomeric blocking events were observed for ceftazidime and meropenem at 0.5 and 10 mM, respectively. It was also observed that the frequency of blockage events was increasing with the concentration of the sensitive antibiotic. Monomeric blockage was produced by partial closure of the single trimeric channel. The observation of monomeric blockage for ceftazidime at low concentration (0.5 mM) indicates that ceftazidime interacted strongly with *BpsOmp38*. Meanwhile meropenem, which is an intermediate antibiotic, demonstrated monomeric blockage at a higher concentration (10 mM). However, the permeation of antibiotic through *BpsOmp38* occurred only at negative voltage. No blocking event of a single trimeric channel was observed for imipenem and cefepime

at concentration up to 10 mM. Current traces from BLM experiments for these antibiotics are presented in Figure 3.21A–D.

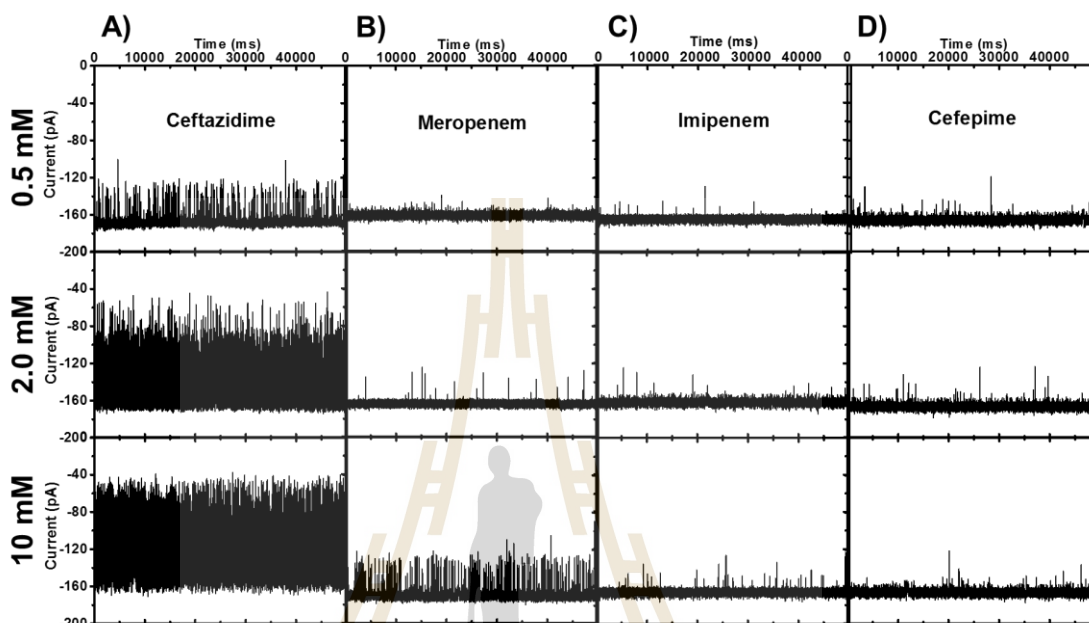


**Figure 3.21** The BLM traces of ion conductance through the single trimeric *BpsOmp38* channel reconstituted into planar lipid membranes in the presence of sensitive drugs: (A) ceftazidime and (B) meropenem, intermediate drugs; (C) imipenem and resistant drugs; (D) cefepime. The traces represent single-monomer blocking events at 0.5, 2, and 10 mM. The membrane was formed from DPhPC; membrane bathing solutions contained 1 M KCl (pH 7.5). Applied voltage was  $-100$  mV.

Antibiotic titrations shown in Figure 3.21 were transformed into the Michaelis-Menten plots for the determination of their dissociation constants. From the plot of  $(G_{\max} - G_c)/G_{\max}$  versus concentration of antibiotics shown in Figure 3.22, the average dissociation constants at  $-100$  mV for ceftazidime, meropenem and imipenem

were calculated to be  $1.51 \pm 0.25$  mM,  $11.96 \pm 2.38$  mM, and  $50.99 \pm 9.74$  mM respectively. However, no blocking event of a *BpsOmp38* single trimeric channel was observed for the resistant drugs (Figure 3.23).

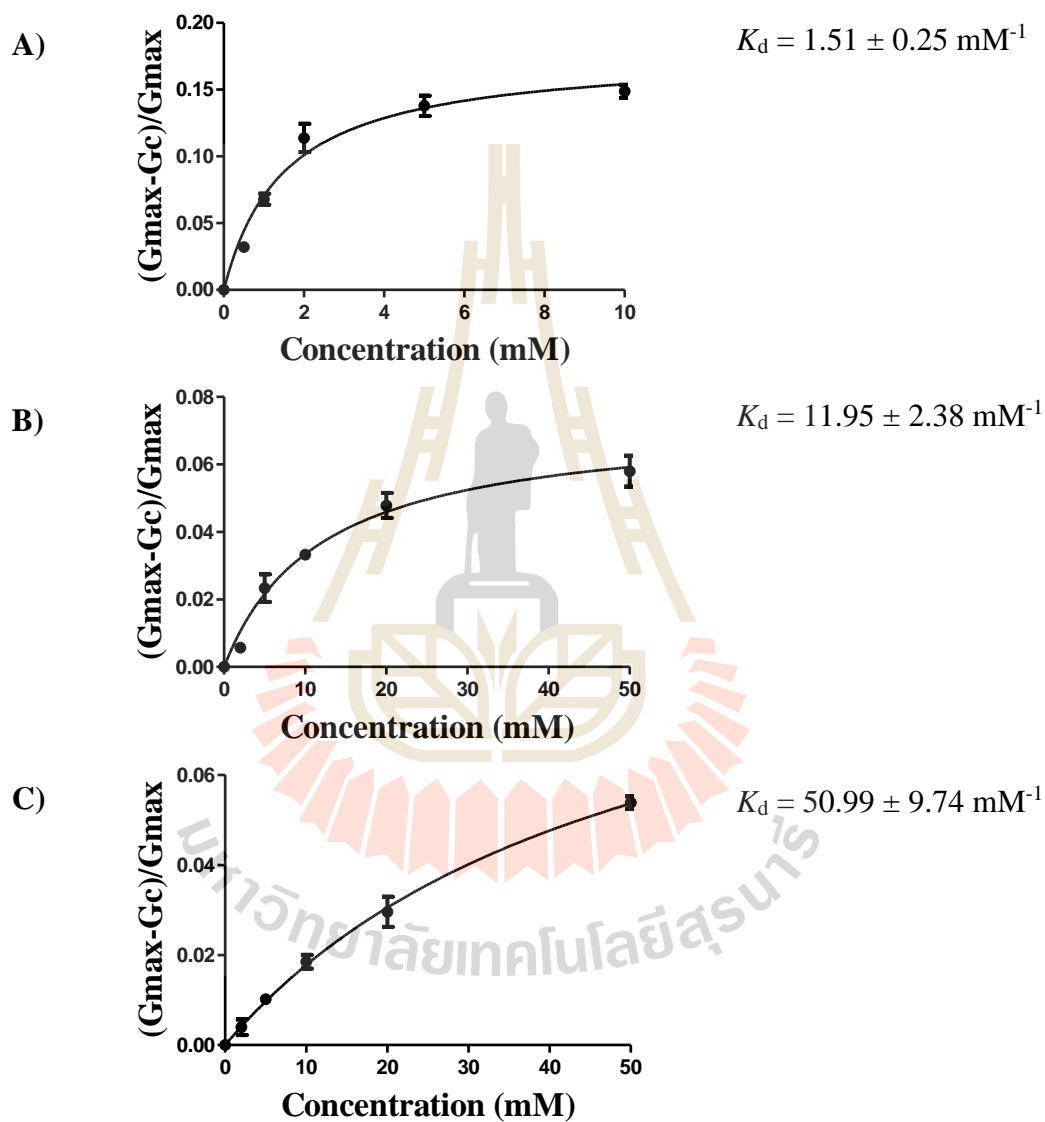


**Figure 3.22** Binding curve plots of *BpsOmp38*-antibiotics interactions. The binding curve plots of  $(G_{\max}-G_c)/G_{\max}$  versus concentration of antibiotics; (A) ceftazidime, (B) meropenem and (C) imipenem were obtained from the data on the Figure 3.21.

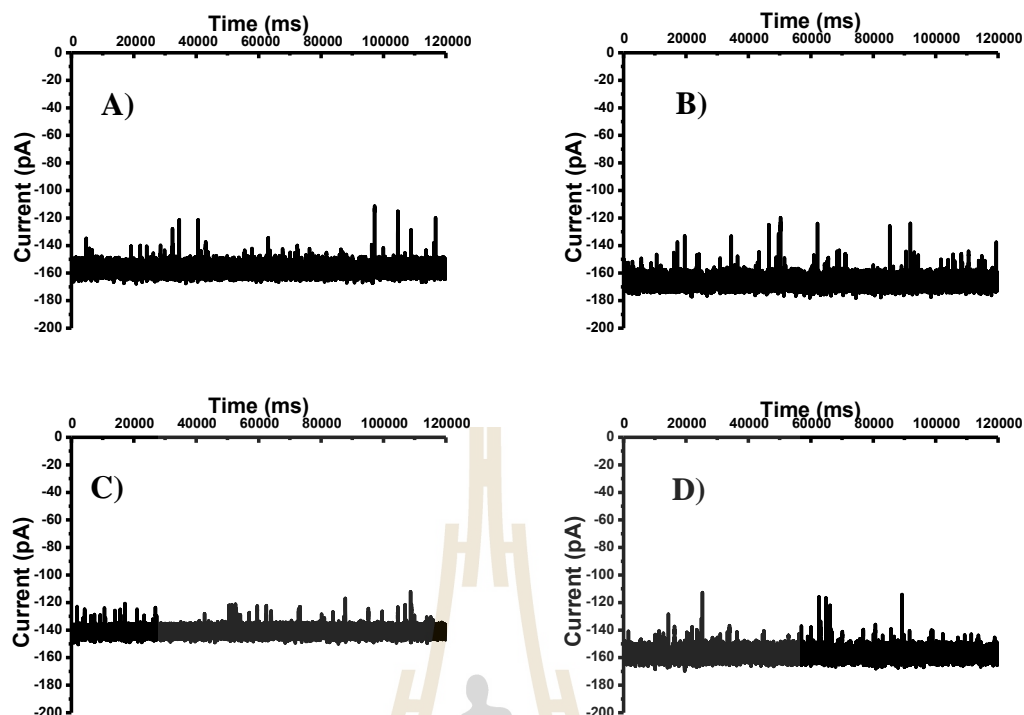


**Figure 3.23** The BLM traces of ion conductance through single trimeric *BpsOmp38* channels reconstituted into planar lipid membranes in the absence and presence of resistance drugs of *B. pseudomallei*. (A) No antibiotic, (B) 20 mM cefepime, (C) 20 mM ceftazidime and (D) 20 mM doripenem. The membrane was formed from DPhPC; membrane bathing solutions contained 1 M KCl (pH 7.5). Applied voltage was  $-100$  mV.

## Part II: Chitoporin (*VhChiP*) from *Vibrio harveyi*

### 3.3 Thermal stability and thermodynamic parameters of mutation effects of Trp136 of outer membrane protein (*VhChiP*) from *Vibrio harveyi*

#### 3.3.1 Model of *VhChiP*

In the modelled 3D-structure, the residue Trp136 is located on the periplasmic side of the outer membrane that precedes the longest loop 3 (L3) (amino acid residues Gly111 – Asn151) and its side chain is situated in the lumen of *VhChiP*. Trp136 is anticipated be involved in controlling sugar passage through the *VhChiP* pore (Figure 3.24). Figures 3.24B and C show the same position of the *VhChiP* WT pore, with Trp136 virtually mutated to phenylalanine (F) and alanine (A), respectively. Amino acid substitution of *VhChiP* generated two single mutants, *VhChiP* W136F and *VhChiP* W136A, which differ in the properties of the side chains at position 136, alanine being small and non-polar, whereas phenylalanine is aromatic and hydrophobic.



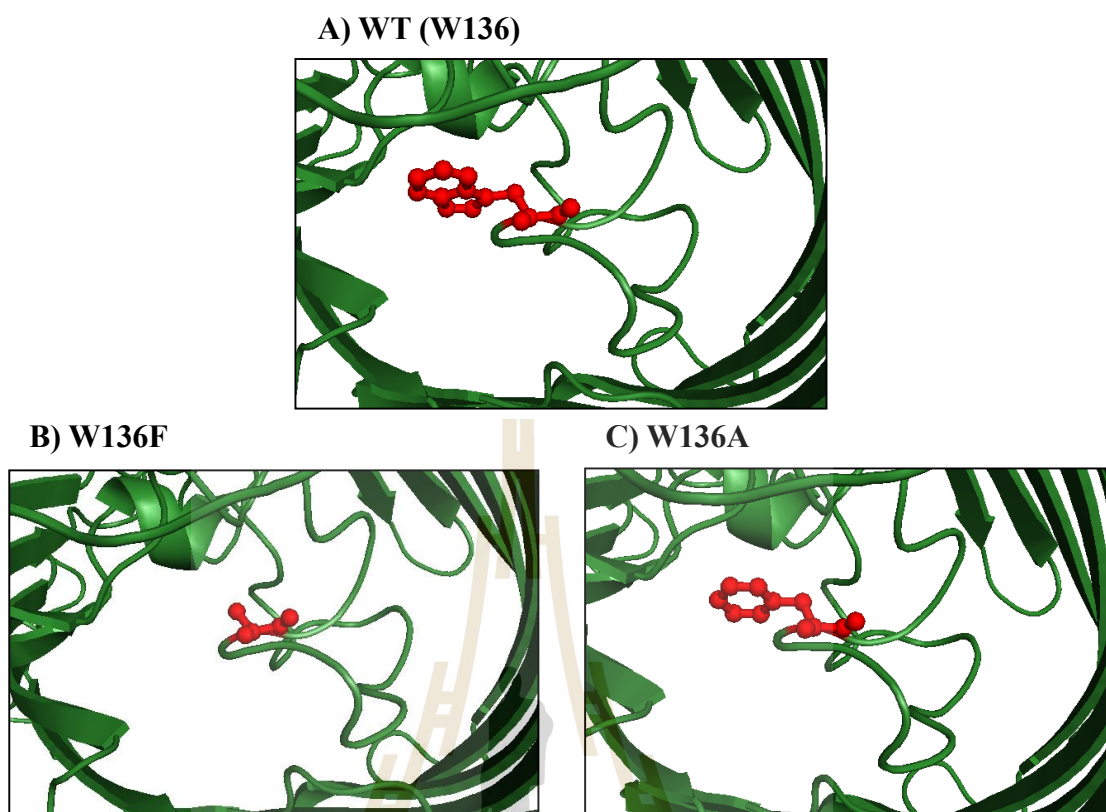


**Figure 3.24** Homology model of *VhChiP* (A) the monomeric *VhChiP* (WT) from *Vibrio harveyi* and mutants W136F (B) and W136A (C). The structures of *VhChiP* and its mutants were modelled using the X-ray structure of *Neisseria meningitidis* PorB (PDB 3VY9 (Kattner *et al.*, 2013)) as a template.

### 3.3.2 Recombinant expression and purification of *VhChiP* variants

In this study, the *VhChiP* expression system was improved by cloning the gene encoding *VhChiP*, including the endogenous signal sequence, to allow the recombinant protein to insert into the *E. coli* cell wall. The protein was then purified from the membrane fraction of the disrupted cells. Site-directed mutagenesis was also conducted to investigate the importance of Trp136 in regulating channel permeability.

The *VhChiP* construct was expressed and accumulated in the cell wall of the *E. coli* host cells. The peptidoglycan fraction was extracted with poly(ethylene glycol)octyl ether (octyl-POE) as detergent. The soluble extract, containing *VhChiP*, was then subjected to ion exchange chromatography followed by gel filtration chromatography as described in Materials and Methods. Bound *VhChiP* was eluted from the Hitrap Q HP ion exchange column with an applied gradient of 0 – 1 M KCl.

Figure 3.25A shows the elution profile of the recombinant of *VhChiP* WT. From the Coomassie blue-stained SDS-PAGE shown in Figure 3.25B, it was observed that the purified *VhChiP* variants migrated as single bands slightly below 42 kDa. *E. coli* outer membrane protein N (OmpN) was often found as contaminant in recombinant of *VhChiP* sample when the protein was expressed in the porin-deficient *E. coli* BL21 (DE3) Omp8 Rosetta strain.

However, only bands of *VhChiP* WT, *VhChiP* W136A and *VhChiP* W136F, which reacted strongly with the *VhChiP* antiserum, were visualised in the immunoblot of the corresponding protein bands when treated with anti-*VhChiP* polyclonal antiserum. The absence of cross-contamination of OmpN in *VhChiP* was verified using anti-OmpN polyclonal antiserum. The anti-OmpN immunoblot revealed the OmpN band in OmpN fraction, but shows no band in the *VhChiP* fractions, indicating that all the purified *VhChiP* fractions were free of OmpN.

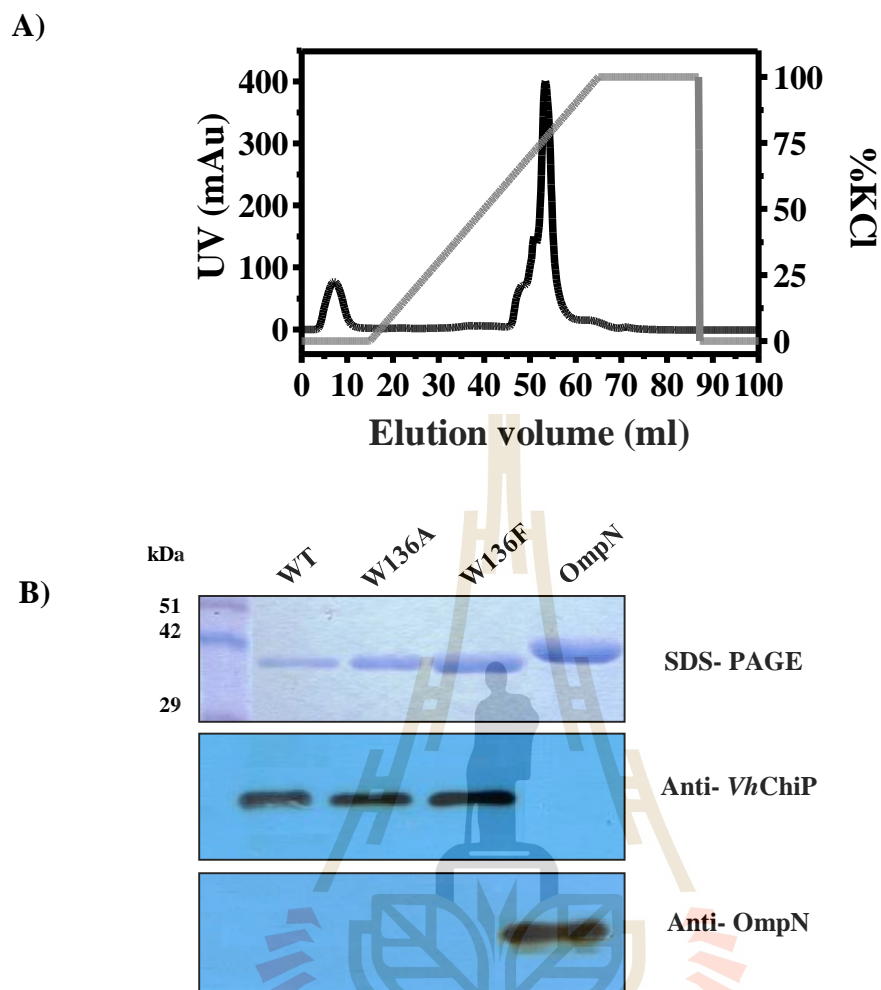


**Figure 3.25** Protein expression, purification and immuno-blotting analysis of WT and its mutants. (A) Chromatographic profile of *VhChiP* WT purification with a Hitrap Q HP column connected to an ÄKTA Prime plus FPLC system. The protein was eluted with a linear gradient of 0 – 1 M KCl. (B) SDS-PAGE analysis of purified WT and its mutants, after IPTG-induced expression for 6 h and chromatography. Immuno-blotting analyses were done with anti-*VhChiP*, and anti-OmpN polyclonal antibodies.

### 3.3.3 Thermal unfolding study using circular dichroism (CD)

The stability of the secondary structure of *VhChiP* WT and mutants was studied with the CD technique. Proteins with different secondary structural elements gave different characteristic CD spectra as illustrated in Figure 3.26A for the three *VhChiPs* under study. *VhGlcNAcase* (Meekrathok and Suginta, 2016), a known ( $\alpha/\beta$ )<sub>8</sub>-barrel protein, was used as a control to indicate the positions of  $\alpha$ -helical and  $\beta$ -strand in the CD spectrum. The protein gave negative bands at 208 nm ( $\alpha$ -helical) and 222 nm ( $\beta$ -strand). For *VhChiP*, the native protein had well-defined antiparallel  $\beta$ -pleated sheets and gave negative bands at 218 nm, while the denatured protein (boiled at 100 °C for 10 min.) showed disappearance of the negative intensity at 218 nm.

In the next series, thermal unfolding experiments were conducted. The normalised unfolding curves of *VhChiP* WT (Figure 3.26B), *VhChiP* W136F (Figure 3.26C) and *VhChiP* W136A (Figure 3.26D) data fitted to a Boltzman sigmoidal function, demonstrated an overall increment in the intensity of all peaks when the temperature was raised from ambient temperature to 100 °C. The  $T_m$  values for all three *VhChiP* variants in the absence and presence of ligands (GlcNAc)<sub>*n*</sub> (where *n* = 1, 2, 3, 4, 5, and 6), maltohexaose (as a negative control) are presented in Table 3.8.

It can be seen that the  $T_m$  value of this trimeric channel protein changed when it interacted with chitoooligosaccharides. The  $T_m$  value of the wild type *VhChiP* alone at 72.7 °C was found to be higher than that of both mutants (W136F and W136A), which were 69.0 and 59.3 °C, respectively. Besides, it was also observed that the increment magnitude became larger as the degree of sugar polymerisation (GlcNAc)<sub>*n*</sub> increased from *n* = 1 to *n* = 6. Ligand (GlcNAc)<sub>6</sub> gave the highest  $T_m$  at 79.7, 74.1, and 63.4 °C respectively for WT, W136F and W136A, while those of ligand GlcNAc were

74.1, 69.4, and 59.8 °C, respectively. This stabilisation effect induced by (GlcNAc)<sub>n</sub> is predicted to be a result of the specific binding of (GlcNAc)<sub>n</sub> to the *Vh*ChiP.

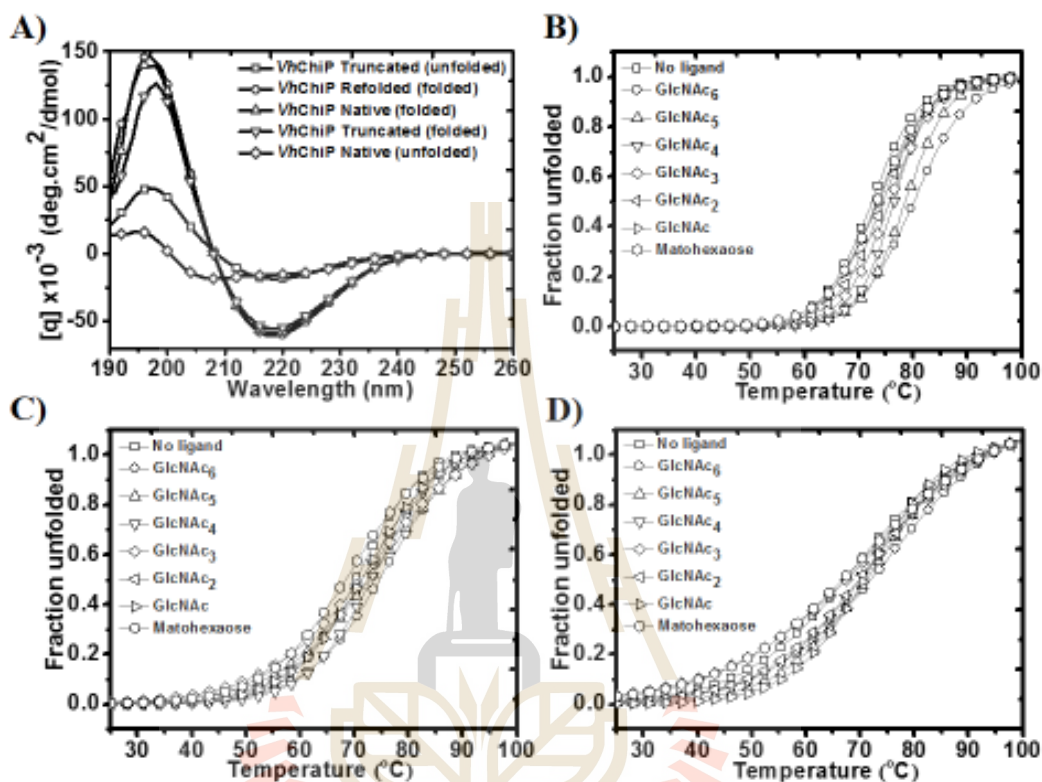


**Figure 3.26** CD spectra and thermal unfolding curves of the WT and mutants. (A) CD spectra of the proteins were recorded with protein (10  $\mu$ M) dissolved in 20 mM phosphate buffer, pH 7.5 and 0.1% LDAO at 25 °C. The unfolded proteins were obtained by boiling at 100 °C for 10 min. The normalised thermal unfolding curves of WT (B) and mutants W136F (C) and W136A (D) were obtained by monitoring CD intensity at 218 nm. The protein concentration used was 10  $\mu$ M with and without the ligand ((GlcNAc)<sub>n</sub>,  $n=1 - 6$ ) at concentration of 10 mM.

The difference of  $T_m$  between protein-ligand complexes and protein without substrate was calculated as  $\Delta T_m$  (Table 3.8). Generally, the  $\Delta T_m$  values of all substrates were found to be higher for WT than for mutants W136F and W136A. This indicates the destabilisation of protein secondary structure when the Trp136 residue was mutated to Phe and Ala. Despite mutation on Trp136 destabilised the secondary structure of the protein, the (GlcNAc)<sub>6</sub>-W136F and (GlcNAc)<sub>6</sub>-W136A complexes were still having the highest  $T_m$  value among the chitooligosaccharides tested. This can be seen from the highest  $T_m$  values given by both the (GlcNAc)<sub>6</sub>-W136F and (GlcNAc)<sub>6</sub>-W136A complexes, when compared to their respective complexes with ligands of lower degree of polymerisation. However, both complexes gave smaller  $\Delta T_m$  values when compared to that of WT. This result shows that all three *VhChiP*s are highly specific for (GlcNAc)<sub>6</sub> binding and that Trp136 is responsible for the higher binding affinity.

#### 3.3.4 Thermal unfolding studies using fluorescence

To study the dissociation binding constants ( $K_d$ ) using fluorescence spectroscopy, the intrinsic fluorescence was used to assess the binding affinity with chitooligosaccharide as a substrate of WT and its mutants. Figure 3.27A reveals the amino acid alignment with the ten tryptophan residues coloured: W73, W105, W123, W136, W157, W188, W220, W233, W275, and W338. Figure 3.27B represents the model of the three-dimensional structure of *VhChiP* channel based on the X-ray structure of *Neisseria meningitidis* PorB (PDB 3VY9). The intrinsic fluorescence intensity of *VhChiP* and its mutants was measured with excitation wavelength of 295 nm.

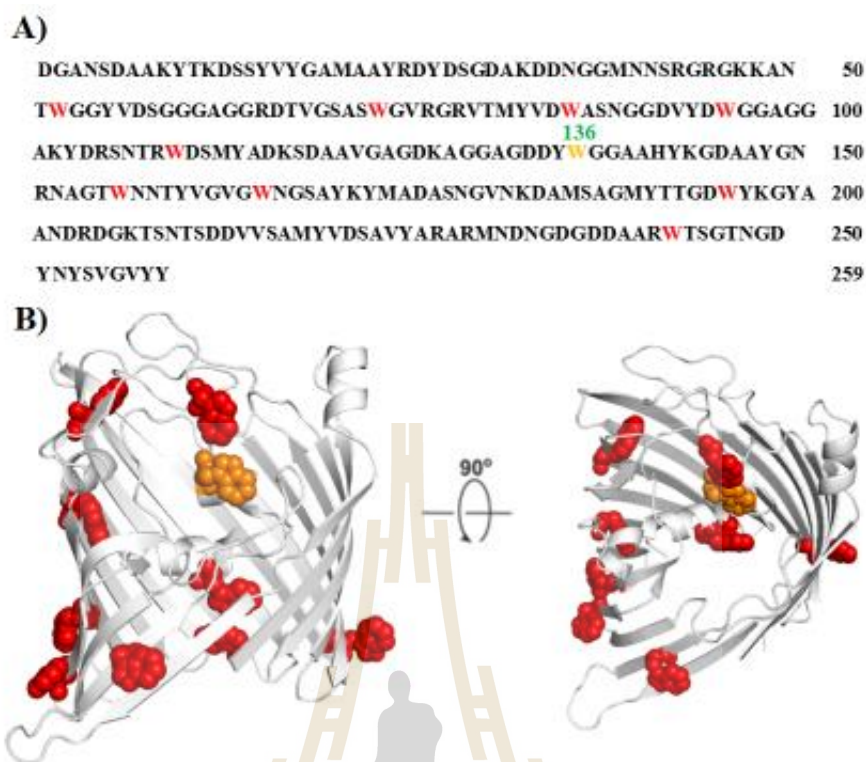


**Figure 3.27** Amino acid sequence and a cross-section of the modelling structure of *V. harveyi* monomeric chitoporin. A) Amino acid sequence of *VhChiP* chitoporin, ten tryptophan residues (red colour) including W73, W105, W123, W157, W188, W220, W233, W275, W338, and W136 (orange). B) Homology model of *VhChiP* show cartoon representations of side and top views with 90-degree rotation. The ten Trp residues are presented in red and orange spheres.

In this experiment, fluorescence spectra of proteins in their folded and unfolded conformations were scanned from 310 nm to 450 nm with 295 nm as the excitation wavelength for Trp (Figure 3.28A). The Trp136 mutations generally affected the intrinsic fluorescence properties of the protein. In the absence of ligand, mutant W136A showed a large reduction in the fluorescence intensity, as compared to that of

the WT channel, while W136F demonstrated a slight intensity decrease at its wavelength of maximum emission (340 nm).

In order to understand the thermal stability of the tertiary structure of *VhChiP* channels, the fluorescence emission intensity of Trp residues from each protein was observed under gradual temperature change. The normalised folding curves of *VhChiP* WT (Figure 3.28B), *VhChiP* W136F (Figure 3.28C) and *VhChiP* W136A (Figure 3.28D) were fitted to a Boltzman sigmoidal function in equation 2.

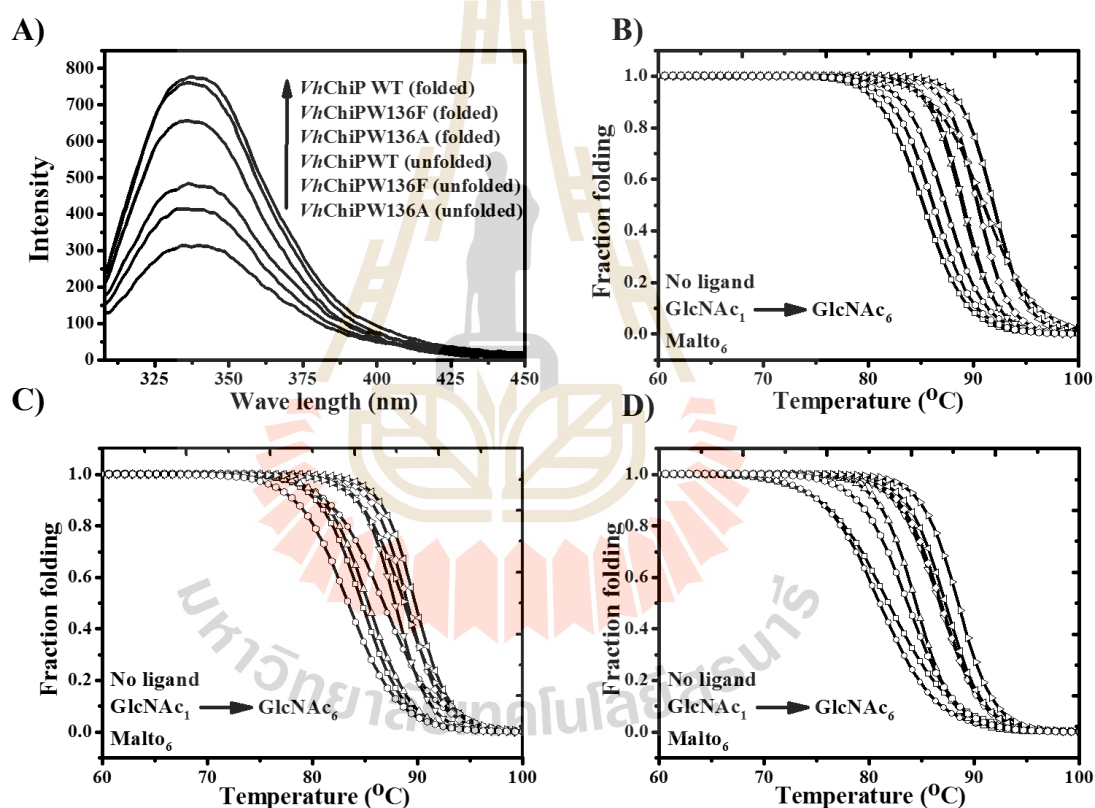


**Figure 3.28** Fluorescence spectra and thermal unfolding curves of the WT and mutants. (A) Fluorescence spectra of the proteins were recorded with protein (1  $\mu$ M) dissolved in 20 mM phosphate buffer pH 7.5 and 0.1 % LDAO at 25  $^{\circ}$ C. The unfolded proteins were obtained by boiling at 100  $^{\circ}$ C for 10 min. The excitation wavelength was 295 nm. The normalised



thermal unfolding curves of WT (B) and mutants W136F (C) and W136A (D) were obtained by monitoring the fluorescence intensity at emission wavelength of 340 nm with excitation wavelength of 295 nm. The protein concentration used was 1  $\mu$ M with 1 mM of ligand ((GlcNAc) $_n$ ,  $n=1-6$ ) and without the ligand.

In thermal unfolding experiments, a decrement of intensity was observed when all three proteins were heated to denaturation. The results obtained from fluorescence showed a similar trend as that of in the CD experiment. The  $T_m$  and  $\Delta T_m$  values of the tertiary protein structural change are listed in Table 3.8. The  $T_m$  of *VhChiP* WT was 85.0  $^{\circ}$ C, while  $T_m$  values for W136F and W136A were determined to be 84.0 and 83.2  $^{\circ}$ C, respectively. The  $T_m$  and  $\Delta T_m$  of all the *VhChiP* WT and mutants increased with increasing length of the (GlcNAc) $_n$  ligand, with the highest values of both parameters given by the (GlcNAc) $_6$ -channel complex.

The  $T_m$  and  $\Delta T_m$  values of the WT-ligand complexes for all six ligands were found to be higher than those of W136F and W136A. Thus, the stabilisation of the tertiary structure of protein by chitooligosaccharides was best observed on the *VhChiP* WT over the W136F and W136A mutants. This shows that the Trp136 residue in WT plays an important role in stabilising the structure of the ligand-bound channel.

**Table 3.8** Thermal unfolding of *VhChiP* with the substrate

Ligands	Circular Dichroism						Fluorescence Spectroscopy					
	WT		W136F		W136A		WT		W136F		W136A	
	$T_m$	$\Delta T_m$	$T_m$	$\Delta T_m$	$T_m$	$\Delta T_m$	$T_m$	$\Delta T_m$	$T_m$	$\Delta T_m$	$T_m$	$\Delta T_m$
No ligand	72.7	0.0	69.0	0.0	59.3	0.0	85.0	0.0	84.0	0.0	83.2	0.0
(GlcNAc) <sub>6</sub>	79.7	7.0	74.1	5.1	63.4	4.1	93.0	8.0	89.1	5.1	88.0	4.8
(GlcNAc) <sub>5</sub>	78.4	5.7	73.3	4.3	62.4	3.1	91.0	6.0	89.0	5.0	87.0	3.8
(GlcNAc) <sub>4</sub>	76.5	3.8	70.4	1.4	61.7	2.4	90.0	5.0	88.1	4.1	86.0	2.8
(GlcNAc) <sub>3</sub>	75.9	3.2	70.0	1.0	60.1	0.8	89.0	4.0	87.0	3.0	85.0	1.8
(GlcNAc) <sub>2</sub>	74.8	2.1	70.0	1.0	59.9	0.6	89.0	4.0	85.1	1.1	84.0	0.8
GlcNAc	74.1	1.4	69.4	0.4	59.8	0.5	87.0	2.0	85.0	1.0	82.0	-1.2
Maltohex <sub>6</sub>	73.7	1.0	69.1	0.1	56.8	-2.5	85.0	0.0	84.0	0.0	82.0	-1.2

$T_m$  is midpoint temperature of thermal unfolding in °C.

$\Delta T_m = T_m$  (with substrate) –  $T_m$  (without the substrate) (in °C).

### 3.3.5 Estimation of binding energies using fluorescence quenching

Intrinsic fluorescence changes were used to assess the binding affinity of *VhChiP* and its mutants for chitooligosaccharides. Each *VhChiP* mutant was titrated with chitooligosaccharides ((GlcNAc)<sub>*n*</sub>, (*n* = 1, 2, 3, 4, 5, and 6) and the plots of Trp fluorescence enhancement were compared with the titration of WT protein (Figure 3.29 – 3.31). In our study, chitooligosaccharides were found to enhance the fluorescence intensity of WT and mutants *VhChiP* in a concentration-dependent manner. Plots of relative changes in fluorescence intensity as a function of chitooligosaccharide concentrations yielded binding curves. Fitting of the binding curve for each *VhChiP* homolog was performed using non-linear regression (Figure 3.32). Curve fitting of the fluorescence intensity plotted against sugar concentration yielded the dissociation constant  $K_d$ , the binding constants  $K$  ( $K = 1/K_d$ ) and  $\Delta G_{\text{binding}}$  ( $\Delta G_{\text{binding}} = -RT \ln K$ ). The values of these parameters are summarised in Table 3.9. Mutations of Trp136 caused a drastic increase in  $K_d$  values for all the chitooligosaccharides tested, indicating a reduced binding affinity. The mutant W136A protein gave the highest  $K_d$  value for all

the chitooligosaccharides, followed by W136F and WT. Since the  $K_d$  is the reciprocal of  $K$ , a large decrease in  $K$  value observed in Figure 3.33 means a large increase in  $K_d$ .  $K$  values for the Phe and Ala mutant were lower than the WT value, and the  $K$  values for chitooligosaccharides for all the three proteins decreased in the following order:  $(\text{GlcNAc})_6 > (\text{GlcNAc})_5 > (\text{GlcNAc})_4 > (\text{GlcNAc})_3 > (\text{GlcNAc})_2 > \text{GlcNAc}$ . Such results again confirm that the binding affinity of *VhChiP* channel towards chitooligosaccharides increases as the size of the sugar molecule increases.



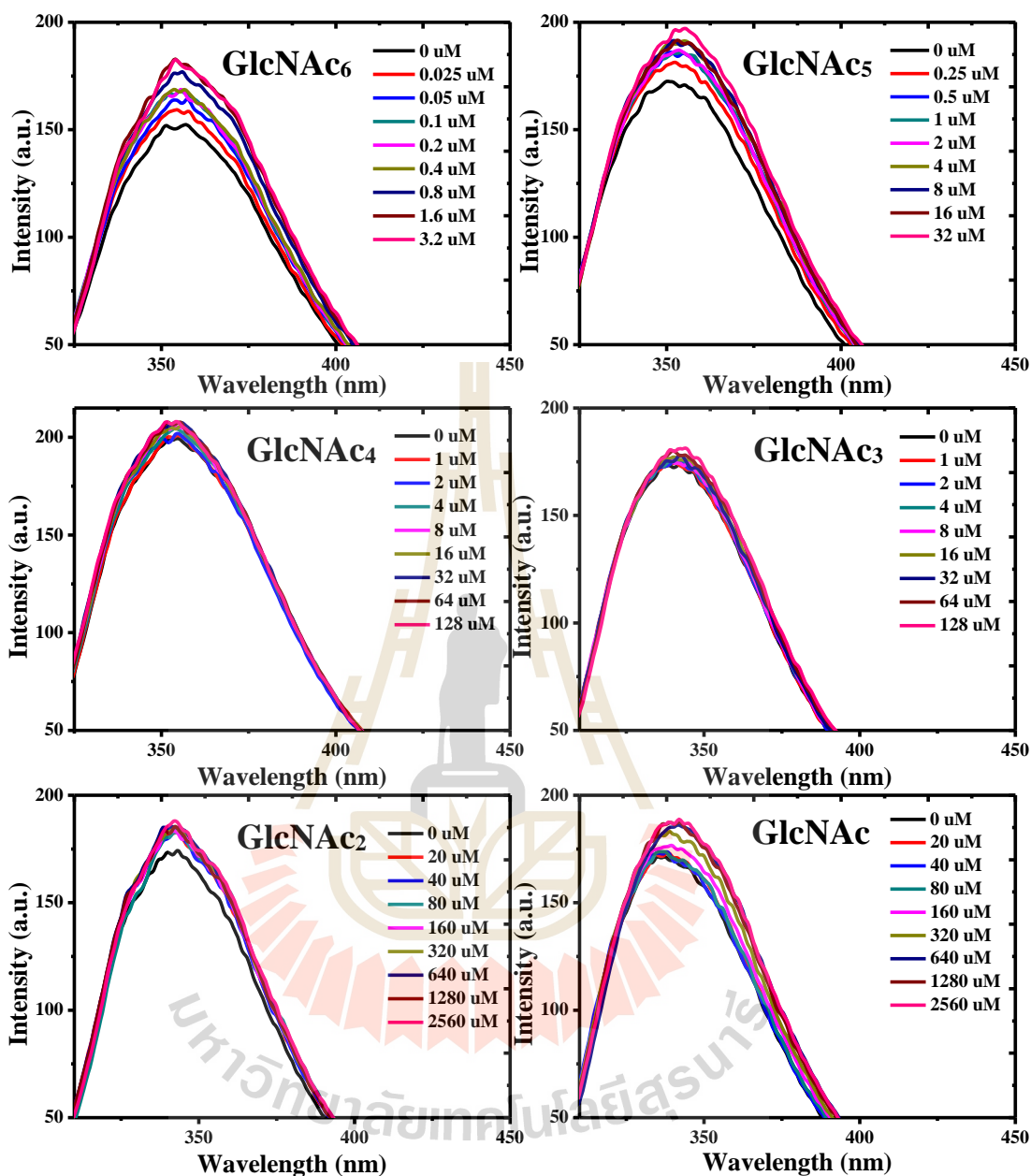


**Figure 3.29** Tryptophan fluorescence quenching spectra of *VhChiP* WT. The titration curves show the changes in the fluorescence intensity with increasing concentration of chitooligosaccharides ((GlcNAc)<sub>n</sub>,  $n = 1 - 6$ ) added to the protein solution.

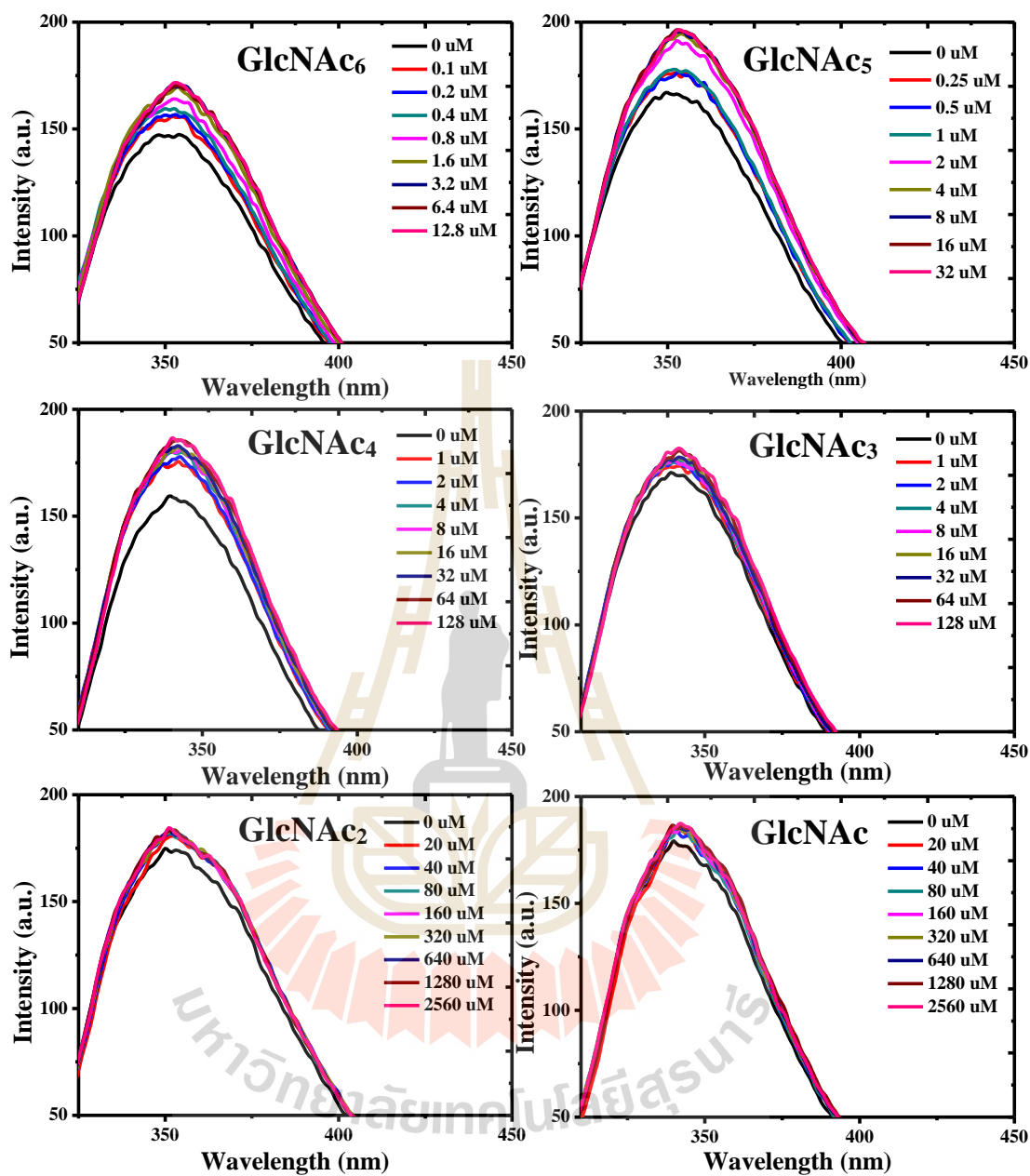


**Figure 3.30** Tryptophan fluorescence quenching spectra of *VhChiP* W136F. The titration curves show the changes in the fluorescence intensity with increasing concentration of chitoooligosaccharides ((GlcNAc)<sub>n</sub>, *n* = 1 – 6) added to the protein solution.

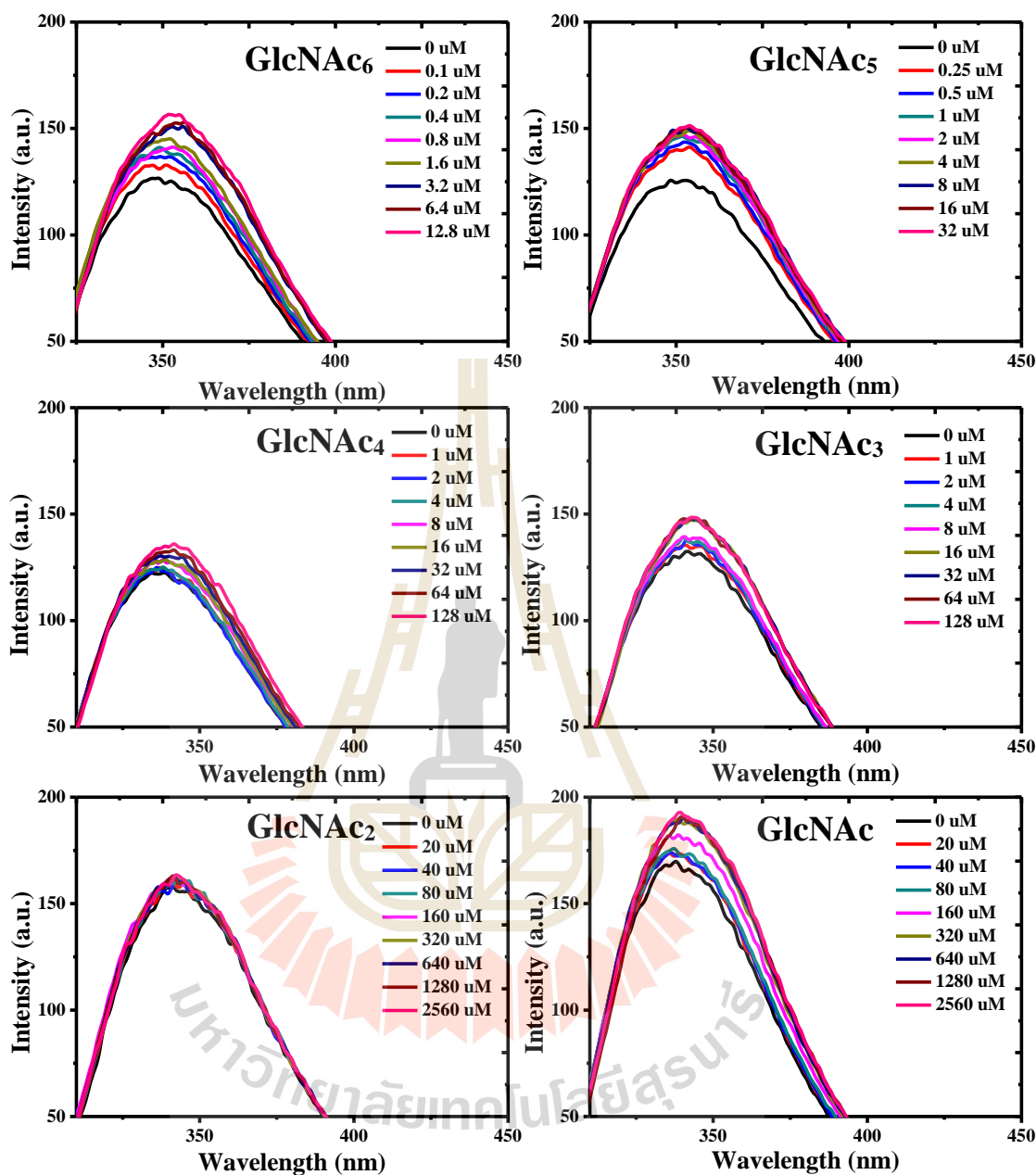


**Figure 3.31** Tryptophan fluorescence quenching spectra of *VhChiP* W136A. The titration curves show the changes in the fluorescence intensity with increasing concentration of chitooligosaccharides ((GlcNAc)<sub>n</sub>, n = 1 – 6) added to the protein solution.

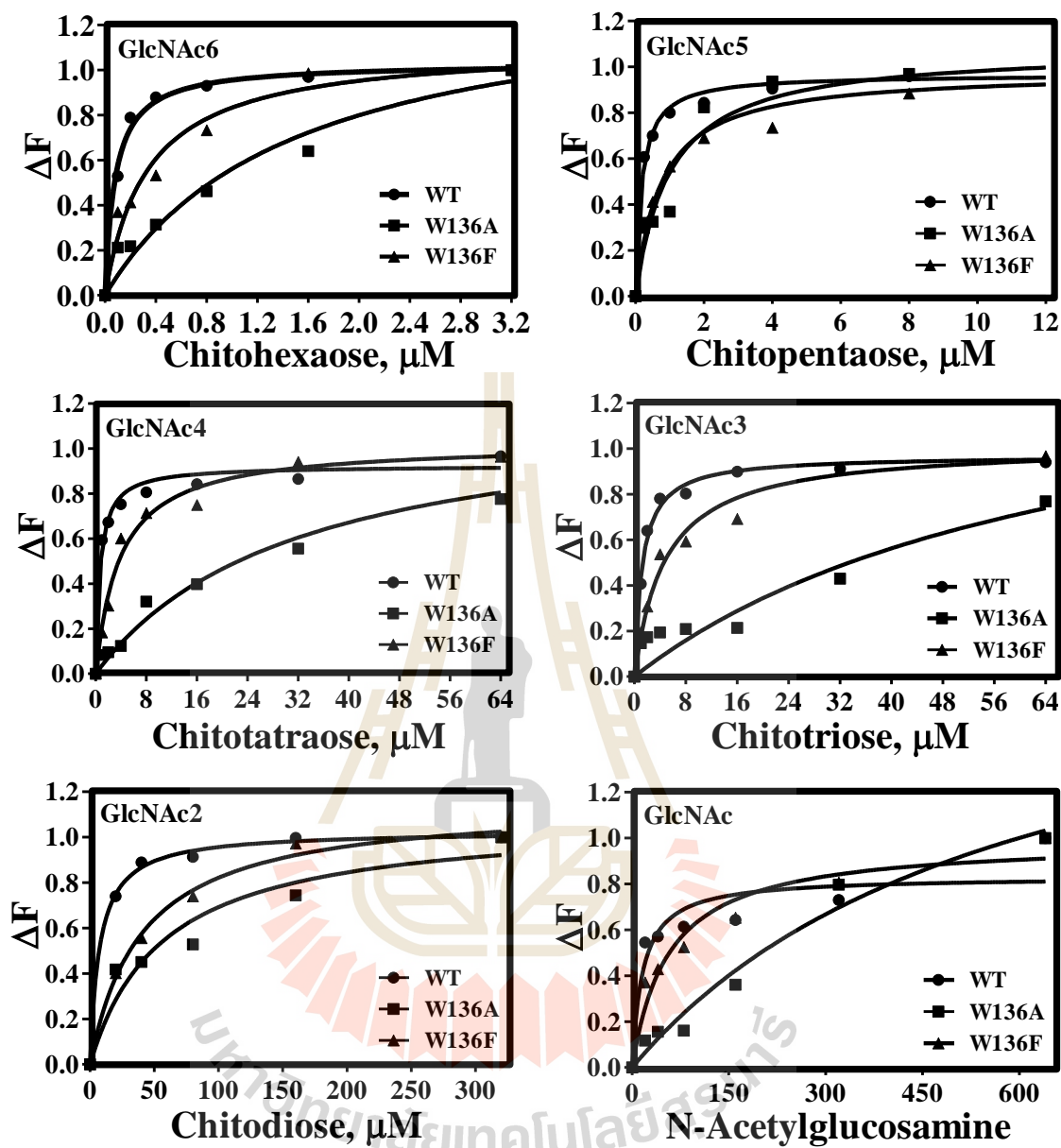


**Figure 3.32** Binding curve plots of WT and its mutants with chitooligosaccharides.

The Michaelis-Menten plots were obtained from the data on the Figure 3.29-3.31. The plot of  $(F_c - F_0)/(F_{max} - F_0)$  versus various concentration of  $(\text{GlcNAc})_n$ ,  $n = 1 - 6$ .

**Table 3.9** The binding constants estimated from fluorescence spectroscopy

Ligand	VhChiP Protein	$K_d$ ( $\mu\text{M}$ )	$K \times 10^6$ ( $\text{M}^{-1}$ )	$\Delta G = -RT \ln K$ ( $\text{kJ mol}^{-1}$ )
(GlcNAc) <sub>6</sub>	Wild type	0.08 $\pm$ 0.03	12.70 $\pm$ 0.46	-57.5 $\pm$ 0.9
	W136A	0.68 $\pm$ 0.37	1.71 $\pm$ 0.07	-52.5 $\pm$ 1.3
	W136F	0.23 $\pm$ 0.09	4.83 $\pm$ 0.21	-55.1 $\pm$ 1.0
(GlcNAc) <sub>5</sub>	Wild type	0.28 $\pm$ 0.10	3.83 $\pm$ 0.16	-54.5 $\pm$ 1.0
	W136A	1.70 $\pm$ 1.29	0.80 $\pm$ 0.04	-50.5 $\pm$ 1.7
	W136F	0.58 $\pm$ 0.17	1.83 $\pm$ 0.05	-52.8 $\pm$ 0.8
(GlcNAc) <sub>4</sub>	Wild type	0.74 $\pm$ 0.09	1.35 $\pm$ 0.01	-52.1 $\pm$ 0.3
	W136A	19.88 $\pm$ 10.50	0.05 $\pm$ 0.02	-44.1 $\pm$ 1.3
	W136F	3.67 $\pm$ 0.55	0.27 $\pm$ 0.04	-48.1 $\pm$ 0.4
(GlcNAc) <sub>3</sub>	Wild type	2.94 $\pm$ 1.62	0.45 $\pm$ 0.033	-49.0 $\pm$ 1.7
	W136A	46.91 $\pm$ 20.20	0.02 $\pm$ 0.008	-41.9 $\pm$ 1.0
	W136F	6.62 $\pm$ 2.17	1.61 $\pm$ 0.040	-46.7 $\pm$ 0.8
(GlcNAc) <sub>2</sub>	Wild type	9.33 $\pm$ 2.93	0.11 $\pm$ 0.040	-45.9 $\pm$ 0.9
	W136A	112.43 $\pm$ 27.20	0.01 $\pm$ 0.002	-39.7 $\pm$ 0.6
	W136F	41.42 $\pm$ 19.80	0.02 $\pm$ 0.010	-42.3 $\pm$ 1.3
GlcNAc	Wild type	15.51 $\pm$ 2.87	0.06 $\pm$ 0.0100	-44.6 $\pm$ 0.5
	W136A	241.63 $\pm$ 84.90	0.004 $\pm$ 0.0010	-37.8 $\pm$ 0.9
	W136F	75.78 $\pm$ 11.10	0.013 $\pm$ 0.0017	-40.6 $\pm$ 0.3

$K_d$  is dissociation constant (M),  $K$  is binding constant ( $\text{M}^{-1}$ ),  $\Delta G^0 =$  Gibbs free-energy change  $R$  is the gas constant ( $8.314472 \text{ J mol}^{-1} \text{ K}^{-1}$ ) and  $T$  is the temperature (in Kelvin).

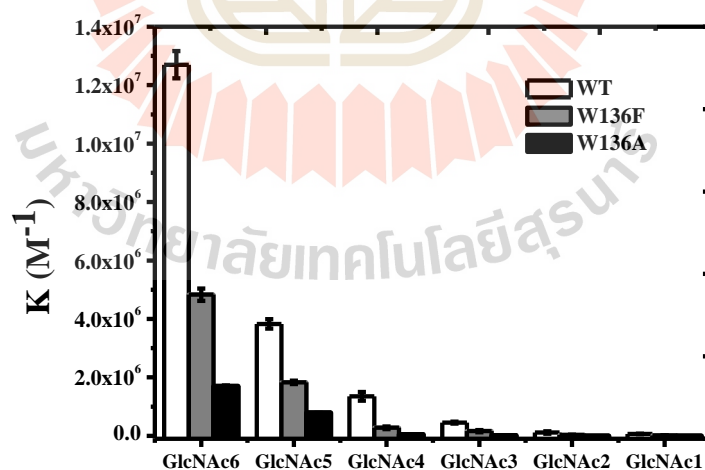


**Figure 3.33** Comparison of protein-chitooligosaccharide binding constants. The bar chart of binding constants of WT and mutants W136F and W136A with chitooligosaccharides were calculated from the binding curve plots (Figure 3.26).



### 3.3.5 Thermodynamic parameters using fluorescence quenching

The fluorescence spectra of the *VhChiP* WT (Figure 3.34), W136F (Figure 3.35) and W136A (Figure 3.36) in the presence of various concentrations of chitohexaose were acquired at 25, 30, 35, 40, and 45 °C.

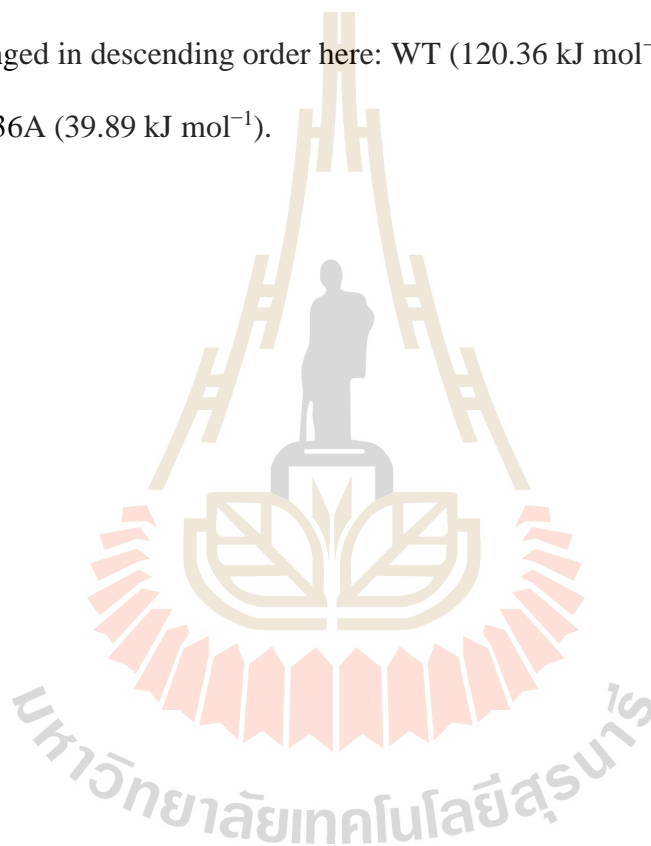
Then, binding curves of *VhChiP* WT (Figure 3.37A – top panel), W136F (Figure 3.37B – top panel) and W136A (Figure 3.37C – top panel) were evaluated with the Michaelis Menten plot to estimate the dissociation constant ( $K_d$ ) which was converted to the binding constant ( $K$ ). The values of the enthalpy change ( $\Delta H$ ) and the entropy change ( $\Delta S$ ) can be estimated by Van't Hoff plots of  $\log K$  against  $1/T$  (Temperature, Kelvin). The Van't Hoff linear equation of the WT (Figure 3.37A – middle panel) is  $y = 19,290x - 48.58$ , W136F (Figure 3.37B – middle panel) is  $y = 10,860x - 22.18$  and W136A (Figure 3.37C – middle panel) is  $y = 8,710x - 16.10$ . The slope of this linear plot represents the term  $-\Delta H/R$  while the y-intercept gives the term  $\Delta S/R$ . The Gibbs free energy of binding can then be calculated by the thermodynamic equation  $\Delta G = \Delta H - T\Delta S$ .

The thermodynamic parameters of the reaction between chitohexaose and the three protein channels were plotted in Figure 3.37 (bottom panel) for easy visualisation. The Gibbs free energy of binding was found to have a negative value for WT, W136F and W136A, suggesting the spontaneity of chitohexaose binding. The WT channel showed the highest Gibbs free energy change of  $-40.02 \text{ kJ mol}^{-1}$ , while W136F and W136A had significantly less negative values at  $-35.34$  and  $-32.52 \text{ kJ mol}^{-1}$ , respectively.

The negative enthalpy changes ( $\Delta H$ ) indicate that the binding of chitohexaose to the three proteins are exothermic processes. The binding to WT releases

160.38 kJ mol<sup>-1</sup> followed by W136F and W136A both releasing 90.29 and 72.41 kJ mol<sup>-1</sup>, respectively to the environment. This significantly higher enthalpy change of WT signifies that the chitohexaose interacts more strongly with the protein.

Entropy change ( $\Delta S$ ) expresses the change in the degree of randomness of the system under study. In this case, the degree of disorder is expressed as a  $-T\Delta S$  term as shown in Figure 3.37 (bottom panel). All three proteins gave positive  $-T\Delta S$  and they are arranged in descending order here: WT (120.36 kJ mol<sup>-1</sup>) > W136F (54.95 kJ mol<sup>-1</sup>) > W136A (39.89 kJ mol<sup>-1</sup>).



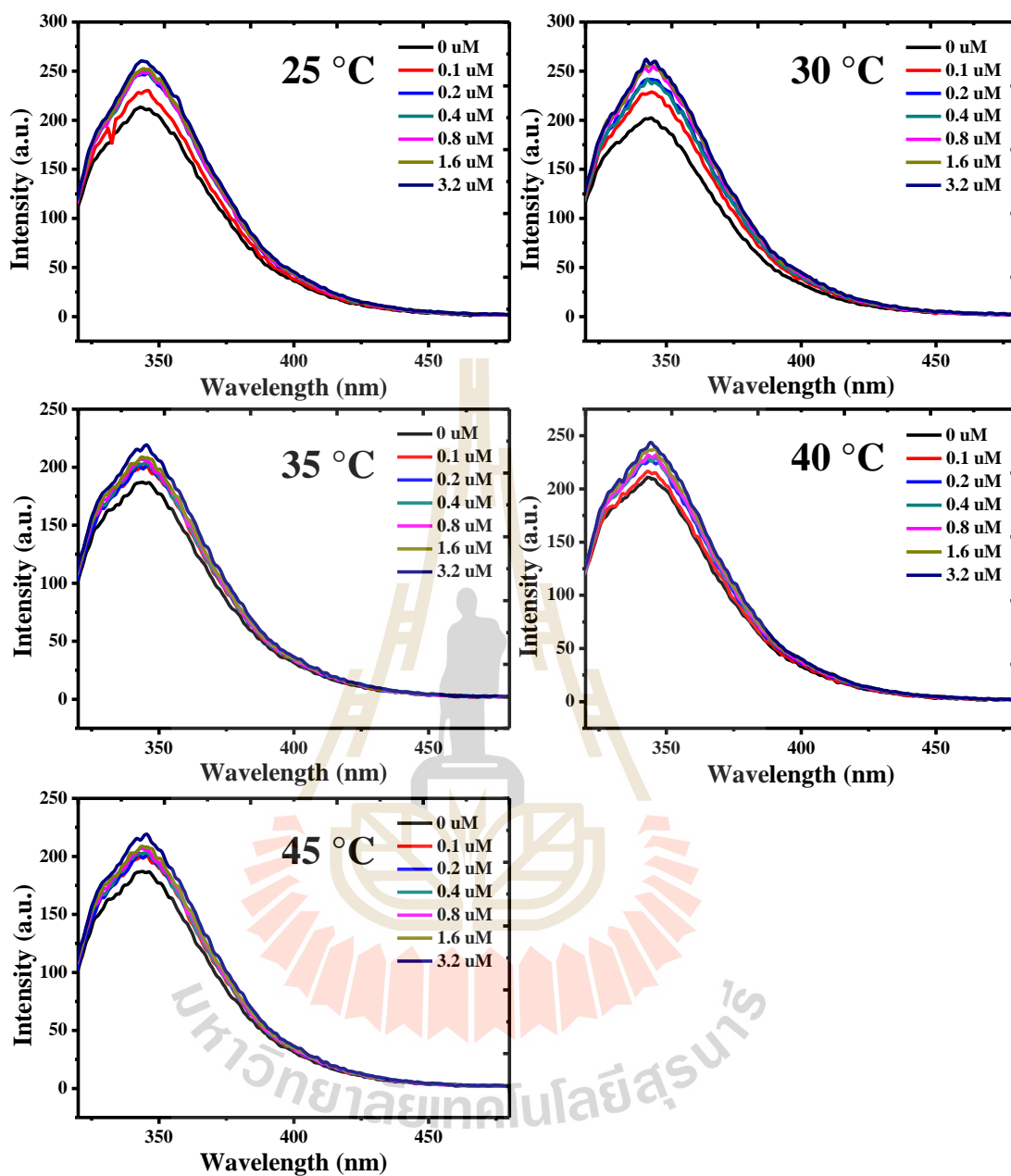


**Figure 3.34** Tryptophan fluorescence quenching spectra of *VhChiP* WT. The titration curves show changes in the fluorescence intensity with increasing concentrations of chitohexaose added to the protein solution at different temperatures: 25, 30, 35, 40, and 45 °C.

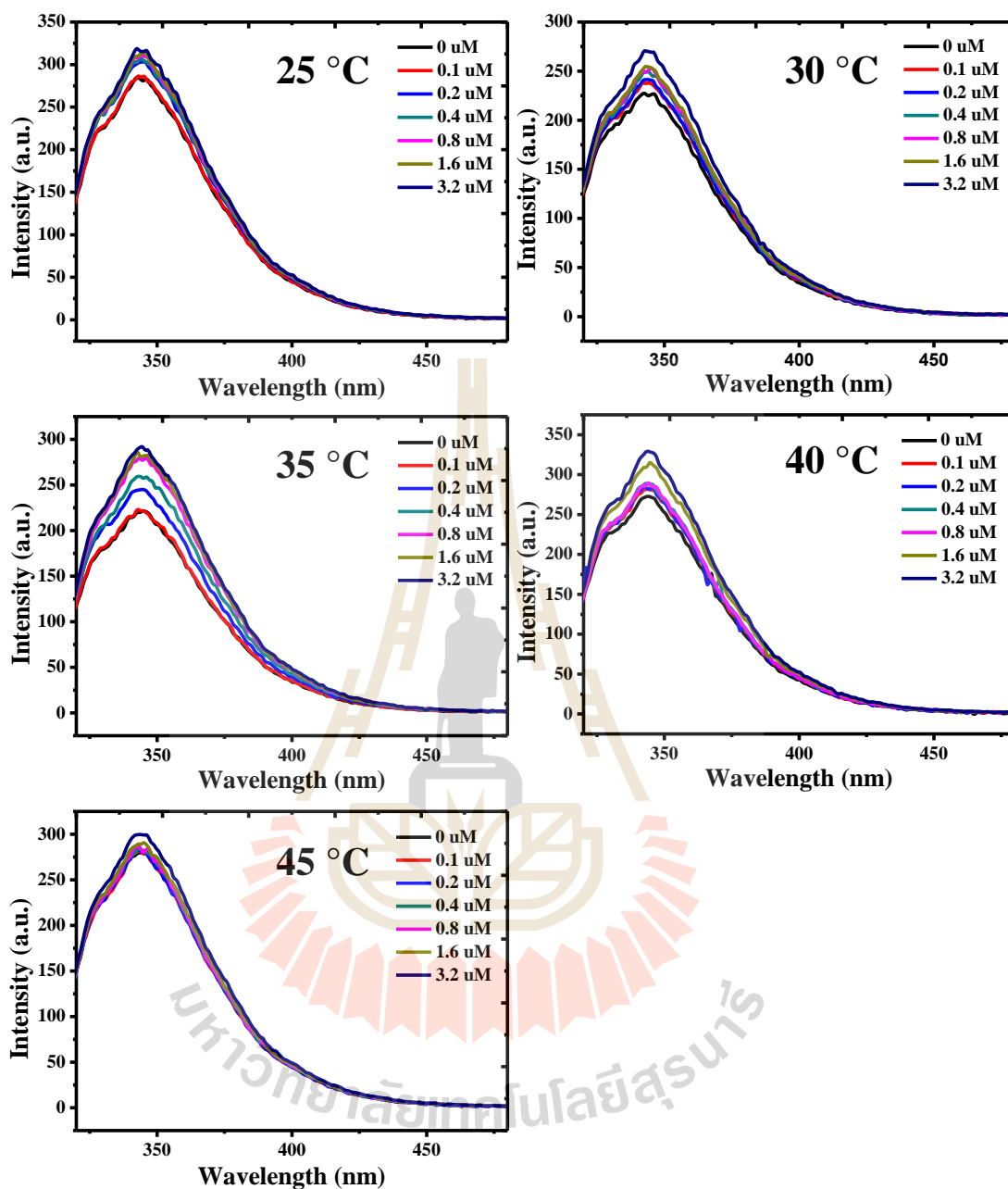


**Figure 3.35** Tryptophan fluorescence quenching spectra of VhChiP W136F. The titration curves show changes in the fluorescence intensity with increasing concentrations of chitohexaose added to the protein solution at different temperatures: 25, 30, 35, 40, and 45 °C.

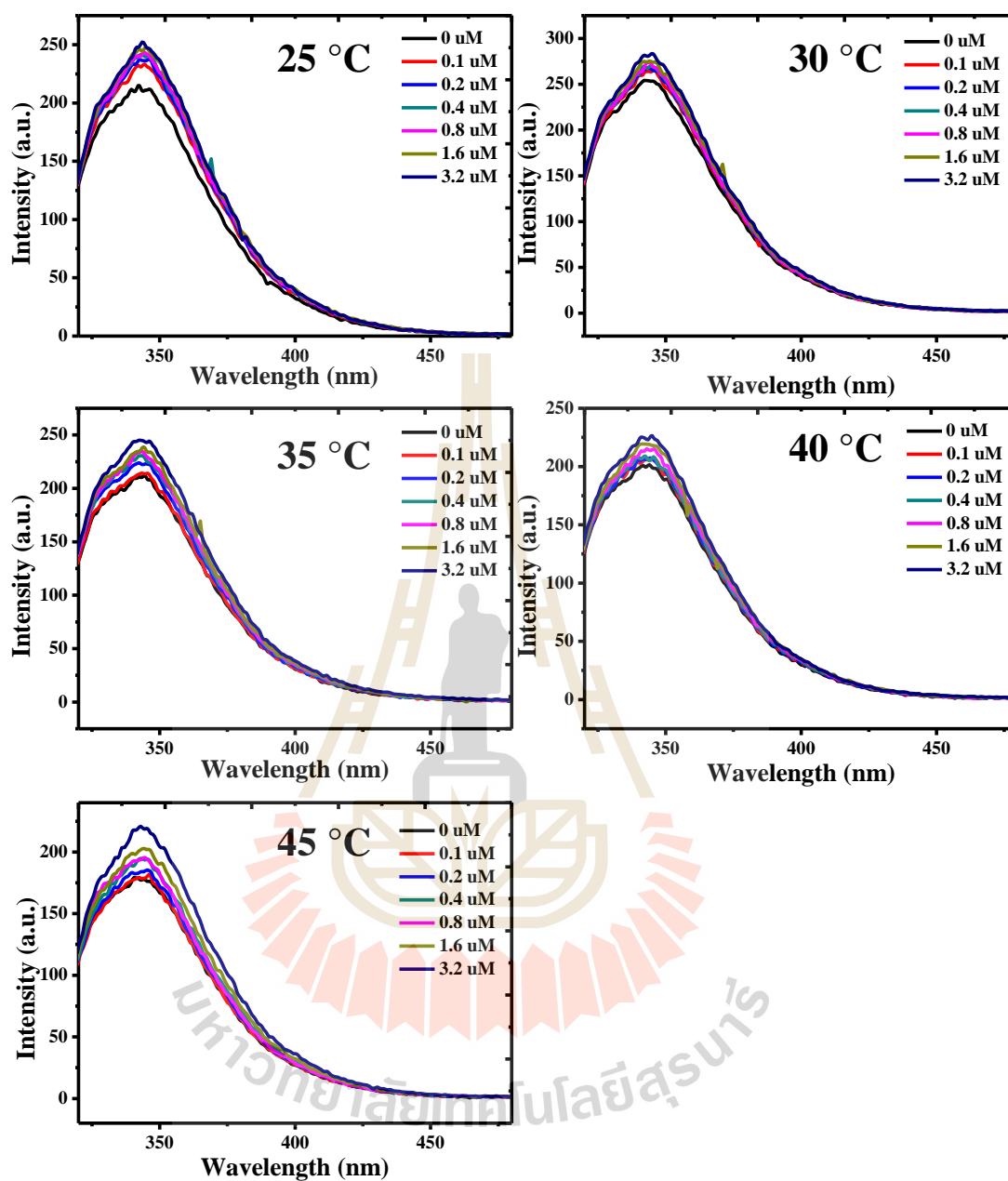


**Figure 3.36** Tryptophan fluorescence quenching spectra of *VhChiP* W136A. The titration curves show changes in the fluorescence intensity with increasing concentrations of chitohexaose added to the protein solution at different temperatures: 25, 30, 35, 40, and 45 °C.

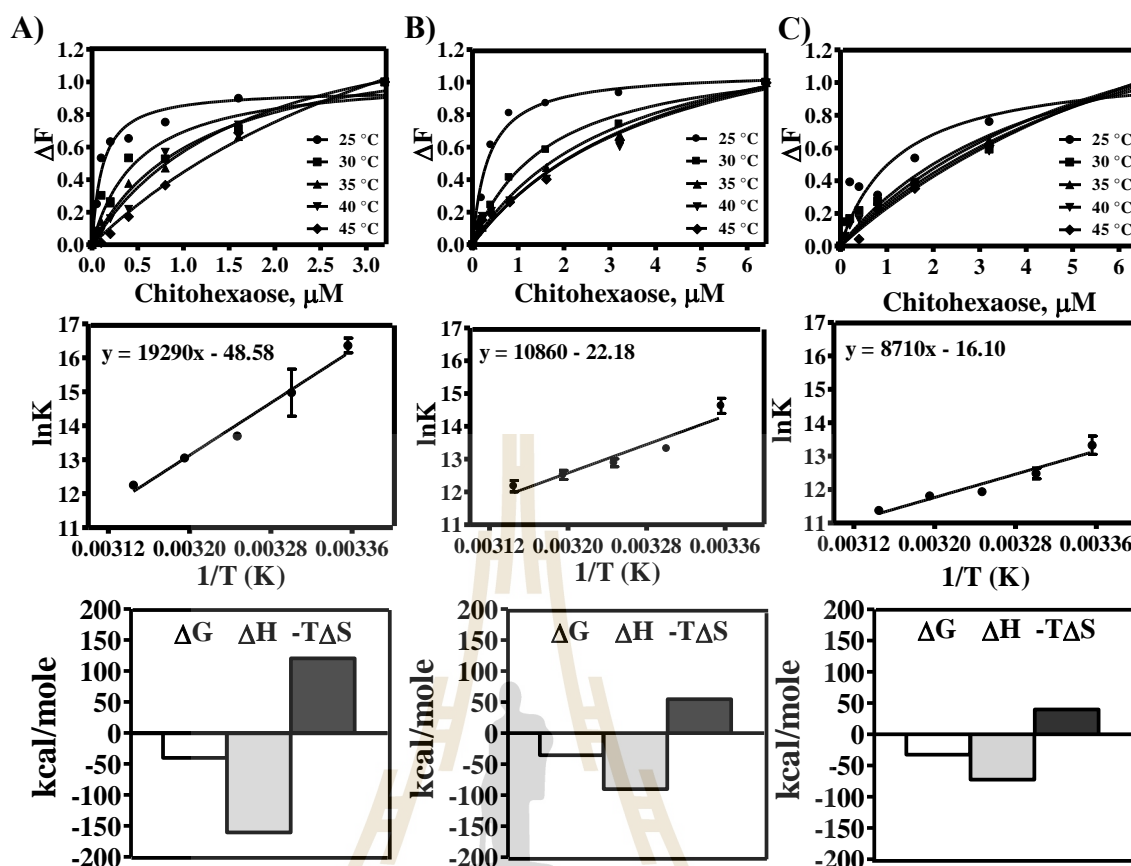


**Figure 3.37** Thermodynamic parameter plots of *VhChiP*- chitohexaose interaction assayed by the fluorescence quenching technique. Thermodynamic parameter plots for *VhChiP* WT (A) and mutants W136F (B) and W136A (C) are presented in their individual columns. The top panels show the Michaelis-Menten plots obtained from the data shown in Figure 3.34 – 3.36. Experiments were conducted at various temperatures: 25, 30, 35, 40, and 45 °C. Binding constant ( $K$ ) for each condition setting was estimated from the  $\Delta F$  versus concentration of chitohexaose plot based on Eq. 3. Middle panels show Van't Hoff plot of the logarithm of the binding constant versus the reciprocal temperature. Thermodynamic parameters can be estimated from the

linearly fitted line (Eq. 5). The bottom panels show the comparison of free energy ( $\Delta G$ ), enthalpy change ( $\Delta H$ ) and the entropy change ( $-T\Delta S$ ).

### 3.4 Structure and functional properties of chitoporin (*VhChiP*) from *Vibrio harveyi*

#### 3.4.1 Expression, purification and crystallisation of *VhChiP*

*VhChiP* was expressed without a His-tag in the outer membrane of the porin-deficient *E. coli* B121 omp8 strain and obtained in reasonable yields (~ 3 mg from 12 liters of culture). Figure 3.38A shows the SDS-PAGE of *VhChiP* native and refolded: in contrast to many other outer membrane proteins, boiled and non-boiled samples gave different mobilities. This indicates that *VhChiP* is heat-modifiable due to a lower thermal stability of the barrel. The folded protein has trimeric porin conformation, while the unfolded protein is in the monomeric form. The size of the trimeric channel was between 66 – 116 kDa and its monomeric form was about 35 – 45 kDa. The purified protein was crystallised in the presence of 0.4% C<sub>8</sub>E<sub>4</sub> detergent. The obtained crystals of *VhChiP* in space group C2 were diffracted to reasonable resolutions of ~2.5 Å (Table 3.10). Despite this, structure solution using molecular replacement (MR) failed, presumably due to the lack of a good homology model. The most likely search models with *VhChiP* gave 20% or less similarity in their sequence identities. Soaking of native crystals with different heavy atoms was also not successful.

Expression of *VhChiP* in minimal media in the presence of selenomethionine (SeMet) for phasing using single/multiple anomalous dispersion (SAD/MAD) approaches was also attempted. However, the cells failed to grow in

accordance with the protein toxicity that was observed in rich medium. Subsequently, *VhChiP* was cloned without a signal sequence and with a *C*-terminal His<sub>6</sub>-tag into pET28a to express the protein into inclusion bodies and to avoid toxicity issues. As expected, the cells grew very well in minimum medium in the presence of SeMet. *VhChiP* from inclusion bodies was folded *in vitro* from 8 M urea and purified as the native protein. Well-diffracting crystals ( $\sim 2 \text{ \AA}$  resolution) in space group P2<sub>1</sub> were obtained and a SAD dataset was collected at the absorption edge of selenium.





**Table 3.10** Structural data and refinement statistics.

	Native	Refolded	Native + (GlcNAc) <sub>4</sub>	Refolded + (GlcNAc) <sub>6</sub>
<b>Data collection</b>				
Space group	C2	P2 <sub>1</sub>	P3 <sub>1</sub> 2 <sub>1</sub>	P2 <sub>1</sub>
Cell dimensions				
a, b, c (Å)	255.7, 148.6, 54.4	146.9, 123.4, 147.0	148.7, 148.7, 158.5	146.5, 121.9, 147.2
$\alpha$ , $\beta$ , $\gamma$ (°)	90, 94.9, 90	90, 117.9, 90	90, 90, 120	90, 117.9, 90
Resolution (Å)	49.15 – 2.5 (2.56 – 2.5)	64.97 – 1.95 (1.98 – 1.95)	99.96 – 2.75 (2.83 – 2.75)	64.75 – 1.90 (1.93 – 1.90)
R <sub>merge</sub> (%)	8.6 (63.6)	7.2 (85.4)	9.2 (70.9)	6.2 (68.2)
I/ $\sigma$ (I)	12.2 (2.1)	13.9 (1.9)	10.4 (2.0)	11.0 (1.8)
Completeness (%)	95.5 (97.5)	100.0 (100.0)	98.0 (96.3)	99.6 (99.5)
Redundancy	4.1 (4.1)	6.8 (6.7)	4.4 (4.1)	3.8 (3.7)
<b>Refinement</b>				
R <sub>work</sub> /R <sub>free</sub>	26.3 / 28.9	17.5 / 19.7	22.5 / 24.8	17.5 / 19.5

Note: Values in parentheses are for the highest resolution shell.

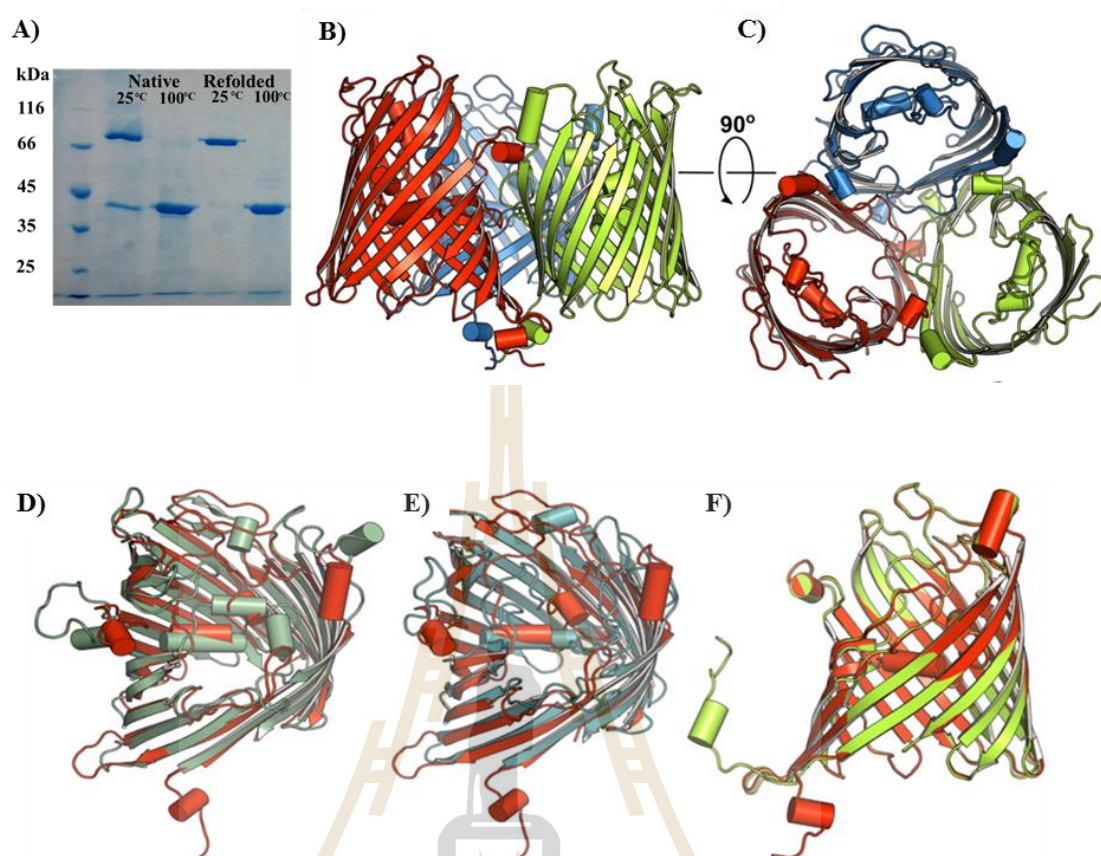


**Figure 3.38** X-ray crystal structure of *in vitro* folded *VhChiP*. A) SDS-PAGE gel of outer membrane-expressed and *in vitro* folded *VhChiP* loaded both as boiled and non-boiled samples. B) Side view and C) top view cartoon presentations of the *in vitro* folded *VhChiP* trimer. D, E) Top view superpositions of *VhChiP* (red) with *Neisseria meningitidis* PorB (green); D) and *Delftia acidovorans* Omp32 (blue); E). F) Superposition of *in vitro* folded *VhChiP* (red) with outer membrane-expressed *VhChiP* (green).

### 3.4.2 *VhChiP* forms trimers with *N*-terminally plugged pores

*In vitro* folded *VhChiP* forms a trimeric assembly of oval  $\beta$ -barrels, each consisting of 16 strands (Figure 3.38), similar to the general diffusion porins OmpF/C

from *E. coli*. Unlike OmpF/C however, the *N*-terminus of *VhChiP* does not form an intramolecular salt bridge with the *C*-terminal carboxyl group. Instead, the first 19 amino acids of the *N*-terminal end of *VhChiP* are not part of the barrel, but extend into the periplasm. The first 9 amino acids of the *N*-terminus are disordered and not visible in the electron density map (Figure 3.38B). The overall topology of the barrel, including the periplasmic *N*-terminal region, is correctly predicted by Boctopus and PRED-TMBB (Hayat *et al.*, 2016; Tsirigos *et al.*, 2016). A DALI search (Holm and Rosenström, 2010) identifies *N. meningitidis* PorB, which has 18% sequence identity similarity to *VhChiP*, as the closest structural homolog in the database ( $Z = 29$ ; r.m.s.d. 2.7 Å over 301 residues). The second-highest similarity is observed for Omp32 from *Delftia acidovorans* ( $Z = 26$ ; r.m.s.d. 2.7 Å over 295 residues), which was used previously for homology modeling of *VhChiP*. Overall, the differences between both structural homologs and *VhChiP* are substantial, especially for most extracellular loops and the functionally important, barrel constricting loop L3.

The crystal structure of the outer membrane-expressed channel is almost identical to that of the *in vitro* folded protein. Strikingly however, in the outer membrane expressed *VhChiP*, the *N*-terminal segment plugs the pore of a neighbouring  $\beta$ -barrel within the trimeric assembly, effectively blocking all  $\beta$ -barrels for sugar transport (Figure 3.39). The blocking of a channel by a neighbour within an oligomeric assembly is, to our knowledge, not yet reported. All residues of the *N*-termini have good electron density in the structure and a number of polar interactions can be identified between the *N*-terminal plugs and the barrels, most notably between Asp1 (carboxylate)-Arg94/148, Asp1 ( $\alpha$ -amino group)-Y118/Asp122, Ala3-Glu53, Asn4-Asn127/Arg312/Glu347, Ser5-Asp122, Asp6-Arg94, and Lys9-Glu76 (Figure 3.39).

Thus, five out of the first six residues of the *N*-terminus make polar interactions with the pore of the protein, suggesting that the plug resides stably in the pore.

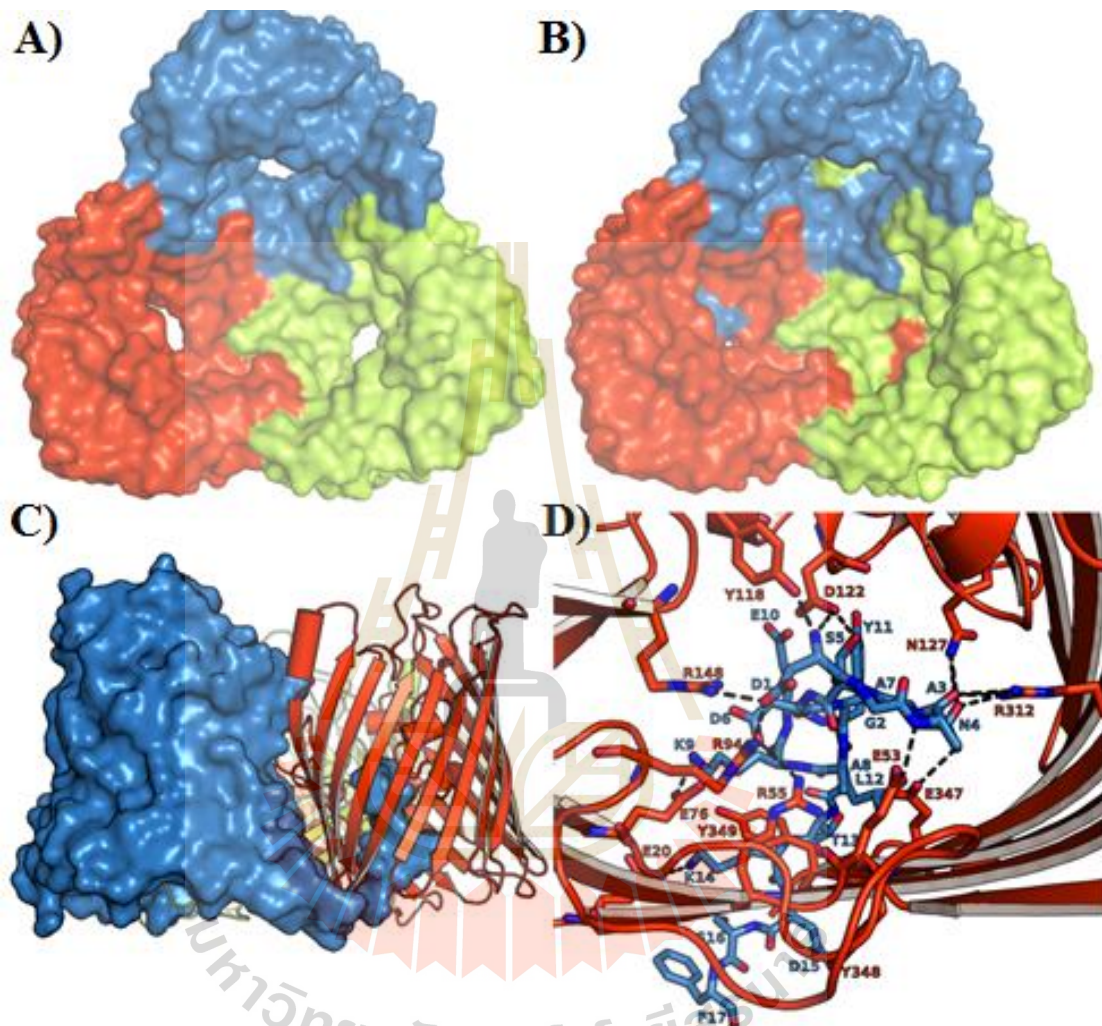


**Figure 3.39** Outer membrane expressed *VhChiP* has *N*-terminally plugged channels. Surface representations (top view) of A) *in vitro* folded *VhChiP* and B) natively-expressed *VhChiP*. The barrel lumen of the natively-expressed *VhChiP* is occupied by the *N*-terminus of a neighbour barrel. C) *N*-terminal insertion mode of natively-expressed *VhChiP*. The *N*-terminus of one barrel (blue) plugs the lumen of a neighbour barrel (red). D) Polar

interactions between the inner barrel wall (red) with the *N*-terminus of a neighbour barrel (blue).

### **3.4.3 Roles of the *N*-terminal plugs in ion and sugar transport through *VhChiP***

In order to obtain experimental evidence for a closed channel, single channel electrophysiological experiments for *in vitro* folded and natively-expressed *VhChiP* were carried out. Based on the crystal structure, a *VhChiP* variant with the first nine *N*-terminal residues removed was also generated, denoted truncated *VhChiP*. At applied potentials of  $-100$  and  $+100$  mV, the single channel conductance is essentially the same ( $\sim 2.0$  nS) for all three *VhChiP* proteins (Figures 3.40A–C). This is fully consistent with the data for the native protein obtained in previous studies (Suginta *et al.*, 2013a; Suginta *et al.*, 2013b). Surprisingly, there is no evidence for channel closing events for any of the three *VhChiP* proteins. The major difference is that the truncated channel exhibited much less gating behavior (Figure 3.40C) and showed an unusually high stability in terms of noise levels at all applied potentials (Figure 3.40-middle panel). The trimers remain fully open even at  $\pm 200$  mV, conditions under which outer membrane channels frequently undergo voltage-induced gating.

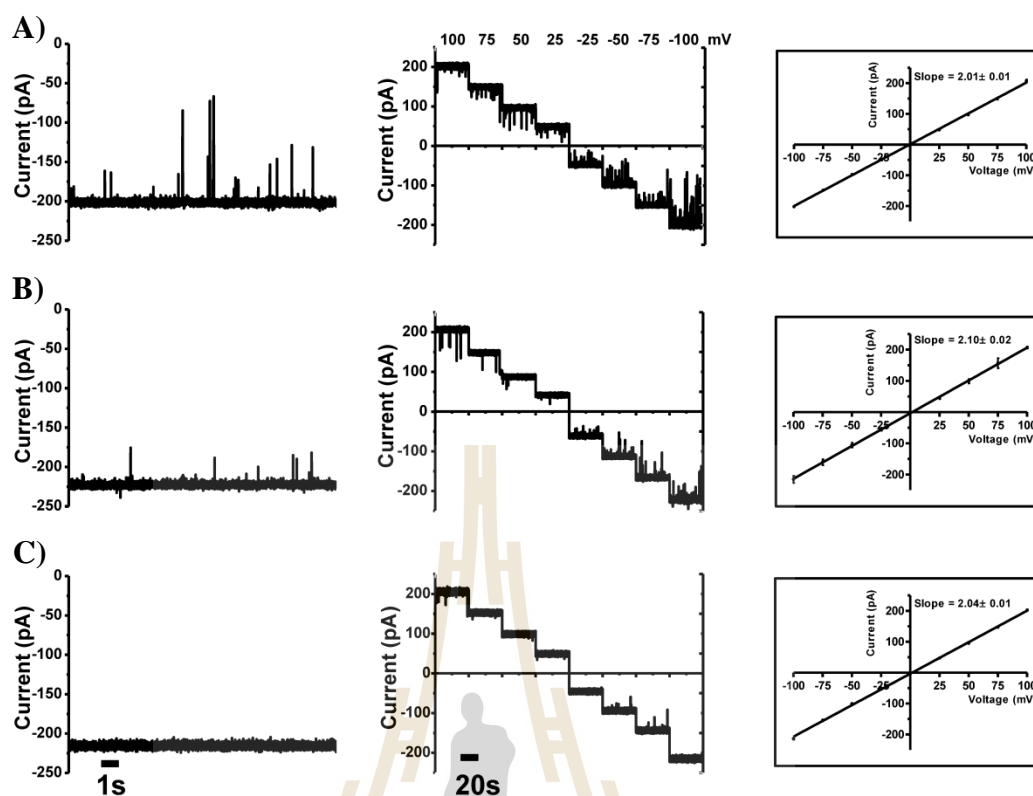


**Figure 3.40** Single channel electrophysiology of *VhChiP*. Single channel insertion of *VhChiP* native (A), *VhChiP* refolded (B) and *VhChiP* truncated (C) were reconstituted into a solvent-free DPhPC lipid membrane, containing 1 M KCl in 20 mM HEPES, pH 7.5 in the absence of chitohexaose. (*Left*) Gating behavior: typical ion current traces of single *VhChiP* variant channels in a fully open state at a transmembrane potential of  $-100$  mV, (*Middle*) The current through a single open *VhChiP* channel was monitored in 1 M KCl, following discrete changes in the voltage across the phospholipid membrane, from  $\pm 25$  to  $\pm 100$  mV. (*Right*) Current-voltage relationship of native *VhChiP* in comparison with its refolded and truncated forms. The slopes of a linear fit yielded the single channel conductance of individual *VhChiP* channels.

### 3.4.4 Chitohexaose binding to *in vitro* folded *VhChiP*

In order to obtain a structure of *VhChiP* in complex with a substrate, *in vitro* folded *VhChiP* was co-crystallised with the preferred substrate chitohexaose. Well-diffracting crystals grew under the same conditions and in the same space group as for the apo-protein (Table 3.10). Following molecular replacement, clear density was observed for all six units of the (GlcNAc)<sub>6</sub> oligosaccharide (Figure 3.41). The substrate is bound in an extended conformation with the reducing end of the molecule (denoted +6GlcNAc) in the extracellular space and stacked against the aromatic ring of Trp331. On the periplasmic side of the channel constriction, the first sugar unit (denoted +1GlcNAc) stacks against Trp123.

Beside the ring stacking, no other interactions are present between +1GlcNAc and +6GlcNAc and *VhChiP*. The aromatic ring of Trp136 stacks against both +4GlcNAc and +5GlcNAc, providing a clear explanation as to why this residue is important for chitohexaose binding to *VhChiP* (Chumjan *et al.*, 2015). Both Trp123 and Trp136 are conserved in *VhChiP* orthologs, whereas Trp331 is not (Figure 3.42). The structure provides a clear rationale for the fact that (GlcNAc)<sub>6</sub> is the best substrate for *VhChiP*, since beyond +1GlcNAc and +6GlcNAc, the channel widens, decreasing the potential for interactions between the substrate and the channel. The central four residues of the sugar chain (+2GlcNAc to +5GlcNAc) form several polar interactions with the channel's interior, some of which are mediated by water molecules (Figure 3.41). The acetamido groups of the successive GlcNAc units point in opposite directions, as is also observed for the chitohexaose molecule bound to the *E. coli* transglycosidase MltA (van Straaten *et al.*, 2007). The acetamido carbonyl groups of +2GlcNAc and +3GlcNAc are likely to be of especial importance for binding. The former interacts closely with the amide of Asn127 and to a lesser extent with Arg312,

whereas the latter makes strong hydrogen bonds to the side chains of Arg94 and Arg148 (Figure 3.41). In addition, the acetamido amides of +2GlcNAc and +3GlcNAc interact with the carboxylates of Glu347 and Asp122, respectively.

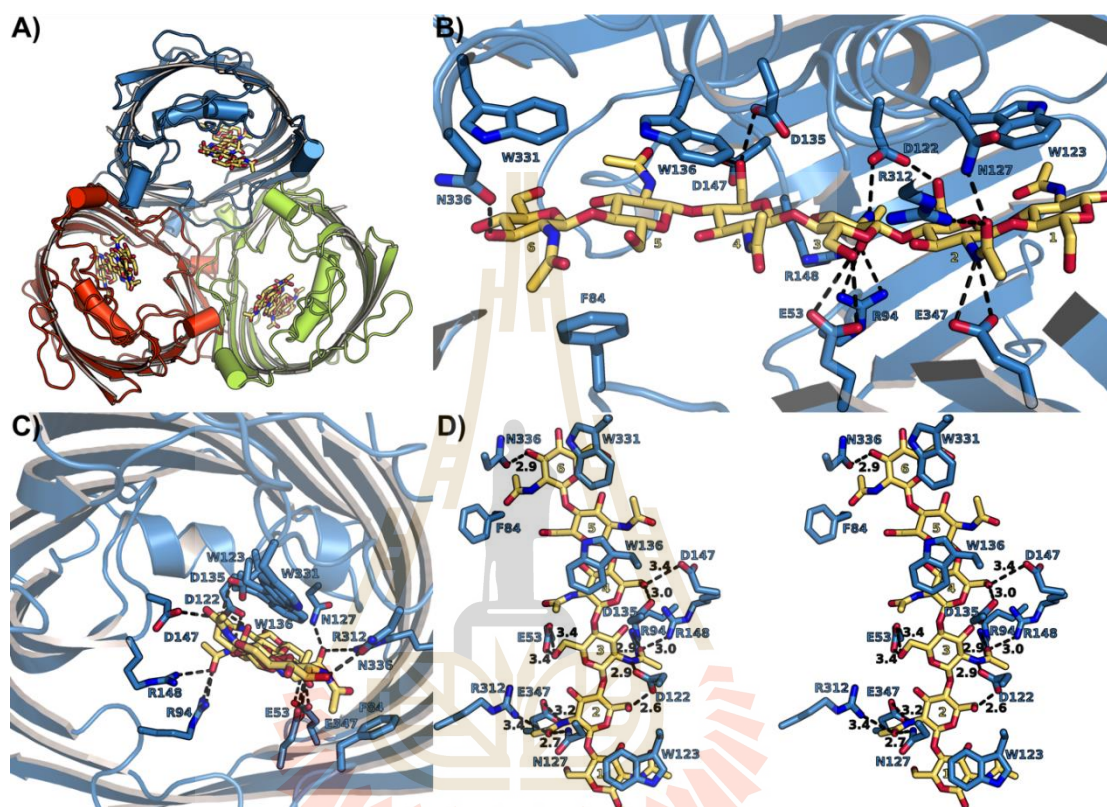


**Figure 3.41** Chitohexaose binding to *VhChiP*. A) Overview from the extracellular side. B) Side view and D) stereo pairs presented on 90°, with selected interactions between the sugar and *VhChiP* labelled. C) Top view schematic showing the interactions of key residues with chitohexaose.



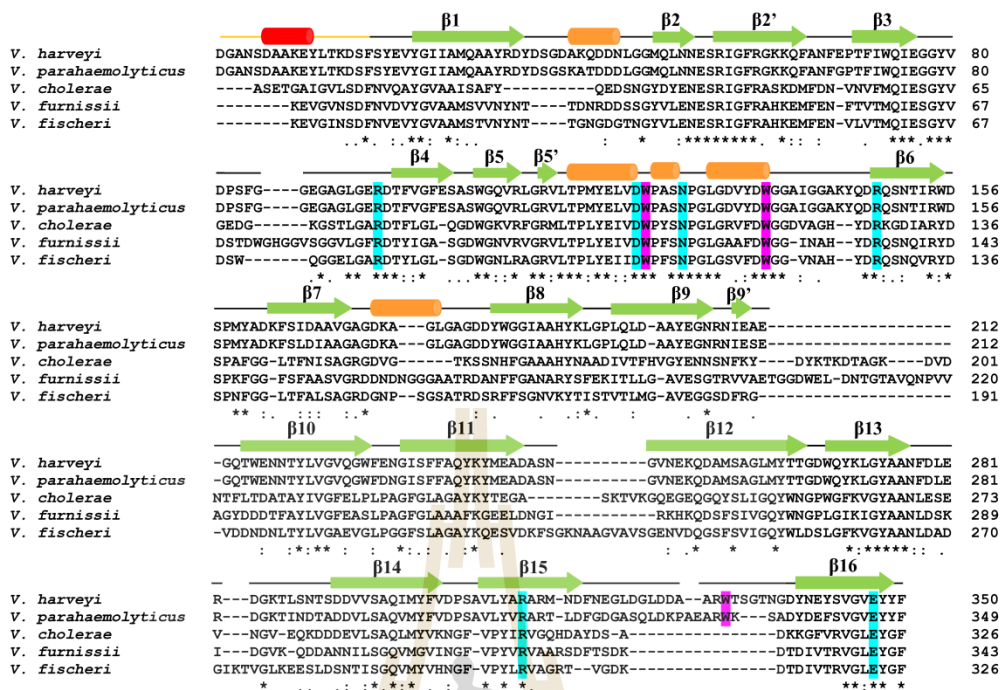


**Figure 3.42** Alignment of *VhChiP* orthologs from *Vibrio* species with observed secondary structure elements indicated (cylinders, helices; arrows,  $\beta$ -sheets). Key hydrophobic (purple) and hydrophilic residues (cyan) interacting with chito-oligosaccharides are coloured. The following orthologs have been aligned: *V. harveyi* (GenBank ID: HF558985.1), *V. parahaemolyticus* (GenBank ID: CPO12950.1), *V. cholera* (GenBank ID: DQ774012.1), *V. furnissii* (GenBank ID : AF129934.1) and *V. fischeri* (GenBank ID : CP001139.1). A BlastP search using chitoporin from *V. harveyi* (UniProtKB/ TrEMBL entry: LORVU0) as protein template identified putative chitoporins. The alignment was generated with “CLASTALW” algorithm in the DNASTAR package and displayed in Genedoc. The secondary structure of *VhChiP* was constructed by ESPript v. 2.2.

### 3.4.5 Chitotetraose binding to natively-expressed *VhChiP*

Given that the channels of the outer membrane-expressed apo-protein are closed due to the insertion of the *N*-terminus of a neighboring monomer (Figure 3.39), it is important to establish whether the incoming substrate from the extracellular space could displace the *N*-terminus and bind in the pore. Outer membrane-expressed *VhChiP* was co-crystallised with chitotetraose ((GlcNAc)<sub>4</sub>). Outer membrane expressed *VhChiP* in the presence of the (GlcNAc)<sub>4</sub> substrate also crystallises under the same conditions and in the same space group as the closed apo protein (Table 3.10). Importantly, the oligosaccharide is bound in the channel and has displaced the *N*-terminus, which is now in the periplasmic space and has the same conformation as that of the *in vitro* folded protein.

The (GlcNAc)<sub>4</sub> substrate occupies approximately the positions of +2GlcNAc to +5GlcNAc of the (GlcNAc)<sub>6</sub> chain (Figure 3.43), suggesting that the central positions of the binding site provide the most binding energy for chitooligosaccharides. However, there are differences of up to 5 Å for individual atoms between the two structures, especially at both ends of the substrate (+2GlcNAc and +5GlcNAc). In most cases, however, this does not dramatically change the interactions between the sugar and the channel. For example, the acetamido carbonyl group +2GlcNAc interacts in both structures with Asn127 and Arg312, whereas that of +3GlcNAc interacts with Arg94 and Arg148 (Figure 3.43). It appears therefore that *VhChiP* accommodates compounds of different length via subtle changes in the way the substrates are bound.

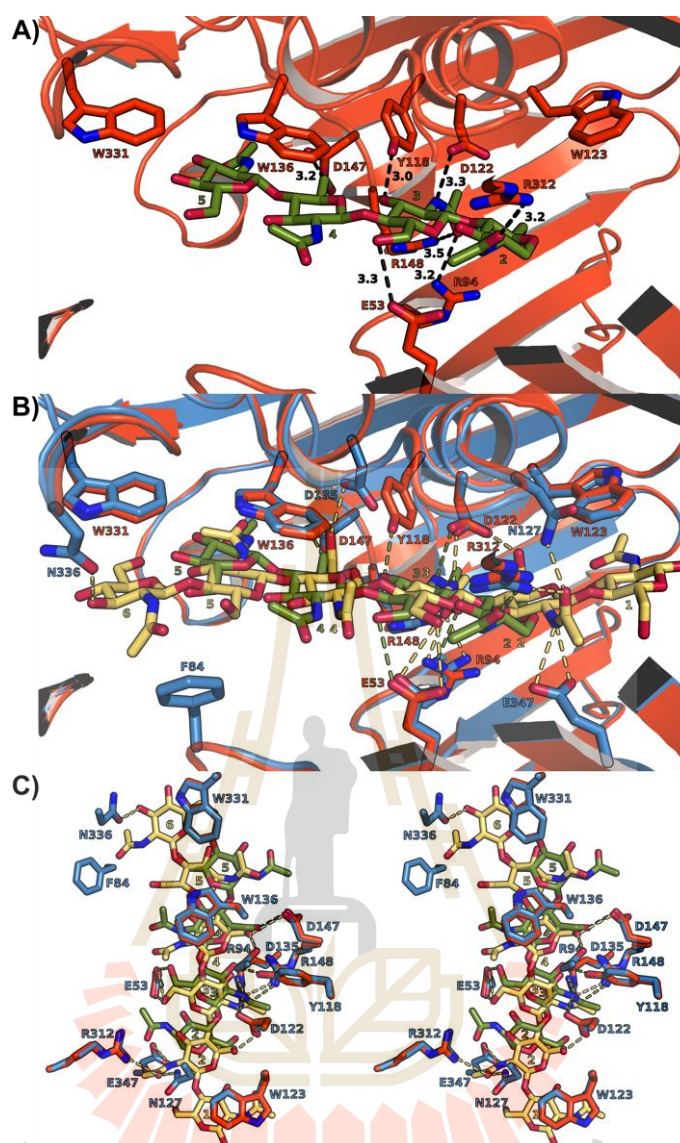


**Figure 3.43** Chitotetraose binding to natively-expressed *VhChiP* displaces the *N*-terminal plug. A–B) Side views showing the bound tetrachitose in natively-expressed *VhChiP* (A) and chitohexaose in *in vitro* folded *VhChiP* (B). C) Stereo pair showing the major interactions between chitotetraose and *VhChiP*.

### 3.4.6 Effect of the *N*-terminus on substrate binding and transport

Single channel electrophysiology of *VhChiP* in the presence of increasing concentrations of chitohexaose at various membrane potentials was

performed to probe the role of the *N*-terminus in substrate binding and transport in more detail (Figure 3.44). The results show that one subunit of the full-length channel was frequently blocked even at low concentrations of chitohexaose (0.5  $\mu\text{M}$ ), while under the same conditions, blocking events were rarely seen with the truncated channel. At 2.5  $\mu\text{M}$ , the sugar occluded all three subunits of the full-length channels, but only two subunits were blocked in truncated *VhChiP*. The data therefore suggest that the truncated channel interacts more weakly with the sugar, compared to the full-length channel. When the equilibrium binding constant  $K$  is evaluated, the full-length channel shows a binding constant of  $\sim 2 - 5 \times 10^5 \text{ M}^{-1}$ , relatively similar to previous reports (Table 3.11) (Chumjan *et al.*, 2015; Suginta *et al.*, 2013b). The binding constant vary somewhat with different membrane potentials and are generally 2- to 3-fold higher for the *in vitro* folded protein, for reasons that are not clear. However, removal of the first nine residues affects substrate binding significantly, with binding constants 10- to 15-fold lower for truncated *VhChiP* compared to outer membrane expressed full-length protein (Table 3.11).

For most systems, there is a common limitation for single channel electrophysiology, that is, the inability to distinguish substrate binding from substrate translocation through the channel, *i.e.* a compound can be released on the same side as where it binds. Therefore, the *in vitro* transport of various sugars is also evaluated via proteoliposome swelling assays. As shown in Figure 3.45, various monomeric sugars translocate efficiently through *VhChiP* in the presence and absence of the *N*-terminus. The truncated variant exhibited a more non-specific channel behavior and was approximately 2-fold more efficient in the transport of various types of small monosaccharides compared to the full-length channels. By contrast, translocation of oligomeric sugars is exquisitely specific, in accordance with previous results (Suginta

*et al.*, 2013a; Suginta *et al.*, 2013b), *i.e.* only chitooligosaccharide substrates are translocated efficiently. Interestingly, for the oligosaccharides the absence of the *N*-terminus leads to a dramatic decrease in transport rates, which is in qualitative agreement with the decreased binding constants observed in electrophysiology. Collectively the results suggest that the *N*-terminal segment plays an important role in substrate translocation through the *VhChiP* channel.

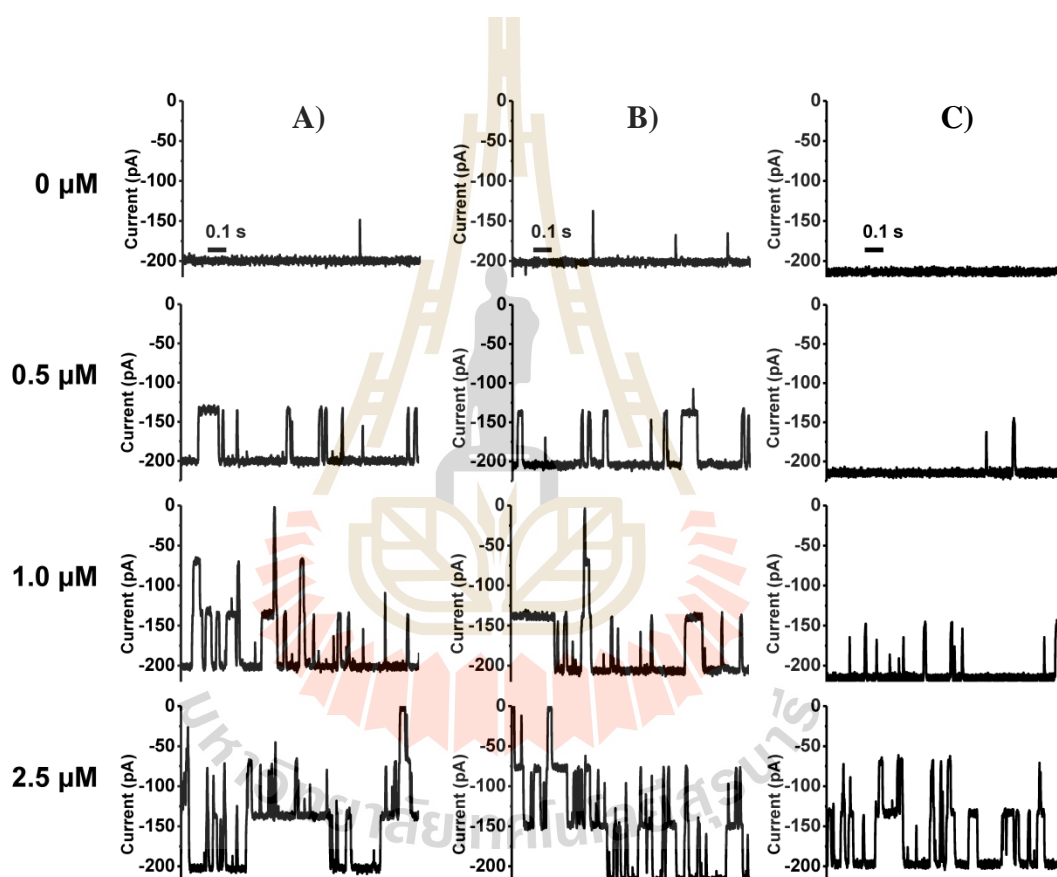


**Figure 3.44** Substrate binding to *VhChiP* probed by single-channel electrophysiology. Effect of transmembrane potentials at various concentrations of chitohexaose on the single channel insertion of *VhChiP* native, refolded and truncated. Single channel insertion of *VhChiP* native (A), *VhChiP* refolded (B) and *VhChiP* truncated (C) were reconstituted into a solvent-free DPhPC lipid membrane, containing 1 M

KCl in 20 mM HEPES, pH 7.5. Various concentrations of chitohexaose (0.25, 1.25, 2.5, and 5  $\mu\text{M}$ ) was added to the *cis* side of the membrane. The data were recorded at a transmembrane potential of  $-100$  mV.

**Table 3.11** The equilibrium binding constants  $K$  obtained by titrating 0 – 5  $\mu\text{M}$  of chitohexaose on single channel of the three *VhChiP* variants reconstituted into the DPhPc bilayers on the HeKÄ BLM setup. The values are mean  $\pm$  SD from at least three independent measurements.

Voltage (mV)	The equilibrium binding constant ( $K$ , $\text{M}^{-1}$ )		
	Native <i>VhChiP</i>	Refolded <i>VhChiP</i>	Truncated <i>VhChiP</i>
+100	245,000 $\pm$ 35,000	424,000 $\pm$ 65,000	34,000 $\pm$ 7,200
-100	434,000 $\pm$ 20,000	602,000 $\pm$ 53,000	97,000 $\pm$ 31,000
+50	154,000 $\pm$ 52,000	309,000 $\pm$ 64,000	19,400 $\pm$ 8,500
-50	386,000 $\pm$ 66,000	591,000 $\pm$ 11,000	35,000 $\pm$ 24,000
+25	103,000 $\pm$ 58,000	287,000 $\pm$ 38,000	7,400 $\pm$ 2,800
-25	242,000 $\pm$ 73,000	376,000 $\pm$ 52,000	19,600 $\pm$ 4,300

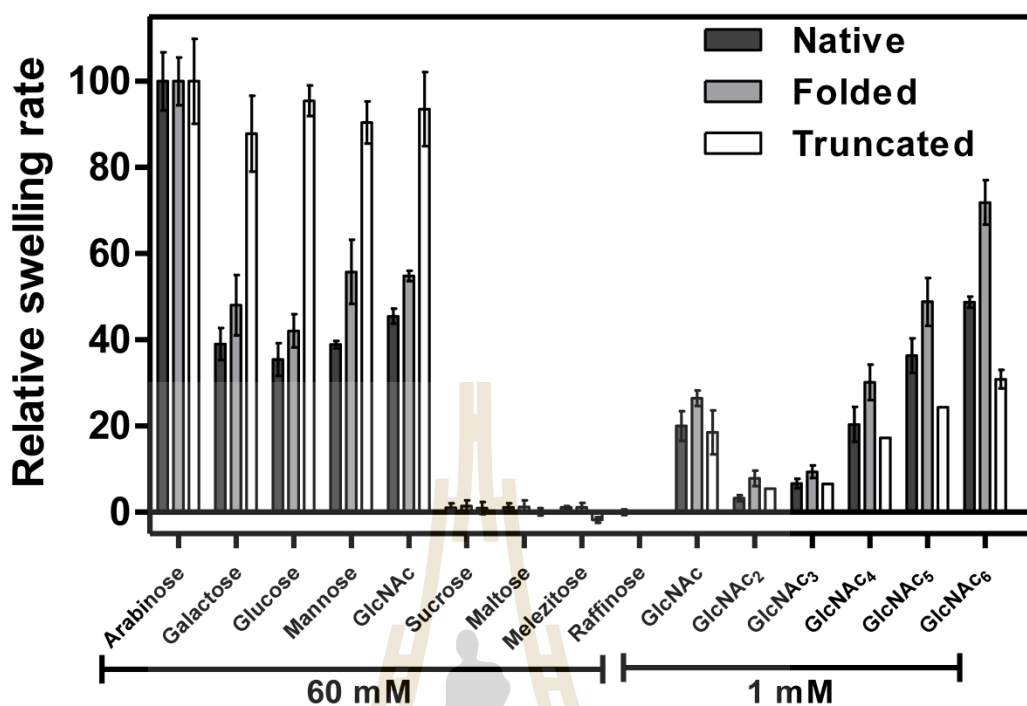


**Figure 3.45** Importance of the *N*-terminus for substrate transport. Proteoliposome swelling assays in the presence of various mono- and oligosaccharides as well as chito-oligosaccharides of different lengths were carried out. Swelling of *Vh*ChiP-containing proteoliposomes was induced by neutral sugars. For each preparation, multilamellar liposomes were reconstituted with 200 ng of purified *Vh*ChiP. The isotonic concentration was determined to be 60 mM *D*-raffinose that caused no change in the absorbance at 500 nm of the proteoliposome suspension, over a period of 60 s. Each swelling rate was normalised to the rate of swelling in arabinose, which was set to 100%, obtained from 3 independent sets of experiments.

## CHAPTER IV

### DISCUSSION

#### Part I: Outer membrane protein (*BpsOmp38*) from *Burkholderia pseudomallei*

##### 4.1 Functional properties and mutation effects of Tyr119 of *BpsOmp38*

Antimicrobial resistance levels of our clinically-derived *B. pseudomallei* strain were evaluated. As shown in Table 3.1, most MIC values were above the breakpoint values, indicating that this *B. pseudomallei* strain is intrinsically resistant to most antimicrobial agents, and sensitive only to ceftazidime and meropenem. When compared with the 65 *B. pseudomallei* isolates reported previously by Thibault *et al.*, (Thibault *et al.*, 2004), our *B. pseudomallei* strain had greater resistance to amoxicillin, cefoxitin, imipenem, and ciprofloxacin, but lower resistance to norfloxacin. Although amoxicillin, imipenem, and co-trimoxazole are commonly prescribed for melioidosis treatment (Cheng *et al.*, 2004; Chetchotisakd *et al.*, 2001; Simpson *et al.*, 1999; Suputtamongkol *et al.*, 1994; Wuthiekanun and Peacock, 2006), our data clearly indicated that such antimicrobial agents would not be applicable to this *B. pseudomallei* strain. This *B. pseudomallei* exhibited particularly high resistance to three antimicrobial agents, penicillin G, cefoxitin and doripenem, with MIC values of 1,024 to > 2,048  $\mu\text{g mL}^{-1}$ . Statistical analysis shows essential agreement of 100% within  $\pm 2 \log_2$  dilution and  $\geq 92\%$  within  $\pm 1 \log_2$  dilution, which is larger than a threshold for the  $\log_2$  dilution analysis (85% essential agreement for  $\pm 2 \log_2$  dilution previously reported by Marley



*et al.* (1995)). This indicates that the differences of MIC values with and without the presence of PA $\beta$ N are insignificant. The correlation of the two-studied groups for all 14 antibiotics yielded  $p > 0.05$  in the one-way ANOVA analysis, further confirming the insignificant differences in the MIC values with and without PA $\beta$ N. Therefore, both statistical analyses clearly suggested that the intrinsic resistance of *B. pseudomallei* to the drugs tested is not mediated by RND-type multidrug efflux pumps.

Recombinant *BpsOmp38* was previously expressed in inclusion bodies that required unfolding/refolding treatment and this often yielded only small ( $\mu$ g) quantities of purified protein, which were insufficient for thorough functional characterisation. However, the new protocol (section 2.5.1.6) allowed trimeric *BpsOmp38* to be expressed and inserted in the cell wall of the *E. coli* host cells, from which it was purified to homogeneity. As shown in Figure 3.3B, the purified protein, which migrated as a band between 29 and 42 kDa on SDS-PAGE, was equivalent to *BpsOmp38* isolated from the outer membrane of native *B. pseudomallei* (lane 4) (Siritapetawee *et al.*, 2004a). After purification, 1 – 2 mg of recombinant *BpsOmp38* per liter of bacterial culture was obtained. This was 5 – 10 times higher than that obtained using the unfolding/refolding protocol (Siritapetawee *et al.*, 2004a). Although in the *E. coli* BL21 (Omp8) Rosetta strain the genes encoding OmpF, OmpC, OmpA and LamB are disrupted (Prilipov *et al.*, 1998b), previous study showed that this bacterium could still express a significant amount of endogenous OmpN, as a major contaminant (Suginta *et al.*, 2013a). Despite the fact that the OmpN gene is quiescent (Prilipov *et al.*, 1998a), with deficiency of the usual porin expression, OmpN seemed to be induced. This is probably as an adaptive response to the nutritional stress and the need for the maintenance of normal growth. However, *E. coli* harboring the heterologous gene used *BpsOmp38* as a major conduit for molecular uptake instead. This is supported by the

data in Table 3.4, which shows some changes in the antimicrobial susceptibility of *E. coli* expressing *BpsOmp38* (column 2) as compared to the control *E. coli* (column 1).

*E. coli* harboring pET23d(+) with and without the *BpsOmp38* DNA insert had exceptionally high MIC values for  $\beta$ -lactam antimicrobial agents. The pET23d(+) vector contains the  $\beta$ -lactamase gene in the same orientation as the target gene, so the high resistance presumably resulted from the degradation of the penicillin antibiotics by  $\beta$ -lactamase. This was verified by the reduction of MIC values from  $>2,048 \mu\text{g mL}^{-1}$  to  $32 \mu\text{g mL}^{-1}$  (Table 3.4, values in brackets) for both penicillin G and amoxicillin when clavulanic acid, a suicide inhibitor of  $\beta$ -lactamases, was included in the culture medium. These results suggested that  $\beta$ -lactamase conferred on *E. coli* a high level of resistance towards the  $\beta$ -lactam antibiotics. The MIC value for kanamycin of *E. coli* harboring both empty and recombinant plasmid was also high, since this pET-series vector carries the kanamycin resistance gene.

*In vivo* investigation in the exogenous *E. coli* system suggested that MIC values of all antimicrobial agents against *E. coli* expressing *BpsOmp38*WT were generally higher than in control cells, which were transfected with a vector containing no insert. These control cells continued to express OmpN to support growth and this was presumably responsible for the observed susceptibility to antimicrobial agents, while over-expression of *BpsOmp38* apparently caused the suppression of OmpN expression. As shown earlier, increased MIC values in *E. coli* expressing *BpsOmp38* suggest that recombinant *BpsOmp38* is used for entry of antibiotic molecules into these cells, its lower permeability lowering the antimicrobial susceptibility of the *E. coli* strain. *BpsOmp38* has poor permeability towards most antimicrobial agents, hence causing decreases in antimicrobial susceptibility in the *E. coli* expressing *BpsOmp38* as shown in Table 3.4.

Log<sub>2</sub> dilution analysis (Table 3.4, column Control and WT) suggests that the difference in MIC values of the three two-group comparisons were significant (essential agreement of  $\leq 85\%$ ) with ceftazidime and gentamicin. Since log<sub>2</sub> dilution analysis gave insufficient statistical resolution, ANOVA analysis using a non-parametric correlation (Spearman) test was further carried out. One-way ANOVA suggests significant differences ( $p < 0.05$ , values marked with an asterisk) with a broader range of antimicrobial agents, including penicillin G, ceftazidime, cefoxitin, imipenem, doripenem, co-trimoxazole, and gentamicin. In *E. coli* expressing *BpsOmp38* Y119A, susceptibility towards certain cephalosporins and carbapenems was regained (Table 3.4). Again, log<sub>2</sub> dilution analysis shows significant difference with penicillin G, ceftazidime and gentamicin. On the other hand, ANOVA analysis shows significant difference for cefoxitin, meropenem and imipenem. The limited significance of mean values with log<sub>2</sub> dilution analysis may reflect inadequate sample sizes. For ANOVA, small but equal sample sizes are generally accepted to give reliable results. The decreasing MIC values with *E. coli* expressing *BpsOmp*Y119A mutant agree well with the enlargement of the pore conductance (as seen in Figure 3.5) as a result of the replacement of the bulky tyrosine side chain with a smaller one. In contrast, *E. coli* expressing the *BpsOmp38* Y118F mutant had decreased susceptibility to the same groups of antimicrobial agents. This may be associated, in part, with the reduced pore conductance due to the 'greasy' phenylalanine side chain at position 119.

The results obtained from our *in vivo* studies indicated that expression of exogenous *BpsOmp38* altered susceptibility of the Omp-deficient *E. coli* host to antimicrobial agents of the cephalosporin and carbapenem classes. In analogous work, a recent study by Bajaj *et al.* (2012) showed that *OmpPst1* porin of *Providencia stuartii*, an opportunistic pathogen found in patients with hospital-acquired urinary tract and

wound infections, developed low membrane permeability as a strategy of resistance against imipenem. Using high-resolution BLM reconstitution measurements, they demonstrated that imipenem blocked the OmpPst1 pore, leading to a progressive decrease in the pore conductance as the concentration of imipenem increased. The low permeability of OmpPst1 was further revealed *in vitro* by liposome swelling assays, which showed slow permeation through the OmpPst1 channel by imipenem.

Small, neutral sugars exhibited reduced rates of permeability through BpsOmp38 with increasing molecular size. The logarithm of the relative permeability rate is inversely proportional to the molecular weight of the sugar, which is characteristic of general diffusion porins, as previously described (Siritapetawee *et al.*, 2004b). The swelling rates of the proteoliposomes in *D*-galactose, *D*-glucose, and *D*-mannose were identical since these sugars are diastereomers of equal size. The permeation rates of the sugars through the BpsOmp38 Y119A mutant were measured and were found to be significantly greater than the rates of permeation through BpsOmp38 WT; in contrast, the permeation rates of these sugars were lower in the BpsOmp38 Y119F mutant.

Unlike sugars, the relative permeability of antimicrobial agents through BpsOmp38 was not correlated with their molecular sizes, as shown in Figure 3.7. Furthermore, liposome swelling rates in ceftazidime and cefoxitin were completely different. Although these antimicrobial agents carry the same net charge, apparently the permeation of these two antibiotics depends on the molecular structure of the drugs, which affects their interaction with the channel. The catalytic role of antibiotic-porin interactions in facilitating drug permeation was first demonstrated for OmpF (Nestorovich *et al.*, 2002). This facilitation effect was further analysed quantitatively by Danelon *et al.* (2006).

## 4.2 Structure, thermal stability and thermodynamic parameters of outer membrane protein (*BpsOmp38*) from *Burkholderia pseudomallei*

Initially, the structure of *BpsOmp38* was predicted using the 3D structure of OmpF porin from *E. coli* (PDB 3K1B), published by Kattner *et al.* (2013). The selection of OmpF as the template for developing the homology model of *BpsOmp38* was based on the extensive report on the structure-function relationship of the antibiotic translocation (Hajjar *et al.*, 2010). The Tyr119 residue of *BpsOmp38* was found to be situated at the same region of Tyr122 in the L3 loop of OmpF, which has been reported to be a key residue for the translocation of antibiotics through OmpF porin (Hajjar *et al.*, 2010). This observation has led to the hypothesis that Tyr119 of *BpsOmp38* plays an important role in the passage of antibiotics into the cytoplasm of *Burkholderia pseudomallei*. The results from microbiological assays, site-directed mutations, liposome swelling assay and biophysical measurements, together with binding kinetic constant, supported this hypothesis.

However, the amino acid sequences of various regions that participate in pore-forming properties were found to be different from that of OmpF. Moreover, BLM experiment showed that the conductance of *BpsOmp38* was 1.6 nS in 1 M KCl at  $\pm 100$  mV while that reported for OmpF was 4 nS (Weichbrodt *et al.*, 2015). This difference can be explained better with the 3D crystal structures of both Omfs.

The 3D crystal structure of *BpsOmp38* was solved at a resolution of 3.0 Å using the 3D structure of Omp32 (*Delftia acidovorans*) as the structure template (Zeth *et al.*, 2000). The overall structure of *BpsOmp38* consists of 16 anti  $\beta$ -strands with eight extracellular long loops and seven periplasmic turns. The longest loop3 (L3) was found

to protrude and hide inside the protein lumen, making the channel selective to only certain antibiotics that pass through the protein pore.

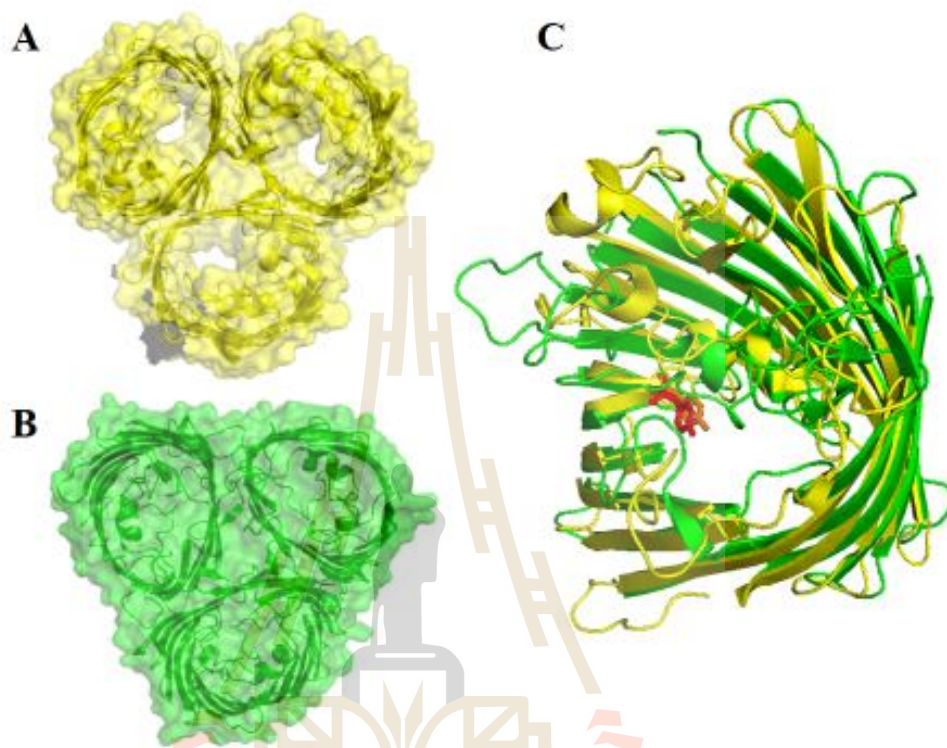


**Figure 4.1** Structural comparison of OmpF and *BpsOmp38*. Surfaces of the top view show the long loops (L3) of A) OmpF and B) *BpsOmp38* hiding in the pores. C) Top view superpositions of OmpF (yellow) and *BpsOmp38* (green) highlighting their respective key residue Y122 (orange) and Y119 (red).

A comparison of the 3D structure of OmpF and *BpsOmp38* explains the electrophysiological difference above. Although both OmpF and *BpsOmp38* have extracellular loops that protrude into their pores, the difference in the length of the loops creates a two different scenarios. OmpF with a shorter 31-residue extracellular loops (L3; Y122-R152) has channels which are not completely closed, leaving a free space

in each channel. In contrast, the longer 44-residue extracellular loops (L3; R117-T160) of *BpsOmp38* protrude and hide in the pores of *BpsOmp38*, thus obstructing the channel to a larger extent. This loop is a characteristic feature of many porins as a pore-confined loop which is responsible for the size-selectivity of the channel (Bredin *et al.*, 2002; Zeth *et al.*, 2000). This is the reason to the higher pore conductance of OmpF where the free space in the channel allows ions to pass through the channel more freely than that of *BpsOmp38*.

MIC assay showed *BpsOmp38* was highly susceptible to two antibiotics; ceftazidime (cephalosporin) and meropenem (carbapenem). Liposome swelling assays showed that both antibiotics can permeate through the *BpsOmp38* channel, while other antibiotics, such as cefipime, ceftaxime, doripenem and imipenem cannot. To compare their ability to bind to the *BpsOmp38* channel, these antibiotics were selected for the studies of thermal unfolding temperature by circular dichroism and fluorescence spectroscopy, along with single channel electrophysiology.

The fluorescence intensity at 340 nm of the denatured *BpsOmp38* was found to be lower than the intensity obtained for the folded *BpsOmp38* (Figure 3.12A). This is because the Trp residues in an unfolded confirmation are more exposed to the hydrophilic aqueous environment. From thermal unfolding experiments, we can anticipate that the tryptophan residues play an important role in the structural stability of the protein. As predicted, addition of the drugs (ceftazidime and meropenem) to which *Bps* was sensitive significantly increased the  $T_m$  values of the *BpsOmp38*, especially ceftazidime which showed the highest  $\Delta T_m$  values (Table 3.6). In contrast, the drugs (doripenem, cefepime and ceftaxime) to which *Bps* was resistant to showed lower  $\Delta T_m$ . The result indicates that interactions of the *BpsOmp38* with the sensitive drugs helped to maintain the structural stability of *BpsOmp38* channel. The results from

both CD and fluorescence spectroscopy were complimentary to each other and indicated that binding of these antibiotics stabilised both the secondary and tertiary structures of *BpsOmp38*.

In our titration experiments, changes in the fluorescence intensity upon titrating *BpsOmp38* with different concentrations of antibiotics gave rise to the quantitative values of the dissociation constant ( $K_d$ ) and the Gibbs free energy of binding ( $\Delta G$ ). The titration of the sensitive drugs (ceftazidem and meripenem) to *BpsOmp38* demonstrated the high binding affinity, when compared to that of the resistant drugs (cefepime, doripenem and ceftazidim).

Thermodynamic parameters obtained by fluorescence quenching technique obtained by varying the temperature of the binding reaction can be used to further understand these protein-drug interactions. The binding between protein and substrate involves several types of interaction, such as hydrogen bonds, electrostatic interactions and van der Waals interaction (Bakkialakshmi and Chandrakala, 2012; Han *et al.*, 2009; Jayabharathi *et al.*, 2012; Lakowicz, 2006; Maltas *et al.*, 2013; Molina-García *et al.*, 2013; Sułkowska and Michnik, 1997; Trynda-Lemiesz, 2004; Xie *et al.*, 2005; Yang *et al.*, 2009; Yu *et al.*, 2009).

The  $\ln K$  against  $1/T$  plots in Figure 3.19 (bottom row) indicate that  $\Delta H$  is relatively constant over the temperature range studied and that  $\Delta H$  and  $\Delta S$  can be determined from the Van't Hoff relationship. Thermodynamically, all four protein-drug pair interactions are found to be exothermic ( $\Delta H < 0$ ). This overall enthalpy change is an overall contribution from (1) heat changes accompanying conformational changes in the peptide molecules; (2) heat changes associated with the formation of new non-covalent bonding such as electrostatic, van der Waals and hydrogen bonding; and (3) heat changes associated with desolvation energies, such as the displacement or the



release of the ordered water molecules from peptide. The total enthalpy can thus be described by the following equation.

$$\Delta H = (-)\Delta H_{conformation} + (-)\Delta H_{interactions} + (+)\Delta H_{desolvation} \text{ (Abraham } et al., 2005).$$

As no significant change in conformation of the overall porin structure can be observed between the 3D structures of porin and its ligand-bound complex, the exothermic contribution from conformational change to the total enthalpy change is thus negligible. This suggests that these drugs form intermolecular bonding with the protein leading to stable complexes which are unfavourable for a conformational change. This can also be seen in Table 3.6 where the  $\Delta T_m$  of both secondary and tertiary structures were generally higher for the protein-ligand complexes. Among the four drugs evaluated, meropenem-protein interaction releases the most heat, which is about 2.5 times of that of ceftazidime, to both of which *Bps* are sensitive. The results demonstrate that antibiotic-channel interactions contribute significantly to the ability of drugs to permeate through the cellular surface of *Bps*. The endothermic effect of desolvation is considered insignificant and is in good agreement with the global decrease in entropy as discussed in the following paragraph.

The degree of freedom decreases when antibiotics are attached to the protein. This leads to an entropy decrease ( $\Delta S_{assoc.} < 0$ ), which signifies that the order of the system increases with the protein-ligand association (Chilom *et al.*, 2004). The positive  $-T\Delta S$  values given by the interaction of the four antibiotics with *Bps*Omp38 indicate that there was a global decrease in entropy ( $\Delta S < 0$ ). Since global change of entropy ( $\Delta S$ ) is contributed by the  $\Delta S_{assoc.}$  and  $\Delta S_{water}$ , the global entropy reduction suggests that there is no significant compensatory effect from the disorganisation of water molecules.

Change in Gibbs free energy ( $\Delta G$ ) is the net effect of the changes in enthalpy ( $\Delta H$ ) and entropy ( $\Delta S$ ). Looking at the histograms in Figure 3.20, it is very clear that

the interactions of ceftazidime, cefoxitin, meropenem and doripenem with *BpsOmp38* are all mainly enthalpically driven as negative entropy change is thermodynamically unfavourable. This enthalpy-entropy compensation effect is a common physical phenomenon for protein-ligand binding (Fenley *et al.*, 2012). Meropenem demonstrated the greatest enthalpic interaction with *BpsOmp38* but this thermodynamic effect was partially compensated by the decrease in entropy. Therefore, the overall effect of this enthalpy-entropy compensation resulted in a negative  $\Delta G$ , which means that the antibiotic-protein interactions are exergonic and their binding processes occur spontaneously (Ross and Subramanian, 1981). The other sensitive drugs, ceftazidime, also demonstrated strong intermolecular interaction when compared to the other two resistance drugs.

Previous study of OmpF and OmpC porins from *E. coli* by Mahendran *et al.* (2010) showed that ceftriaxone strongly interacted with OmpF and cefepime and ceftazidime produced partial monomeric closures of a single channel in their BLM experiment. It was also demonstrated that cefepime and ceftriaxone strongly interacted with the OmpC. This shows that different porins demonstrate different sensitivity towards different antibiotics. The BLM data supported this observation.

Ceftazidime, which gave partial monomeric closure with OmpF and no blockage event with OmpC, demonstrated monomeric blockage events at low concentration (0.5 mM) with *BpsOmp38*. This can be correlated to its high binding constant ( $K$ ) from fluorescence quenching experiments, which suggests that the ceftazidime-bound form is more favourable ( $\Delta G < 0$ ) at the equilibrium state. This is because the permeability and selectivity of a porin channel is determined by the constriction zone formed by the L3 loop together with the opposite barrel wall (Delcour, 2009).

In the case of meropenem, despite having high negative  $\Delta H$ , which indicates its strong interaction with protein, blockage events can only be seen at high concentration (10 mM). This phenomenon is due to the fact that for general diffusion Omp has a size exclusion limit of about 600 Da, as reported for OmpF (Delcour, 2009; Nikaido and Rosenberg, 1983), while for *BpsOmp38*, the size exclusion limit was previously reported to be 650 Da (Siritapetawee *et al.*, 2004b). Therefore, the small meropenem molecule (383 Da), together with its strong interaction with the pore, may pass through the *BpsOmp38* channel freely and quickly without blocking the channel. As a result, no regular current drop event from channel blockage is recorded in the BLM traces for meropenem at low concentration, i.e. 0.5 and 2.0 mM. However, frequency of translocation increases as the concentration of meropenem increases to 10 mM and multiple translocations may happen at the same time, causing channel blockages (Figure 3.21). This explains the high permeability for meropenem in *B. pseudomallei* demonstrated by liposome swelling assay. On the other hand, ceftazidime, which has a molecular size about the exclusion limit for general diffusion through *BpsOmp38*, blocks the pore and obstructs the passage of ions in the electrolyte when the molecules are translocating through the channel. This is recorded as ion current fluctuation in the BLM traces as shown in Figure 3.21. No channel activity was observed for the resistance drugs (imipenem and cefepime) even at high concentration (10 mM). This is correlated with their weak interaction with the *BpsOmp38* porin as displayed in titration studies with CD and fluorescence spectroscopy.

## Part II: Chitoporin (*VhChiP*) from *Vibrio harveyi*

### 4.3 Mutation effects of Trp136 on binding affinity and thermostability of *VhChiP*

Substrate-specific porins are selective for one particular solute and contain binding site(s) for that solute inside the pores. For example, maltoporin (LamB) is specific for maltooligosaccharides (Schirmer *et al.*, 1995), ScrY specific for sucrose (Forst *et al.*, 1998) and OprD specific for a fragment of amino acids (Biswas *et al.*, 2007). Recently, chitoporin (*VhChiP*) has been isolated from the outer membrane of the marine bacterium *Vibrio harveyi*, namely *VhOmp* (Schulte *et al.*, 2009). Chitoporin expressed in *E. coli* host, is a chitooligosaccharides specific channel, and is especially specific for chitohexaose (Suginta *et al.*, 2013a; Suginta *et al.*, 2013b).

The *VhChiP* from this study, expressed in *E. coli* Omp8 rosetta, was found to be a heat-sensitive trimer. The single band on SDS-PAGE was further confirmed for its purity by using anti-ChiP polyclonal antibody. The structure of *VhChiP* (Figure 3.24) showed that Trp136 protrudes into the channel lumen. This residue at this position is presumed to have effect on the binding affinity and the permeability of sugar through the *VhChiP* channel. In order to verify this assumption, Trp136 was mutated to Ala and Phe, which have different physicochemical properties. According to the standard scales of hydrophobicity (Eisenberg *et al.*, 1984), the side chain of Ala is small and neutral, while Phe has increased aromaticity and hydrophobicity. These mutants together with the *VhChiP* WT were then subjected to a series of experiments so that the importance of this residue in the structural stability of this *VhChiP* can be better understood.

The unfolding curves plotted from the CD and fluorescence spectroscopy experiments demonstrate the transition profile of the secondary and tertiary structural

change of protein, respectively. The number of intermediate states is seen as the turning points in the unfolding curve between the folded and unfolded conformational states (Honda *et al.*, 1999). Thermal unfolding profiles in Figures 3.26 and 3.28 show that secondary structural unfolding of the three *VhChiP* subunits is a two-state transition involving no intermediate state. The  $T_m$  values observed in the CD measurements and fluorescence spectroscopy are not the same as they are determined by the stability of the secondary and tertiary structures of proteins, respectively. Based on the reduction of  $T_m$  values of mutants in both experiments, one can anticipate that this tryptophan residue is important for maintaining the structural integrity of *VhChiP*. As expected, all chitooligosaccharides gave significant increase to the thermal stability of the *VhChiPs*, where chitohexaose showed the highest  $\Delta T_m$  value (Table 3.8).

The linear plots of  $\ln K$  against  $1/T$  in Figure 3.37 (middle row) show that there is no significant shift of  $\Delta H$  over the temperature range studied and that  $\Delta H$  and  $\Delta S$  can be calculated from the Van't Hoff relationship. Therefore, from the thermodynamic point of view, all three protein-chitohexaose pair binding reactions are exothermic ( $\Delta H < 0$ ). This overall enthalpy change is a measure of (1) heat changes accompanying conformational changes in the peptide molecules; (2) heat changes associated with the formation of new non-covalent bonding such as electrostatic, van der Waals and hydrogen bonding; and (3) heat changes associated with desolvation energies such as the displacement or the release of the ordered water molecules from peptide. Therefore, the overall enthalpy can be conveniently shown as:

$$\Delta H = (-)\Delta H_{conformation} + (-)\Delta H_{interactions} + (+)\Delta H_{desolvation} \text{ (Abraham } et al., 2005).$$

Since no significant change in conformation of the overall porin structure is seen in the 3D structures of porin and its ligand-bound complex, its exothermic contribution of conformational change to the overall enthalpy change is negligible. This suggests

that the chitohexaose forms intermolecular bonding, especially hydrogen bonds, with the protein, leading to a more stable complex, which is unfavourable for a conformational change. This can also be seen in Table 3.8 where the  $\Delta T_m$  of both secondary and tertiary structures were generally higher for the protein-ligand complexes. When comparing the  $\Delta H$  of WT and mutants, the heat release of from the interaction of chitohexaose with the WT porin is about 77% higher than with W136F. This is predicted to be an effect of the stacking of aromatic ring of Trp136 with the +4GlcNAc and +5GlcNAc rings (Figure 3.41), forming a productive interaction compared to W136F and W136A which lack this structural feature (Ranok *et al.*, 2015).

Change in Gibbs free energy ( $\Delta G$ ) is the net effect of the changes in enthalpy ( $\Delta H$ ) and entropy ( $\Delta S$ ). Looking at the histograms in Figure 3.37, it is clear that the interactions of chitohexaose with WT, W136A and W136F are all mainly enthalpy driven, with negative entropy change which is thermodynamically unfavourable. This enthalpy-entropy compensation effect is a common physical phenomenon for protein-ligand binding (Fenley *et al.*, 2012). Chitohexaose displayed the greatest enthalpic interaction with WT but this thermodynamic effect was partially counteracted by a decrease in entropy. In our case, the overall effect of this enthalpy-entropy compensation resulted in negative  $\Delta G$ , which means that the interactions are exergonic and binding processes between chitohexaose and protein occur spontaneously (Ross and Subramanian, 1981).

The free energy changes ( $\Delta G$ ) for the three *VhChiP* variants are not very much different. However, it is seen that Trp136 in the WT channel has a stronger exothermic interaction with chitohexaose when compared to the other mutant-ligand pairs. This is also in good agreement with its high binding constant value ( $K = 12.70 \times 10^6 \text{ M}^{-1}$ ), showing that the WT-chitohexaose interaction forms more WT-chitohexaose complex

molecules at equilibrium. The drastic decrease in the thermodynamic parameters for the interactions of chitohexaose with W136A and W136F is an indication that Trp136 contributes significantly to the strong binding affinity of *VhChiP* to its substrates. This observation of the important role of Trp136 is consistent with the chitooligosaccharide translocation pattern through *VhChiP* observed by Chumjan *et al.* (2015).

#### **4.4 Structure and functional properties of outer membrane protein (*VhChiP*) from *Vibrio harveyi***

The X-ray crystal structure of trimeric outer membrane-purified *VhChiP* shows an unprecedented closing of the open pore by the *N*-terminus of a neighbouring monomer. Meanwhile, in native *VhChiP* complexed to chitotetraose substrate the *N*-terminus swings out-side the pore. In order to confirm the functional properties of  $\Delta 1-19$  amino acids at the *N*-terminus, the three *VhChiP* variants were further investigated using both electrophysiological techniques and liposome swelling assays.

Single channel pore conductance of truncated and refolded *VhChiP* was found to be similar to that of the native *VhChiP*. The conductance of the three protein channels ranges from 1.8 to 2.0 nS in 1 M KCl, which is in agreement with previous reports (Chumjan *et al.*, 2015; Schulte *et al.*, 2009; Suginta *et al.*, 2013a; Suginta *et al.*, 2013b). This suggests that the 19 amino acids at the *N*-terminal end have no effect to the passage of ions in the electrolyte through *VhChiP*.

The effect of  $\Delta 1-19$  truncated protein on the binding affinity of *VhChiP* was also investigated by single channel BLM experiments. The *K* value of truncated *VhChiP* decreased 7-fold in comparison to that of native and refolded *VhChiP*. This confirms that the  $\Delta 1-19$  amino acids at *N*-terminal end residue play an important role in the binding affinity between sugar substrate and the *VhChiP* channel.

The liposome swelling assay shows that the removal of  $\Delta 1 - 19$  amino acids at *N*-terminal end of *VhChiP* (Figure 3.45) has significantly affected the specificity of the porin, causing it to behave more like a general diffusion porin. This truncated porin, in comparison to the native and refolded proteins, gave a higher permeation rate for sugars with molecular weight less than 200 Da. However chitohexaose, which is specific to *VhChiP*, demonstrated a lower permeation rate than with the native and refolded proteins. This experimental data indicates that the  $\Delta 1 - 19$  amino acids at the *N*-terminal end is responsible for the specific binding interactions between *VhChiP* and chitohexaose.

Previous studies on the characteristics of chitooligosaccharides (i.e. chitobiose, -triose, -tetraose, -pentaose and -hexaose) in the single channel artificial membrane have shown that the trimeric pore of *VhChiP* is highly specific for chitooligosaccharides with higher MW ((GlcNAc)<sub>n</sub>, *n*= 4, 5 and 6) (Suginta *et al.*, 2013b). This can be clearly seen from the protein-ligand interactions of *VhChiP*-chitohexaose and *VhChiP*-chitotetraose shown in Figure 3.41 and Figure 3.43, respectively. The (GlcNAc)<sub>4</sub> occupies approximately the positions of ring 2 to ring 5 of the (GlcNAc)<sub>6</sub>. Chitooligosaccharides of shorter chain length do not have these key protein-substrate interactions, which leads to the loss of binding specificity.

Apart from *VhChiP*, LamB (maltoporin) is the well-studied outer membrane channel dedicated to oligosaccharide transport for which structural information is available. The crystal structure of *E. coli* LamB complexed with maltohexaose has been solved previously (PDB ID 1MPO) (Dutzler *et al.*, 1996), providing an opportunity for comparison with the *VhChiP*-chitohexose structure reported in this study. Both channels form stable trimers, but the LamB barrel is larger since it consists of 18 strands rather than the 16 strands of *VhChiP*. Beyond the difference in size, the channel shapes



of *VhChiP* and *EcLamB* also differ substantially, with *LamB* having a more funnel-shaped channel with a pronounced pore constriction region. The difference in pore architecture is most likely the reason for the strikingly different conformation of the bound oligosaccharide, being a left-handed helix in *LamB* and an extended chain in *VhChiP* (Figure 4.1A and B).

An interesting question is why the affinity of *EcLamB* for maltohexaose ( $K = 9 \times 10^3$ ) (Dumas *et al.*, 2000) is much lower (~ 50-fold) than the affinity of *VhChiP* for chitohexaose. Thus, it is worth comparing the ion conductance and gating behaviour of *EcLamB* and *VhChiP* using the single channel BLM experiments. *EcLamB* has a tiny conductance (0.3 nS), while *VhChiP* has 1.8 nS. Besides, the transportation of maltohexaose through *EcLamB* gave a saturation at >30  $\mu\text{M}$ , while that of chitohexaose through *VhChiP* showed a saturation at >5  $\mu\text{M}$ . Chitohexaose interacts with *VhChiP* strongly through the acetamido group on each GlcNAc residue, while maltohexaose, which lacks this functionality, interacts weakly with *EcLamB*. This explains the low affinity of *EcLamB* for maltohexaose in comparison to that of *VhChiP* for chitohexaose.

Qualitatively, the binding interaction of hexaoses with both the proteins is very similar, both having the aromatic stacking and polar interactions. The X-ray *LamB* structure is a successive sequence of aromatic residues including Trp74, Tyr41, Tyr6, Trp420, Trp358, Phe227 that are arranged inside the channel along a left-handed helical path. This stretch of aromatic residues was named the “greasy slide” and is actually believed to be the structural element responsible for substrate binding and specificity. A chain of polar residues (namely, Arg8, Arg33, Glu43, Arg82, Arg109, Asp111, Asp116), the so called polar track, is also situated around the constriction site and plays an important role in maltose and maltodextrin translocation (Ranquin and Van Gelder, 2004).

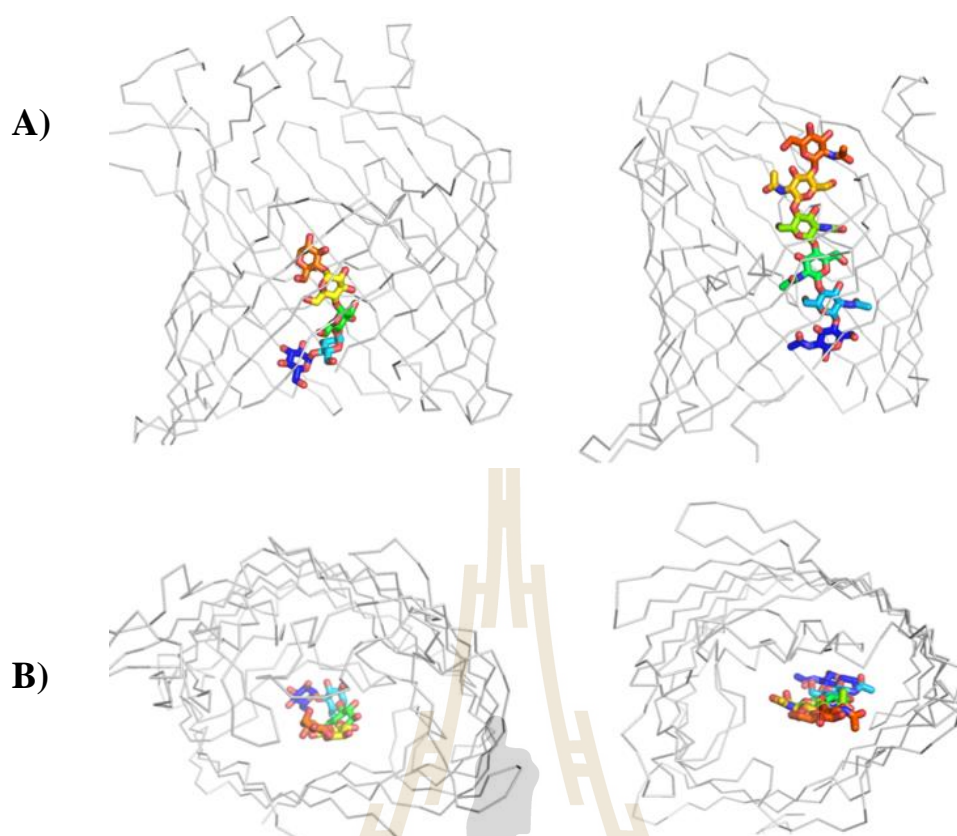


**Figure 4.2** Comparison of sugar binding in LamB and *VhChiP*. Side-by-side comparison of LamB (left) and *VhChiP* (right) with their respective substrates, viewed from the plane of the OM (A) and from the extracellular side (B). The orientations of the proteins are comparable. The substrates are coloured in rainbow representation starting at their reducing ends. Only 5 substrate units are visible in the LamB structure.

## CHAPTER V

### CONCLUSION

In this study, the structural and functional characteristics of two outer membrane proteins, namely *BpsOmp38* from *B. pseudomallei* and *VhChiP* from *V. harveyi*, were investigated.

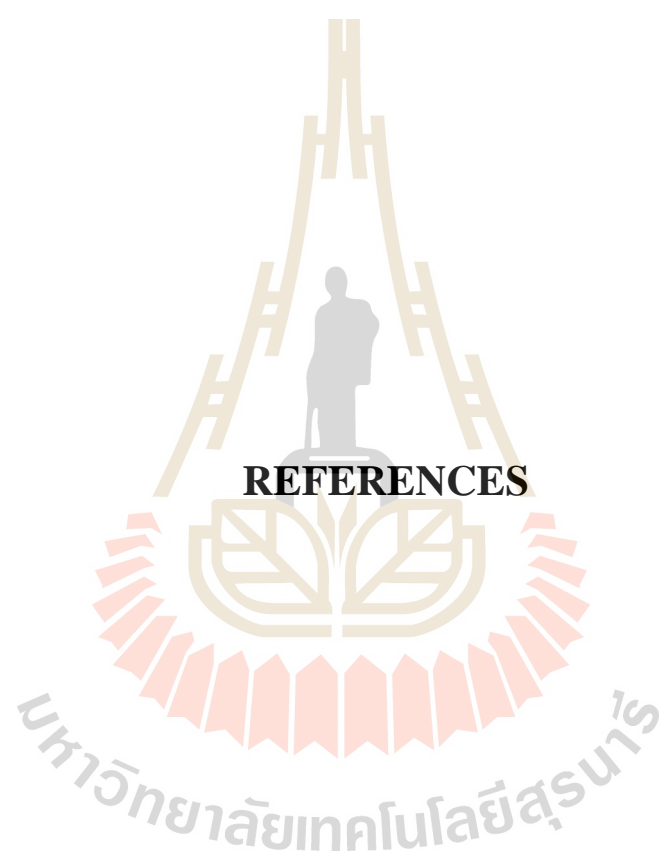
In the first part of this work, *BpsOmp38* with His<sub>6</sub>-tag from *B. pseudomallei* was successfully cloned, expressed and purified. Mutation of tyrosine at position 119 of *BpsOmp38* to alanine and phenylalanine using site-directed mutagenesis technique has yielded mutants Y119A and Y119F, respectively. The 3D-structures of these *BpsOmp38* proteins were elucidated with single-wavelength anomalous dispersion (SAD) and molecular replacement (MR) techniques.

The functional role of the residue at position 119 was evaluated using a series of characterisation techniques which include MIC values, liposome swelling assay, circular dichroism spectroscopy, fluorescence spectroscopy and black lipid membrane translocation studies. Detailed comparison of these experimental data, from WT and mutants, revealed that the amino acid residue at position 119 plays an important role in the passage of antibiotic through the pore channel of *BpsOmp38*. The antibiotic meropenem from carbapenems and ceftazidime from cephalosporins demonstrated the strongest structural stabilisation effect upon forming complexes with *BpsOmp38*.

In the second part of this work, *VhChiP* WT and mutants W136A and W136F were successfully expressed and purified. Besides, truncated *VhChiP*, which has no signal peptide and 19 amino acids deleted at the *N*-terminal end, was also expressed.

The 3D structures of these proteins were solved using SAD and MR techniques. Their functional properties were investigated with a series of experiments which comprised of liposome swelling assay, circular dichroism spectroscopy, fluorescence spectroscopy, and black lipid membrane translocation studies. These experimental data suggested that *VhChiP* is selective for chitohexaose, of the six chitooligosaccharides investigated. Assessment of the experimental evidence suggested that the structural feature at position 136 of WT has a significant contribution to this selectivity.

The functional characterisation of *BpsOmp38* (Tyr119) and *VhChiP* WT (Trp136) along with their mutants showed that certain structural features at these positions are largely responsible for the translocation of drugs and nutrients into their cells. This finding provides a fundamental understanding of the significance of certain amino acid residues in controlling the functional properties of *BpsOmp38* and *VhChiP* porins. This knowledge is expected to be utilised for future research, especially in designing effective drugs for the treatment of diseases.



**REFERENCES**

## REFERENCES

- Abraham, T., Lewis, R. N. A. H., Hodges, R. S., and McElhaney, R. N. (2005). Isothermal Titration Calorimetry Studies of the Binding of a Rationally Designed Analogue of the Antimicrobial Peptide Gramicidin S to Phospholipid Bilayer Membranes. *Biochemistry*, 44(6): 2103-2112.
- Adl, S. M., Simpson, A. G. B., Farmer, M. A., Andersen, R. A., Anderson, O. R., Barta, J. R., Bowser, S. S., Brugerolle, G. U. Y., Fensome, R. A., Fredericq, S., James, T. Y., Karpov, S., Kugrens, P., Krug, J., Lane, C. E., Lewis, L. A., Lodge, J., Lynn, D. H., Mann, D. G., McCourt, R. M., Mendoza, L., Moestrup, Ø., Mozley-Standridge, S. E., Nerad, T. A., Shearer, C. A., Smirnov, A. V., Spiegel, F. W., and Taylor, M. F. J. R. (2005). The New Higher Level Classification of Eukaryotes with Emphasis on the Taxonomy of Protists. *Journal of Eukaryotic Microbiology*, 52(5): 399-451.
- Aldhous, P. (2005). Tropical Medicine: Melioidosis? Never Heard of It. *Nature*, 434(7034): 692-693.
- Amsler, K., Santoro, C., Foleno, B., Bush, K., and Flamm, R. (2010). Comparison of Broth Microdilution, Agar Dilution, and Etest for Susceptibility Testing of Doripenem against Gram-Negative and Gram-Positive Pathogens. *Journal of Clinical Microbiology*, 48(9): 3353-3357.

- Andersen, C., Jordy, M., and Benz, R. (1995). Evaluation of the Rate Constants of Sugar Transport through Maltoporin (LamB) of *Escherichia coli* from the Sugar-Induced Current Noise. *The Journal of General Physiology*, 105(3): 385-401.
- Ashdown, L. R. (1979). Identification of *Pseudomonas pseudomallei* in the Clinical Laboratory. *Journal of Clinical Pathology*, 32(5): 500-504.
- Bajaj, H., Tran, Q.-T., Mahendran, K. R., Nasrallah, C., Colletier, J.-P., Davin-Regli, A., Bolla, J.-M., Pagès, J.-M., and Winterhalter, M. (2012). Antibiotic Uptake through Membrane Channels: Role of *Providencia stuartii* OmpPst1 Porin in Carbapenem Resistance. *Biochemistry*, 51(51): 10244-10249.
- Bakkialakshmi, S., and Chandrakala, D. (2012). A Spectroscopic Investigations of Anticancer Drugs Binding to Bovine Serum Albumin. *Spectrochimica Acta Part A: Molecular and Biomolecular Spectroscopy*, 88: 2-9.
- Baslé, A., Rummel, G., Storici, P., Rosenbusch, J. P., and Schirmer, T. (2006). Crystal Structure of Osmoporin OmpC from *E. coli* at 2.0 Å. *Journal of Molecular Biology*, 362(5): 933-942.
- Bassler, B. L., Yu, C., Lee, Y. C., and Roseman, S. (1991). Chitin Utilization by Marine Bacteria. Degradation and Catabolism of Chitin Oligosaccharides by *Vibrio furnissii*. *Journal of Biological Chemistry*, 266(36): 24276-24286.
- Benz, R., and Hancock, R. E. (1987). Mechanism of Ion Transport through the Anion-Selective Channel of the *Pseudomonas aeruginosa* Outer Membrane. *The Journal of General Physiology*, 89(2): 275-295.
- Berkane, E., Orlik, F., Charbit, A., Danelon, C., Fournier, D., Benz, R., and Winterhalter, M. (2005). Nanopores: Maltoporin Channel as a Sensor for Maltodextrin and Lambda-Phage. *Journal of Nanobiotechnology*, 3(1): 3.

- Biswas, S., Mohammad, M. M., Patel, D. R., Movileanu, L., and Van Den Berg, B. (2007). Structural Insight into OprD Substrate Specificity. *Nature Structural & Molecular Biology*, 14(11): 1108.
- Braun, V., and Rehn, K. (1969). Chemical Characterization, Spatial Distribution and Function of a Lipoprotein (Murein-Lipoprotein) of the *E. coli* Cell Wall. *European Journal of Biochemistry*, 10(3): 426-438.
- Braun, V., and Wolff, H. (1970). The Murein-Lipoprotein Linkage in the Cell Wall of *Escherichia coli*. *European Journal of Biochemistry*, 14(2): 387-391.
- Bredin, J., Saint, N., Malléa, M., Emmanuelle, D., Molle, G., Pagès, J.-M., and Simonet, V. (2002). Alteration of Pore Properties of *Escherichia coli* OmpF Induced by Mutation of Key Residues in Anti-Loop 3 Region. *Biochemical Journal*, 363(3): 521-528.
- Centers for Disease Control and Prevention. (2012). Melioidosis. Retrieved from [www.cdc.gov/nczved/divisions/dfbmd/diseases/melioidosis](http://www.cdc.gov/nczved/divisions/dfbmd/diseases/melioidosis)
- Charalambous, K., O'Reilly, A. O., Bullough, P. A., and Wallace, B. A. (2009). Thermal and Chemical Unfolding and Refolding of a Eukaryotic Sodium Channel. *Biochimica et Biophysica Acta (BBA) - Biomembranes*, 1788(6): 1279-1286.
- Cheng, A. C., and Currie, B. J. (2005). Melioidosis: Epidemiology, Pathophysiology, and Management. *Clinical Microbiology Reviews*, 18(2): 383-416.
- Cheng, A. C., Fisher, D. A., Anstey, N. M., Stephens, D. P., Jacups, S. P., and Currie, B. J. (2004). Outcomes of Patients with Melioidosis Treated with Meropenem. *Antimicrobial Agents and Chemotherapy*, 48(5): 1763-1765.



- Chetchotisakd, P., Porramatikul, S., Mootsikapun, P., Anunnatsiri, S., and Thinkhamrop, B. (2001). Randomized, Double-Blind, Controlled Study of Cefoperazone-Sulbactam Plus Cotrimoxazole Versus Ceftazidime Plus Cotrimoxazole for the Treatment of Severe Melioidosis. *Clinical Infectious Diseases*, 33(1): 29-34.
- Chilom, G., Bestetti, G., Sello, G., and Rice, J. A. (2004). Formation of Bound Residues by Naphthalene and Cis-Naphthalene-1, 2-Dihydrodiol. *Chemosphere*, 56(9): 853-860.
- Chumjan, W., Winterhalter, M., Schulte, A., Benz, R., and Suginta, W. (2015). Chitoporin from the Marine Bacterium *Vibrio harveyi* Probing the Essential Roles of Trp136 at the Surface of the Constriction Zone. *Journal of Biological Chemistry*, 290(31): 19184-19196.
- Cowan, S. W., Garavito, R. M., Jansonius, J. N., Jenkins, J. A., Karlsson, R., König, N., Pai, E. F., Pauptit, R. A., Rizkallah, P. J., Rosenbusch, J. P., Rummel, G., and Schirmer, T. (1995). The Structure of OmpF Porin in a Tetragonal Crystal Form. *Structure*, 3(10): 1041-1050.
- Cowan, S. W., Schirmer, T., Rummel, G., Steiert, M., Ghosh, R., Pauptit, R. A., Jansonius, J. N., and Rosenbusch, J. P. (1992). Crystal Structures Explain Functional Properties of Two *E. coli* Porins. *Nature*, 358(6389): 727-733.
- Currie, B., Smith-Vaughan, H., Golledge, C., Buller, N., Sriprakash, K. S., and Kemp, D. J. (1994). *Pseudomonas pseudomallei* Isolates Collected over 25 Years from a Non-Tropical Endemic Focus Show Clonality on the Basis of Ribotyping. *Epidemiology and Infection*, 113(2): 307-312.
- Dance, D. A. B. (1991). Melioidosis: The Tip of the Iceberg? *Clinical Microbiology Reviews*, 4(1): 52-60.

- Danelon, C., Nestorovich, E. M., Winterhalter, M., Ceccarelli, M., and Bezrukov, S. M. (2006). Interaction of Zwitterionic Penicillins with the OmpF Channel Facilitates Their Translocation. *Biophysical Journal*, 90(5): 1617-1627.
- Delcour, A. H. (2009). Outer Membrane Permeability and Antibiotic Resistance. *Biochimica et Biophysica Acta (BBA) -Proteins and Proteomics*, 1794(5): 808-816.
- Dumas, F., Koebnik, R., Winterhalter, M., and Van Gelder, P. (2000). Sugar Transport through Maltoporin of *Escherichia coli* Role of Polar Tracks. *Journal of Biological Chemistry*, 275(26): 19747-19751.
- Dutzler, R., Wang, Y. F., Rizkallah, P. J., Rosenbusch, J. P., and Schirmer, T. (1996). Crystal Structures of Various Maltooligosaccharides Bound to Maltoporin Reveal a Specific Sugar Translocation Pathway. *Structure*, 4(2): 127-134.
- Džidić, S., Šušković, J., and Kos, B. (2008). Antibiotic Resistance Mechanisms in Bacteria: Biochemical and Genetic Aspects. *Food Technology and Biotechnology*, 46(1): 11-21.
- Eisenberg, D., Schwarz, E., Komaromy, M., and Wall, R. (1984). Analysis of Membrane and Surface Protein Sequences with the Hydrophobic Moment Plot. *Journal of Molecular Biology*, 179(1): 125-142.
- Elschner, M. C., Hnizdo, J., Stamm, I., El-Adawy, H., Mertens, K., and Melzer, F. (2014). Isolation of the Highly Pathogenic and Zoonotic Agent *Burkholderia pseudomallei* from a Pet Green Iguana in Prague, Czech Republic. *BMC Veterinary Research*, 10(1): 283.
- Eswar, N., Eramian, D., Webb, B., Shen, M.-Y., and Sali, A. (2008). Protein Structure Modeling with Modeller. *Structural proteomics: high-throughput methods*: 145-159.

- Evans, W. H., and Graham, J. M. (1989). *Membrane Structure and Function*: Oxford, England ; New York : IRL Press at Oxford University Press, 1989.
- Fenley, A. T., Muddana, H. S., and Gilson, M. K. (2012). Entropy–Enthalpy Transduction Caused by Conformational Shifts Can Obscure the Forces Driving Protein–Ligand Binding. *Proceedings of the National Academy of Sciences*, 109(49): 20006-20011.
- Forst, D., Welte, W., Wacker, T., and Diederichs, K. (1998). Structure of the Sucrose-Specific Porin ScrY from *Salmonella typhimurium* and Its Complex with Sucrose. *Nature Structural & Molecular Biology*, 5(1): 37-46.
- Galdiero, S., Galdiero, M., and Pedone, C. (2007).  $\beta$ -Barrel Membrane Bacterial Proteins: Structure, Function, Assembly and Interaction with Lipids. *Current Protein and Peptide Science*, 8(1): 63-82.
- Garavito, R. M., and Rosenbusch, J. P. (1980). Three-Dimensional Crystals of an Integral Membrane Protein: An Initial X-Ray Analysis. *The Journal of Cell Biology*, 86(1): 327-329.
- Garavito, R. M., and Rosenbusch, J. P. (1986). Isolation and Crystallization of Bacterial Porin. *Methods in Enzymology*, 125: 309-328.
- Hajjar, E., Mahendran, K. R., Kumar, A., Bessonov, A., Petrescu, M., Weingart, H., Ruggerone, P., Winterhalter, M., and Ceccarelli, M. (2010). Bridging Timescales and Length Scales: From Macroscopic Flux to the Molecular Mechanism of Antibiotic Diffusion through Porins. *Biophysical Journal*, 98(4): 569-575.

- Han, X.-L., Mei, P., Liu, Y., Xiao, Q., Jiang, F.-L., and Li, R. (2009). Binding Interaction of Quinlorac with Bovine Serum Albumin: A Biophysical Study. *Spectrochimica Acta Part A: Molecular and Biomolecular Spectroscopy*, 74(3): 781-787.
- Hardesty, C., Ferran, C., and DiRienzo, J. M. (1991). Plasmid-Mediated Sucrose Metabolism in *Escherichia coli*: Characterization of ScrY, the Structural Gene for a Phosphoenolpyruvate-Dependent Sucrose Phosphotransferase System Outer Membrane Porin. *Journal of Bacteriology*, 173(2): 449-456.
- Harris, P., Engler, C., and Norton, R. (2011). Comparative *in vitro* Susceptibility of *Burkholderia pseudomallei* to Doripenem, Ertapenem, Tigecycline and Moxifloxacin. *International Journal of Antimicrobial Agents*, 37(6): 547-549.
- Hayat, S., Peters, C., Shu, N., Tsigros, K. D., and Elofsson, A. (2016). Inclusion of Dyad-Repeat Pattern Improves Topology Prediction of Transmembrane  $\beta$ -Barrel Proteins. *Bioinformatics*, 32(10): 1571-1573.
- Holm, L., and Rosenström, P. (2010). Dali Server: Conservation Mapping in 3d. *Nucleic Acids Research*, 38(suppl\_2): W545-W549.
- Honda, Y., Fukamizo, T., Okajima, T., Goto, S., Boucher, I., and Brzezinski, R. (1999). Thermal Unfolding of Chitosanase from *Streptomyces Sp.* N174: Role of Tryptophan Residues in the Protein Structure Stabilization. *Biochimica et Biophysica Acta (BBA) - Protein Structure and Molecular Enzymology*, 1429(2): 365-376.
- Huijbregts, R. P. H., de Kroon, A. I. P. M., and de Kruijff, B. (2000). Topology and Transport of Membrane Lipids in Bacteria. *Biochimica et Biophysica Acta (BBA) - Reviews on Biomembranes*, 1469(1): 43-61.

- Hunt, D. E., Gevers, D., Vahora, N. M., and Polz, M. F. (2008). Conservation of the Chitin Utilization Pathway in the *Vibrionaceae*. *Applied and Environmental Microbiology*, 74(1): 44-51.
- Ichihara, S., Hussain, M., and Mizushima, S. (1981). Characterization of New Membrane Lipoproteins and Their Precursors of *Escherichia coli*. *Journal of Biological Chemistry*, 256(6): 3125-3129.
- Irwin, J. J., Sterling, T., Mysinger, M. M., Bolstad, E. S., and Coleman, R. G. (2012). Zinc: A Free Tool to Discover Chemistry for Biology. *Journal of Chemical Information and Modeling*, 52(7): 1757-1768.
- Jayabharathi, J., Thanikachalam, V., Sathishkumar, R., and Jayamoorthy, K. (2012). Fluorescence Investigation of the Interaction of 2-(4-Fluorophenyl)-1-Phenyl-1h-Phenanthro [9,10-D] Imidazole with Bovine Serum Albumin. *Journal of Photochemistry and Photobiology B: Biology*, 117: 222-227.
- Jung, B.-O., Roseman, S., and Park, J. K. (2008). The Central Concept for Chitin Catabolic Cascade in Marine Bacterium, *Vibrios*. *Macromolecular Research*, 16(1): 1-5.
- Kanaphun, P., Thirawattanasuk, N., Suputtamongkol, Y., Naigowit, P., Dance, D. A. B., Smith, M. D., and White, N. J. (1993). Serology and Carriage of *Pseudomonas pseudomallei*: A Prospective Study in 1000 Hospitalized Children in Northeast Thailand. *The Journal of Infectious Diseases*, 167(1): 230-233.
- Kattner, C., Zaucha, J., Jaenecke, F., Zachariae, U., and Tanabe, M. (2013). Identification of a Cation Transport Pathway in *Neisseria meningitidis* PorB. *Proteins: Structure, Function, and Bioinformatics*, 81(5): 830-840.

- Kern, W. V., Steinke, P., Schumacher, A., Schuster, S., Baum, H. v., and Bohnert, J. A. (2006). Effect of 1-(1-Naphthylmethyl)-Piperazine, a Novel Putative Efflux Pump Inhibitor, on Antimicrobial Drug Susceptibility in Clinical Isolates of *Escherichia coli*. *Journal of Antimicrobial Chemotherapy*, 57(2): 339-343.
- Kespichayawattana, W., Intachote, P., Utaisincharoen, P., and Sirisinha, S. (2004). Virulent *Burkholderia pseudomallei* Is More Efficient Than Avirulent *Burkholderia thailandensis* in Invasion of and Adherence to Cultured Human Epithelial Cells. *Microbial Pathogenesis*, 36(5): 287-292.
- Kullman, L., Winterhalter, M., and Bezrukov, S. M. (2002). Transport of Maltodextrins through Maltoporin: A Single-Channel Study. *Biophysical Journal*, 82(2): 803-812.
- Lakowicz, J. R. (2006). *Principles of Fluorescence Spectroscopy*: New York : Springer, c2006. 3rd ed.
- Li, X., and Roseman, S. (2004). The Chitinolytic Cascade in *Vibrios* Is Regulated by Chitin Oligosaccharides and a Two-Component Chitin Catabolic Sensor/Kinase. *Proceedings of the National Academy of Sciences of the United States of America*, 101(2): 627-631.
- Lightner, D. V. (1993). Diseases of Cultured Penaeid Shrimp. In J. P. McVey (Ed.), *Crc Handbook of Mariculture* (Vol. 1, pp. 393-486).
- Limmathurotsakul, D., Wongratanacheewin, S., Teerawattanasook, N., Wongsuvan, G., Chaisuksant, S., Chetchotisakd, P., Chaowagul, W., Day, N. P. J., and Peacock, S. J. (2010). Increasing Incidence of Human Melioidosis in Northeast Thailand. *The American Journal of Tropical Medicine and Hygiene*, 82(6): 1113-1117.

- Luber, P., Bartelt, E., Genschow, E., Wagner, J., and Hahn, H. (2003). Comparison of Broth Microdilution, E Test, and Agar Dilution Methods for Antibiotic Susceptibility Testing of *Campylobacter jejuni* and *Campylobacter coli*. ***Journal of Clinical Microbiology***, 41(3): 1062-1068.
- Luckey, M., and Nikaido, H. (1980). Specificity of Diffusion Channels Produced by  $\lambda$  Phage Receptor Protein of *Escherichia coli*. ***Proceedings of the National Academy of Sciences***, 77(1): 167-171.
- Lugtenberg, B., and Van Alphen, L. (1983). Molecular Architecture and Functioning of the Outer Membrane of *Escherichia coli* and Other Gram-Negative Bacteria. ***Biochimica et Biophysica Acta (BBA) - Reviews on Biomembranes***, 737(1): 51-115.
- Mahendran, K. R., Kreir, M., Weingart, H., Fertig, N., and Winterhalter, M. (2010). Permeation of Antibiotics through *Escherichia coli* OmpF and OmpC Porins. ***Journal of Biomolecular Screening***, 15(3): 302-307.
- Maltas, E., Ozmen, M., Yildirimer, B., Kucukkolbasi, S., and Yildiz, S. (2013). Interaction between Ketoconazole and Human Serum Albumin on Epoxy Modified Magnetic Nanoparticles for Drug Delivery. ***Journal of nanoscience and nanotechnology***, 13(10): 6522-6528.
- Marley, E. F., Mohla, C., and Campos, J. M. (1995). Evaluation of E-Test for Determination of Antimicrobial MICs for *Pseudomonas aeruginosa* Isolates from Cystic Fibrosis Patients. ***Journal of Clinical Microbiology***, 33(12): 3191-3193.
- Meekrathok, P., and Suginta, W. (2016). Probing the Catalytic Mechanism of *Vibrio harveyi* Gh20  $\beta$ -N-Acetylglucosaminidase by Chemical Rescue. ***PloS One***, 11(2): e0149228.

- Mima, T., and Schweizer, H. P. (2010). The BpeAB-OprB Efflux Pump of *Burkholderia pseudomallei* 1026b Does Not Play a Role in Quorum Sensing, Virulence Factor Production, or Extrusion of Aminoglycosides but Is a Broad-Spectrum Drug Efflux System. *Antimicrobial Agents and Chemotherapy*, 54(8): 3113-3120.
- Molina-García, L., Santos, J. L. M., Ruiz-Medina, A., and Llorent-Martínez, E. J. (2013). Determination of Ketoprofen Based on Its Quenching Effect in the Fluorescence of Quantum Dots. *Journal of Food and Drug Analysis*, 21(4): 426-431.
- Nestorovich, E. M., Danelon, C., Winterhalter, M., and Bezrukov, S. M. (2002). Designed to Penetrate: Time-Resolved Interaction of Single Antibiotic Molecules with Bacterial Pores. *Proceedings of the National Academy of Sciences*, 99(15): 9789-9794.
- Neves, P., Berkane, E., Gameiro, P., Winterhalter, M., and de Castro, B. (2005). Interaction between Quinolones Antibiotics and Bacterial Outer Membrane Porin OmpF. *Biophysical Chemistry*, 113(2): 123-128.
- Nikaido, H. (2003). Molecular Basis of Bacterial Outer Membrane Permeability Revisited. *Microbiology and Molecular Biology Reviews*, 67(4): 593-656.
- Nikaido, H., and Rosenberg, E. Y. (1983). Porin Channels in *Escherichia coli*: Studies with Liposomes Reconstituted from Purified Proteins. *Journal of Bacteriology*, 153(1): 241-252.
- Nikaido, H., and Vaara, M. (1985). Molecular Basis of Bacterial Outer Membrane Permeability. *Microbiological Reviews*, 49(1): 1-32.
- Owens, L., and Busico-Salcedo, N. (2006). *Vibrio harveyi*: Pretty Problems in Paradise. In *The Biology of Vibrios*: American Society of Microbiology.



- Pagès, J.-M., James, C. E., and Winterhalter, M. (2008). The Porin and the Permeating Antibiotic: A Selective Diffusion Barrier in Gram-Negative Bacteria. *Nature reviews. Microbiology*, 6(12): 893.
- Parameswaran, U., Baird, R. W., Ward, L. M., and Currie, B. J. (2012). Melioidosis at Royal Darwin Hospital in the Big 2009–2010 Wet Season: Comparison with the Preceding 20 Years. *The Medical Journal of Australia*, 196(5): 345-348.
- Peacock, S. J. (2006). Melioidosis. *Current Opinion in Infectious Diseases*, 19(5): 421-428.
- Phale, P. S., Philippsen, A., Kiefhaber, T., Koebnik, R., Phale, V. P., Schirmer, T., and Rosenbusch, J. P. (1998). Stability of Trimeric OmpF Porin: The Contributions of the Latching Loop L2. *Biochemistry*, 37(45): 15663-15670.
- Phale, P. S., Philippsen, A., Widmer, C., Phale, V. P., Rosenbusch, J. P., and Schirmer, T. (2001). Role of Charged Residues at the OmpF Porin Channel Constriction Probed by Mutagenesis and Simulation. *Biochemistry*, 40(21): 6319-6325.
- Prilipov, A., Phale, P. S., Koebnik, R., Widmer, C., and Rosenbusch, J. P. (1998a). Identification and Characterization of Two Quiescent Porin Genes, NmpC and OmpN, in *Escherichia coli* B<sup>c</sup>. *Journal of Bacteriology*, 180(13): 3388-3392.
- Prilipov, A., Phale, P. S., Van Gelder, P., Rosenbusch, J. P., and Koebnik, R. (1998b). Coupling Site-Directed Mutagenesis with High-Level Expression: Large Scale Production of Mutant Porins from *E. coli*. *FEMS Microbiology Letters*, 163(1): 65-72.
- Raetz, C. R., and Whitfield, C. (2002). Lipopolysaccharide Endotoxins. *Annual Review of Biochemistry*, 71(1): 635-700.

- Randall-Hazelbauer, L., and Schwartz, M. (1973). Isolation of the Bacteriophage Lambda Receptor from *Escherichia coli*. *Journal of Bacteriology*, 116(3): 1436-1446.
- Ranok, A., Wongsantichon, J., Robinson, R. C., and Suginta, W. (2015). Structural and Thermodynamic Insights into Chitooligosaccharide Binding to Human Cartilage Chitinase 3-Like Protein 2 (CHI3L2 or YKL-39). *Journal of Biological Chemistry*, 290(5): 2617-2629.
- Ranquin, A., and Van Gelder, P. (2004). Maltoporin: Sugar for Physics and Biology. *Research in Microbiology*, 155(8): 611-616.
- Ross, P. D., and Subramanian, S. (1981). Thermodynamics of Protein Association Reactions: Forces Contributing to Stability. *Biochemistry*, 20(11): 3096-3102.
- Saraya, S., Soontornpas, C., Chindavijak, B., and Mootsikapun, P. (2009). *In Vitro* Interactions between Cotrimoxazole and Doxycycline in *Burkholderia pseudomallei*: How Important Is This Combination in Maintenance Therapy of Melioidosis? *Indian Journal of Medical Microbiology*, 27(1): 88.
- Schirmer, T., Keller, T. A., Wang, Y.-F., and Rosenbusch, J. P. (1995). Structural Basis for Sugar Translocation through Maltoporin Channels at 3.1 Å Resolution. *Science*, 267(5197): 512.
- Schmid, K., Ebner, R., Altenbuchner, J., Schmitt, R., and Lengeler, J. (1988). Plasmid-Mediated Sucrose Metabolism in *Escherichia coli* K12: Mapping of the Scr Genes of Pur400. *Molecular Microbiology*, 2(1): 1-8.
- Schmid, K., Ebner, R., Jahreis, K., Lengeler, J., and Titgemeyer, F. (1991). A Sugar-Specific Porin, ScrY, Is Involved in Sucrose Uptake in Enteric Bacteria. *Molecular Microbiology*, 5(4): 941-950.

- Schülein, K., Andersen, C., and Benz, R. (1995). The Deletion of 70 Amino Acids near the *N*-Terminal End of the Sucrose-Specific Porin ScrY Causes Its Functional Similarity to Lamb *in vivo* and *in vitro*. *Molecular Microbiology*, 17(4): 757-767.
- Schülein, K., Schmid, K., and Benzl, R. (1991). The Sugar-Specific Outer Membrane Channel ScrY Contains Functional Characteristics of General Diffusion Pores and Substrate-Specific Porins. *Molecular Microbiology*, 5(9): 2233-2241.
- Schulte, A., Ruamchan, S., Khunkaewla, P., and Suginta, W. (2009). The Outer Membrane Protein *VhOmp* of *Vibrio harveyi*: Pore-Forming Properties in Black Lipid Membranes. *Journal of Membrane Biology*, 230(2): 101-111.
- Schulz, G. E. (2002). The Structure of Bacterial Outer Membrane Proteins. *Biochimica et Biophysica Acta (BBA) - Biomembranes*, 1565(2): 308-317.
- Shih, H.-I., Chuang, Y.-C., Cheung, B. M.-H., Yan, J.-J., Chang, C.-M., Chang, K., Lee, N.-Y., Lee, H.-C., Wu, C.-J., Chen, P.-L., Lee, C.-C., Wang, L.-R., Ko, N.-Y., and Ko, W.-C. (2008). Sporadic and Outbreak Cases of Melioidosis in Southern Taiwan: Clinical Features and Antimicrobial Susceptibility. *Infection*, 37(1): 9.
- Simpson, A. J. H., Suputtamongkol, Y., Smith, M. D., Angus, B. J., Rajanuwong, A., Wuthiekanun, V., Howe, P. A., Walsh, A. L., Chaowagul, W., and White, N. J. (1999). Comparison of Imipenem and Ceftazidime as Therapy for Severe Melioidosis. *Clinical Infectious Diseases*, 29(2): 381-387.
- Siritapetawee, J., Prinz, H., Krittanai, C., and Suginta, W. (2004a). Expression and Refolding of Omp38 from *Burkholderia pseudomallei* and *Burkholderia thailandensis*, and Its Function as a Diffusion Porin. *Biochemical Journal*, 384(3): 609-617.

- Siritapetawee, J., Prinz, H., Samosornsuk, W., Ashley, R. H., and Suginta, W. (2004b). Functional Reconstitution, Gene Isolation and Topology Modelling of Porins from *Burkholderia pseudomallei* and *Burkholderia thailandensis*. *Biochemical Journal*, 377(3): 579-587.
- Songsiriritthigul, C., Pantoom, S., Aguda, A. H., Robinson, R. C., and Suginta, W. (2008). Crystal Structures of *Vibrio harveyi* Chitinase a Complexed with Chitooligosaccharides: Implications for the Catalytic Mechanism. *Journal of Structural Biology*, 162(3): 491-499.
- Srivastava, D. B., Ethayathulla, A. S., Kumar, J., Singh, N., Sharma, S., Das, U., Srinivasan, A., and Singh, T. P. (2006). Crystal Structure of a Secretory Signalling Glycoprotein from Sheep at 2.0Å Resolution. *Journal of Structural Biology*, 156(3): 505-516.
- Stock, I., and Wiedemann, B. (1998). Natural Antibiotic Susceptibility of *Providencia stuartii*, *P. rettgeri*, *P. alcalifaciens* and *P. rustigianii* Strains. *Journal of Medical Microbiology*, 47(7): 629-642.
- Suginta, W., Chumjan, W., Mahendran, K. R., Janning, P., Schulte, A., and Winterhalter, M. (2013a). Molecular Uptake of Chitooligosaccharides through Chitoporin from the Marine Bacterium *Vibrio harveyi*. *PloS One*, 8(1): e55126.
- Suginta, W., Chumjan, W., Mahendran, K. R., Schulte, A., and Winterhalter, M. (2013b). Chitoporin from *Vibrio harveyi*, a Channel with Exceptional Sugar Specificity. *Journal of Biological Chemistry*, 288(16): 11038-11046.

- Suginta, W., Mahendran, K. R., Chumjan, W., Hajjar, E., Schulte, A., Winterhalter, M., and Weingart, H. (2011). Molecular Analysis of Antimicrobial Agent Translocation through the Membrane Porin *BpsOmp38* from an Ultrasensitive *Burkholderia pseudomallei* Strain. *Biochimica et Biophysica Acta (BBA) - Biomembranes*, 1808(6): 1552-1559.
- Sułkowska, A., and Michnik, A. (1997). Interaction of Purine Bases and Nucleosides with Serum Albumin. *Journal of Molecular Structure*, 410: 27-29.
- Sun, S.-F., Zhou, B., Hou, H.-N., Liu, Y., and Xiang, G.-Y. (2006). Studies on the Interaction between Oxaprozin-E and Bovine Serum Albumin by Spectroscopic Methods. *International Journal of Biological Macromolecules*, 39(4): 197-200.
- Suputtamongkol, Y., Rajchanuwong, A., Chaowagul, W., Dance, D. A. B., Smith, M. D., Wuthiekanun, V., Walsh, A. L., Pukrittayakamee, S., and White, N. J. (1994). Ceftazidime Vs. Amoxicillin/Clavulanate in the Treatment of Severe Melioidosis. *Clinical Infectious Diseases*, 19(5): 846-853.
- Szmelcman, S., and Hofnung, M. (1975). Maltose Transport in *Escherichia coli* K-12: Involvement of the Bacteriophage Lambda Receptor. *Journal of Bacteriology*, 124(1): 112-118.
- Szmelcman, S., Schwartz, M., Silhavy, T., and Boo, W. (1976). Maltose Transport in *Escherichia coli* K12: A Comparison of Transport Kinetics in Wild-Type and a-Reigent Mutants with the Dissociation Constants of the Maltose Binding Protein as Measured by Fluorescence Quenching. *European Journal of Biochemistry*, 65: 13-19.
- Tenover, F. C. (2006). Mechanisms of Antimicrobial Resistance in Bacteria. *The American Journal of Medicine*, 119(6): S3-S10.

- Thamlikitkul, V., and Trakulsomboon, S. (2010). *In vitro* Activity of Biapenem against *Burkholderia pseudomallei*. ***International Journal of Antimicrobial Agents***, 35(5): 514.
- Thibault, F. M., Hernandez, E., Vidal, D. R., Girardet, M., and Cavallo, J. D. (2004). Antibiotic Susceptibility of 65 Isolates of *Burkholderia pseudomallei* and *Burkholderia mallei* to 35 Antimicrobial Agents. ***Journal of Antimicrobial Chemotherapy***, 54(6): 1134-1138.
- Tien, H. T., and Ottova, A. L. (2001). The Lipid Bilayer Concept and Its Experimental Realization: From Soap Bubbles, Kitchen Sink, to Bilayer Lipid Membranes. ***Journal of Membrane Science***, 189(1): 83-117.
- Tran, Q.-T., Mahendran, K. R., Hajjar, E., Ceccarelli, M., Davin-Regli, A., Winterhalter, M., Weingart, H., and Pagès, J.-M. (2010). Implication of Porins in  $\beta$ -Lactam Resistance of *Providencia stuartii*. ***Journal of Biological Chemistry***, 285(42): 32273-32281.
- Trunck, L. A., Propst, K. L., Wuthiekanun, V., Tuanyok, A., Beckstrom-Sternberg, S. M., Beckstrom-Sternberg, J. S., Peacock, S. J., Keim, P., Dow, S. W., and Schweizer, H. P. (2009). Molecular Basis of Rare Aminoglycoside Susceptibility and Pathogenesis of *Burkholderia pseudomallei* Clinical Isolates from Thailand. ***PLoS Neglected Tropical Diseases***, 3(9): e519.
- Trynda-Lemiesz, L. (2004). Paclitaxel–Hsa Interaction. Binding Sites on Hsa Molecule. ***Bioorganic & Medicinal Chemistry***, 12(12): 3269-3275.
- Tsirigos, K. D., Elofsson, A., and Bagos, P. G. (2016). PRED-TMBB2: Improved Topology Prediction and Detection of Beta-Barrel Outer Membrane Proteins. ***Bioinformatics***, 32(17): i665-i671.

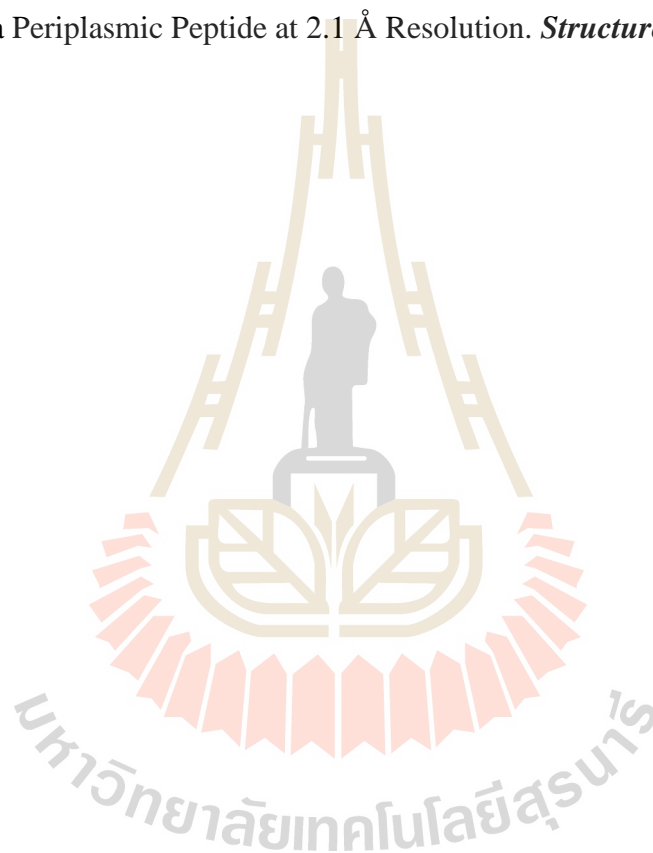
- van Straaten, K. E., Barends, T. R., Dijkstra, B. W., and Thunnissen, A.-M. W. (2007). Structure of *Escherichia coli* Lytic Transglycosylase MltA with Bound Chitohexaose Implications for Peptidoglycan Binding and Cleavage. *Journal of Biological Chemistry*, 282(29): 21197-21205.
- Varma, S., Chiu, S.-W., and Jakobsson, E. (2006). The Influence of Amino Acid Protonation States on Molecular Dynamics Simulations of the Bacterial Porin OmpF. *Biophysical Journal*, 90(1): 112-123.
- Vedros, N. A., Chow, D., and Liong, E. (1988). Experimental Vaccine against *Pseudomonas pseudomallei* Infections in Captive Cetaceans. *Diseases of Aquatic Organisms*, 5(3): 157-161.
- Wallner, B., and Elofsson, A. (2003). Can Correct Protein Models Be Identified? *Protein Science*, 12(5): 1073-1086.
- Wang, Y.-F., Dutzler, R., Rizkallah, P. J., Rosenbusch, J. P., and Schirmer, T. (1997). Channel Specificity: Structural Basis for Sugar Discrimination and Differential Flux Rates in Maltoporin. *Journal of Molecular Biology*, 272(1): 56-63.
- Weichbrodt, C., Bajaj, H., Baaken, G., Wang, J., Guinot, S., Kreir, M., Behrends, J. C., Winterhalter, M., and Fertig, N. (2015). Antibiotic Translocation through Porins Studied in Planar Lipid Bilayers Using Parallel Platforms. *Analyst*, 140(14): 4874-4881.
- Weingart, H., Petrescu, M., and Winterhalter, M. (2008). Biophysical Characterization of in- and Efflux in Gram-Negative Bacteria. *Current Drug Targets*, 9(9): 789-796.
- White, N. J., Chaowagul, W., Wuthiekanun, V., Dance, D. A. B., Wattanagoon, Y., and Pitakwatchara, N. (1989). Halving of Mortality of Severe Melioidosis by Ceftazidime. *The Lancet*, 334(8665): 697-701.

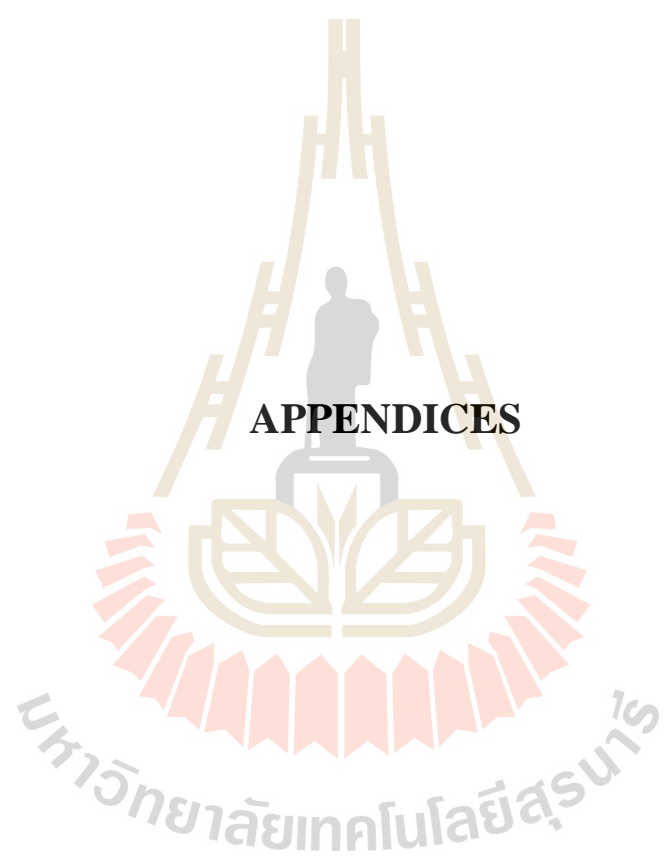
- Wiersinga, W. J., Van der Poll, T., White, N. J., Day, N. P., and Peacock, S. J. (2006). Melioidosis: Insights into the Pathogenicity of *Burkholderia pseudomallei*. *Nature reviews. Microbiology*, 4(4): 272.
- Wikler, M. A. (2006). *Methods for Dilution Antimicrobial Susceptibility Tests for Bacteria That Grow Aerobically: Approved Standard*: Clinical and laboratory standards institute.
- Wimley, W. C. (2003). The Versatile  $\beta$ -Barrel Membrane Protein. *Current Opinion in Structural Biology*, 13(4): 404-411.
- Winterhalter, M. (2000). Black Lipid Membranes. *Current Opinion in Colloid & Interface Science*, 5(3): 250-255.
- Woods, J. B. (2005). Antimicrobials for Biological Warfare Agents. In L. E. Lindler, F. J. Lebeda, & G. W. Korch (Eds.), *Biological Weapons Defense: Infectious Diseases and Counterbioterrorism* (pp. 285-315). Totowa, NJ: Humana Press.
- Wuthiekanun, V., and Peacock, S. J. (2006). Management of Melioidosis. *Expert Review of Anti-Infective Therapy*, 4(3): 445-455.
- Xie, M.-X., Xu, X.-Y., and Wang, Y.-D. (2005). Interaction between Hesperetin and Human Serum Albumin Revealed by Spectroscopic Methods. *Biochimica et Biophysica Acta (BBA) - General Subjects*, 1724(1): 215-224.
- Yang, J., Jing, Z. H., Jie, J. J., and Guo, P. (2009). Fluorescence Spectroscopy Study on the Interaction between Gossypol and Bovine Serum Albumin. *Journal of Molecular Structure*, 920(1): 227-230.
- Yoshimura, F., and Nikaido, H. (1985). Diffusion of Beta-Lactam Antibiotics through the Porin Channels of *Escherichia coli* K-12. *Antimicrobial Agents and Chemotherapy*, 27(1): 84-92.



Yu, J., Li, B., Dai, P., and Ge, S. (2009). Molecular Simulation of the Interaction between Novel Type Rhodanine Derivative Probe and Bovine Serum Albumin. *Spectrochimica Acta Part A: Molecular and Biomolecular Spectroscopy*, 74(1): 277-281.

Zeth, K., Diederichs, K., Welte, W., and Engelhardt, H. (2000). Crystal Structure of Omp32, the Anion-Selective Porin from *Comamonas acidovorans*, in Complex with a Periplasmic Peptide at 2.1 Å Resolution. *Structure*, 8(9): 981-992.





**APPENDICES**

มหาวิทยาลัยเทคโนโลยีสุรนารี

# APPENDIX A

## COMPETENT CELL PREPARATIONS AND PLASMID TRANSFORMATIONS

### 1. Preparation of calcium chloride competent cells

The *E. coli* DH5 $\alpha$  and omp8 Rosetta strain are bacterial strain used for the competent cell preparations. The single colony was picked up from LB agar plate and grown in 5 mL of LB broth and incubated at 37 °C for overnight (18 hr) at 200 rpm. Then 1 mL the overnight cell cultured was subjected into 100 mL of LB broth (ratio 1:100) and grown at 37 °C until OD<sub>600</sub> reached about 0.4-0.5. The cell cultured was transferred into a pre-chilled polypropylene tube, chilled on ice for 10 min, and the cell pellets were collected by centrifugation at 4,500 rpm at 4 °C for 10 min. The cell pellets were gently resuspended in 10 mL of pre-chilled CaCl<sub>2</sub> solution (100 mM CaCl<sub>2</sub> and 15% glycerol) on ice, then centrifuged at 4,500 rpm at 4 °C for 10 min. then, the cell pellets were gently resuspended again in 10 mL of pre-chilled CaCl<sub>2</sub> solution. The cell pellets were collected as describe above, then resuspended in 4 mL of pre-chilled CaCl<sub>2</sub> and kept on ice for 10 min. aliquot 100  $\mu$ L of suspension competent cells into 1.5 mL eppendroft tube. The competent cells were frozen using snap-freeze technique under liquid nitrogen and store at -80 °C.

## 2. Plasmid transformation (Heat shock method)

The frozen competent cells were gently thawed on ice and then added 50-100 ng recombinant plasmid DNAs of *VhChiP* into 100  $\mu$ L of the competent cells and kept on ice. The mixture were immediately placed at 42 °C for 45 second and then rapidly placed on ice again for 10 min. adding 900  $\mu$ L of pre-warmed LB broth at 37 °C into the transformed cells and incubated at 37 °C for 60 min. centrifugation at 4,500 rpm for 5 min, the 900  $\mu$ L of supernatant were removed. The 100  $\mu$ L of cells were spread on an LB agar plate containing the appropriate antibiotic and then incubated at 37 °C overnight.



## APPENDIX B

### PREPARATION OF SOLUTIONS AND REAGENTS

#### 1. Reagents for bacterial culture and competent cell transformation

##### 1.1 Luria-Bertani (LB) broth containing $100 \mu\text{g mL}^{-1}$ of ampicillin

Dissolve 10 g Bacto tryptone, 5 g Bacto yeast extract and 10 g NaCl in 950 mL distilled water. Stir until the solutes have been dissolved. Adjust the volume of the solution to 1,000 mL with distilled water. The solution is then sterilised by autoclaving at  $121^\circ\text{C}$  for 15 min. The medium is allowed to cool down to  $50^\circ\text{C}$  before ampicillin is added to the final concentration of  $100 \mu\text{g mL}^{-1}$ . The medium is freshly used or store at  $4^\circ\text{C}$  until used.

##### 1.2 LB broth containing $100 \mu\text{g mL}^{-1}$ of ampicillin and $25 \mu\text{g mL}^{-1}$ of kanamycin

Dissolve 10 g Bacto tryptone, 5 g Bacto yeast extract and 10 g NaCl in 950 mL distilled water. Stir until the solutes have been dissolved. Adjust the volume of the solution to 1,000 mL with distilled water. The solution is then sterilised by autoclaving at  $121^\circ\text{C}$  for 15 min. The medium is allowed to cool down to  $50^\circ\text{C}$  before ampicillin and kanamycin were added to the final concentration of 100 and  $25 \mu\text{g mL}^{-1}$ , respectively. The medium is freshly used or store at  $4^\circ\text{C}$  until used.

##### 1.3 LB agar medium containing $100 \mu\text{g mL}^{-1}$ of ampicillin

Dissolve 10 g Bacto tryptone, 5 g Bacto yeast extract and 10 g NaCl and 15 g Bacto agar in 950 mL distilled water. Stir until the solutes have been dissolved. Adjust the volume of the solution to 1,000 mL with distilled water. The solution is then

sterilised by autoclaving at 121 °C for 15 min. the medium is allowed to cool down to 50 °C before adding ampicillin to the final concentration of 100 µg mL<sup>-1</sup>. Pour medium into petri-dishes and allowed the agar to harden and store at 4 °C.

1.4 LB agar medium containing 100 µg mL<sup>-1</sup> of ampicillin and 25 µg mL<sup>-1</sup> of kanamycin.

Dissolve 10 g Bacto tryptone, 5 g Bacto yeast extract and 10 g NaCl and 15 g Bacto agar in 950 mL distilled water. Stir until the solutes have been dissolved. Adjust the volume of the solution to 1,000 mL with distilled water. The solution is then sterilised by autoclaving at 121 °C for 15 min. the medium is allowed to cool down to 50 °C before adding ampicillin to the final concentration of 100 and 25 µg mL<sup>-1</sup>, respectively. Pour medium into petri-dishes and allowed the agar to harden and store at 4 °C.

### 1.5 Antibiotic stock solutions

#### 1.5.1 Ampicillin stock solution (100 mg mL<sup>-1</sup>)

Dissolve 1 g of ampicillin in 10 mL of sterile distilled water. Filter sterile solution with 0.2 µm filtration, then ampicillin solution is aliquoted and stored at -20 °C until used.

#### 1.5.2 Kanamycin stock solution (50 mg mL<sup>-1</sup>)

Dissolve 50 g of kanamycin in 10 mL of sterile distilled water. Filter sterile solution with 0.2 µm filtration, then kanamycin solution is aliquoted and stored at -20 °C until used.

#### 1.6 Isopropyl thio-β-D-galactoside (IPTG) stock solution (1 M)

Dissolve 2.38 g of IPTG in distilled water and make up to a final volume of 10 mL. The stock solution is filtered to sterilisation and aliquoted to small volume and stored at -20 °C.

## 2. Reagents for competent *E. coli* cell preparation

2.1 CaCl<sub>2</sub> solution (100 mM CaCl<sub>2</sub> contains 15% (v/v) glycerol)

Preparation of 100 mL CaCl<sub>2</sub> working solution, mixed the stock solution as follows:

- 10 mL of 1 M CaCl<sub>2</sub> (14.7 g/100 mL, filtered to sterilisation)
- 15 mL of 100% (v/v) sterilised glycerol (autoclaved at 121 °C, for 15 min)

Adding sterile distilled water to bring a volume to 100 mL. Store the solution at 4 °C.

## 3. Reagent for agarose gel electrophoresis

3.1 50x TAE buffer

Mix 242 g Tris-base, 57.1 mL glacial acetic acid, and 100 mL of 0.5 M EDTA (pH 8.0). Adjust the final volume to 1,000 mL with distilled water. Store the solution at room temperature.

3.2 6x DNA loading solution (10 mL)

Mix 0.025 g Bromophenol blue and/or 0.025 g xylene cyanol and 3 mL of 100% (v/v) of glycerol. Adjust to the final volume of 10 mL with distilled water and store at 4 °C.

## 4. Solutions for protein expression and purification

4.1 200 mM Lysis buffer (200 mM Tris-HCl, 25 mM MgCl<sub>2</sub>, 1 mM CaCl<sub>2</sub>)

Dissolve 4.84 g of Tris-base, 1 g of  $\text{MgCl}_2$ , and 29.4 mg of  $\text{CaCl}_2$  in 100 mL of distilled water. Adjust pH to 8.0 with 6 M HCl and make up the volume to 200 mL with distilled water and stored the solution at 4 °C.

#### 4.2 0.2 M $\text{Na}_2\text{HPO}_4$ ( $M_r = 358.14 \text{ g mol}^{-1}$ )

Dissolve 71.63 g of  $\text{Na}_2\text{HPO}_4$  in 500 mL of distilled water and make up the volume to 1,000 mL with distilled water.

4.3 0.2 M  $\text{Na}_2\text{H}_2\text{PO}_4$  ( $M_r = 136 \text{ g mol}^{-1}$ ) Dissolve 27.2 g of  $\text{NaH}_2\text{PO}_4$  in 500 mL of distilled water and make up the volume to 1000 mL with distilled water.

#### 4.4 0.1 M phosphate buffer (PB), pH 7.4

Preparation of 100 mL of 0.1 M PB, pH 7.4 working solution, mixed the stock solution as follows:

- 40.5 mL of 0.2 M  $\text{Na}_2\text{HPO}_4$

- 9.5 mL of 0.2 M  $\text{NaH}_2\text{PO}_4$

Adjust the volume to 100 mL with distilled water and stored the solution at room temperature.

#### 4.5 DNase I ( $10 \text{ mg mL}^{-1}$ )

Dissolve 0.001 g of DNase I in 20 mM PB (pH 7.4) to the final volume of 100  $\mu\text{L}$  and kept at  $-20 \text{ }^\circ\text{C}$  before used.

#### 4.6 RNase A ( $10 \text{ mg mL}^{-1}$ )

Dissolve 0.01 g of RNase A in 20 mM PB (pH 7.4) to the final volume of 1,000  $\mu\text{L}$  and kept at  $-20 \text{ }^\circ\text{C}$  before used.

#### 4.7 20% SDS stock solution

Dissolve 20 g of SDS in distilled water to final volume of 100 mL and stored at room temperature.

#### 4.8 3% Octyl-POE



Dilute 3 mL of octyl-POE in 20 mM PB (pH 7.4) to the final volume of 100 mL and stored at 4 °C before used.

#### 4.9 0.125% Octyl-POE

Dilute 0.125 mL of octyl-POE in 20 mM PB (pH 7.4) to the final volume of 100 mL and stored at 4 °C before used.

#### 4.10 0.2% LDAO

Dilute 0.6 mL of LDAO in 20 mM PB (pH 7.4) to the final volume of 100 mL and stored at 4 °C before used.

4.11 SDS-gel loading buffer (3x stock) contains 0.15 M Tris-HCl (pH 6.8), 6% SDS, 0.1% bromophenol blue and 30% glycerol

Dissolve 6 g of SDS, 0.1 g bromophenol blue, 30 mL of glycerol and add 0.15 M Tris-HCl (pH 6.8) to the final volume of 100 mL. Store the solution at -30 °C. Before used, add 20 µL of 2-mercapthoethanal to the final volume of 40 µL of the solution mixture.

#### 4.12 1.5 M Tris-HCl (pH 8.8)

Dissolve 18.17 g of Tris-base in 80 mL distilled water. Adjust pH to 8.8 with 6 M HCl and bring the volume up to 100 mL with distilled water and stored at 4 °C.

#### 4.13 1.0 M Tris-HCl (pH 6.8)

Dissolve 12.10 g of Tris-base in 80 mL distilled water. Adjust pH to 6.8 with 6 M HCl and bring the volume up to 100 mL with distilled water and stored at 4 °C.

#### 4.14 30% (w/v) Acrylamide solution

Dissolve 29 g of Tacrylamide and 1 g N, N'-methylene-bis-acrylamide in distilled water to a final volume of 100 mL. Mix the solution by stirring for 1 hr until

the solution is homogeneous and filter through a whatman filter paper membrane No.

1. Store the solution in the dark bottle at 4 °C.

#### 4.15 Tris-glycine electrode buffer (5x stock solution)

Dissolve 30.29 g of Tris-base, 144 g of glycine, 5 g of SDS in distilled water. Adjust pH to 8.3 with 6 M HCl and bring the final volume up to 1 liter with distilled water.

#### 4.16 Staining solution with Coomassie Brilliant Blue for protein

Mix 1 g of Coomassie Brilliant Blue R-250, 400 mL methanol, 500 mL distilled water and 100 mL glacial acetic acid and filter through a whatman filter paper membrane No. 1 and Store the solution in the dark bottle at room temperature.

#### 4.17 Destaining solution for Coomassie stain

Mix 400 mL methanol, 100 mL glacial acetic acid, and then add distilled water to the final volume of 1,000 mL.

#### 4.18 10% (w/v) Ammonium persulfate

Dissolve 100 mg of ammonium persulfate in 1 mL of distilled water. Store the solution at -20 °C.

#### 4.19 12% (w/v) Separating SDS-PAGE gel

Mix the solution as follows:

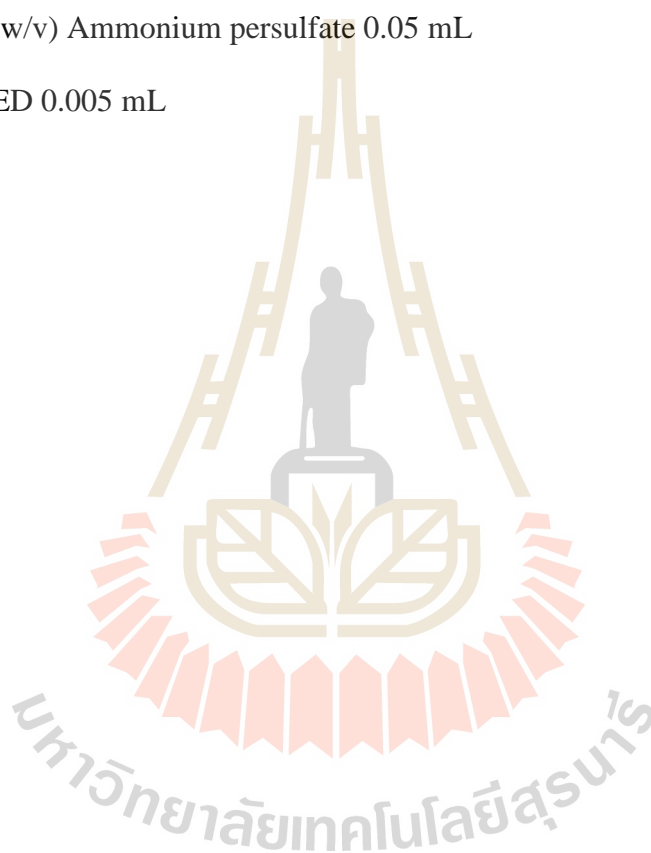
- 1.5 M Tris-HCl (pH 8.8) 2.5 mL
- Distilled water 3.3 mL
- 10% (w/v) SDS 0.1 mL
- 30% (w/v) Acrylamide solution 4.0 mL
- 10% (w/v) Ammonium persulfate 0.1 mL
- TEMED 0.004 mL

Adjust the volume with distilled water to 10 mL

#### 4.20 5% (w/v) Stacking SDS-PAGE gel

Mix the solution as follows:

- 0.5 M Tris-HCl (pH 6.8) 0.63 mL
- Distilled water 3.4 mL
- 10% (w/v) SDS 0.05 mL
- 30% (w/v) Acrylamide solution 0.83 mL
- 10% (w/v) Ammonium persulfate 0.05 mL
- TEMED 0.005 mL



## APPENDIX C

### PUBLICATIONS

#### Publication output:

1. Aunkham, A., Schulte, A., Winterhalter, M., and Suginta, W. (2014). Porin Involvement in Cephalosporin and Carbapenem Resistance of *Burkholderia pseudomallei*, *PLoS ONE*. 9(5): (2014) e95918.

#### Submitted for publication:

2. Aunkham, A., Zahn, M., Kesireddy, A., Baslè, A., Kleinekathöfer, U., Suginta, W., and van den Berg, B. (2017). Structural basis for chitin acquisition 1 by marine *Vibrio* species, *Nature Communications*.

#### In preparations:

3. Aunkham, A., Sim, WC., Chumjan, W. and Suginta, W. (2017). Probing the effect of Trp136 on the uptake of Chitooligosaccharides through Chitoporin from *Vibrio harveyi*.

4. Aunkham, A., Sim, WC. and Suginta, W. (2017). Antibiotic permeating studies of the interaction of cephalosporins and carbapenems with *BpsOmp38* channel from *Burkholderia pseudomallei*.

## CURRICULUM VITAE

**Name:** Anuwat Aunkham  
**Status:** Ph.D.candidate (Biochemistry)  
**Birthday:** 4th October 1986  
**Place of Birth:** Nakhon Ratchasima, Thailand  
**Nationality:** Thai

### Educations:

- 2004, High school  
Pakthongchai Phachaniramit School, Nakhon Ratchasima
- 2009, B.Sc., Environmental Health  
(First class honors), Schools of Environmental Health, Institute of Medicine,  
Suranaree University of Technology, Nakhon Ratchasima
- 2011-2017 Start as Ph.D. student  
School of Chemistry, Institute of Science, Suranaree  
University of Technology, Nakhon Ratchasima

### Scholarship

The Royal Golden Jubilee (RGJ) Ph.D. Programme, Thailand, 2010-2017.